



**Inward currents in mouse corpus cavernosum  
smooth muscle cells**

A thesis submitted to the  
School of Health and Science  
Dundalk Institute of Technology

For the degree of **Doctor of Philosophy**

By

**Xin Rui Lim B.Sc (Hons)**

September 2022

Under the supervision of Professor Keith Thornbury  
and co-supervision of  
Professor Gerard Sergeant  
Smooth Muscle Research Centre,  
Dundalk Institute of Technology

## Declaration

We, the undersigned declare that this thesis entitled 'Inward currents in mouse corpus cavernosum smooth muscle cells' is entirely the author's own work and has not been taken from the work of others, except as cited and acknowledged within the text.

The thesis has been prepared according to the regulations of Dundalk Institute of Technology and has not been submitted in whole or in part for an award in this or any other institution.

Author Name: Xin Rui Lim

Author Signature: Xin Rui Lim

Date: 28<sup>th</sup> Sept 2022

Supervisor Name: Professor Keith Thornbury

Supervisor Signature: 

Date: 29<sup>th</sup> September 2022

## Acknowledgement

Being drawn to SMRC since my undergraduate years, I am incredibly grateful to have the opportunity to explore research in the smooth muscle field. I would like to thank Professor Keith Thornbury for his invaluable advice and guidance. I especially enjoyed his insightful talks and research discussions – his passion is contagious. I'm proud to be his mentee. I would also like to thank Professor Gerard Sergeant and Professor Mark Hollywood for their tremendous support, helpful suggestions, and for showing me the spirit of enthusiasm needed to make this happen. Thank you all for the extra support, especially on my last lap of the race.

*“If I have seen further, it is by standing on the shoulders of giants”-Isaac Newton*

I would like to acknowledge Dr Eamonn Bradley, Dr Roddy Large, Dr Nicholas Mullins, Dr Srikanth Dudem, Dr Bernard Drumm, Dr Caoimhim Griffin, and Dr Tuleen Alkawadri for their assistance, advice, and for answering my unending science questions. Eamonn, thank you for bestowing me with scientific knowledge and skills - once a patcher, always a patcher. Roddy, your dad jokes kept me going. It was great craic - go raibh maith agat. Niki, thank you for the Mac. Above all, I sincerely thank you for being a good listener, comedian, and translator. Caoimhim, thank you for having my back in Reno, I'm grateful. Ben, Srikanth, and Tuleen, I enjoyed learning from and working with you all.

善之本在教，教之本在师 - 李觏

“The foundation of goodness lies in teaching, and the foundation of teaching lies in teachers”

Special thanks to Billie McIlveen, who shares my love for cats, and for putting up with my requests. I would like to thank my collaborators at the University of Reno, Nevada for their intracellular recording data in Appendix. Thank you, Karen Hannigan for sharing your career path and experience, and for being supportive. Also, many thanks to Thomas Curran and Stephen Fedigan for their advice and friendship. I would also like to thank my fellow colleagues, past and present, for the stimulating conversations, and for teaching me the value of endurance.

锲而舍之，朽木不折；锲而不舍，金石可镂 - 荀况

“Perseverance is key”

Thank you, Irish Research Council, for the small raise back in February 2021. Both my cats: Olive, Bobby, and I really appreciate it. Many thanks to DkIT research office staff, especially Aideen Gaynor, for the continuous support, and for helping me secure a visa extension for the last few months of my research. Thank you, Brainin Lennon for your kind words, for coordinating our work trips, and for helping me secure the Mac for data analysis. A massive thank you to all the Science technicians: Fiona McGovern, Fiona Finn, Ciara Martin, Marie McDonnell, Paddy McEntee, Laura Heffernan, Martina Carolan, Allison Murdock, and Muhammad Faisal Jamil for the good times and for keeping me sane. To all the friendly staff in RDC, especially Moyra, Grainne, and Margaret, I enjoyed our pleasant conversations. To the academic staff and lecturers in Science, those whom I had the pleasure to learn from, and especially those who have reached out, and encouraged me during my time as a PhD student – thank you.

一言之善，重于千金 - 晋·葛洪

“A kind word is worth more than gold”

I am incredibly indebted to my mom, dad, and brother, for without their love and support, this journey would have been impossible. Thank you for the laughter on videocalls, I miss you all dearly. Thank you, Theresa, for listening to my rants, for imparting words of wisdom, for all the wine and laughter, and for being my shelter in the storm. Ignatius has been a true, great supporter and has unconditionally loved me during my good and bad times during this project. You're my rock - I honestly couldn't have done it without you. Ixora, Tye Sween, Jing Yin, Jo Ann, and Iman, thank you for being with me every step of the way.

Finally, thank you self – You finally did it. Onwards and upwards.

## Abstract

*“Inward currents in mouse corpus cavernosum smooth muscle cells”*

*Xin Rui Lim*

Tonic contraction of CCSM is a pivotal component of the erectile dysfunction mechanism. Numerous studies have suggested that the penile contractile tone is regulated by its membrane potential. However, the precise expression and functional contributions of ion channels in corpus cavernosum smooth muscle of the mouse species have yet to be fully ascertained.

Whole cell ruptured patch and perforated patch technique revealed the presence of 1) voltage-gated sodium channels and 2)  $\text{Ca}^{2+}$ -activated  $\text{Cl}^-$  channels, respectively, in freshly dispersed mouse CCSM cells. Pharmacology studies revealed 2 populations of sodium currents, where TTX-insensitive current was mediated by  $\text{Nav}1.5$ , and TTX-sensitive current was mediated by a mixture of subtypes. Immunocytochemistry studies confirmed the presence of  $\text{Nav}1.4$ ,  $\text{Nav}1.5$ , and  $\text{TMEM16A}$ . Steady-state activation and inactivation curves revealed a small  $\text{Na}_V$  window current at the resting membrane potential. Veratridine, a  $\text{Na}_V$  activator, reduced time-dependent inactivation of the current and increased the duration of evoked action potentials. In CCSM tissue, veratridine-induced phasic contractions were a result of direct membrane depolarisation by sustained  $\text{Na}^{2+}$ -influx, hence activating L-type  $\text{Ca}^{2+}$  current to cause contractions. Phenylephrine induced phasic contractions of intact corpus cavernosum muscle strips were inhibited by  $\text{Na}_V$  and  $\text{CaCC}$  antagonists, highlighting the importance of these ion channels in the regulation of contractility by the sympathetic nerves. CCSM cells exhibited spontaneous transient inward currents and spontaneous transient depolarisations when voltage-clamped at  $-60$  mV, and in current clamp mode, respectively. STICs were carried by  $\text{Cl}^-$  ions. Both STICs and STDs involved  $\text{Ca}^{2+}$ -activated  $\text{Cl}^-$  channels. They were dependent on  $\text{Ca}^{2+}$  release from intracellular  $\text{Ca}^{2+}$  stores involving RyR and  $\text{IP}_3\text{R}$  and were also reliant on store-operated calcium entry. L-type  $\text{Ca}^{2+}$  currents contributed to the plateau of STDs.

This study suggests that contraction of CCSM is regulated by activation of  $\text{Na}_V$  channels and  $\text{TMEM16A}$  channels and therefore inhibition of these channels could lead to penile erection. A graphical abstract summarising the findings in mouse CCSM is shown in Figure I.

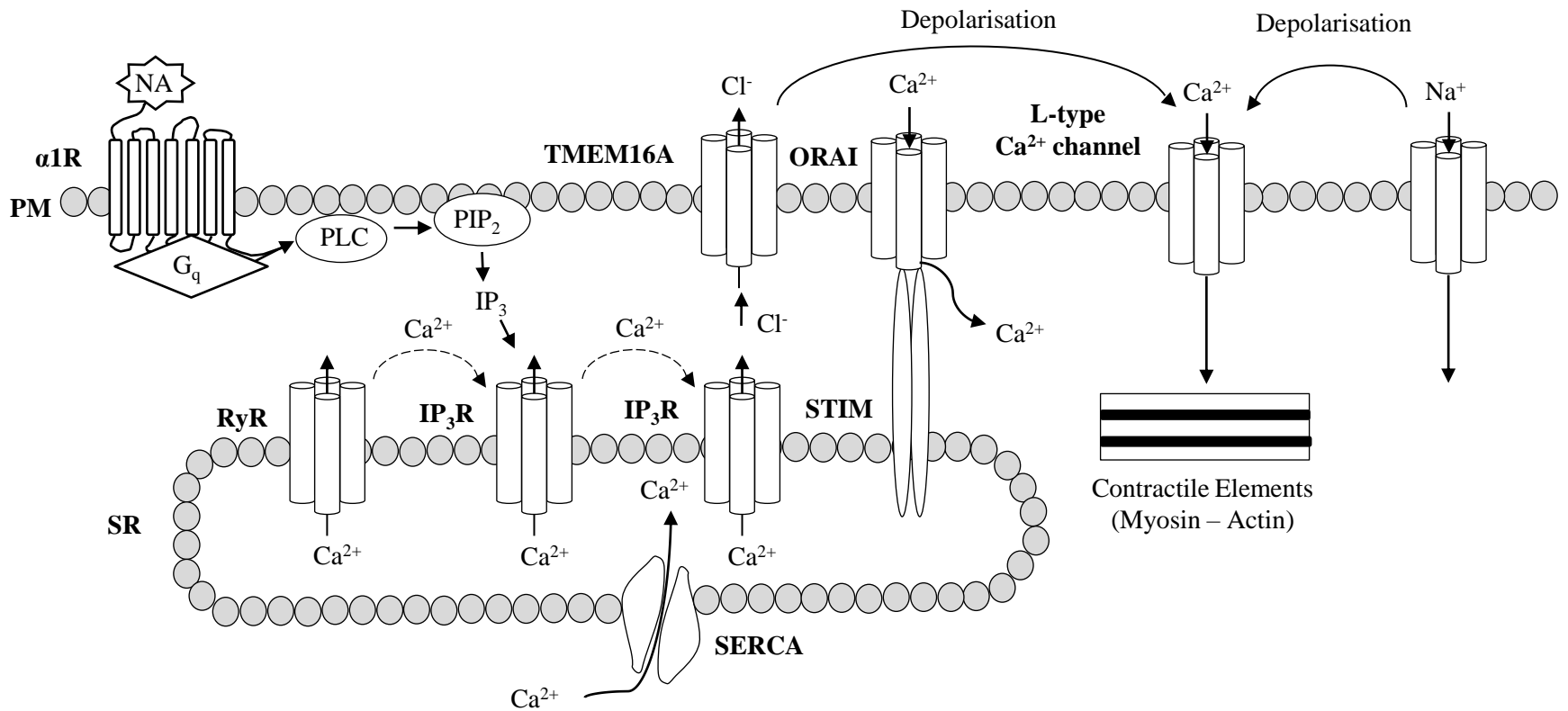


**Figure I: Mechanisms underlying inward currents in mouse CCSM.**

## Research Dissemination

### Publications

Lim, X.R., Bradley, E., Griffin, C.S., Hollywood, M.A., Sergeant, G.P., and Thornbury, K.D. (2021). Fast voltage-dependent sodium (Nav) currents are functionally expressed in mouse corpus cavernosum smooth muscle cells. *British Journal of Pharmacology*. DOI: 10.1111/bph.15728

### Publication and conference contributions

- Gordon Research Conference 2022  
Poster communication  
“The functional role of voltage-dependent sodium (Nav) currents in mouse corpus cavernosum smooth muscle tissue”
- Gordon Research Seminar 2022  
Poster communication  
“The functional role of voltage-dependent sodium (Nav) currents in mouse corpus cavernosum smooth muscle tissue”
- Annual Physiology 2021 virtual conference  
Oral communication  
OC46 “Fast voltage-dependent sodium (Nav) currents are functionally expressed in mouse corpus cavernosum smooth muscle cells”
- FASEB 2019, Florida, United States  
Poster Communication  
“Sodium current in mouse corpus cavernosum”

## Table of Content

<b>Declaration</b> .....	<b>1</b>
<b>Acknowledgement</b> .....	<b>2</b>
<b>Abstract</b> .....	<b>4</b>
<b>Research Dissemination</b> .....	<b>6</b>
<b>Glossary</b> .....	<b>11</b>
<b>Chapter 1: Literature Review</b> .....	<b>18</b>
1.1 Anatomy.....	19
1.1.1 Anatomy of the corpus cavernosum.....	20
1.1.2 Arterial supply to the penis.....	21
1.1.3 Venous drainage of the penis.....	21
1.1.4 Blood circulation within the corpus cavernosum.....	22
1.2 Innervation.....	24
1.2.1 Peripheral innervation.....	24
1.3 Physiological regulation of penile contraction.....	30
1.3.1 Ca <sup>2+</sup> signalling cascade.....	30
1.3.2 RhoA/Rho-kinase pathway.....	31
1.3.3 Physiological regulation of penile relaxation.....	32
1.4 Erectile dysfunction.....	33
1.4.1 Contributing factors to ED.....	33
1.4.2 Treating ED.....	34
1.5 Electrophysiology.....	35
1.5.1 Ion channels in corpus cavernosum.....	35
1.5.2 K <sup>+</sup> channels.....	35
1.5.3 Ca <sup>2+</sup> -activated K <sup>+</sup> (BK <sub>Ca</sub> ) channels.....	35
1.5.4 K <sub>v</sub> channels.....	37
1.5.5 Ca <sup>2+</sup> -activated Cl <sup>-</sup> channels.....	38
1.5.6 L-and T-type Ca <sup>2+</sup> channel.....	39
1.5.7 P2X receptor-mediated cation current.....	40
1.5.8 STIM ORAI proteins.....	41
1.6 Review of voltage-gated sodium (Na <sub>v</sub> ) channel.....	42
1.6.1 Na <sub>v</sub> channels in smooth muscles.....	42
1.6.2 Structure of Na <sub>v</sub> channels.....	43
1.6.3 Biophysical properties of Na <sub>v</sub> channels.....	45
1.6.3.1 Activation.....	46

1.6.3.2 Inactivation.....	48
1.6.3.3 Fast inactivation .....	48
1.6.3.4 Slow inactivation.....	51
1.6.4 Channelopathies.....	51
1.6.5 Pharmacology of Nav channels .....	54
1.7 Review of Ca <sup>2+</sup> -activated Cl <sup>-</sup> (TMEM16A) channels .....	61
1.7.1 Ca <sup>2+</sup> -activated Cl <sup>-</sup> channels.....	62
1.7.2 Chloride accumulation in smooth muscle.....	62
1.7.3 Role of Ca <sup>2+</sup> -activated Cl <sup>-</sup> channels in smooth muscle.....	63
1.7.4 Structure of TMEM16A channel .....	66
1.7.5 Biophysical properties of CaCCs.....	67
1.7.6 Channelopathies.....	70
1.7.7 Pharmacology of TMEM16A channels .....	70
1.8 Project aims and objectives .....	74
<b>Chapter 2: Materials and methods.....</b>	<b>75</b>
2.1 Tissue preparation .....	76
2.2 Isometric tension recording .....	76
2.3 Isolation of corpus cavernosum smooth muscle cells .....	77
2.4 Human embryonic kidney cells .....	78
2.5 Total RNA isolation .....	78
2.5.1 Tissue sample.....	78
2.6 Reverse Transcription-Polymerase Chain Reaction (RT-PCR) .....	79
2.6.1 cDNA synthesis .....	79
2.7 Polymerase Chain Reaction (PCR) .....	80
2.8 Agarose Gel Electrophoresis and Gel Imaging .....	83
2.9 Real-time quantitative PCR.....	84
2.10 Immunocytochemistry .....	85
2.11 Immunohistochemistry .....	86
2.12 Electrophysiology.....	88
2.12.1 Patch-clamp equipment.....	88
2.12.2 Voltage clamp .....	89
2.12.3 Current clamp .....	89
2.12.4 Patch-clamp .....	90
2.12.4.1 Whole-cell ruptured patch.....	90
2.12.4.2 Whole-cell perforated patch.....	91

2.13 Liquid junction potential .....	92
2.14 Pipette resistance .....	92
2.15 Formation of a gigaseal .....	93
2.16 Cell capacitance.....	93
2.17 Series resistance .....	95
2.18 Space clamp.....	96
2.19 Leak subtraction .....	97
2.20 Statistical analysis .....	98
2.21 Solutions.....	99
2.22 Drugs .....	101
<b>Chapter 3: Biophysical properties of Nav currents in CCSM.....</b>	<b>112</b>
3.1 Introduction .....	113
3.2 Results .....	115
3.2.1 Low external sodium abolished the evoked inward current .....	115
3.2.2 Reveal of sodium-dependent difference currents .....	115
3.2.3 Reversal potential of sodium-dependent difference currents .....	115
3.2.4 Biophysical properties of the sodium current.....	116
3.2.5 TTX sensitivity reveals the presence of $\geq$ two populations of Nav current	117
3.2.6 Voltage-dependent kinetics of TTX <sub>sens</sub> and TTX <sub>insens</sub> currents.....	118
3.2.7 Effect of subtype-specific Nav inhibitors on TTX <sub>sens</sub> current .....	119
3.2.8 Effect of A803467 on CCSM TTX <sub>insens</sub> current and HEK Nav1.5 current...	120
3.2.9 Effect of OD1 on CCSM TTX <sub>sens</sub> and TTX <sub>insens</sub> current and HEK Nav1.5 current.....	120
3.3 Discussion .....	122
<b>Chapter 4: Functional study of Nav in CCSM.....</b>	<b>138</b>
4.1 Introduction .....	139
4.2 Results .....	140
4.2.1 Effect of veratridine on CCSM cells.....	140
4.2.2 Effect of veratridine on evoked action potential (AP).....	140
4.2.3 Effect of veratridine and TTX On CCSM cells .....	141
4.2.4 Effect of KB-R7943 on currents in CCSM.....	141
4.2.5 Veratridine evokes contractions in mouse corpus cavernosum tissue.....	142
4.2.6 TTX inhibited PE-induced transient depolarisations.....	143
4.2.7 TTX reduced the frequency of PE-induced contractions in CCSM tissue ...	143
4.3 Discussion .....	145

<b>Chapter 5: Transcriptional and immunocytochemistry study of Nav in CCSM..</b>	<b>160</b>
5.1 Introduction .....	161
5.2 Results .....	162
5.2.1 Transcriptional expression of Nav channels in CCSM tissue.....	162
5.2.2 Relative transcriptional expression of Nav channels in CCSM tissue.....	162
5.2.3 Expression of Nav1.5 and Nav1.4 in CCSM cells.....	162
5.3 Discussion .....	164
<b>Chapter 6: Ca<sup>2+</sup>-activated Cl<sup>-</sup> channels in CCSM.....</b>	<b>175</b>
6.1 Introduction .....	176
6.2 Results .....	178
6.2.1 Protein expression of TMEM16A in CCSM cells.....	178
6.2.2 Two different TMEM16A specific blockers inhibited chloride tail currents	178
6.2.3 The effect of low Cl <sup>-</sup> Hanks on tail current .....	179
6.2.4 Two different TMEM16A specific blockers abolished STICs and STDs ...	179
6.2.5 Contribution of Ca <sup>2+</sup> stores to STICs and STDs in CCSMC .....	180
6.2.6 Involvement of both RyR and IP <sub>3</sub> R in the activation of STICs and STDs...	181
6.2.7 Involvement of L-type Ca <sup>2+</sup> channel in the activation of STICs and STDs .	181
6.2.8 Ani9 inhibited PE-induced transient inward currents and transient depolarisations.....	182
6.2.9 Ani9 reduced the frequency of PE-induced contractions in CCSM tissue ...	182
6.3 Discussion .....	183
<b>Chapter 7: General discussion and future work .....</b>	<b>210</b>
<b>References .....</b>	<b>217</b>
<b>Appendix .....</b>	<b>256</b>
A.1 Materials and methods.....	256
A.1.1 Intracellular recording.....	256
A.1.2 Tissue Ca <sup>2+</sup> imaging.....	256

## Glossary

2APB	2-Aminoethoxydiphenyl borate
A9C	Anthracene-9-carboxylic acid
AB	Antibody
AD/DA	Analog-digital
ADP	Adenosine diphosphate
AMP	Adenosine monophosphate
ANGII	Angiotensin II
ANO1	Anoctamin-1
ANOVA	One way analysis of variance
AP	Action potential
ARG	Arginine
ATP	Adenosine triphosphate
BK <sub>Ca</sub>	Large-conductance, Ca <sup>2+</sup> -activated K <sup>+</sup> channel
bp	Base pair
[Ca <sup>2+</sup> ]	Calcium concentration
CaCC	Ca <sup>2+</sup> -activated Cl <sup>-</sup> channel
CAM	Calmodulin
CaMKII	Calmodulin kinase II
cAMP	Cyclic adenosine monophosphate
CAS	Chemical Abstracts Service
CC	Corpora cavernosa
CCSM	Corpus cavernosum smooth muscle
CFTR	Cystic fibrosis transmembrane conductance regulator

cGMP	Cyclic guanosine monophosphate
CIP	Congenital insensitivity to pain
CO <sub>2</sub>	Carbon dioxide
COX	Cyclooxygenase
CPA	Cyclopiazonic acid
CRAC	Ca <sup>2+</sup> -release-activated Ca <sup>2+</sup>
DAG	Diacylglycerol
DEKA	Asp, Glu, Lys, and Ala
DIDS	4,4'-diisothiocyanatostilbene-2,2'-disulfonic acid
DMEM	Dulbecco's Modified Eagle Medium
DMSO	Dimethyl sulfoxide
DNA	Deoxyribonucleic acid
dNTP	Deoxynucleoside triphosphate
DOG	Discovered on GIST-1
DPBS	Dulbecco's phosphate-buffered saline
DS	Dravet syndrome
DTT	Dithiothreitol
EC <sub>50</sub>	Half-maximal excitatory concentration
ECG	Electrocardiogram
E <sub>Cl</sub>	Chloride equilibration potential
ED	Erectile dysfunction
EDTA	Ethylenediaminetetraacetic acid
EFS	Electrical field stimulation
EGTA	Ethylene glycol-bis(β-aminoethyl ether)- <i>N,N,N',N'</i> -tetraacetic acid

EMCCD	Electron-multiplying charge-coupled device
EMG	Electromyography
EP	Prostaglandin E
ER	Endoplasmic reticulum
ET <sub>A</sub>	Endothelin receptor subtype A
ET <sub>B</sub>	Endothelin receptor subtype B
FASEB	Federation of American Societies of Experimental Biology
FHF	Fibroblast growth factor homologous factors
FPS	Frames per second
GDI	Guanosine dissociation inhibitors
GDP	Guanosine diphosphate
GEFS	Genetic epilepsy with febrile seizures plus
GEFs	Guanine nucleotide exchange factors
GIST	Gastrointestinal squamous tumour
GMP	Guanosine monophosphate
GTP	Guanosine 5'-triphosphate
HEK	Human embryonic kidney
IC <sub>50</sub>	Half-maximal inhibitory concentration
IFM	Isoleucine-phenylalanine-methionine
IP <sub>3</sub>	Inositol 1,4,5-trisphosphate
IP <sub>3</sub> R	Inositol 1,4,5-trisphosphate receptor
IQ-motif	Isoleucine (commonly) and glutamine (invariably) motif
IV	Current-voltage
K <sub>v</sub>	Voltage-gated K <sup>+</sup> channel

LDL	Low density lipid
L-NOARG	N $\omega$ -nitro-l-arginine
LSM	Laser scanning microscopy
MAE	Myoclonic astatic epilepsy
mg	Milligram
min	Minutes
MLC	Myosin light chain
MLCK	Myosin light chain kinase
MLCP	Myosin light chain phosphatase
mm	Millimetre
mM	Millimolar
mN	Millinewton
ms	Millisecond
mV	Millivolt
N	Animal number
n	Sample number
NANC	Non-adrenergic, non-cholinergic
NCX	Na <sup>+</sup> /Ca <sup>2+</sup> exchanger
NFA	Niflumic acid
NIH	National institutes of health
NKCC	Sodium-potassium-chloride (Na <sup>+</sup> , K <sup>+</sup> , Cl <sup>-</sup> ) cotransport
nM	Nanomolar
NMDG	N-methyl-d-glucamine
NO	Nitric oxide

NTC	No template control
O <sub>2</sub>	Oxygen
°C	Degrees Celsius
P2X	ATP-gated ion channel
P2Y	Purinergic G-protein coupled receptor
PACAP	Pituitary adenylate-cyclase-activating polypeptide
PCR	Polymerase chain reaction
PDE	Phosphodiesterase
PE	Phenylephrine
PFA	Paraformaldehyde
PGE1	Prostaglandin E1
PIP <sub>2</sub>	Phosphatidylinositol 4,5-bisphosphate
PKA	Protein kinase A
PKC	Protein kinase C
PKG	Protein kinase G
PLC	Phospholipase C
qPCR	Real-time quantitative PCR
RCF	Relative Centrifugal Force/G-force
RMP	Resting membrane potential
RNA	Ribonucleic acid
ROCK	Rho-kinase
RPM	Revolutions per minute
RT-PCR	Reverse transcriptase polymerase chain reaction
RyR	ryanodine receptor

s or sec	Second
S.E.M.	Standard error of the mean
SCN	Sodium channel
SERCA	Sarco/endoplasmic (Ca <sup>2+</sup> )-ATPase pump
SM	Smooth muscle
SMEI	Severe myoclonic epilepsy of infancy
SNP	Sodium nitroprusside
SNS	Somatic nervous system
SOCE	Store-operated Ca <sup>2+</sup> entry
SR	Sarcoplasmic reticulum
SS	Short membrane-associated segments
SMC	Smooth muscle cell
STD	Spontaneous transient depolarisations
STIC	Spontaneous transient inward current
STIM	Stromal interaction molecule
STOC	Spontaneous transient outward current
STX	Saxitoxin
TAE	Tris, acetic acid
TEA	Tetraethylammonium
TIFF	Tag Image File Format
TMEM16A	Transmembrane protein 16A
TRPC	Transient receptor potentials: canonical channel
TRPV	Transient receptor potentials: vanilloid-related channel
TTX	Tetrodotoxin

VEGF	Vascular Endothelial Growth Factor
VIP	Vasoactive intestinal peptide
VPAC	Vasoactive intestinal peptide receptor
VRAC	Volume regulated anion channel
$\Delta\Delta CT$	Delta delta threshold cycle method
$\mu\text{l}$	Microlitre
$\mu\text{m}$	Micrometre
$\mu\text{M}$	Micromolar
$\alpha$	Alpha
$\beta$	Beta
$\gamma$	Gamma
$\Delta$	Delta
$\mu$	Micro
$\tau$	Time constant
$\omega$	Omega
%	Percentage

## **Chapter 1: Literature Review**

## 1.1 Anatomy

The penis is located within the urogenital triangle (Sam and LaGrange, 2018). It has three components: the paired corpora cavernosa and the corpus spongiosum, which contains the urethra (Figure 1.1). The corpus spongiosum expands into the glans at the distal end, where the urethra opens to the outside of the body, termed the meatus. The corpora cavernosa stem from the crura; the corpus spongiosum stems from the bulb. The root of the penis consists of the diverging crura (covered by the ischiocavernosus muscles) and the median bulb (covered by the bulbospongiosus muscles). The bulb is anchored to the perineal membrane while the crura are fixed to the ischiopubic rami as two separate structures to prevent the penis from sinking into the perineum during intercourse. Two ligaments support the penis root: the suspensory ligament that arises from the anterior surface of the pubic symphysis, and the superficially located fundiform ligament (Drake *et al.*, 2015). A layer of fibrous tissue, the tunica albuginea, envelops both the corpora cavernosa and the corpus spongiosum, but it is thicker around the corpora cavernosa (Figure 1.1). A second fibrous layer, Buck's fascia, also known as the deep fascia of the penis, envelops the corpora cavernosa and divides them from the corpus spongiosum (Pretorius *et al.*, 2001). Corpora cavernosa are the main structure responsible for erection, maintained by both tunica albuginea and Buck's fascia.

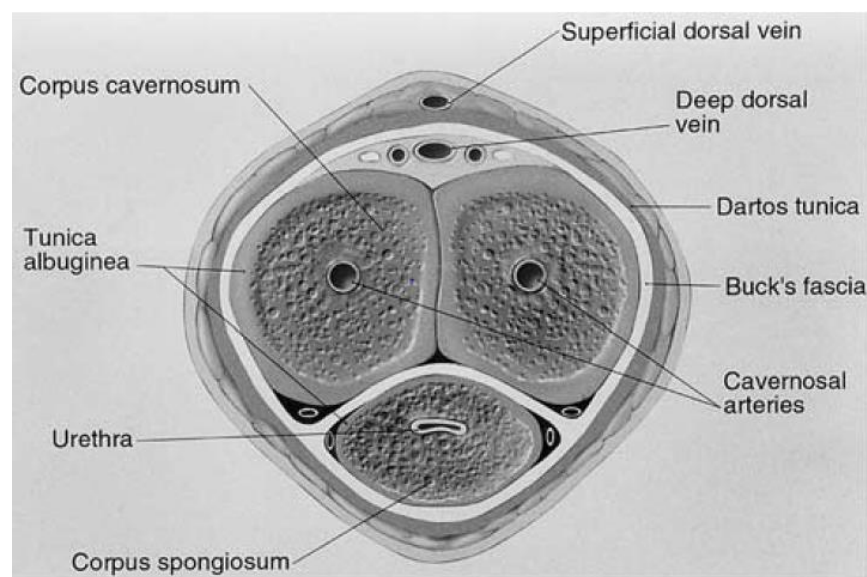


**Figure 1.1: Axial illustration of penile anatomy (Pretorius *et al.*, 2001).**

### 1.1.1 Anatomy of the corpus cavernosum

The paired corpora cavernosa are linked to each other for the distal two-thirds of their lengths. According to Pretorius *et al.* (2001), they are connected by fenestrations in the intracavernous septum, allowing communication and cross talk, effectively rendering the pair a single functional unit. The corpus cavernosa contains a high abundance of smooth muscle bundles oriented in all directions. Embedded within the mass of smooth muscle is a meshwork of intercommunicating vascular spaces (sinusoids) lined with endothelium (Goldstein and Padma-Nathan, 1990).

The tunica albuginea enveloping corpus cavernosa consists of undulating collagen fibres and longitudinal elastic fibres. Investigations have suggested that the collagen fibres are characteristically transversely linked by elastic fibres (Bitsch *et al.*, 1990). The fibre arrangement functions to meet the mechanical demands imposed during erection by preventing the overstretching of collagen fibres. It allows for elongation and can accommodate a certain degree of intracavernosal pressure to provide rigidity and axial strength when erect, yet be supple when flaccid (Iacono *et al.*, 1995; Bitsch *et al.*, 1990; Gelbard, 1982). It has been suggested that reduction in the elastic fibre content, but not the collagen content of the tunica albuginea, may contribute to the development of erectile dysfunction (Costa *et al.*, 2006; Iacono *et al.*, 1995; Luangkhot *et al.*, 1992).

Projections from the internal surface of tunica albuginea, also known as trabeculae, cross the corpus cavernosa interior in all directions to form a fibrous framework (Nakano, 1995; Hsu *et al.*, 1992). The smooth muscle bundles have attachments to the tunica albuginea and its columns, the periarterial and perineural fibrous sheaths, and the intracavernosal framework of collagen fibres (Goldstein and Padma-Nathan, 1990). Gap junctions formed by connexin-43 are found between the smooth muscle cells of the human corpus cavernosum (De Carvalho *et al.*, 1993). It was suggested that the initiation, maintenance, and modulation of synchronised relaxation and contraction commonly observed in the corpus cavernosum, occurs by the diffusion of ions and second messenger molecules intercellularly through gap junctions (Christ *et al.*, 1992; 1991).

### 1.1.2 Arterial supply to the penis

The arterial supply to the penis arises from the internal pudendal arteries, which stem from the internal iliac arteries. The internal pudendal artery branches into the bulbourethral artery, the dorsal artery of the penis, and the cavernosal artery (Sam and LaGrange, 2018; Pretorius *et al.*, 2001; Juskiewenski *et al.*, 1982). The bulbourethral artery supplies the penile bulb, the bulbourethral gland, and the corpus spongiosum, and it gives rise to the urethral artery, which runs in parallel to the course of the urethra within the corpus spongiosum (Figure 1.2).

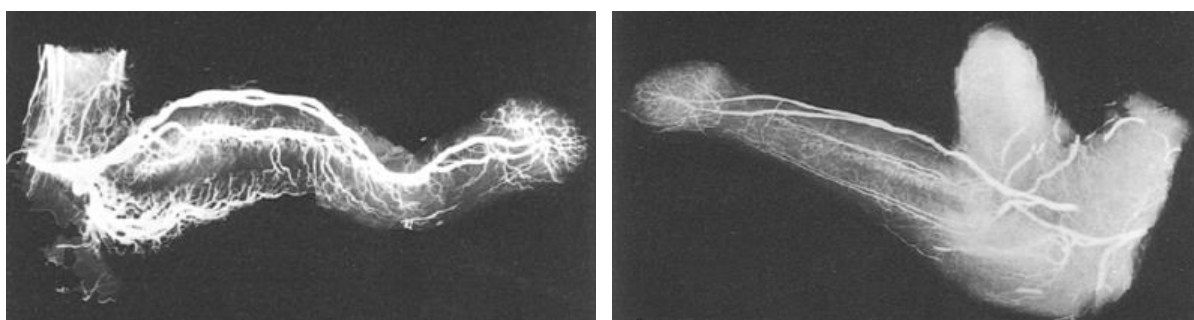


**Figure 1.2: Distribution of the penile bulb arteries [left] and urethral arteries [right] (Juskiewenski *et al.*, 1982).**

The dorsal arteries supply the penile skin, the glans penis, the fibrous tissue surrounding the corpus cavernosa, corpus spongiosum, and the spongy urethra (Drake *et al.*, 2015). The cavernosal arteries run in the centre of each corpus cavernosum, which gives rise to multiple helicine arteries to supply the corpus cavernosum sinusoids (Figure 1.4). The bulbourethral, dorsal and cavernosal arteries all anastomose with each other, providing extensive blood supply to the penis (Drake *et al.*, 2015).

### 1.1.3 Venous drainage of the penis

The superficial dorsal vein lies outside the Buck's fascia. It drains blood from the skin and prepuce and empties into the great saphenous vein (Drake *et al.*, 2015). The emissary vein carries blood from sinusoids of distal two-thirds of the penis before joining the

circumflex vein. The circumflex and deep dorsal vein drain the glans and the corpus spongiosum into the prostatic venous plexus (Tank *et al.*, 2005; Hsu *et al.*, 2003). Blood from sinusoids of proximal one-third of the penis is carried by the emissary vein before joining the cavernosal vein. Crural veins drain the crura of the penis. The cavernosal and crural veins drain into the internal pudendal veins, which empty into the internal iliac vein (Hsu *et al.*, 2003).

#### 1.1.4 Blood circulation within the corpus cavernosum

The intracorporal circulation sequence can be summarised as in the flow chart below (Figure 1.3).

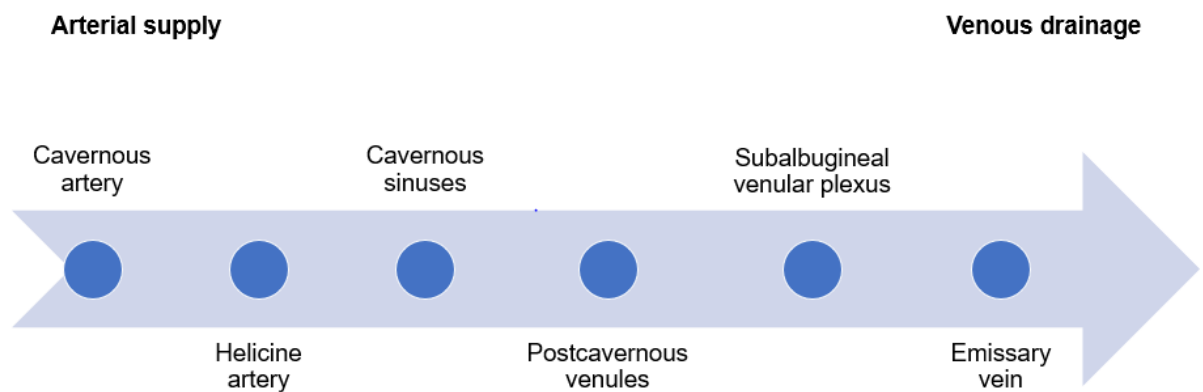


**Figure 1.3: The sequence of the intracorporal circulation (MacLennan *et al.*, 2012).**

During the flaccid state, the contracted state of the helicine arteries and the sinusoidal smooth muscle causes high vascular resistance in the penis. After stimulation, the release of neurotransmitters causes dilation of the arteriolar wall and relaxation of sinusoidal smooth muscle, thereby increasing blood flow to enlarge the corpora cavernosa and thus stretching the tunica albuginea. Expansion of the cavernous space compresses the subalbugineal venular plexuses between the tunica albuginea and the peripheral sinusoids. Stretching of tunica albuginea to its capacity ultimately leads to occlusion of the emissary veins, resulting in minimum venous outflow and maintenance of an erection (Dean and Lue, 2005; Lue, 2000). Thus, erection involves, arterial dilatation sinusoidal relaxation,

and venous compression. An overview of the vascular anatomy of penile erection is shown in Figure 1.4.

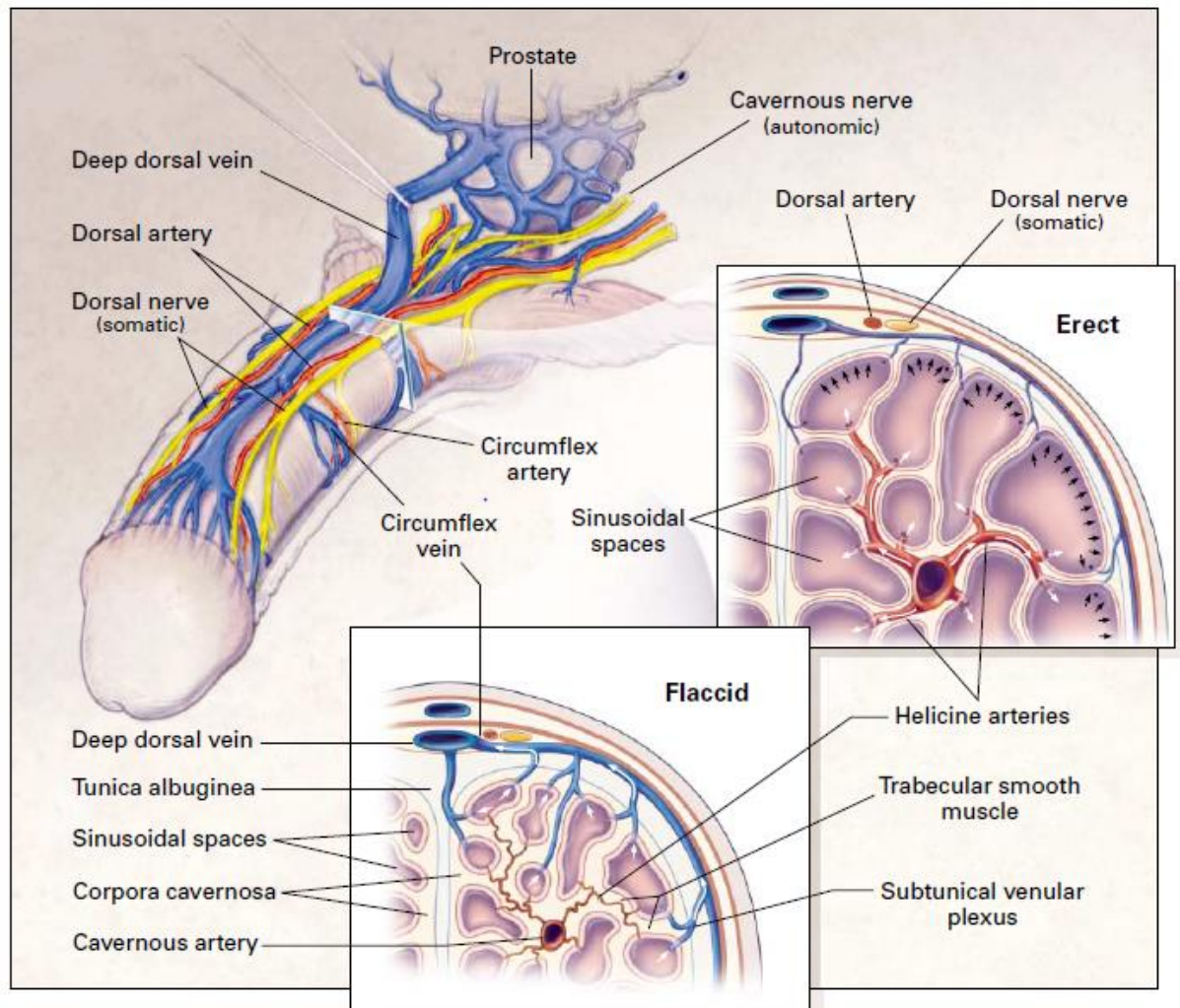


**Figure 1.4: Vascular anatomy of penile erection.** Reproduced with permission from (Lue, 2000), Copyright Massachusetts Medical Society.

## **1.2 Innervation**

Penile erection is a complex neurovascular process in which nerves, endothelium, and smooth muscle cells are involved. It is initiated by the processing and integration of sexual stimuli (for example, visual, olfactory, and imaginary) in the central nervous system superimposed upon a spinal reflex and the release of neurotransmitters in the peripheral nervous system, which can be either excitatory or inhibitory (Andersson, 2011). There is also a somatic innervation, where the pudendal nerve is responsible for penile sensation, and somatic motor nerves control the striated bulbospongiosus and ischiocavernosus muscles (Vein, 2003). The balance between excitatory and inhibitory factors determines the contractile degree of corpora cavernosa smooth muscle, and subsequently, the functional state of the penis (Andersson, 2011).

### **1.2.1 Peripheral innervation**

In humans, the sympathetic innervation originates from T10 to L2 spinal cord segments (Lue *et al.*, 1984). Some preganglionic fibres traverse the lumbar splanchnic nerves to the superior hypogastric plexus, which is at the level of the third lumbar and first sacral vertebrae (Dean and Lue, 2005). The fibres then travel in the hypogastric nerves to the pelvic plexus. On the other hand, the parasympathetic innervation arises from the S2 to S4 spinal cord segments (Lue *et al.*, 1984). The preganglionic fibres pass in the pelvic nerves to the pelvic plexus, where they are joined by the sympathetic nerves from the superior hypogastric plexus (Dean and Lue, 2005). Branches of the pelvic plexus then travel through the cavernous nerves to innervate the penis (Dean and Lue, 2005).

It is generally accepted that the sympathetic innervation is responsible for maintaining detumescence and vasoconstriction, while the parasympathetic innervation is responsible for tumescence and vasodilatation. The primary neurotransmitter involved in sympathetic stimulation is noradrenaline (adrenergic), while the ones mainly involved in parasympathetic stimulation are acetylcholine (cholinergic) and nitric oxide (non-adrenergic non-cholinergic NANC).

However, all types of nerves may contain more than one type of neurotransmitter. The endothelium of sinusoids and blood vessels in the penis also release modulators that influence the state of contraction or relaxation of the penis. Examples of such neurotransmitters and modulators are listed in Table 1.1 below.

Neurotransmitter	Origin	Receptor	Mechanism	Smooth muscle response
Noradrenaline	Sympathetic, adrenergic nerves	Postsynaptic $\alpha_1$ , Postsynaptic $\alpha_2$ (De Tejada <i>et al.</i> , 1989)	Activation of L-type $\text{Ca}^{2+}$ channels, receptor-operated $\text{Ca}^{2+}$ channels, PKC, Rho-kinase (Takahashi <i>et al.</i> , 2003)	Contraction
		Presynaptic $\alpha_2$ (De Tejada <i>et al.</i> , 1989)	Downregulate its own release (De Tejada <i>et al.</i> , 1989)	
			Downregulate the release of nervous nitric oxide (Prieto, 2008)	
Adrenaline	Adrenal medulla	$\beta_2$ -adrenoreceptor on CCSM tissue (Dhabuwala <i>et al.</i> , 1985)	Induces cAMP-dependent relaxation (Palmer <i>et al.</i> , 1994)	Relaxation
Neuropeptide Y	Sympathetic nerves	Postsynaptic $\text{Y}_1$ (Prieto, 2008) Postsynaptic $\text{Y}_2$	Enhance noradrenaline contractions depolarising arterial smooth muscle and by	Contraction

(co-localised and co-released with noradrenaline)		(Prieto, 2008)	inhibiting cAMP-mediated relaxations (Prieto, 2008)	
		Presynaptic Y <sub>2</sub> (Prieto, 2008)	Limit noradrenaline release from nerve terminals (Prieto, 2008)	Relaxation
Nitric oxide (neural)	Nonadrenergic, non-cholinergic (NANC) nerve	Soluble guanylyl cyclase on CCSM cells (Nimmegeers <i>et al.</i> , 2008)	Guanylate cyclase/cGMP/PKG (Prieto, 2008)	Relaxation
Nitric oxide (endothelial)	Shear stress on the endothelium lining activates membrane-bound endothelium nitric oxide synthase (Prieto, 2008)			

Acetylcholine	Cholinergic nerves	M <sub>3</sub> on endothelial cells (Traish <i>et al.</i> , 1995)	Release endothelial nitric oxide (Lue, 2000)	Relaxation
		Nicotinic receptors on nitrenergic nerves (Bozkurt <i>et al.</i> , 2007)	Release of nitric oxide from nitrenergic terminals (Bozkurt <i>et al.</i> , 2007)	Relaxation
		Muscarinic receptors on adrenergic nerve (Andersson, 2011)	Inhibit the release of noradrenaline from adrenergic nerve terminals (Andersson, 2011)	Relaxation
Angiotensin II	Endothelial cells (Kifor <i>et al.</i> , 1997)	ANG II receptor subtype AT <sub>1</sub> on smooth muscle (Iwamoto <i>et al.</i> , 2001; Park <i>et al.</i> , 1997)	IP <sub>3</sub> /diacylglycerol/Ca <sup>2+</sup> /PKC (Andersson, 2011).	Contraction
Endothelin I	Endothelial cells (Prieto, 2008)	Postsynaptic ET <sub>A</sub> (Prieto, 2008) Presynaptic ET <sub>B</sub> (Prieto, 2008)	IP <sub>3</sub> /diacylglycerol /Ca <sup>2+</sup> /PKC (Vein, 2003)	Contraction
Prostaglandin E	Blood vessel endothelium (Andersson, 2011)	EP1 on CCSM cell (Moreland <i>et al.</i> , 2003)	Causes relaxation <i>in vitro</i> at concentrations below 300 nM via cAMP/PKA (Hedlund and Andersson, 1985). At higher concentrations (> 300 nM), cross-reacts with thromboxane A2	Relaxation

			(TP) receptors to induce contraction (Moreland <i>et al.</i> , 2003; Moreland <i>et al.</i> , 2000)	
		EP2/EP4 on CCSM cells (Moreland <i>et al.</i> , 2003)	Adenylate cyclase/cAMP/PKA (Andersson, 2011)	Relaxation
Thromboxane A <sub>2</sub>	Blood vessel endothelium	Prostanoid Thromboxane receptor (TP) on CCSM	PKC/Rho-kinase (Grann <i>et al.</i> , 2016)	Contraction
Vasointestinal peptide (VIP)	Nonadrenergic, non-cholinergic nerves (Vein, 2003)	VPAC <sub>2</sub> on CCSM cells (Guidone <i>et al.</i> , 2002)	cGMP/PKG (Kim <i>et al.</i> , 1994)  Adenylate cyclase/cAMP/protein kinase A (Prieto <i>et al.</i> , 2008)	Relaxation

**Table 1.1: Neurotransmitters and mediators in corpus cavernosum.**

### 1.3 Physiological regulation of penile contraction

Smooth muscle contraction occurs through two main mechanisms:  $\text{Ca}^{2+}$  signalling cascades and altered  $\text{Ca}^{2+}$  sensitivity via Rho/Rho-kinase signalling pathways (Berridge, 2008). According to Thornbury *et al.* (2019), the rhythmical contractions of CCSM depend on spontaneous  $\text{Ca}^{2+}$  oscillations induced by  $\text{Ca}^{2+}$  release from  $\text{IP}_3$  receptors and ryanodine receptors. Spontaneous  $\text{Ca}^{2+}$  waves act as a primary event, driving transient depolarisation to synchronise and amplify the oscillatory mechanism.

#### 1.3.1 $\text{Ca}^{2+}$ signalling cascade

Many agonists, for example,  $\alpha_1$ -adrenergic agonists and angiotensin, bind to specific plasmalemmal receptors coupled to phosphoinositide-specific phospholipase C via GTP-binding proteins. Phospholipase C then hydrolyses phosphatidylinositol 4,5-bisphosphate ( $\text{PIP}_2$ ) to 1,2-diacylglycerol (DAG) [DAG activates PKC] and inositol-1,4,5-triphosphate ( $\text{IP}_3$ ).  $\text{IP}_3$  then binds to its receptor,  $\text{IP}_3\text{R}$ , on the store to cause  $\text{Ca}^{2+}$  release. Given that the  $\text{Ca}^{2+}$  concentration in the cytosol and the store are  $\sim 100$  nM and  $\sim 0.4$  mM, respectively (Bootman, 2012),  $\text{Ca}^{2+}$  from the store is driven into the cytoplasm by the concentration gradient, triggering smooth muscle contraction.

The increase in sarcoplasmic  $\text{Ca}^{2+}$  concentration may lead to calcium-induced calcium release from the ryanodine receptor, RyR, channel of the sarcoplasmic reticulum, causing a larger  $\text{Ca}^{2+}$  release and propagation of calcium wave (Karaki *et al.*, 1997). Normally, RyR is closed at low cytosolic  $\text{Ca}^{2+}$  concentration (100–200 nM). However, when cytosolic  $[\text{Ca}^{2+}]$  is between sub-micromolar to 10  $\mu\text{M}$ ,  $\text{Ca}^{2+}$  ions can bind to RyR, which increases the open probability ( $P_o$ ) of the channel to release  $\text{Ca}^{2+}$ . Elevated cytosolic  $\text{Ca}^{2+}$  beyond this point leads to negative feedback and reduction in  $P_o$  (Bezprozvanny *et al.* 1993).

In the smooth muscle cell,  $\text{Ca}^{2+}$  binds to calmodulin to form the  $\text{Ca}^{2+}$ -calmodulin complex, which then binds to and activates myosin light-chain kinase (MLCK). The activated MLCK then catalyses the phosphorylation of myosin light chain (MLC20). Phosphorylated MLC20 activates myosin ATPase to trigger cycling of the myosin heads

(cross-bridges) along the actin filaments, ultimately resulting in smooth muscle contraction (Andersson, 2011). Conversely, a decrease in sarcoplasmic  $\text{Ca}^{2+}$  induces dissociation of the  $\text{Ca}^{2+}$ -calmodulin MLCK complex, resulting in dephosphorylation of the MLC20 by myosin light chain phosphatase (MLCP) and in smooth muscle relaxation (Andersson, 2011).

Smooth-muscle myosin comprises a pair of myosin heavy chains and two pairs of myosin light chains (MLC17 and MLC20) that are closely interlaced (Andersson, 2011). It has been shown that myosin heavy chain pre-mRNA is alternatively spliced to form: SM-A, which is more tonic [for example, aorta], and SM-B, which is more phasic [for example, urinary bladder] (DiSanto *et al.*, 1998). Intriguingly, DiSanto *et al.* (1998) have demonstrated that the CCSM possesses an overall myosin isoform composition intermediate between the bladder and aortic smooth muscle.

### **1.3.2 RhoA/Rho-kinase pathway**

DeFeo and Morgan (1985) have shown that besides intracellular  $[\text{Ca}^{2+}]_i$ , smooth muscle contraction is also regulated by a  $\text{Ca}^{2+}$ -sensitisation mechanism. They demonstrated that the  $\alpha$ -adrenergic agonist phenylephrine increased the contraction of ferret aorta strips. However, the contractions were associated with only a transient increase in intracellular  $[\text{Ca}^{2+}]_i$ , as the  $\text{Ca}^{2+}$  level declined quickly to near basal levels despite continued contractions. This disconnection between contraction and continued level of  $[\text{Ca}^{2+}]_i$  indicated the presence of a  $\text{Ca}^{2+}$ -sensitisation mechanism.

Since then, it has generally been accepted that calcium sensitisation depends on MLC20 phosphorylation-dependent mechanism (Andersson, 2011). Calcium sensitisation is brought on by agonist activation of G protein-coupled receptors, leading to the exchange of GTP for GDP on the small monomeric GTPase RhoA, catalysed by guanine exchange factor (Sopko *et al.*, 2014). Thus, RhoA-GTP dissociates from RhoA-GDP dissociation inhibitor (RhoGDI). This activates RhoA to bind to downstream targets and translocate to the membrane, where it binds to and causes autophosphorylation of Rho-kinase (ROCK), increasing its activity to phosphorylate MLCP (Sopko *et al.*, 2014). Phosphorylation of MLCP by Rho-kinase inhibits phosphatase activity, heightening the contractile response at a constant intracellular calcium concentration (Andersson, 2011).

ROCK-1 and ROCK-2 isoforms are differentially expressed throughout the body (Amano *et al.*, 2000). Interestingly, their involvement in erectile dysfunction varies according to the conditions. For example, ROCK-2 is upregulated in cavernosal-nerve-crush rat models, whereas ROCK-1 overexpression is prominent in diabetes-associated ED (Sopko *et al.*, 2014). Theoretically, the suppression of elevated RhoA/Rho-kinase activity presents an attractive target for treatment for ED. However, the RhoA/Rho-kinase pathway's abundant occurrence throughout the body limits the use of Rho-kinase inhibitors (Sopko *et al.*, 2014).

### 1.3.3 Physiological regulation of penile relaxation

CCSM relaxation is regulated via intracellular cyclic nucleotide/protein kinase messenger systems. Atrial natriuretic peptide stimulates particulate guanylate cyclase, whereas nitric oxide stimulates soluble guanylyl cyclase, both generating cyclic GMP (cGMP) to activate protein kinase G (PKG) and cGMP-dependent protein kinase I (Andersson, 2011). On the other hand, agonists activate membrane-bound adenylyl cyclase, generating cyclic AMP to activate protein kinase A (PKA). Activated PKA and cGMP-dependent protein kinase I then phosphorylate phospholamban. In the unphosphorylated state, phospholamban binds to and inhibits the sarcoplasmic reticulum  $\text{Ca}^{2+}$ -ATPase (SERCA) to reduce  $\text{Ca}^{2+}$  uptake (Masterson *et al.*, 2011). Thus, phosphorylated phospholamban is activated to increase  $\text{Ca}^{2+}$  uptake, resulting in smooth muscle relaxation. Furthermore, the protein kinases phosphorylate and thus inactivate voltage-gated  $\text{Ca}^{2+}$  channels, leading to a decreased sarcoplasmic concentration and, subsequently, relaxation (Berridge, 2008). Through phosphorylation, PKG may also elicit CCSM relaxation by other mechanisms including activating large-conductance  $\text{Ca}^{2+}$ -activated  $\text{K}^+$  (BK) channels (hence causing membrane hyperpolarisation and closing of L-type  $\text{Ca}^{2+}$  channels), inhibiting the RhoA/Rho-kinase pathway, and inhibiting the  $\text{IP}_3$  receptor to slow down  $\text{IP}_3$ -mediated release of calcium and the cytosolic oscillator (Berridge, 2008).

A study from Hashitani *et al.* (2002) suggested that reduced  $\text{Ca}^{2+}$  sensitivity may be the primary mechanism of nitric oxide-induced relaxation in CCSM. In noradrenaline pre-contracted guinea pig CCSM, they found that nitric oxide donor SIN-1 inhibited 80% of the contraction and 20% of the intracellular calcium. Inversely, L-type  $\text{Ca}^{2+}$  channel

blocker nifedipine inhibited intracellular  $\text{Ca}^{2+}$  by 80%, whereas the contraction level was inhibited by only 20%.

## **1.4 Erectile dysfunction**

Erectile dysfunction (ED) is characterised by the inability to reach or maintain a penile erection sufficient for sexual activity (NIH Consensus Conference, 1993). It is estimated that more than 150 million men worldwide are affected by ED (Costa *et al.*, 2006). However, this number may be significantly underestimated due to the social stigma attached to the condition.

### **1.4.1 Contributing factors to ED**

The origin of ED can be psychogenic [e.g. performance anxiety or depression], neurologic [e.g. cerebral trauma or spinal cord injury], endocrinologic [e.g. hyperprolactinemia inhibiting central dopaminergic activity], vasculogenic [e.g. atherosclerosis, hypertension, Type II diabetes, and Peyronie's disease], or caused by other systemic diseases [e.g. chronic renal failure and coronary heart disease] and old age (Lue, 2000). It may also be a side effect of pharmacological agents. For example, certain antidepressants, or nicotine from smoking, may inhibit the autonomic nervous system and consequently inhibit normal sexual function (Higgins *et al.*, 2010).

Cardiovascular risk factors and vascular abnormalities are highly prevalent in modern ED cases (Prieto, 2008). In fact, vasculogenic ED was found to account for approximately 75% of ED patients (NIH Consensus Conference, 1993). The underlying causes for vasculogenic ED include but are not limited to: endothelial dysfunction, nitric oxide synthase dysfunction or reduced nitric oxide bioavailability, impaired vasodilatory signalling, smooth muscle cell hypercontractility, veno-occlusive disorder, and changes to the tunica albuginea or corporal elastic fibres (Andersson, 2011; Costa *et al.*, 2006; Lue 2000).

## 1.4.2 Treating ED

A large selection of drugs has been recommended for the treatment of ED. The various options have been extensively studied, majorly advancing our understanding of drug pharmacology and erectile mechanism in the last decade (Andersson, 2011). Current options include drugs for non-intracavernosal administration [e.g. oral treatment by sildenafil], drugs for intracavernosal administration [e.g. injection of PGE<sub>1</sub>], vacuum constriction devices, and finally, prosthesis implantation when all other ED treatment options fail (McMahon, 2014).

Phosphodiesterase 5 (PDE-5) inhibitors such as sildenafil (Viagra<sup>TM</sup>), reduce the breakdown of cGMP and have had a tremendous impact on the treatment of ED, but they are not always effective (Andersson, 2011). Indeed, approximately 30–40% of ED patients with diabetes are resistant to such drugs (De Tejada, 2004). In addition, decreased nitric oxide synthase activity or impaired nitric oxide release may cause insufficient cGMP formation, thus limiting the action of PDE-5 (De Tejada, 2004). Furthermore, 60 to 70% of patients who begin treatment with PDE-5 inhibitors stop the treatment after 2 to 3 years due to unwanted side effects (Corona *et al.*, 2011; Chen *et al.*, 2015). Therefore, there is an unmet medical need to develop new treatments for ED.

The significance of CCSM in sexual function is highlighted by the fact that ED is mostly caused by the inability of CCSM to relax (Steers, 2002). This could be due to either nerve damage, endothelial dysfunction, or alterations in receptors or signal transduction pathways in CCSM. Ultimately, contractile state of the penile smooth muscle depends on the concentration of intracellular Ca<sup>2+</sup> (Andersson, 2001). Elevated levels of intracellular Ca<sup>2+</sup> induce myosin light chain phosphorylation and subsequently smooth muscle contraction. Importantly, the balance of intracellular Ca<sup>2+</sup> concentration is regulated by ion channels and intracellular mediators. In the present study, we discovered, for the first time, the presence of voltage-gated sodium channels channels in mouse CCSM and confirmed that the mouse also has Ca<sup>2+</sup>-activated Cl<sup>-</sup> channels (TMEM16A). Our findings suggest that these ion channels could contribute to the mechanisms of detumescence and potentially serve as a clinically relevant target for pharmaceutical intervention for ED.

## **1.5 Electrophysiology**

Electromyography recordings from CC tissue using extracellular electrodes show that they exhibit electrical waves (Shafik *et al.*, 2004; Wagner *et al.*, 1989). Indeed, electromyography can potentially diagnose different types of ED (Jiang *et al.*, 2005; Shafik *et al.*, 2004). As outlined by Christ (2000), activities of the CCSM are a synchronised network of events. Thus, the firing rate of the autonomic nervous system, myocyte excitability, signal transduction processes via gap junctions, and intercellular communication must be coordinated and integrated to ensure normal erectile function.

### **1.5.1 Ion channels in corpus cavernosum**

A variety of plasmalemmal ion channels that can alter membrane potential have been found in corpus cavernosum, including large-conductance  $\text{Ca}^{2+}$ -activated  $\text{K}^+$  ( $\text{BK}_{\text{Ca}}$ ) channels (Hannigan *et al.*, 2016; Werner *et al.* 2005), voltage-dependent  $\text{K}^+$  ( $\text{K}_{\text{V}}$ ) channels (Malysz *et al.*, 2002; Malysz *et al.*, 2001),  $\text{Ca}^{2+}$ -activated  $\text{Cl}^-$  channels (Hannigan *et al.*, 2017; Craven *et al.*, 2004), L- and T-type voltage-gated  $\text{Ca}^{2+}$  channels (McCloskey *et al.*, 2009; Höppner *et al.*, 1996), and P2X receptors (Doyle *et al.*, 2014).

### **1.5.2 $\text{K}^+$ channels**

Opening of potassium channels leads to the efflux of  $\text{K}^+$  from the cell, down the electrochemical gradient. The movement of positive charge out of the cell results in hyperpolarisation, thus inhibiting transmembrane  $\text{Ca}^{2+}$ -influx through voltage-dependent  $\text{Ca}^{2+}$  channels.

### **1.5.3 $\text{Ca}^{2+}$ -activated $\text{K}^+$ ( $\text{BK}_{\text{Ca}}$ ) channels**

$\text{BK}_{\text{Ca}}$  channels have large conductance (several hundred pS) and increased open probability in response to both increased cytosolic  $\text{Ca}^{2+}$  and membrane depolarisation

(Dudem, 2021). Four identical  $\alpha$ -subunits, encoded by the KCNMA1 (Slo1) gene, form the channel pore. Their gating kinetics and pharmacology are modulated by tissue-specific expression of regulatory  $\beta$  and  $\gamma$  subunits (Thornbury *et al.*, 2019).

Transcriptional and protein expressions of BK<sub>Ca</sub> channel have been detected in both freshly isolated human corporal tissues and cultured corporal smooth muscle cells (Andersson, 2011). Interestingly, this channel's activity in CCSM cells increased after cellular activation of either the cAMP pathway by 8-bromo-cAMP or PGE1 (Lee *et al.*, 1999) or the cGMP pathway by 8-bromo-cGMP (Wang *et al.*, 2000). However, in freshly isolated rabbit CCSM cells, attempts to activate inside-out patches with an alpha isoform of cGMP-dependent kinase I (PKG I $\alpha$ ) were in vain (Thornbury *et al.*, 2019). This was unexpected as BK<sub>Ca</sub> channels have phosphorylation sites for both PKG and PKA.

A study by Zhou *et al.* (2001) demonstrated the importance of BK channel  $\alpha$  subunit splice variants (BK<sub>A</sub>, BK<sub>B</sub>, and BK<sub>C</sub>) and their regulation by cyclic nucleotide-dependent protein kinases. They showed that the 3 isoforms have nearly identical single channel conductance, Ca<sup>2+</sup>-, voltage-, and iberiotoxin- sensitivity. However, cGMP kinase but not cAMP kinase shifted the voltage dependence of BK<sub>A</sub> and BK<sub>B</sub> to more negative potentials. On the other hand, BK<sub>C</sub> was exclusively stimulated by cAMP kinase. Given that the successful activation by PKA and PKG depends on the BK<sub>Ca</sub>  $\alpha$ -subunit splice variant, this may explain the variability in activation of the channel by PKG.

Werner *et al.* (2005) studied the functional role of BK<sub>Ca</sub> channels in the CC using a Slo gene knock-out (Slo(-/-)) mouse. In the presence of phenylephrine, the phasic contractions in Slo(-/-) mice CCSM strips quadrupled. Furthermore, EFS-induced relaxations of pre-contracted strips were reduced by half, both in strips from Slo(-/-) mice and by blocking BK channels with iberiotoxin in the Slo+/+ strips. As shown by *in vivo* intracavernosal pressure, significant oscillations were present in Slo(-/-) mice but absent in Slo+/+ mice. Additionally, EFS-induced rise in intracavernosal pressure was inhibited by 22% in Slo(-/-) mice. These authors asserted that BK channels are vital for erectile function, and showed that loss of BK channels causes impaired relaxation of the corpus cavernosum.

BK<sub>Ca</sub> channel openers such as NS11021, 4-aryl-3-(mercapto)quinolin-2-ones, and 3-thioquinolinones had been used to study the relaxation of the corpus cavernosum or penile arteries (Thornbury *et al.*, 2019). GoSlo-SR5-130, a novel BK<sub>Ca</sub> channel opener [developed by the Smooth Muscle Research Centre, DkIT], was used by Hannigan *et al.* (2016) to investigate its effects on BK<sub>Ca</sub> channels and tension in rabbit corpus cavernosum.

This compound activated channels in excised inside-out patches and inhibited spontaneous contractions, an effect that was reversed by iberiotoxin. However, as the expression of BK<sub>Ca</sub> channels is common in vascular and visceral smooth muscle and neurons (Thornbury *et al.*, 2019), targeted treatment for erectile dysfunction may be complex. Interestingly, the effects of GoSlo-SR-5-130 are dependent on the presence of regulatory  $\beta$ 1 or  $\beta$ 4 subunits. However, expression of  $\beta$  subunits did not affect the efficacy of GoSlo-SR-5-6, a similar compound (Large *et al.*, 2015). Thus, differential tissue expression of regulatory subunits may allow drugs to target specific tissues in the future.

#### 1.5.4 K<sub>V</sub> channels

When BK<sub>Ca</sub> channels are blocked or genetically deleted, corpus cavernosum myocytes still display considerable voltage-dependent outward currents (Werner *et al.*, 2005; Malysz *et al.*, 2001). Werner *et al.* (2005) found two components of a voltage-dependent K<sup>+</sup> current: one which had little time-dependent inactivation and was TEA-sensitive (delayed rectifier K<sub>V</sub> current), while the other was fast-activating, rapidly inactivating and TEA-resistant ('A-type current'). Individual cells expressed mainly either one or the other K<sub>V</sub> component, suggesting the presence of at least two different groups of mouse CCSM cells.

Malysz *et al.* (2001) also suggested the presence of two phenotypes in rabbit CC, based on the expression or non-expression of a delayed rectifier current in individual cells. In a follow-up study, Malysz *et al.* (2002) showed the transcriptional expression of K<sub>V</sub>2.2 in CCSM cells, and that this channel contributed to the delayed rectifier K<sub>V</sub> current, which was inhibited by 4-aminopyridine, and the K<sub>V</sub>2-selective blocker Hanatoxin-1, but not the K<sub>V</sub>1-selective blocker  $\alpha$ -dendrotoxin. Delayed rectifier K<sup>+</sup> channels are activated at approximately -50 to -40 mV (at resting membrane potential), thus contributing to the regulation of excitability (Malysz *et al.*, 2002).

Transcriptional expression of K<sub>V</sub>7.1 and K<sub>V</sub>7.3-7.5 channels and plasmalemmal expression of K<sub>V</sub>7.4 and K<sub>V</sub>7.5 were found in rat corpus cavernosum (Jepps *et al.*, 2016). K<sub>V</sub>7 activators, ML213 and BMS204352, relaxed pre-contracted corpus cavernosum and a K<sub>V</sub>7 channel blocker, linopirdine, reduced the effect of sildenafil and sodium nitroprusside (SNP). In CCSM of spontaneously hypertensive rats, the transcriptional

expression of all bar Kv7.1 was downregulated (Jepps *et al.*, 2016). The tissues were also less responsive to sildenafil and SNP (Jepps *et al.*, 2016).

These studies suggest that Kv channels play a role in erectile function and may contribute to erectile diseases.

### 1.5.5 Ca<sup>2+</sup>-activated Cl<sup>-</sup> channels

The presence of these currents in CC was confirmed based on their susceptibility to blockade by Ca<sup>2+</sup>-activated Cl<sup>-</sup> channel antagonists, their activation by intracellular Ca<sup>2+</sup>, and reversal potential change due to Cl<sup>-</sup> gradient in ion substitution experiments (Hannigan *et al.*, 2017; Craven *et al.*, 2004; Karkanis *et al.*, 2003). In 2008, the molecular identity of Ca<sup>2+</sup>-activated Cl<sup>-</sup> channels was determined to be TMEM16A, also known as ANO1 (Caputo *et al.*, 2008; Schroeder *et al.*, 2008; Yang *et al.*, 2008).

Due to high cytosolic Cl<sup>-</sup> concentration (32-44 mM) in smooth muscle cells, E<sub>Cl</sub> falls within -38 mV to -19 mV and is positive to the resting membrane potential, E<sub>m</sub> (Chipperfield and Harper, 2000). Hence, activating Cl<sup>-</sup> channels generate an inward current due to the efflux of Cl<sup>-</sup> ions. This depolarises the cell, which may be excitatory by opening L-type Ca<sup>2+</sup> channels (Thornbury *et al.*, 2019).

Freshly isolated rabbit, rat, and human CCSM cells exhibit spontaneous transient inward currents (STICs) due to the activation of Cl<sup>-</sup> currents by Ca<sup>2+</sup> spontaneously released from the sarcoplasmic reticulum (Craven *et al.*, 2004; Karkanis *et al.*, 2003). In rabbit CC, these are evidenced by blockade of STICs by cyclopiazonic acid (CPA), a SERCA pump inhibitor, and 2APB, suggesting that STICs are induced by Ca<sup>2+</sup> release from the sarcoplasmic reticulum, and are mediated by IP<sub>3</sub>R (Craven *et al.*, 2004). Craven *et al.* (2004) also found that this mechanism can be modulated via the NO-cGMP pathway. In rat CC, Williams and Sims (2007) showed that Ca<sup>2+</sup> sparks activate Ca<sup>2+</sup>-activated Cl<sup>-</sup> channels. Interestingly, Sergeant *et al.* (2009) revealed that oscillatory Ca<sup>2+</sup> waves in rabbit CC were associated with an inward current typical of the Ca<sup>2+</sup>-activated Cl<sup>-</sup> currents. The waves depended on the SERCA pump, both IP<sub>3</sub> receptors and ryanodine receptors, and could be modulated by cGMP (Sergeant *et al.*, 2009).

Few papers have studied the functional role of Ca<sup>2+</sup>-activated Cl<sup>-</sup> channels in CC. Karkanis *et al.* (2003) found that EFS-induced rise in pressure was enhanced and prolonged in the presence of chloride channel blockers, suggesting the contribution of Cl<sup>-</sup> current to the regulation of intracavernosal pressure. Kuo *et al.* (2009) and Chu and Adaikan (2008) also underlined the importance of chloride channels in regulating erectile activity and CC tone. In the rabbit CCSM, they showed that CaCC antagonists abolished spontaneous contractile activity and tone. The antagonists also reversed both neurogenic and agonist-induced contractions in the CC tissue.

### 1.5.6 L-and T-type Ca<sup>2+</sup> channel

Development of phasic contractions and phasic electrical activity in human, rabbit, and rat CC suggests that intracellular Ca<sup>2+</sup> levels are oscillatory (Hashitani *et al.*, 2005). This was confirmed by Sergeant *et al.* (2009), where oscillatory Ca<sup>2+</sup> waves trigger both phasic and tonic components of contraction, contributing to pacemaker-like activity. McCloskey *et al.* (2009) demonstrated the presence of both L-type and T-type Ca<sup>2+</sup> currents in freshly dispersed rabbit CCSM cells. They were able to separate the two components of Ca<sup>2+</sup> currents by their pharmacology: L-type Ca<sup>2+</sup> current was nifedipine-sensitive but mibefradil- and Ni<sup>2+</sup>-resistant, whereas T-type Ca<sup>2+</sup> current was Ni<sup>2+</sup>- or mibefradil-sensitive, but nifedipine-resistant. The two Ca<sup>2+</sup> currents also had different kinetics. T-type (transient) Ca<sup>2+</sup> channels activated and inactivated more rapidly than L-type Ca<sup>2+</sup> channels (McCloskey *et al.*, 2009; Perez-Reyes, 2003). They also activated and inactivated over more negative voltage ranges than L-type Ca<sup>2+</sup> current (McCloskey *et al.*, 2009; Perez-Reyes, 2003). Interestingly, the steady-state activation and inactivation curves of L-type Ca<sup>2+</sup> current intersected at around -30 mV, and overlapped from -45 to -10 mV, resulting in a small but sustained inward Ca<sup>2+</sup> (window) current (McCloskey *et al.*, 2009). Continuous Ca<sup>2+</sup> influx via window current might explain the maintenance of CC tone. Interestingly, the maximal Ca<sup>2+</sup> window current at -30 mV also corresponds to E<sub>Cl</sub> in smooth muscle (Thornbury *et al.*, 2019). Thus, activation of Ca<sup>2+</sup>-activated Cl<sup>-</sup> currents in CCSM cells would depolarise and clamp the membrane potential at the value where the maximal sustained Ca<sup>2+</sup> influx via L-type Ca<sup>2+</sup> channels is possible (Thornbury *et al.*, 2019).

### 1.5.7 P2X receptor-mediated cation current

Within smooth muscle tissues, sources of ATP release include nerves, endothelium/epithelium, smooth muscle cells, erythrocytes, platelets, and other cell types (Gordon, 1986). Depending on the animal species and basal tension of the tissue, it can either be excitatory or inhibitory (Wu *et al.*, 1993).

In the vas deferens and some blood vessels, ATP acts as an excitatory co-transmitter with noradrenaline, inducing contraction by activating P2X purinoceptors, which are a family of cation-permeable ligand-gated ion channels (Burnstock, 2018). In contrast, shear stress in arteries can induce the release of ATP from the endothelium, which feeds back onto the endothelial P2Y receptors, typically G-protein-coupled receptors, in this situation causing the release of nitric oxide and subsequent relaxation of arterial smooth muscle (Shalev *et al.*, 1999). ATP can also be rapidly metabolically broken down into adenosine diphosphate (ADP) and adenosine, the latter stimulating P1 purinoceptors to cause relaxation, which is seemingly distinct from the classic P2Y and P2X receptor subtypes (Burnstock, 2018). The combination of P2Y receptor-mediated endothelium-release of nitric oxide and adenosine activated P1 receptor-induced relaxation in CC have been found in a few studies (Phatarpekar *et al.*, 2010). However, ATP can also be excitatory.  $\alpha,\beta$ -methylene ATP, a P2X receptor agonist, caused contraction of human corpus cavernosum *in vitro*, while ATP itself causes contraction in the rabbit corpus cavernosum when resting tension was initially low (Wu *et al.*, 1993).

In freshly dispersed rabbit CCSM cells, Doyle *et al.* (2014) provided functional evidence that ATP induces an inward cationic current, partly carried by Na<sup>+</sup> ions. This current was blocked by desensitisation of P2X receptors to  $\alpha,\beta$ -methylene ATP, and by NF449, a P2X1 antagonist. Intriguingly, P2X receptors have been suggested to be pathologically involved in the development of erectile dysfunction in diabetes (Gur *et al.*, 2009). Gur *et al.* (2009) demonstrated abundant P2X1 receptors immunoreactivity in penile tissues from diabetic rats in comparison to control rats. They also showed that although P2X1 antagonist failed to rescue intracavernous pressure/mean arterial pressure values, it improved EFS-induced relaxation in isolated CCSM from diabetic rats.

Suadicani *et al.* (2009) found increased expression of the P2X1 receptor as erectile capacity decreased during the development of streptozotocin-induced diabetes. They also demonstrated a negative correlation between P2X1 expression and erectile capacity as normal healthy animals matured (Suadicani *et al.*, 2009).

### 1.5.8 STIM ORAI proteins

Although replenishment of intracellular  $\text{Ca}^{2+}$  stores has been associated with a range of  $\text{Ca}^{2+}$  influx pathways including through the L-type  $\text{Ca}^{2+}$  channels, the most recent consensus is that this process is mainly achieved by the interaction of STIM and Orai proteins (Emrich *et al.*, 2021; Giachini *et al.*, 2011). Stromal interaction molecules, STIM1 and STIM2 are single transmembrane proteins that are expressed on the ER and to a lesser extent on the plasma membrane. Their N-terminus EF-hand allows them to sense  $[\text{Ca}^{2+}]$  in intracellular store (Huang *et al.*, 2009). In response to a decrease in intracellular store  $[\text{Ca}^{2+}]$ ,  $\text{Ca}^{2+}$ -binding STIM proteins oligomerise to form discrete clusters that tether Orai proteins. This physical coupling activates Orai (Orai 1, 2, and 3) proteins, which are a highly conserved,  $\text{Ca}^{2+}$  selective pore-forming subunits, thereby promoting extracellular  $\text{Ca}^{2+}$  entry (Hill-Eubank *et al.*, 2011). This mechanism is termed store operated calcium entry (SOCE). Interestingly, Orai 1 and Orai 3 upregulation in human cavernosal tissues is related to ageing (Sevilleja-Ortiz *et al.*, 2020). In the same study, Orai inhibition was also shown to reverse hypercontractility of aged human penile smooth muscle, thus implicating their contribution to erectile function.

## 1.6 Review of voltage-gated sodium (Nav) channel

### 1.6.1 Nav channels in smooth muscles

Voltage-gated sodium channels are usually expressed in excitable cells such as cardiac smooth muscle cells, neurons, and skeletal cells. However, they have also been studied in cell types that are not considered to be electrically excitable, including differentiated myofibroblasts, metastatic cancer cells, macrophages, and vascular endothelial cells (Sun *et al.*, 2019; Chatelier *et al.*, 2012; Brackenbury, 2012; Andrikopoulos *et al.*, 2011).

Previously a rarity, Nav channels have been discovered in various smooth muscle cells over the years. They are largely found in phasic tissues, including the lymphatic, gastrointestinal tract, vas deferens, uterine, and portal vein (Neshatian *et al.*, 2015; Telinius *et al.*, 2015; Teramoto *et al.*, 2012; Seda *et al.*, 2007; Saleh *et al.*, 2005; Holm *et al.*, 2002; Hollywood *et al.*, 1997; Sperelakis *et al.*, 1992). They have also been found in smooth muscle cells generally thought to be non-spontaneously active, such as the airway (Matthews *et al.*, 2022; Bradley *et al.*, 2013) and the pulmonary arteries (Okabe *et al.*, 1988).

Aside from being involved in the initiation and/or propagation of spontaneous electrical activity, the expression of Nav channels in smooth muscle has also been implicated in pathological conditions. In the rabbit, Nav1.7 channels are prominently expressed in balloon-injured aorta, but not in normal aorta (Meguro *et al.*, 2009). Conversely, in healthy vascular tissues, for example in the mouse portal vein, Nav channels are not involved in myogenic rhythmicity, but they contribute to veratridine-induced contractions via reverse mode Na<sup>+</sup>-Ca<sup>2+</sup> exchange pathway (Saleh *et al.*, 2005). In other phasic tissue types, TTX-sensitive Nav channels mediate myometrial rhythmic contractions in non-pregnant rat (Seda *et al.*, 2007). Interestingly, there appears to be species differences regarding the contribution of Nav channels in generating action potentials. For example, Hollywood *et al.* (1997) successfully demonstrated the presence of TTX-sensitive Nav currents in isolated sheep lymphatic SMCs, and the contribution of Nav channels to spontaneous lymphatic tissue contractions. On the other hand, TTX failed to inhibit spontaneous activity in isolated guinea-pig lymphatics (Van Helden, 1993), suggesting variable Nav channel contribution.

As mentioned before, the corpus cavernosum is a phasic tissue known to exhibit coordinated contraction and synchronised relaxation. The presence of gap junction connexin-43 found in the human corpus cavernosum (De Carvalho *et al.*, 1993) may induce electrical coupling between cells, effectively rendering it to function as a syncytium. Synchronised excitability and conduction of these electrical responses might be important in detumescence, but little is known about the underlying mechanism. Although they have never been investigated in corpus cavernosum, Nav channels could play a part in coordinating contractions in the corpus cavernosum. As a major part of the experimental work presented in this thesis will be to explore the role of Nav channels, their structure and function will now be reviewed in detail.

### **1.6.2 Structure of Nav channels**

Voltage-gated sodium (Nav) channels play a pivotal role in the initiation and propagation of action potentials in neurons, cardiac muscle and skeletal muscle. They are a membrane-embedded, multiprotein complex, typically consist of a pore-forming  $\alpha$  subunit associated with one or more  $\beta$  subunits (Catterall, 2000). The subunits fall into different molecular weight ranges:  $\alpha$  subunits are approximately 240-260 kDa while  $\beta$  subunits are approximately 30.4-45 kDa (Isom *et al.*, 1995). Functionally, the  $\alpha$  subunits can facilitate conductance by themselves, but  $\beta$  subunits can modulate their gating.

In mammals, ten  $\alpha$  subunit genes encoding the channels Nav1.1 to Nav1.9, and an atypical protein, Nav<sub>x</sub>, have been identified (Namadurai *et al.*, 2015). The expression of  $\alpha$  subunit isoforms is tissue specific. According to Waxman (2012), they exhibit different gating kinetics, which may interact with each other and with the currents produced by other channels, effectively tailoring them for distinct physiological roles.

The  $\alpha$  subunits of Nav channels are composed of the following three parts: four highly homologous but non-identical transmembrane domains (D1- D4, with amino acid homology >75%); three intracellular loops (2 long loops, L1 and L2, and 1 short loop, L3); and the N-terminus and C-terminus (Figure 1.5). The four transmembrane domains each contain six transmembrane helical segments (S1–S6) and short membrane-associated segments (SS1/SS2), also known as the re-entrant loops or P loops (Ahern, 2013). The channel pore is formed by the S5 and S6 segments and the re-entrant loops,

where the inner narrowest part is lined with residues Asp, Glu, Lys, and Ala (DEKA) to function as the selectivity filter (Cestèle *et al.*, 1998; Terlau *et al.*, 1991; Noda *et al.*, 1989).

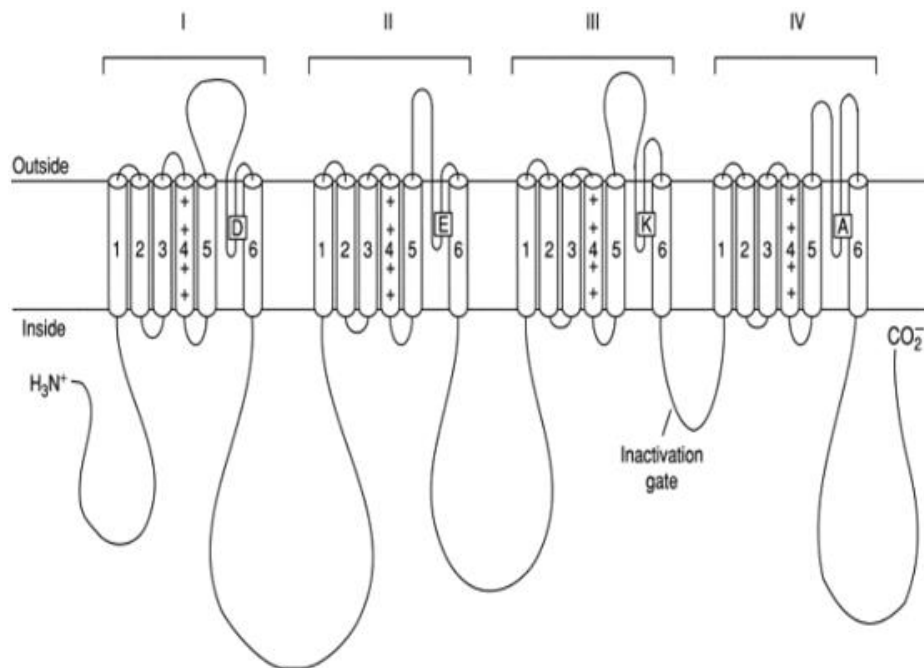


**Figure 1.5: Structure of  $\alpha$  subunit of Nav channel (Soderlund *et al.*, 2010).**

The chemistry of  $Na^+$  selectivity and conductance is opposite to that of  $K^+$ . Negatively charged residues interact with  $Na^+$  to remove most (but not all) of its waters of hydration, and  $Na^+$  is conducted as a hydrated ion interacting with the pore through its inner shell of bound water molecules (Catterall, 2014). Interestingly, several high-resolution studies have described the C-terminal portion of mammalian Nav channels to exhibit an EF-hand domain after the S6 segment, followed by an IQ-motif (Gardill *et al.*, 2018). The EF-hand domain and the IQ motif are interaction sites for intracellular modulatory proteins.

To date, five mammalian  $\beta$  subunits have been discovered:  $\beta 1$ ,  $\beta 1$ 's alternative splice variant  $\beta 1B$ ,  $\beta 2$ ,  $\beta 3$ , and  $\beta 4$  (Brackenbury and Isom, 2011). They are encoded by four genes: SCN1B–SCN4B. All of them are type I topology transmembrane proteins, except for  $\beta 1B$ . Furthermore,  $\beta 1$ ,  $\beta 2$ ,  $\beta 3$ , and  $\beta 4$  have an intracellular C-terminal domain, transmembrane domain, and an extracellular N-terminal immunoglobulin (Ig) loop. While  $\beta 1B$  also contains an Ig loop, it lacks the transmembrane domain and is thus a secreted and soluble protein (Patino *et al.*, 2011).  $\beta 1$  and  $\beta 3$  subunits have an amino acid sequence similarity of 45%, and they are non-covalently linked to Nav  $\alpha$  subunits. On the

other hand,  $\beta 2$  and  $\beta 4$  subunits have amino acid sequence similarity of 35%, and they associate with Nav  $\alpha$  subunits by disulphide bonds (Yu *et al.*, 2003; Isom *et al.*, 1995; 1992).

Nav  $\beta$  subunits are multifunctional. They are typically N-linked glycosylated members of the immunoglobulin superfamily known to regulate cell adhesion, cell migration and also serve as the substrate for sequential proteolytic cleavage by secretases (Chopra *et al.*, 2007). In addition, Nav  $\beta$  subunits have been found to promote channel trafficking to the cell membrane. For instance, hippocampal neurons from  $\beta 2$  null mice show approximately halved sodium current density and reduced number of  $\alpha$  subunits at the plasma membrane (Chen *et al.*, 2002).

Another feature of the Nav  $\beta$  subunits is that functional interaction between  $\alpha$  and  $\beta$  subunits regulates cellular excitability. They alter gating, voltage-dependence, and kinetics of Nav  $\alpha$  subunits. For example, co-expression of the  $\beta 1$  subunit with  $\alpha$  subunit of Nav1.2 increases peak sodium current, accelerates its inactivation, and shifts the voltage dependence of inactivation to more negative membrane potentials (Isom *et al.*, 1992). A hyperpolarising shift of voltage-dependence of inactivation is also evident in  $\beta 1$  interactions with skeletal muscle, cardiac, or neuronal  $\alpha$  subunits (Goldfarb, 2012). Interestingly, the  $\beta 4$  subunit is found to antagonise fast inactivation (Bant and Raman, 2010). It is a transmembrane protein that blocks open Nav channels and unblocks upon repolarisation, thereby mediating resurgent current (Bant and Raman, 2010). Nav channel block and resurgent current have been the most extensively studied for Nav 1.6 in neurons, but they have also been demonstrated in Nav1.1, Nav1.5, and Nav1.7 (Goldfarb, 2012).

### **1.6.3 Biophysical properties of Nav channels**

During an action potential, Nav channels first activate, opening the channels to facilitate conductance, driving the upstroke of the action potential, and then inactivate, along with activation of delayed rectifier  $K^+$  channels, promoting repolarisation to the resting potential. Both activation and inactivation gates must be open for the current to pass through.

After depolarisation, Nav channels activate in a few steps to an open state, followed by inactivation. Previous work has shown that only the activation gate is voltage-sensitive (Bezanilla and Armstrong, 1977; Armstrong and Bezanilla, 1977). Inactivation is a steeply voltage-dependent process that helps terminate all-or-none depolarisation and action potential. Kinetics of inactivation, as for activation, is accelerated by depolarisation, again indicative of strong voltage-dependence. According to Armstrong (2006) and Horn *et al.* (1981), channel inactivation occurs when the activation gate is open (open-state inactivation), but can also occur before the channel reaches the conducting state (closed-state inactivation).

At the resting potential, the favourable state of Nav channels is fully deactivated. After depolarisation, a few sequential steps are required to move the activation gate from a fully deactivated state through the partially activated states to the completely activated state. Each step is voltage-dependent and will generate gating current from the movement of charges in the transmembrane helices of Nav channels (Horn *et al.*, 2000). Conversely, inactivation following activation is voltage-independent, generating no gating current.

Upon repolarisation, the channel recovers from inactivation. Deactivation of the channel precedes the recovery of the channel. While the inactivation gate remains closed, the activation gate is closed in this step, generating a gating current from its movement. This is important functionally since recovery occurs at negative voltages, where sodium influx through any conducting channels would be large (Armstrong 2006). Failure of the Nav channels to proceed as normal at any of the activated, inactivated, or deactivated stages may lead to diseases, termed channelopathies.

### 1.6.3.1 Activation

Certain properties of the Nav channel domains are detailed in Table 1.2, where coupling between activation and inactivation has been taken into account.

Domain	1	2	3	4
Positive residues in S4 (Yang <i>et al.</i> , 1996)	4	5	6	8
Kinetics	Fast	Fast	Fast	Slow

(Chanda and Bezanilla, 2002)				
Immobilised by inactivation (Chanda and Bezanilla, 2002; Horn <i>et al.</i> , 2000; Cha <i>et al.</i> 1999)	No	No	Yes	Yes

**Table 1.2: Properties of Nav channel domains.**

The S4 transmembrane segments contain several positively charged arginine or lysine residues (Table 1.2) at every third position, with non-polar residues intervening between the basic residues (Stühmer *et al.*, 1989; Noda, 1984). Nav channels are activated when the electric field changes, caused by membrane depolarisation, to move S4 segments toward the extracellular face of the membrane, thus initiating conformational changes that open the pore (Namadurai *et al.*, 2015).

Even though the voltage sensors in all four domains contribute to the voltage-sensing process, the outward movement of the S4 segments is sequential. For D1—D3, S4 segments activate rapidly in a process that so far cannot be kinetically distinguished from a single step (Armstrong, 2006). Following this is a slow movement (Table 1.2) via activation of S4/D4 to step one of a two-step process, as suggested by Horn *et al.* (2000), which would then open the channel to allow conductance. The opening of the activation gate only requires S4 segment activation in D1, D2, D3, and partial activation of S4/D4 (Armstrong 2006). It should be noted that subsequent full activation of S4/D4 will then inactivate the channel.

Prediction from models of voltage sensor function has revealed the structural basis for S4 gating charge movement in Nav. Based on the modelling of the voltage-sensing domain of the bacterial sodium channel NaChBac, Yarov-Yarovoy *et al.* (2012) believe that the S4 segment slides 6-8 Å outward through a narrow groove formed by the S1, S2, and S3 segments, rotates ~ 30°, and tilts sideways at a pivot point formed by a highly conserved hydrophobic region near the centre of the voltage sensor. Also, S4 has a 3<sub>10</sub>-helical conformation, which is believed to interact with the narrow inner gating pore, allowing linear movement of gating charges across the inner one-half of the membrane. They also proposed that a conformational change of S4 due to the combination of outward, rotating,

and tilting motions imposes a lateral movement (3–5 Å) of the S4-S5 linker, which could induce the movement of S5 and S6 segments, opening the intracellular gate of the pore to conduct sodium ions.

### 1.6.3.2 Inactivation

Inactivation follows activation by either occlusion or rearrangement of the channel pore. There are several types of inactivation (Table 1.3).

Inactivation type	Inactivation time constant
Fast open-state	1-2 milliseconds (Groome <i>et al.</i> , 2011)
Fast closed-state	1-2 milliseconds (Groome <i>et al.</i> , 2011)
Intermediate	A few hundred milliseconds (Wagner <i>et al.</i> , 2006)
Slow	Hundreds of milliseconds to seconds (Catterall, 2014)
Ultra-slow	Hundreds of seconds (Hilber <i>et al.</i> , 2002)

**Table 1.3: Types of inactivation and their time constant.**

However, only fast inactivation and slow inactivation will be discussed below.

### 1.6.3.3 Fast inactivation

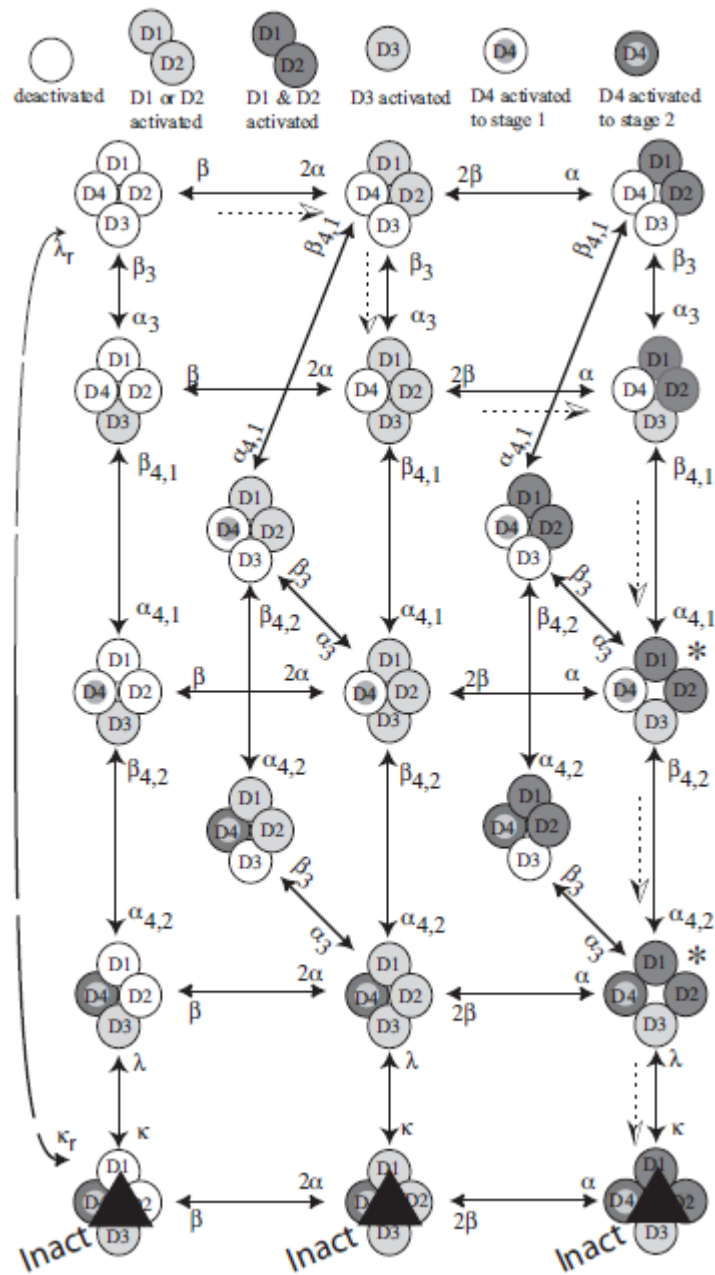
Fast inactivation can only proceed if S4 segments in D3 and D4 are activated to completion (as mentioned above, activation of S4/D4 is a two-step process), exhibiting coupling of activation to inactivation (Ji *et al.*, 1996; Rogers *et al.*, 1996). In addition, a cluster of three hydrophobic residues: isoleucine-phenylalanine-methionine (known as IFM motif), has been found in the loop connecting S6 of domain 3 and S1 of domain 4 (Abriel and Kass, 2005). These hydrophobic triplet residues (IFM) are believed to occlude the open pore during fast inactivation.

Fast inactivation generally occurs when the activation gate is open, termed fast open-state inactivation. However, it can also occur before the channel reaches the conducting state, termed fast closed-state inactivation. Armstrong (2006) suggests that small depolarisations extend the occupancy of channels in a partially activated state. Thus, few channels are open, and the majority of inactivation occurs via closed-state inactivation. In contrast, large depolarisations drive the S4s outward rapidly to minimise the period of closed-state occupancy, making closed-state inactivation small and open-state inactivation large. The same study also detailed the most likely kinetic pathway for closed-state inactivation and open-state inactivation to occur. Open-state inactivation likely takes place via the activation of S4 segments in all domains. Contrastingly, in closed-state inactivation, activation of S4 segments in D1 and D2 is not needed, they remain deactivated to shut the activation gate, but inactivation can still occur. Therefore, it is likely that only the activation of S4/D3 and full activation of S4/D4 are needed for closed-state inactivation (Armstrong, 2006).

The first event on repolarisation after open-state inactivation is the inward movement of the S4s of D1 and D2, which generates the gating current to shut the activation gate, and to functionally prevent leak during recovery (As noted in Table 1.2, S4s of D1 and D2 are not immobilised from inactivation). Then, the deactivation of S4s in D3 and D4 occurs slowly to generate a slow gating current that parallels recovery from inactivation (Armstrong and Gilly, 1979; Armstrong and Bezanilla, 1977). This allows the channel to recover without passing through the open conducting state.

Since S4/D3 and S4/D4 are involved in both open-state and closed-state fast inactivation, and only these 2 segments are immobilised from fast inactivation (Table 1.2), the charge immobilised during both states of fast inactivation should be similar, which aligns with the findings from Groome *et al.* (2011). It was discovered that the extent of charge immobilised from closed-state inactivation approximated that observed during open-state fast inactivation (Groome *et al.*, 2011). Armstrong (2006) also suggested that the inward movement of S4/D4 will displace the inactivation particle from its blocking position. In the absence of this push to dislocate the inactivation particle, recovery would have to happen from the spontaneous dissociation of the particle, making it very slow.

Kinetic schemes showing the probable paths for Nav channels activation and different modes of inactivation are detailed below in Flowchart1.



**Flow chart 1: Kinetic schemes for activation and inactivation (Armstrong, 2006).** A horizontal step represents activation (rightward movement) or deactivation (leftward movement) of D1 or D2, which are kinetically indistinguishable. A vertical step represents activation or deactivation of D3, first-stage activation of D4, second-stage activation of D4, or closing of the inactivation gate. The dotted arrows indicate the most probable path from fully deactivated (upper left corner) to inactivated at 0 mV. Conducting states are marked with asterisks. Full paper can be accessed at DOI: 10.1073/pnas.0607603103

#### 1.6.3.4 Slow inactivation

Slow inactivation is a process distinct from fast inactivation. It reduces the availability of channels after a prolonged depolarising pulse or high-frequency stimulation. Mutational work that alters slow inactivation is targeted throughout the Nav channels. For example, based on permeant ions, toxins, and pore blockers, the selectivity filter has been implicated in mediating slow inactivation, akin to the C-type inactivation in potassium channels (Capes *et al.*, 2012; Szendroedi *et al.*, 2007; Balsler *et al.*, 1996). On the other hand, mutations in other parts of the protein, for instance in the voltage-sensing domain, the S4-S5 loop, and the S6 C-terminal end, also modulates slow inactivation (Lenaeus *et al.*, 2017; Silva and Goldstein, 2013; Capes *et al.*, 2012; Chen *et al.*, 2006; Kontis and Goldin, 1997). However, the consensus on slow inactivation involves rearranging the channel pore (Catterall, 2014; Savio Galimberti *et al.*, 2012; Goldin, 2003). In fact, by studying prokaryotic Nav channels, Chatterjee *et al.* (2018) discovered profound conformational flexibility of the pore in the slow-inactivated state, which may lead to an extensive conformational change in the selectivity filter region. The movement of pore helices also changes the volume of both the central and inter-subunit cavities, forming pathways for lipophilic drugs that modulate slow inactivation (Chatterjee *et al.*, 2018).

#### 1.6.4 Channelopathies

As mentioned above, abnormal Nav channel activity can lead to various diseases - channelopathies. Abnormal Nav channel activities are often a result of spontaneous or inherited mutations, leading to hypo- or hyper-excitable phenotypes. Hypo- and hyper-excitable phenotypes are related to loss-of-function defects and gain-of-function defects, respectively (Cannon, 2011). Hypo-excitable phenotypes can be caused by deficient or defective Nav channel expression, leading to sodium current loss and reduced excitability (Ahern *et al.*, 2016). On the other hand, hyper-excitable phenotypes can be caused by defective channel inactivation, or in rare cases, enhancement of activation, leading to excessive sodium current, resulting in prolonged or unstable depolarisation (Ahern *et al.*, 2016). In fact, more than 1,000 mutations in neuronal Nav channels are associated with an array of epilepsy syndromes (Claes *et al.*, 2009). Nav channelopathies associated with

the central nervous system, heart, skeletal muscle, and peripheral nervous system, including pain, myopathy, and cancer, are detailed in Table 1.4. It should be noted that the list in Table 1.4 is not exhaustive.

Nav isoforms	Channelopathies
1.1	<p>Genetic epilepsy with febrile seizures plus [GEFS+] (Escayg and Goldin, 2010)</p> <p>Dravet syndrome (DS) [Severe myoclonic epilepsy of infancy (SMEI)] (Escayg and Goldin, 2010)</p> <p>Myoclonic astatic epilepsy [MAE/Doose syndrome] (Yordanova <i>et al.</i>, 2011)</p> <p>Lennox-Gastaut Syndrome (Selmer <i>et al.</i>, 2009)</p> <p>Familial autism (Weiss <i>et al.</i>, 2003)</p> <p>Familial hemiplegic migraine (Castro <i>et al.</i>, 2009)</p> <p>Rasmussen encephalitis (Ohmori <i>et al.</i>, 2008)</p> <p>Ovarian cancer (Brackenbury, 2012)</p>
1.2	<p>Febrile seizures and epilepsies (Sugawara <i>et al.</i>, 2001)</p> <p>Dravet syndrome (DS) [Severe myoclonic epilepsy of infancy (SMEI)] (Lossin <i>et al.</i>, 2012)</p> <p>Cervical cancer, mesothelioma cancer, ovarian cancer, prostate cancer (Brackenbury, 2012)</p>
1.3	<p>Cryptogenic pediatric partial epilepsy (Holland <i>et al.</i>, 2008)</p> <p>A potential contributor to neuropathic pain following spinal cord injury (Hains <i>et al.</i>, 2003)</p> <p>Ovarian cancer, prostate cancer, small cell lung cancer (Brackenbury, 2012)</p>

1.4	<p>Hypokalaemic periodic paralysis (Struyk <i>et al.</i>, 2008)</p> <p>Hyperkalemic periodic paralysis (Cannon, 2011)</p> <p>Myotonia (Cannon, 2011)</p> <p>Malignant hyperthermia susceptibility (Moslehi <i>et al.</i>, 1998)</p> <p>Congenital myasthenic syndrome (Habbout <i>et al.</i>, 2016)</p> <p>Sudden infant death syndrome (Männikkö <i>et al.</i>, 2018)</p> <p>Cervical cancer, ovarian cancer, prostate cancer (Brackenbury, 2012)</p>
1.5	<p>Long QT syndrome (Wang <i>et al.</i>, 1995)</p> <p>Idiopathic ventricular fibrillation [Brugada syndrome] (Chen <i>et al.</i>, 1998)</p> <p>Atrial Standstill (Groenewegen <i>et al.</i>, 2003)</p> <p>Congenital sick sinus syndrome (Benson <i>et al.</i>, 2003)</p> <p>Sudden infant death syndrome (Plant <i>et al.</i>, 2006)</p> <p>Dilated cardiomyopathy (Moreau <i>et al.</i>, 2015)</p> <p>Arrhythmia (Moreau <i>et al.</i>, 2015)</p> <p>Breast cancer, colon cancer, lymphoma, neuroblastoma, non-small cell lung cancer, prostate cancer, small cell lung cancer (Brackenbury, 2012)</p>
1.6	<p>Epileptic encephalopathy (O'Brien and Meisler, 2013)</p> <p>Intellectual disability (O'Brien and Meisler, 2013)</p> <p>Breast cancer, cervical cancer, lymphoma, melanoma, mesothelioma, non-small cell lung cancer, prostate, small cell lung cancer (Brackenbury, 2012)</p>
1.7	<p>Hereditary primary erythromelalgia (Dib-Hajj <i>et al.</i>, 2005)</p> <p>Paroxysmal extreme pain disorder (Drenth and Waxman, 2007)</p> <p>Congenital insensitivity to pain [CIP] (Drenth and Waxman, 2007)</p> <p>Paroxysmal itch (Devigili <i>et al.</i>, 2014)</p> <p>Anosmia (Weiss <i>et al.</i>, 2011)</p>

	Breast cancer, cervical cancer, lymphoma, mesothelioma, non-small cell lung cancer, ovarian cancer, prostate cancer (Brackenbury, 2012)
1.8	Upregulated in inflammatory and pain model (Jarvis <i>et al.</i> , 2007) Cerebellar dysfunction in multiple sclerosis (Shields <i>et al.</i> , 2012)
1.9	Familial episodic pain syndrome (Okuda <i>et al.</i> , 2016) Lymphoma, small-cell lung cancer (Brackenbury, 2012)

**Table 1.4: Nav isoforms and their associated channelopathies.**

Due to the central role of Nav channels in normal physiology and pathophysiology, the development of selective pharmacological Nav channel modulators is of utmost interest to the scientific and medical community.

### 1.6.5 Pharmacology of Nav channels

Nav channels can be targeted with many toxins. They bind to specific receptor sites to alter channel function, posing as effective tools to study the structure and function of Nav channels by affecting both permeation and gating properties (Cestèle and Catterall, 2000). In fact, pharmacological studies have separated Nav channels into two groups based on their sensitivity to a neurotoxin, tetrodotoxin (TTX).

1. TTX-sensitive channels can be inhibited by TTX in the nanomolar concentration range. These include Nav1.1, Nav1.2, Nav1.3, Nav1.4, Nav1.6, and Nav1.7 isoforms (Catterall *et al.*, 2005).

2. TTX-resistant channels can be inhibited by TTX in the micromolar to millimolar concentration range. These include Nav1.5, Nav1.8, and Nav1.9 isoforms (Catterall *et al.*, 2005).

Interestingly, TTX-sensitive and TTX-resistant Nav channels have different biophysical and pharmacological properties. Commonly, TTX-resistant Nav channels exhibit smaller single-channel conductance and slower kinetics (Yoshida, 1994; Weiss and Horn, 1986).

Most sodium channel antagonists have increased affinity for channels in the activated or inactivated state, and reduced affinity for channels in the resting state (Savio Galimberti, 2012). Thus, the drug binds to Nav channels to block them during depolarisation, and then dissociates from it during repolarisation to unblock the channels.

Dissociation rate is critical in determining the steady-state block of Nav channels. The voltage, frequency, duration, and physicochemical properties of the drug will determine the rate of recovery from blockade. Savio Galimberti (2012) explained that as depolarisation frequency increases, the rest interval decreases to limit the time available for the drug to dissociate from the channels. Thus, the binding time of the drug to the channel increases to improve the steady-state block. In fact, for certain drugs with use-dependent block, a train of depolarisation pulses causes repetitive opening of the channel pore, which gives cumulative access for drugs to bind to the intracellular site of the channels (Hille 2001; 1977). On the other hand, state-dependent inhibition occurs when the pharmacological modulators bind to a channel when it is in a particular voltage-dependent conformational state. For example, certain anticonvulsants and antiarrhythmics function by binding to and stabilising an inactivated conformation of the channels (Karoly *et al.*, 2010).

In Table 1.5 below, some pharmacological modulators of Nav channels, including channel-specific agonists and antagonists that have been used in this project, are detailed. Some of them are well-established, whereas the others are more recently discovered. Their binding sites on the channels, as well as their functional effects, are also listed.

Toxin	Interaction Site	Voltage/frequency-dependent	Function
<p><math>\beta</math>-Scorpion toxin C<sub>ss</sub>IV</p>	<p>Extracellular loops of S3-S4/D2 (Cestèle <i>et al.</i>, 1998), S1-S2/D2, and SS2-S6/D3 (Zhang <i>et al.</i>, 2012)</p>	<p>Binds preferentially to activated channels (Cestèle <i>et al.</i>, 1998)</p>	<p>Non-selective Nav channel agonist</p> <p>Negatively shifts the voltage-dependence of activation (Cestèle <i>et al.</i>, 1998)</p> <p>Enhance fast closed-state inactivation (Cestèle <i>et al.</i>, 1998)</p>
<p>Tetrodotoxin (TTX)</p>	<p>The single amino acid Cys374 in Nav1.5 and the equivalent position Ser356 in Nav1.8 imparts TTX resistance (Triggle <i>et al.</i>, 2006)</p>	<p>Inhibition of TTX-insensitive channels has been found to be both voltage and frequency-dependent</p>	<p>Non-selective Nav channel antagonist</p> <p>Physically block the pore to prevent sodium conductance (Cestèle and Catterall, 2000)</p>

		(Carmeliet, 1987; Gonoj <i>et al.</i> , 1985)	
	Both TTX and STX also interact with Asp <sup>400</sup> , Glu <sup>755</sup> , and Lys <sup>1237</sup> residues of the selectivity filter (Noda <i>et al.</i> , 1989; Terlau <i>et al.</i> , 1991; Penzotti <i>et al.</i> , 1998)		
Saxitoxin (STX)	Interacts strongly with the more extracellular residues of the channel vestibule, Glu <sup>758</sup> and Asp <sup>1532</sup> , in comparison with TTX (Penzotti <i>et al.</i> , 1998)	Exhibits voltage-dependent block (French <i>et al.</i> , 1984)	Non-selective Nav channel antagonist  Physically block the pore to prevent sodium conductance (Cestèle and Catterall, 2000)
Veratridine	S6/D1 and S6/D4 (Catterall <i>et al.</i> , 2005; Cestèle and Catterall, 2000)	Binds preferentially to activated channels (Ulbricht, 2005)	Non-selective Nav channel agonist

			Slows inactivation and shifts activation to more negative potentials (Ulbricht, 2005; Denac 2000)
ICA-1211431	Ser <sup>1510</sup> , Arg <sup>1511</sup> , and Glu <sup>1559</sup> of S2 and S3 of D4 (McCormack <i>et al.</i> , 2013)	Binds preferentially to inactivated channels (McCormack <i>et al.</i> , 2013)	Selective inhibitor of Nav1.1 and Nav1.3 channels (McCormack <i>et al.</i> , 2013)
PF- 05089771	Voltage-sensor region of D4 (Alexandrou <i>et al.</i> , 2016)	Binds preferentially to half-inactivated channels (Alexandrou <i>et al.</i> , 2016)	Selective inhibitor of Nav1.7 channels (Alexandrou <i>et al.</i> , 2016)
A-803467	Phe <sup>1710</sup> of S6 segments (Browne <i>et al.</i> , 2009)	Binds preferentially to inactivated channels, although there is significant	Selective inhibitor of Nav1.8 channels (Jarvis <i>et al.</i> , 2007)

		<p>block at all holding potentials. (Jarvis <i>et al.</i>, 2007)</p> <p>Did not show significant frequency-dependent block (Jarvis <i>et al.</i>, 2007)</p>	
4,9 anhydroTTX	Unknown	<p>Tonic, state-independent block (Rosker <i>et al.</i>, 2007)</p>	<p>Selective inhibitor of Nav1.6 channels (Rosker <i>et al.</i>, 2007)</p> <p>Shifts steady-state inactivation to more negative potentials (Rosker <i>et al.</i>, 2007)</p>
OD1	Extracellular loops of DIV S3–S4 (Xu <i>et al.</i> , 2019).	Unknown	Inhibits fast inactivation of Nav1.7, Nav1.4, and Nav1.6 (De Lera Ruiz and Kraus, 2015).

			<p>Shifts Nav1.4 And Nav1.6 channel activation in the hyperpolarising direction (Durek <i>et al.</i>, 2013)</p> <p>Slow the inactivation process of Nav 1.5/b1 at micromolar concentrations (Jalali <i>et al.</i>, 2005)</p>
--	--	--	--

**Table 1.5: Pharmacological modulators of Nav channel.**

## **1.7 Review of Ca<sup>2+</sup>-activated Cl<sup>-</sup> (TMEM16A) channels**

### 1.7.1 Ca<sup>2+</sup>-activated Cl<sup>-</sup> channels

Ca<sup>2+</sup>-activated Cl<sup>-</sup> channels (CaCCs) play diverse roles in cellular physiology, including epithelial secretion, sensory transduction, smooth muscle contraction, cardiac and neuronal excitability, and nociception (Hartzell *et al.*, 2005). The direction of Cl<sup>-</sup> movement through CaCCs is dictated by membrane potential, and the Cl<sup>-</sup> concentration gradient. If the membrane potential is positive to E<sub>Cl</sub>, then the activation of CaCCs will cause Cl<sup>-</sup> influx, contributing towards repolarisation of the cell. On the other hand, if the membrane potential is negative to E<sub>Cl</sub>, then CaCC activation will cause Cl<sup>-</sup> efflux, contributing towards depolarisation of the cell. In some cells, this depolarisation increases the open probability of voltage gated Ca<sup>2+</sup> channels, which results in further depolarisation (Hartzell *et al.*, 2005). CaCCs were first described in *Xenopus* oocytes (Barish, 1983; Miledi, 1982) and salamander retinas (Bader *et al.*, 1982) in the early 1980's, however it was not until 28 years later that the proteins responsible for these channels were identified. In 2008, three independent teams of investigators used different strategies, yet reached the same conclusion simultaneously: Transmembrane protein 16A (TMEM16A) is a *bona fide* Ca<sup>2+</sup>-activated Cl<sup>-</sup> channel (Caputo *et al.*, 2008; Schroeder *et al.*, 2008; Yang *et al.*, 2008). The approaches they used include expression cloning and functional genomics, RNA silencing of TMEM16A gene expression, as well as heterologous expression of TMEM16A in null cell systems. The consistent results support the proposal that TMEM16A is a CaCC. Before this, several other candidates, including CLCA (Chloride Channel Calcium Activated), CLC-3 (a voltage-activated Cl<sup>-</sup> channel), Tweety, and Bestrophins had been proposed to be the molecular candidates for native CaCC. The evolution of this story, and the current evidence supporting TMEM16A, has been recently reviewed by Hawn *et al.* (2021).

### 1.7.2 Chloride accumulation in smooth muscle

Smooth muscle cells are known to possess a range of chloride accumulation mechanisms, leading to higher intracellular Cl<sup>-</sup> concentration and Cl<sup>-</sup> equilibrium potential (E<sub>Cl</sub>) within the range of -38 mV to -19 mV (Chipperfield and Harper, 2000; Aickin and Brading, 1982). The known mechanisms include chloride-bicarbonate exchange (Cl<sup>-</sup>/HCO<sub>3</sub><sup>-</sup>),

sodium-potassium-chloride ( $\text{Na}^+$ ,  $\text{K}^+$ ,  $\text{Cl}^-$ ) cotransport (NKCC), and another mechanism designated 'Pump III' by Chipperfield and Harper (2000).

The importance of  $\text{HCO}_3^-$  in intracellular  $\text{Cl}^-$  accumulation was demonstrated by Aickin and Brading (1984) in guinea pig vas deferens. They showed that the removal of  $\text{HCO}_3^-$  reversibly slowed the depletion of intracellular  $\text{Cl}^-$ , and that  $\text{Cl}^-/\text{HCO}_3^-$  was important in the regulation of intracellular pH. Importantly, the depletion and reuptake of  $\text{Cl}^-$  was slowed but not completely abolished (Aickin and Brading, 1984), suggesting the existence of more than one chloride accumulation pathway. In another tissue type, it was observed that furosemide impeded chloride exchange and resulted in a hyperpolarisation in rabbit aortic tissue (Kreye *et al.*, 1981). In 1990, Aickin and Brading provided evidence of the presence of the sodium-potassium-chloride cotransporter (NKCC) in guinea pig vas deferens smooth muscle. They showed marked inhibition of  $\text{Cl}^-$  accumulation with  $\text{Na}^+$ -free and  $\text{K}^+$ -free solutions, in the presence of the anion exchange blocker, DIDs, supporting NKCC as a contributor towards intracellular  $\text{Cl}^-$  accumulation.

Interestingly, Chipperfield *et al.* (1993) found that rat femoral artery had  $\text{Cl}^-$  accumulation unaccounted for by either NKCC or  $\text{Cl}^-/\text{HCO}_3^-$ -exchange. By manipulating  $[\text{Cl}]_i$  and using a pharmacological agent, they found that the additional mechanism, which they referred to as pump III, was sensitive to acetazolamide. Blockade of all three  $\text{Cl}^-$  transports brought the  $E_{\text{Cl}}$  in line with  $E_m$  (Chipperfield *et al.*, 1993). This is similar to findings from Davis *et al.* (1997) in rat arterial smooth muscle, where in addition to blockade of NKCC, application of ethacrynic acid and N-ethyl maleimide (a known inhibitor of a range of ATP-dependent transport processes), cause a fall in  $[\text{Cl}]_i$  to a value similar to the predicted passive equilibrium value in the absence of any active  $\text{Cl}^-$  accumulation mechanisms. This ATP-dependent  $\text{Cl}^-$  pump is known as pump III.

### **1.7.3 Role of $\text{Ca}^{2+}$ -activated $\text{Cl}^-$ channels in smooth muscle**

Intracellular  $[\text{Cl}^-]$  ranging from ~30 to ~50 mM has been recorded in smooth muscle cells using radioisotopes, fluorescent dyes, and ion-selective electrodes (Kitamura and Yamazaki, 2001). Due to the high cytosolic  $\text{Cl}^-$  concentration in smooth muscle cells,  $E_{\text{Cl}}$  falls within -38 mV to -19 mV, a range that is positive to  $E_m$  (Chipperfield and Harper,

2000). Hence,  $\text{Ca}^{2+}$ -activated  $\text{Cl}^-$  channel activation would cause  $\text{Cl}^-$  efflux. This would depolarise the membrane and activate L-type  $\text{Ca}^{2+}$  channel, resulting in  $\text{Ca}^{2+}$  influx. The elevation in intracellular  $[\text{Ca}^{2+}]$  would ultimately lead to smooth muscle contraction.

In vascular smooth muscle cells, TMEM16A transcripts and/or proteins have been found in rat cerebral artery (Thomas-Gatewood *et al.*, 2011), murine carotid artery (Davis *et al.*, 2010), murine portal vein (Davis *et al.*, 2010), murine thoracic aorta (Davis *et al.*, 2010), and cultured rat pulmonary artery smooth muscle cells (Manoury *et al.*, 2010). On the other hand, they have also been found in non-vascular smooth muscle cells. These include the sheep, rat, and mouse urethra smooth muscle (Sancho *et al.*, 2012), mouse airway, oviduct, epididymis (Huang *et al.*, 2009), as well as the rabbit corpus cavernosum (Hannigan *et al.*, 2017).

Importantly, their functional significance has been demonstrated in pharmacological studies involving both vascular and non-vascular SMCs. TMEM16A potentiator,  $F_{act}$ , increased single channel and whole cell CaCC currents in rabbit pulmonary arteries (Davis *et al.*, 2013). On the other hand, CaCC antagonists inhibited the currents in rabbit pulmonary artery myocytes (Davis *et al.*, 2013), and STICs in rabbit portal vein SMCs (Hogg *et al.*, 1994). In some non-vascular SMC types, including those from sheep urethra (Cotton *et al.*, 1997) and rabbit corpus cavernosum (Craven *et al.* 2004), CaCC antagonists had profound inhibition on their electrical and mechanical activity.

At the organ level, T16Ainh-A01 relaxed methoxamine-contracted murine and human blood vessels, suggesting the contribution of agonist-induced  $\text{Cl}^-$  currents in contraction (Davis *et al.*, 2013). In the urethra, EFS- and NE-induced contractions were inhibited by CaCC blockers and exposure to  $\text{Cl}^-$  free Krebs solution (Sancho *et al.*, 2012). In the corpus cavernosum, Chu and Adaikan (2008) and Kuo *et al.* (2009) showed that CaCC antagonists abolished myogenic, neurogenic, and agonist-induced contractions in the rabbit CC tissue.

In disease models, TMEM16A contributes to agonist-induced contraction in airway smooth muscle tissue. Moreover, Zhang *et al.* (2013) has demonstrated that TMEM16A expression in ASM cells is up-regulated in ovalbumin-induced mouse model of chronic asthma. They also showed that inhibition of these channels by niflumic acid and benzbramarone reduced airway hyperresponsiveness *in vivo* and hypercontraction *in vitro*. In vascular SMCs, TMEM16A protein expression is upregulated in pulmonary artery

SMCs of rats with hypoxic pulmonary hypertension (Sun *et al.*, 2012). Similarly, Forrest *et al.* (2012) showed that CaCC currents and TMEM16A expression were also increased in conduit and intralobar pulmonary artery from monocrotaline-induced pulmonary hypertensive rats. They also demonstrated that the contractions in the hypertensive rat models exhibited greater sensitivity to nifedipine, NFA, and T16AInh-A01 in comparison to control animals, suggesting that TMEM16A channel plays a major role in electromechanical coupling changes of pulmonary artery in this model of pulmonary hypertension. Since vascular dysfunction can compromise cavernosal function (Lue, 2000), we investigated the role of Ca<sup>2+</sup>-activated Cl<sup>-</sup> channels in the CCSM of the mice, a model commonly used to study ED (Leong *et al.*, 2015). Hence, in the next section the structure and function of TMEM16A will be reviewed in detail.

#### 1.7.4 Structure of TMEM16A channel

TMEM16A is a homo-dimeric  $\text{Ca}^{2+}$ -activated  $\text{Cl}^-$  channel belonging to a family of 10 membrane proteins, also known as anoctamins (Yang *et al.*, 2008). 'Anoctamin' was coined as these channels are anion-selective and were predicted to have eight (octa) transmembrane segments [Anion + octa]. The channel was, however, discovered to have 10 transmembrane helices at a later stage. TMEM16 family members all share considerable sequence homology (Milenkovic *et al.*, 2010). Each subunit has hydrophobic helices ( $\alpha$ -helices 1-10) anticipated to be transmembrane domains, with cytosolic N- and C-termini (Scudieri *et al.*, 2012). So far, the evidence points toward TMEM16A (Ano1) and TMEM16B (Ano2) being  $\text{Ca}^{2+}$ -activated  $\text{Cl}^-$  channels, whereas most others are scramblases, which induce membrane lipid bilayer deformations associated with lipid translocation (Kalienkova *et al.*, 2021). Although TMEM16B has  $\text{Ca}^{2+}$ -activated  $\text{Cl}^-$  channels activity, it requires higher intracellular  $\text{Ca}^{2+}$  concentrations and has faster activation and deactivation kinetics in comparison with TMEM16A (Pifferi *et al.*, 2009).

Interestingly, various isoforms of TMEM16A can be generated from alternative splicing, which involves inclusion or exclusion of five exons in different combinations (Ferrera *et al.*, 2009). Different varieties of isoforms have been found in different organ and tissue types, where they have altered biophysical properties, in particularly their  $\text{Ca}^{2+}$ -sensitivity (Ferrera *et al.*, 2009). Splice segment *a*, which starts the protein at the N-terminal end, is under the control of an alternative promoter, and is likely to be involved in expression at the plasma membrane. On the other hand, expression of splice segment *b* (encoded by exon 6b) reduces  $\text{Ca}^{2+}$  sensitivity of TMEM16A (Ferrera *et al.*, 2009). Splice variant segment *c*, encoded by exon 13, is located in the first intracellular loop, and alters the voltage and time-dependence, as well as  $\text{Ca}^{2+}$ -sensitivity of TMEM16A (Xiao *et al.*, 2011). Splice segment *d*, encoded by exon 15, has been shown by Mazzone *et al.* (2011) to decelerate both activation and deactivation kinetics. There is also evidence for an additional isoform encoded by exon 0 that is upstream of exon 1 (Mazzone *et al.*, 2015), which has been found to enhance TMEM16A current.

The proposed secondary structure of TMEM16A illustrating important domains,  $\text{Ca}^{2+}$  binding, and splice variants is shown in Figure 1.6.

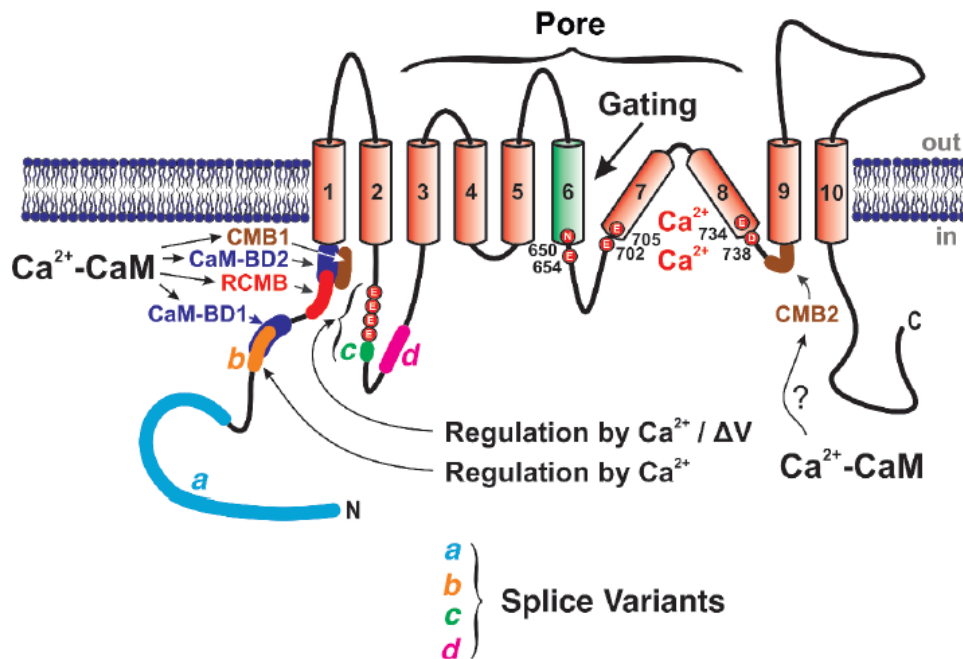


**Figure 1.6: The current proposed model of TMEM16A channel (Hawn *et al.*, 2021).**

### 1.7.5 Biophysical properties of CaCCs

Biophysical hallmarks of CaCCs include:

- They are activated by cytosolic  $\text{Ca}^{2+}$  with half-maximal concentrations for activation in the sub-micromolar range (Kuruma and Hartzell, 2000).

However, the exact value varies with specific channel splice variant. For example, Ferrera *et al.* (2009) found that skipping of exon 6b changes the  $\text{Ca}^{2+}$  sensitivity by nearly 4-fold, resulting in  $\text{Cl}^-$  currents requiring lower  $\text{Ca}^{2+}$  concentrations to be activated. On the other hand, Xiao *et al.* (2011) showed that omitting segment *c* considerably reduced the apparent affinity for  $\text{Ca}^{2+}$ , but the currents were still voltage-dependent.

- They exhibit outward rectification at low intracellular  $\text{Ca}^{2+}$  but display a linear current-voltage relationship at higher intracellular  $\text{Ca}^{2+}$  concentrations (Kuruma and Hartzell, 2000).

- The channels can conduct other divalent ions [preferentially larger anions] with the ionic selectivity being  $\text{NO}_3^- > \text{I}^- > \text{Br}^- > \text{Cl}^- > \text{F}^-$  (Large and Wang, 1996)

Although calmodulin (CaM) can activate TMEM16A channels (Vocke *et al.*, 2013), it is not responsible for the calcium dependent TMEM16A activation. This is supported by studies showing the lack of effect of exogenous CaM on TMEM16A currents in inside-out excised patches (Yu *et al.*, 2014). Furthermore, TMEM16A in excised patches can be activated by  $\text{Ba}^{2+}$ , which does not activate CaM (Yu *et al.*, 2014). Importantly, both loss-of-function CaM mutations and mutations in the CaM binding domain did not affect the channels' apparent calcium sensitivity (Tien *et al.*, 2014).

Contained within each subunit of TMEM16A is an ion conduction pore formed by  $\alpha 3$ – $\alpha 7$  helices. It resembles an hourglass, with a small extracellular and a large intracellular vestibule bridged by a narrow neck region about 20 Å long (Paulino *et al.*, 2017). The vestibules are highly hydrophilic and lined with excess basic amino acids, conferring a positive electrostatic environment throughout the pore, thus lowering the energy barrier for anion conduction. In the closed state, the proximity of hydrophobic residues at the intracellular entrance of the narrow neck prevents water and ions access (Lam *et al.*, 2021). The closed channel also has relaxed protein helices, allowing cytoplasmic  $\text{Ca}^{2+}$  to access the vacant ligand-binding site.

Activation of TMEM16A channel is a multi-step process. Binding of two  $\text{Ca}^{2+}$  ions to the five acidic residues (Yu *et al.*, 2012; Scudieri *et al.*, 2012) between the 5th and 7th putative transmembrane segments on  $\alpha 7$  and  $\alpha 8$  helices (Figure 1.7) precedes pore opening (Paulino *et al.*, 2017).  $\text{Ca}^{2+}$  binding shifts the conformational equilibrium by facilitating the attraction between the high positive charge density  $\alpha 7$ -8 helices with the distant  $\alpha 6$  helix. This hinge-like process simultaneously stabilises the contact between helices, closes off the aqueous path to the  $\text{Ca}^{2+}$  binding site, and opens the channel pore (Paulino *et al.*, 2017). Coupling of ligand binding to pore opening is consistent with less voltage dependence observed with  $\text{Ca}^{2+}$ -binding as opposed to without (Xiao *et al.*, 2011). Stabilisation of the fully activated channel conformation by  $\text{Ca}^{2+}$ -binding also results in slow deactivation kinetics (Peter *et al.*, 2018).

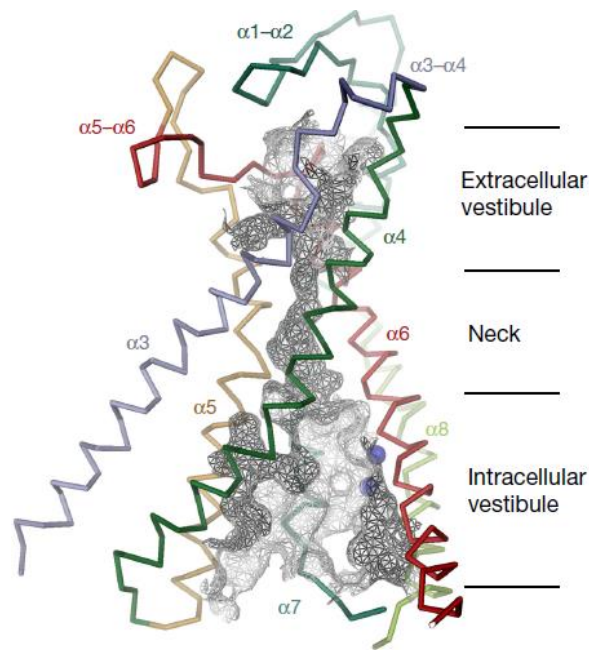


**Figure 1.7: Pore and Ca<sup>2+</sup>-binding site in the Ca<sup>2+</sup>-bound TMEM16A structure (Paulino *et al.*, 2017).**

Importantly, TMEM16A exhibits intrinsic voltage dependence for activation. Xiao *et al.* (2011) showed that the channels can be opened by  $V_m$  in the absence of Ca<sup>2+</sup> or other divalent cations by strong depolarisations. In their study, under conditions with zero intracellular Ca<sup>2+</sup>, depolarisations >100 mV evoke outward currents. One plausible mechanism for Ano1 voltage-dependent activation would be voltage-dependent protonation of the residues in the Ca<sup>2+</sup>-binding pocket. A depolarising pulse could push H<sup>+</sup> ions into the electrical field, where they can interact with and protonate the residues within the Ca<sup>2+</sup>-binding pocket, turning the channel into a conductive state to permeate ions (Segura-Covarrubias *et al.*, 2020).

Selective anion permeation occurs via attraction from positively charged side chains at both ends of the neck. Peters *et al.* (2015) identified four basic residues (R515, K603, R621 and R788) in the putative pore region associated with anion selection. In the narrow pore, polar residues compensate for the shedding of anion hydration shell, while the hydrophobic residues increase the energetic penalty for smaller ions. This is evident with the observed lyotropic permeability sequence, which favours larger anions (Ni *et al.*, 2014). Replacement of external Cl<sup>-</sup> with more permeant ions, for example I<sup>-</sup>, results in increased interaction with anions in the outer pore due to lower hydration energy and

higher permeability in comparison with Cl<sup>-</sup> (Xiao *et al.*, 2011). Higher occupancy in the pore stabilises and favours the voltage-dependent conformational changes at less depolarising voltages, thus reducing the Ca<sup>2+</sup>-dependence of activation, demonstrating that the gating of Ano1 by voltage is affected by permeant anions (Peter *et al.*, 2018).

### **1.7.6 Channelopathies**

Before its molecular identification as CaCC in 2008, TMEM16A/DOG1 (Discovered on GIST-1) was described as a biomarker for gastrointestinal squamous tumour (GIST) (West *et al.*, 2004). Since then, TMEM16A overexpression has been described in different tumour cells, including head and neck squamous cell carcinoma, gastric cancer, breast cancer, and colon cancer (Ji *et al.*, 2019). TMEM16A has been implicated in tumour proliferation, metastasis, as well as apoptosis resistance (Crottès and Jan, 2019). In other pathophysiological diseases, TMEM16A hyperactivity plays a role in asthma and neuropathic pain. In contrast, TMEM16A hypoactivity is associated with dry eye and dry mouth syndromes (Mitri *et al.*, 2021). Importantly, TMEM16A has been implicated in hypertension models (Cil *et al.*, 2021; Heinze *et al.*, 2014). Knockdown of TMEM16A is associated with vascular diseases. In one of the hypertension models, TMEM16A acts as a negative regulator. Its downregulation contributes to cerebrovascular remodelling during hypertension by promoting basilar smooth muscle cell proliferation (Wang *et al.*, 2012). Contrary to the paper by Wang *et al.* (2012), various independent studies have found TMEM16A to be upregulated in pulmonary hypertension (Papp *et al.*, 2019; Forrest *et al.*, 2012; Sun *et al.*, 2012).

### **1.7.7 Pharmacology of TMEM16A channels**

Modulation of TMEM16A activity presents an opportunity for therapeutic intervention in pathological conditions. Several TMEM16A channel modulators are natural products, for example, tannic acid and related gallotannins are derived from tea and wine (Namkung *et al.*, 2010). On the other hand, synthetic TMEM16A channel modulators also exist, for example, niflumic acid (NFA) and 4,4'-diisothiocyanatostilbene-2,2'-disulfonic acid

(DIDS) (Ji *et al.*, 2019). Some of these modulators are broad-spectrum, and can block endogenous CaCCs in *Xenopus laevis* oocytes, but they are also known to have off-targeted effect on other channels. For instance, while NFA is a CaCC antagonist, it can also activate BK<sub>Ca</sub> channels (Li *et al.*, 2008), inhibit Kv4 channels (Wang *et al.*, 1997), as well as modulate volume regulated anion channel (VRAC) (Liu *et al.*, 2021). It has been an ongoing challenge to develop compounds that can potently and specifically modulate CaCCs, however the recently developed TMEM16A antagonist Ani9 seems promising. Some activators and inhibitors of TMEM16A are included in Table 1.6.

Ano1 modulator	Function	Specificity
NFA	Inhibitor IC <sub>50</sub> 7-37 μM (Liu <i>et al.</i> , 2021)	Activate BK <sub>Ca</sub> channels (Li <i>et al.</i> , 2008)  Inhibit Kv4 channels (Wang <i>et al.</i> , 1997)  Inhibit volume regulated anion channel (VRAC) (Liu <i>et al.</i> , 2021).  Voltage-dependent bimodal effect (Bradley <i>et al.</i> , 2014)
DIDS	Inhibitor IC <sub>50</sub> 11-550 μM (Liu <i>et al.</i> , 2021)	Inhibit Kv4 channels (Wang <i>et al.</i> , 1997)  Agonist-dependent potentiation of TRPV1 channel (Zhang <i>et al.</i> , 2012)
Tannic Acid	Inhibitor IC <sub>50</sub> 6-25 μM	Does not block CFTR or ENaC (Namkung <i>et al.</i> , 2011)

	(Liu <i>et al.</i> , 2021)	Inhibits Ano2 (Namkung <i>et al.</i> , 2011)
CaCCinh-A01	Inhibitor IC <sub>50</sub> 1-7.8 μM (Liu <i>et al.</i> , 2021)	Inhibits L-type Ca <sup>2+</sup> channels at 30 μM (Hannigan <i>et al.</i> , 2017)
T16Ainh-A01	Inhibitor IC <sub>50</sub> 1 μM (Namkung <i>et al.</i> , 2011)	Inhibits L-type Ca <sup>2+</sup> channels at 10 μM (Hannigan <i>et al.</i> , 2017; Boedtkjer <i>et al.</i> , 2015)
A9C	Inhibitor IC <sub>50</sub> 58 μM (Bradley <i>et al.</i> , 2014)	Cardiac CFTR Sorota (1999)  Voltage-dependent bimodal effect (Bradley <i>et al.</i> , 2014)
Monna	Inhibitor IC <sub>50</sub> 80 nM (Oh <i>et al.</i> , 2013)	Inhibits VRAC and TMEM16B Liu <i>et al.</i> (2021)
Ani9	Inhibitor IC <sub>50</sub> 77 nM (Seo <i>et al.</i> , 2016)	NA
Niclosamide	Inhibitor IC <sub>50</sub> 140 nM (Miner <i>et al.</i> , 2019)	Also inhibits TMEM16F, the SERCA pump, and Ca <sup>2+</sup> influx channels (Centeio <i>et al.</i> , 2020)
TM <sub>Inh</sub> -23	Inhibitor	NA

	$IC_{50}$ ~30 nM (Cil <i>et al.</i> , 2021)	
GRb1	Activator $EC_{50}$ 38.5 nM (Guo <i>et al.</i> , 2017)	NA
ETD002 (or ETX001)	Activator $EC_{50}$ 116 nM (Danahay <i>et al.</i> , 2020)	NA

**Table 1.6: Pharmacological modulators of TMEM16A channel.**

## 1.8 Project aims and objectives

Corpus cavernosum smooth muscle (CCSM) exhibits phasic contractions that are coordinated by a variety of ion channels. Mouse models are commonly used to study erectile dysfunction, but there are few published electrophysiological studies of mouse CCSM.

We describe a novel voltage-dependent sodium current in mouse CCSM and aim to investigate its function by:

- Characterising its biophysical properties
- Estimating its reversal potential
- Studying its TTX-sensitivity
- Examining the effect of subtype-specific blockers
- Studying the effect of  $\text{Na}_V$ -activator
- Investigating its functional role in tissue
- Performing transcriptional and immunocytological studies

$\text{Ca}^{2+}$ -activated  $\text{Cl}^-$  current is another inward current that contributes towards excitation in CCSM. Transcripts for TMEM16A have been identified in rabbit CCSM (Hannigan *et al.*, 2017), but neither  $\text{Ca}^{2+}$ -activated  $\text{Cl}^-$  currents nor TMEM16A channels have been studied in mouse CCSM. We describe  $\text{Ca}^{2+}$ -activated  $\text{Cl}^-$  current in mouse CCSM by studying spontaneous transient inward currents (STICs) and spontaneous transient depolarisations (STDs) in mouse CCSM cells. Hence, we aim to:

- Investigate the effect of TMEM16A-specific antagonists
- Study the reversal potential of STICs
- Determine the mechanism of activation of STICs and STDs
- Investigate if  $\text{Ca}^{2+}$ -activated  $\text{Cl}^-$  channels contribute to adrenergic responses
- Perform immunocytological studies

## **Chapter 2: Materials and methods**

## **2.1 Tissue preparation**

C57BL/6 mice aged between 10 – 18 weeks were euthanised via intraperitoneal injection of sodium pentobarbital. This was carried out in accordance with the EU Directive 2010/63/EU and was approved by the Dundalk Institute of Technology Animal Care and Use committee.

The anterior pelvis was cut at the superior ramus of the pubis and the ischial ramus to ensure excision of the entirety of the corpus cavernosum. The remainder of the penis was dissected away from the pelvic bone and immediately placed in a Sylgard base Petri dish (9 cm in diameter) containing fresh Krebs solution (solution 1). Surrounding skeletal muscles, fat tissues, connective tissues, penile bulb, and corpus spongiosum were trimmed by sharp dissection to expose the proximal corpus cavernosum. The crura were then excised and opened at the proximal end to expose the inner muscle of the corpus cavernosum (Figure 2.1).

For experiments using urinary bladder smooth muscle, the bladder was removed from the animal and placed in Krebs solution. The bladder was opened along from the ureter end to the dome and pinned flat into a sheet. The urothelium was then carefully peeled away using fine forceps. To isolate segments of jejunum, the entire small intestine was removed and placed in Krebs solution. A small section of jejunum (2 cm) was cut away and pins were inserted into the mesentery along the axis of the tissues. The tissue was then opened in a longitudinal direction and the mucosal layer was removed.

For experiments using skeletal muscle, skin, connective, and fatty tissues were removed from the thigh to reveal the skeletal muscle underneath. Using a surgical blade, the muscle was thinly sliced (<1mm) along the longitudinal plane.

## **2.2 Isometric tension recording**

For isometric tension recording, crura sections of the corpus cavernosum ~3 mm in length and 1.5 mm in diameter were removed. The sections were hooked transversely through the tunica albuginea, and one side of the tissue was cut open, exposing the tunica albuginea connected by the inner smooth muscle. The tissue sections were then mounted

between electrical field stimulating (EFS) electrodes in organ baths containing Krebs (solution 1) at 37°C constantly bubbled with 95% O<sub>2</sub> and 5% CO<sub>2</sub> throughout the experiments. Tissue sections were adjusted to a tension of 4-6 mN and left to equilibrate for 45 minutes before experimentation.

Drugs were added directly to the organ bath from stock solutions to achieve their final stated concentrations via dilution in the chamber. Drugs were manually drained from the chamber, followed by Krebs replacement from a heated reservoir.

Corpus cavernosum smooth muscle contraction was recorded in a four-chamber tissue bath system (SI-Heidelberg, Europe; Figure 2.2). Tension was measured through transducers connected to a SI-BAM21-LCB Force Transducer Amplifier (World Precision Instruments, Europe), which converts the output of the transducer to an amplified analogue voltage that is proportional to the force applied to the force transducer. The analogue signal was then converted to a digital signal by a LabTrax 4/16 Channel Data Acquisition A/D converter (World Precision Instruments, Europe) and recorded via Data-Trax 2 software (World Precision Instruments, Europe) on a PC.

### **2.3 Isolation of corpus cavernosum smooth muscle cells**

Cells were obtained from the corpus cavernosum via enzymatic dispersal. The corpus cavernosum tissue was cut into small (<1 mm) pieces and these were placed in a 5 mL test tube, along with a small stir bar. Then, 4 mL enzyme mix containing 15 mg collagenase (Sigma, Type 1A), 10 mg bovine serum albumin (Sigma, heat shock fraction) and 10 mg Trypsin inhibitor (Sigma, from Glycine max soybean) dissolved in Ca<sup>2+</sup> free Hanks (solution 2) was added. The tube was placed in a 37°C water bath for 2.5 minutes while its contents were magnetically stirred. This was followed by the addition of 1 mL containing 1 mg proteinase (Sigma, Type XXIV) and vigorous trituration. The tissue was left in the enzyme mix for 2 more minutes, while being checked under the microscope every 30 seconds, before centrifugation for 30 seconds at 1000 RPM/ 78 RCF (Clifton 010 series). Then, the supernatant was removed, and the cell pellet was washed carefully at room temperature in Ca<sup>2+</sup> free Hanks (solution 2) three times. After washing, the cells were re-suspended in Ca<sup>2+</sup> free Hanks (solution 2) at 37°C for a further wash of 10 minutes. 1 mL Ca<sup>2+</sup> free Hanks (solution 2) containing dispersed cells were placed onto

a Nunclon dish along with (with  $\text{Ca}^{2+}$  added to a concentration of 100  $\mu\text{M}$ ). The dish was stored in the fridge at 4°C, and removed and left to equilibrate at room temperature for 30 minutes before use.

## **2.4 Human embryonic kidney cells**

A stable cell line expressing human  $\text{Na}_v1.5$  in human embryonic kidney (HEK-293) cells was purchased from CreaCell (France) and cultured at 37°C in DMEM (Invitrogen) containing 10% fetal bovine serum, glutamine, penicillin-streptomycin, and 1.2 mg/mL G418 in a humidified incubator under 5%  $\text{CO}_2$ .

## **2.5 Total RNA isolation**

### **2.5.1 Tissue sample**

Total RNA was isolated from tissue samples using the TRIZOL method. Approximately 50 mg to 100 mg of tissue was homogenised, either by cutting the tissue into small pieces with sterile scissors or flash-frozen in liquid nitrogen to be ground into a powder using a chilled pestle and mortar. The tissue was then transferred into a ribonuclease (RNase) free eppendorf tube containing 1 mL Trizol reagent, followed by gentle trituration through an 18-gauge needle and then a 21-gauge needle to physically disrupt the mammalian cell membranes. The sample was then incubated for 5 minutes at room temperature. After that, 200  $\mu\text{L}$  chloroform was added to cause organic and aqueous phase separation. The sample was capped and agitated for 15 seconds, followed by incubation at room temperature for 3 minutes, and then centrifugation at 14500 RPM in a cold room for 15 minutes. Centrifugation separated the sample into a lower layer of red phenol-chloroform, an interlayer, and a clear upper aqueous layer. The upper aqueous layer contained the RNA and was transferred into a sterile Eppendorf tube. Care was taken to avoid touching the inter-layer. The addition of 500  $\mu\text{L}$  isopropanol then precipitated RNA. The sample was then vortexed briefly before being incubated at room temperature for 10 minutes and then centrifuged for 10 minutes in the cold room. Next, the pellet was recovered and washed

with 1 mL 75% ethanol. Then, the sample was vortexed and centrifuged for 5 minutes in a cold room. This was followed by supernatant removal and air-drying for 5 minutes. Finally, the pellet was resuspended in 25  $\mu$ L RNase free water by trituration.

All isolated RNA samples were treated with deoxyribonuclease (DNase) to eliminate DNA contamination. DNase 1 (Invitrogen) digests single and double-stranded DNA enzymatically by hydrolytic cleavage of phosphodiester links. 1  $\mu$ L DNase 1 enzyme was added per 10  $\mu$ L dissolved RNA before incubation at room temperature for 15 minutes. The enzymatic reaction was inactivated by EDTA and 10 minutes of heating at 65°C. After DNase treatment, the samples were deemed suitable for cDNA synthesis.

RNA yield was quantified via absorbance using a NanoDrop Spectrophotometer. Nucleic acids and proteins absorb ultraviolet light at 260 nm and 280 nm, respectively. On the other hand, absorbance at 230 nm is typically the result of salt contamination. Hence, A260/A280 and A260/A230 ratios are used to estimate sample purity. Thus, RNA samples with an A260/A280 ratio between the range of 1.8 and 2 and a A260/A230 ratio between 2.0 and 2.2 were considered pure.

## **2.6 Reverse Transcription-Polymerase Chain Reaction (RT-PCR)**

### **2.6.1 cDNA synthesis**

Complementary DNA (cDNA) is double-stranded DNA synthesised from RNA using the enzyme reverse transcriptase. A total reaction volume of 20  $\mu$ L was used to synthesise cDNA from 1  $\mu$ g of total sample RNA. First, random hexamers (200  $\mu$ g), RNA (1  $\mu$ g), and dNTP mix (10 mM) were added into a nuclease-free microcentrifuge tube. The thermal protocol involved heating the sample to 65°C for 5 minutes, followed by a quick chill on ice. Then, the contents were collected by brief centrifugation, followed by the addition of 4  $\mu$ L 5x First-Strand Buffer and 2  $\mu$ L of 0.1 M DTT. The contents were then mixed gently by trituration and then incubated at 25°C for 2 minutes. After that, 1  $\mu$ L of Superscript II RNase-H Reverse Transcriptase (Invitrogen) was added and mixed by gentle trituration. The incubation temperature was then set at 25°C for 10 minutes and then 42°C for 50 minutes. Finally, inactivation of the reaction was carried out by heating

the sample to 70°C for 15 minutes. All cDNA sample was stored at -20 degrees until further use.

## 2.7 Polymerase Chain Reaction (PCR)

Polymerase chain reaction is a molecular biology technique used to amplify DNA or cDNA to generate millions of copies of the targeted DNA sequence. This technique was created by Kary B. Mullis in 1983 and involves 3 crucial steps of denaturation (double-stranded DNA/cDNA separation) at high temperature, followed by annealing of forward and reverse primers to the DNA/cDNA, and finally, the extension of new DNA strand. For these steps to be carried out successfully, thermo-stable DNA polymerase, buffer containing magnesium ions (co-factor for DNA polymerase), and deoxynucleotide triphosphates (dNTPs) were needed. A commercially available PCR mastermix – Amplitaq Gold PCR Mastermix (Applied Biosystems) containing all of these reagents was used for all PCR experiments. The reactions also required the use of forward and reverse primers, along with the cDNA template.

The typical PCR reaction contained the following:

Reagents	Volume (µL)
Amplitaq Gold	12.5
PCR grade water	8.5
Forward primer	1
Reverse primer	1
cDNA template	2
Total volume	25

**Table 2.1: PCR reaction reagents.**

PCR reactions were carried out using a Techne TC-512 thermal cycler. The temperature-programmed protocol used is shown below in Table 2.2 and the products were stored at 4 °C until further use.

<u>Step</u>	<u>Temperature (°C)</u>	<u>Time (minutes)</u>
Initial denaturation	95	5
Denaturation	95	0.5
Annealing	56	0.5
Extension	72	0.5
X 40 cycles		
Final extension	72	7

**Table 2.2: Temperature-programmed protocol.**

Primer	Sequence (5'-3')	Product Length (bp)	Accession #
<i>Actb</i> -F	CTAGGCACCAGGGTGTG	205	NM_007393.5
<i>Actb</i> -R	GTGAGCAGCACAGGGT		
<i>SCN1A</i> -F	AACAAGCTTCATTACATAACAATAAG	150	NM_001313997.1
<i>SCN1A</i> -R	AGGAGGGCGGACAAGCTG		
<i>SCN2A</i> -F	ATTTTCGGCTCATTCTTCACACT	176	NM_001099298.3
<i>SCN2A</i> -R	GGGCGAGGTATCGGTTTTTGT		
<i>SCN3A</i> -F	CAGACCATGTGCCTTATTGTGT	154	NM_001355166.1
<i>SCN3A</i> -R	CCGCGATCTGGAGGTTGTT		
<i>SCN4A</i> -F	AGTCCCTGGCAGCCATAGAA	140	NM_133199.2
<i>SCN4A</i> -R	CCCATAGATGAGTGGGAGGTT		
<i>SCN5A</i> -F	ATGGCAAACCTCCTGTTACCTC	104	NM_021544.4
<i>SCN5A</i> -R	CCACGGGCTTGTTTTTCAGC		
<i>SCN8A</i> -F	CACTACTGCTTCAACGAGAC	182	NM_001077499.2
<i>SCN8A</i> -R	CCTTTGAAGGTTGCCACTTG		

(qPCR)

<i>SCN8A-F</i>	GCAAGCTCAAGAAACCCACCC	115	NM_011323
<i>SCN8A-R</i>	CCGTAGATGAAAGGCAAACCTCT		
(end-point PCR)			
<i>SCN9A-F</i>	TGGATTCCCTTCGTTACACAGA	115	NM_001290674.1
<i>SCN9A-R</i>	GTCGCAGATACATCCTCTTGTTT		
<i>SCN10A-F</i>	TCCGTGGGAACTACCAACTTC	190	NM_001205321.1
<i>SCN10A-R</i>	GCTCGCCATAGAACCTGGG		
<i>SCN11A-F</i>	CGACTCTTTGGCTGCAATAGA	134	NM_011887.3
<i>SCN11A-R</i>	AGAGCTTAGGTAACCTCCTGGAG		

**Table 2.3: Primer details used in this study.**

Details of each primer sequence, including their accession number and expected amplicon size, are listed above in Table 2.3.

## 2.8 Agarose Gel Electrophoresis and Gel Imaging

Agarose gel electrophoresis employs an electrical field to move DNA samples across an agarose gel to separate DNA fragments according to their sizes. Agarose is extracted from seaweed, and its gel serves as a molecular sieve. The higher the agarose concentration, the smaller the pore size. Smaller DNA fragments can move through the pores faster and travel down the gel further than larger DNA fragments. Amplicons move from cathode to anode as they are polyanionic.

Due to the small sizes of the targeted amplicons, 2% agarose gel was used to resolve the PCR products in this project. This was prepared by dissolving 2 g of Ultra-Pure agarose powder (Invitrogen) in 100 ml 1x TAE (Tris, acetic acid, EDTA) buffer (Sigma), and then heating the mixture in a microwave until boiling point. The solution was allowed to cool until approximately 50°C before 6 µL of 1X SYBR Safe (Invitrogen) was added and mixed. SYBR Safe dye intercalates between the DNA backbone, and its excitation under the U.V. light causes fluorescence. This facilitates the visualisation of resolved DNA fragments and is a less hazardous alternative to the traditional nucleic acid stain ethidium bromide. The solution was then poured into an electrophoresis-casting tray, and a comb was inserted before the solution was allowed to cool and solidify for about 20 minutes. Removal of the comb leaves a negative impression to form wells for sample loading. The gel was fully immersed in 1x TAE buffer within a horizontal electrophoresis chamber unit (Scie-Plas U.K.). 10 µL of post-PCR sample was mixed with 2 µL of 6x DNA loading buffer (Thermo Scientific) before being loaded into the gel. A 100 base pair (bp) DNA ladder (Thermo Scientific) was loaded into a lane parallel to the samples to facilitate amplicon size estimation. Electrophoresis was carried out at 80 V for 90 minutes.

Following completion of electrophoresis, the gel was moved to an INGENIUS gel documentation system (Syngene Bio Imaging) and placed onto the glass plate of a U.V.-transilluminator (312 nm) linked to the imaging system. U.V. light was used to illuminate SYBR Safe bound to DNA fragments. The resolved amplicons were then compared to the predicted bp size.

## **2.9 Real-time quantitative PCR**

Real-time quantitative PCR (qPCR) is a molecular technique capable of simultaneous amplification and quantification of a specific DNA sequence using the principles of PCR described earlier. This technique provides “real-time” feedback of the PCR reaction by measuring the fluorescence intensity emitted during each cycle. In this study, qPCR was used to measure the relative quantity of different genes of interest in RNA extracted from the mouse CCSM. SYBR Green (Applied Biosystems) chemistry on a Techne-Quantica real-time thermal cycler was used to quantify PCR products. SYBR Green is a dye that binds to double-stranded DNA (dsDNA) with high specificity. This dye absorbs light at

488 nm and emits light at 522 nm when dye-DNA interaction occurs. Therefore, fluorescence intensity is proportional to dsDNA quantity. The primer pairs and thermal protocol were described previously in Table 2.2 and 2.3. The efficiency of each primer pair was calculated by constructing a standard curve from amplicons obtained from a series of serial dilutions of template cDNA. Standard curve for each individual primer set was obtained from mouse brain cDNA used at concentrations of 1:3, 1:10, 1:30 and 1:100. Primer efficiency was calculated from each standard curve using the Quanta computer software. Only primers possessing efficiency values within a 90-110% range were used for qPCR analysis. To validate that the observed fluorescence was mostly amplicon-based, melting curve analysis was performed on each reaction. This involved ramping the temperature from 70°C to 90°C to melt the dsDNA. The presence of one peak indicated that one PCR product was produced in the reaction. The presence of > 1 peak would indicate non-specific binding or primer dimer occurring, thus being deemed unsuitable for further analysis. Each gene and their subsequent standard curve were compared to a standard curve generated from a reference housekeeping gene.  $\beta$ -Actin, a highly conserved cell structural protein, was used as a housekeeping gene for qPCR in this study. Reactions without template cDNA served as contamination controls. qPCR data were normalised to  $\beta$ -actin and analysed using the  $\Delta\Delta$ CT method (Livak and Schmittgen, 2001).

## **2.10 Immunocytochemistry**

250  $\mu$ L of 100  $\mu$ M  $\text{Ca}^{2+}$  Hanks (dissolve 1.1 mg of CaCl in 100 mL of Solution 2) were added to freshly dispersed corpus cavernosum smooth muscle cells in a glass-bottom dish. The cells were left at room temperature for an hour and a half to adhere to the bottom of the dish. This step was not considered necessary for HEK cells, as they have adherent growth. Then, they were incubated in fixative of 2% paraformaldehyde for 45 minutes in the fridge at 4°C, before being washed with 1x DPBS thrice. After that, the cells were permeabilised with 0.3% Triton X-100 and blocked with donkey serum for 10 minutes, before being washed with 1x DPBS three times. Then, cells were incubated in anti-Nav1.4 antibody (rabbit polyclonal anti-mouse, 1:200 dilution, Alomone), anti-Nav1.5 antibody (rabbit polyclonal anti-mouse, 1:100 dilution, Alomone), anti-TMEM16A antibody (rabbit polyclonal anti-human, 1:200 dilution, Alomone), or anti-smooth muscle myosin

heavy chain 11 antibody (rabbit polyclonal anti-mouse, 1:200 dilution, Abcam) for 24 hours in the fridge at 4°C and then washed with 1x DPBS three times. This was followed by incubating cells in secondary antibody conjugated to Alexa Fluor™ 488 (donkey polyclonal anti-rabbit antibody, 1:1000 dilution, Invitrogen) for 1 hour in the fridge at 4°C, and then washed with 1x DPBS for half an hour with a solution change every 5 minutes. All the antibodies used are detailed in Table 2.4 below.

All solution removal was done using a peristaltic pump (Watson Marlow, Europe) at 13 RPM and 2 bar (30 psi) pressure. The suction tip of the peristaltic pump was placed at the sidewall of the dish for solution removal, while solution addition was done by pipetting very slowly down the sidewall of the dish.

Controls were prepared simultaneously. Secondary antibody only control omitted the primary antibody incubation while the negative control contained only cells in serum and 1x DPBS. Both controls were imaged with the same parameters as each experimental image.

Cells were imaged using an iXon 887 electron-multiplying charge-coupled device (EMCCD) camera (Andor Technology, Belfast) coupled to a Nipkow spinning disk confocal head (CSU22, Yokogawa, Japan). A 488 nm krypton-argon laser (Melles Griot, UK) was used to excite the Alexa Fluor™ conjugated to the secondary antibody bound to the cells, which has a peak emission at 520 nm. Images were acquired under a x60 objective (Nikon eclipse Ti) using the Andor IQ software, producing images of pixel sizes 0.266 x 0.266 µm. The sampling frequency used was 15 frames per second (FPS). The frames were collected as a stack of TIFF images and then imported into Image J (National Institute of Health, MD, USA) to be analysed with Z-stack protocol.

## **2.11 Immunohistochemistry**

The protocol is similar to immunocytochemistry protocol, except that the tissue was incubated in paraformaldehyde for 40 min at room temperature, and the only primary antibody used was the anti-TMEM16A antibody.

Immunofluorescence was imaged using an Axioskop 2 LSM 510 Meta confocal microscope (Zeiss, Germany). A water-dripping x20 objective lens was lowered into the

dish and cells were focused with transmitted light. Using a laser, excitation wavelength of 488 nm was used to visualise immunoreactivity in the cells. The emission filter used was 505-530 nm (green). Confocal micrographs were composited of Z-series scans taken at 0.3  $\mu\text{m}$  depth intervals. Final images were constructed using the z-stack function within Image J software (Rasband, 2011).

Note: Z-series scans were also carried out on CCSM cells. They had ~25 to 36 optical sections, taken at 0.3  $\mu\text{m}$  depth intervals, suggesting that they have a height of ~ 7.5 to 10.8  $\mu\text{m}$ .

Antibody	Clonality	Dilution	Supplier
Anti-Nav1.5	rabbit polyclonal anti-mouse	1:100	Alomone Labs Cat# ASC-005
Anti-Nav1.4	rabbit polyclonal anti-mouse	1:200	Alomone Labs Cat# ASC-020
Anti-TMEM16A	rabbit polyclonal anti-human	1:200	Alomone Labs Cat# ab72984
Anti-smooth muscle myosin heavy chain 11	rabbit polyclonal anti-mouse	1:100	Abcam Cat# ab53219
Donkey anti-rabbit 488	donkey polyclonal anti-rabbit	1:1000	Molecular Probes Cat# A-21206

**Table 2.4: Antibodies used in immunocytochemical and immunohistochemical studies.**

## **2.12 Electrophysiology**

Electrophysiology is the study of the electrical properties of biological cells and tissues. By measuring the voltage or current changes, it allows the study of the ionic basis of the electrical activity of corpus cavernosum smooth muscle cells.

### **2.12.1 Patch-clamp equipment**

The bath was constantly perfused with Hanks solution (solution 3) throughout all experiments. Typically, patch-clamp experiments involving studying of the sodium currents were carried out at room temperature (22°C). However, depending on the temperature requirement, a glass heat exchanger was used to maintain bath temperature at 37°C, which was monitored at regular intervals using a handheld, battery-operated temperature probe.

In addition to bath perfusion, the cell under study was constantly superfused via a custom-built system (Figure 2.3). This allowed rapid delivery of drugs or rapid changes in the perfusion solution. A series of syringes, acting as reservoirs, were gravity-fed via tubing to a 1 ml syringe and sealed using a silicon-based gel to prevent backflow. At the end of the syringe was a glass pipette with a tip size of around 200-300 µm, placed around 100 µm from the cell using a micromanipulator. Three-way taps allowed individual reservoirs to be turned on or off as required. To avoid mechanical artefacts, changes were made by switching the new reservoir on before switching the current reservoir off.

Patch pipettes were pulled from borosilicate glass capillaries (Havard Apparatus, UK) with an outer diameter of 1.5 mm and an inner diameter of 1.17 mm, using a Flaming/Brown micropipette puller (model-P97, Sutter Instruments, CA, USA). Pipette tips were around 1-2 µm in diameter. New glass pipettes were used for each experiment. Pipettes were filled with solutions 5 or 6, depending on the experiment. Patch pipettes were applied to the cell membranes using a micromanipulator system (Burleigh PCS-6000).

Voltage commands were delivered via an Axopatch 1D patch-clamp amplifier (Molecular Devices, Sunnyvale, CA, USA). For recording purposes and to specify voltage-clamp

protocols, this was connected to a Digidata 1440A AD/DA converter (Molecular Devices) interfaced to a Dell PC running Clampex 10.2 software (Molecular Devices). The acquisition frequency was 100 kHz, and this was further filtered at 1 kHz by the amplifier. A Humbug device (HumBug, Quest Scientific) was inserted between the patch-clamp amplifier and AD/DA converter. This device is not a filter. It effectively eliminates 50/60 Hz noise and harmonics without altering the frequency characteristics of the physiological signal. It achieves this by using an advanced signal processing unit to continuously construct a replica of the noise present on the input, which it then subtracts, to leave a clean signal free from distortion. A diagrammatic representation of the patch-clamp set-up used is shown in Figure 2.3.

### **2.12.2 Voltage clamp**

At the end of the 1940s, Marmont and Cole pioneered the conception of voltage clamp by inventing an electronic feedback system that could "clamp" the membrane potential at a set value along the squid axon and measure the feedback current. Shortly after, Hodgkin and Huxley used that recording technique to advance their quantitative theory of the action potential based on voltage-dependent ionic currents (Hodgkin and Huxley, 1952).

In voltage-clamp experiments, the cell membrane potential is controlled while the ionic current that crosses the membrane is measured. This technique is essential to study ion channels, as many of them are voltage-gated, and their biophysical properties are dependent on the cell membrane potential (for example, activation and inactivation within certain range of membrane potential).

### **2.12.3 Current clamp**

In current-clamp experiments, the amount of injected current is controlled while the cell membrane potential is measured. In contrast to voltage-clamp mode, the cell membrane potential is free to vary, either from its own myogenic activities (for example, resting membrane potential and spontaneous depolarisations) or as a result of stimulation (for example, injection of current to mimic synaptic input or application of drugs to open

membrane ion channels). It should be noted that current clamp means clamping the current applied through the electrode at a constant value and not the current flowing through the membrane (Hammond, 2014).

However, it should be noted that the injected current may leak through bad seals, leading to inadequate clamping and therefore inaccurate recordings. This is especially important in the estimation of resting membrane potential. Thus, high seal resistance and high input resistance are required so that small current injections will produce high voltage responses: Ohm's law ( $V = IR$ ).

#### **2.12.4 Patch-clamp**

Over time, various patch-clamp methods had evolved: cell-attached, excised inside-out, whole-cell, and excised outside-out patches may be used (Figure 2.4). Excised inside-out patch exposes the intracellular membrane surface to the bath, allowing the study of environmental factors on the intracellular components of single ion channels (Ogden and Stanfield, 1994). This technique can be employed to study the activation of ion channels by different concentrations of intracellular ligands.

The excised outside-out patch is complementary to the excised inside-out patch. The original outside of the cell membrane is facing outward from the pipette, which means that the pipette solution serves as the intracellular fluid, and the outside of the membrane may be exposed to any drug of choice. The excised outside-out patch allows the exposure of an isolated ion channel to different solutions, while maintaining a controlled and known concentration of intracellular constituents, i.e. the pipette solution.

##### **2.12.4.1 Whole-cell ruptured patch**

Whole-cell recordings allow the recording of currents through multiple channels simultaneously, over the entire cell membrane. Once a seal is formed, suction and/or current pulses can be used to break into the cell. One advantage of the whole-cell technique is that the larger pipette tip size has lower resistance and allows better electrical access to the inside of the cell. This is especially important to record fast ionic currents,

such as sodium current. However, the cytosol of the cell will be slowly replaced by the pipette solution, resulting in the subsequent loss of constituents essential for certain intracellular pathways or ion channel functions (Byerly and Yazejian, 1986).

#### **2.12.4.2 Whole-cell perforated patch**

Dialysis of cytosolic components can be overcome by using the perforated patch, where electrical access to the cell is provided by amphotericin B. Instead of rupturing the cell membrane, amphotericin B can be included in the pipette solution. This antibiotic forms channels in cholesterol or ergosterol containing membranes, providing electrical access to the cell. These pores have an effective radius of approximately 4 Å (Holz and Finkelstein, 1970). The small pore sizes are readily permeable to monovalent but not large anions (Holz and Finkelstein, 1970), limiting the dialysis of cellular components (Rae *et al.*, 1991; Horn and Marty, 1988).

For this reason, the perforated patch was used to study electrical activity in mouse corpus cavernosum cells, to prevent the loss or 'run-down' of intracellular constituents that might contribute to an electrical event, for example, the calcium currents. Mouse corpus cavernosum smooth muscle cells were also studied under the current-clamp mode, where the injected current was controlled while the changes in membrane potential in response to drugs was monitored.

Amphotericin B was added to DMSO at a concentration of 60 mg/ml. Next, 14 µl of this solution was then added to 1 ml of pipette solution to give a final amphotericin B concentration of 840 µg/ml. Perforation of the patch, and hence the development of electrical access to the cell interior, was monitored by holding the cell at -60 mV and applying steps to 0 mV for 100 ms, at intervals of 500 ms. After roughly 1-5 minutes, amphotericin B perforated the cell membrane, and electrical access improved. This was observed as the gradual development of an inward current and reduction in the width of the capacitive transient. The evolution of current during patch perforation using Cs<sup>+</sup> pipette solution (solution 7) is shown in Figure 2.5.

An example of freshly dispersed corpus cavernosum cell under whole-cell patch-clamp conditions and its equivalent circuit is shown in Figure 2.6.

## 2.13 Liquid junction potential

Liquid junction potentials are caused by ionic movement at the junction between pipette solution and extracellular bath solution due to their differences in ionic compositions and ion mobilities.

The liquid junction potential between Normal Hanks and caesium pipette solutions, measured using the method set out by Neher (1992), was calculated previously by Craven (2006). A 3M KCl agar solution was placed in a pipette containing a silver chloride wire. This acted as the bath electrode. At the outset, both the patch pipette and bath solutions contained the pipette solution. In current clamp mode, the resting voltage was set to 0 mV.

Following this, the bath solution was exchanged with the solution used in this study (Hank's solution). This resulted in a change in the voltage reading and this new value was taken as the liquid junction potential. The bath solution was then changed back to the pipette solution to test reversibility. The liquid junction potential was found not to exceed 3 mV (Craven, 2006), and therefore was not compensated for.

## 2.14 Pipette resistance

When a current is applied through the electrically conductive fluid-filled micropipette, the micropipette's electrical resistance is computed as the ratio of the voltage drop across the tip of the applied current. The resistance is affected by its tip geometry and is governed by the tip diameter and cone angle.

Pipette resistance ( $R_p$ ) can be calculated using Ohm's law:

$$R_p = \frac{V_T}{I_p} \quad \text{Equation 1}$$

With a micropipette in the bath, a square test pulse of 5 millivolts for 400 ms was used to indicate the resistance of the pipette. Typically, a current response to the test pulse would be around 2000 pA. Hence, the typical pipette resistance would be:

$$R_P = \frac{5 \times 10^{-3}}{2 \times 10^{-15}}$$

$$R_P = 2.5 \text{ M}\Omega$$

2.5 M $\Omega$  is within the acceptable range of 1-5 M $\Omega$  for whole-cell patch application.

### **2.15 Formation of a gigaseal**

As the pipette advanced through the bath solution, slight positive pressure was applied to the inside of the patch pipette to keep the tip contamination-free. The current was set to zero using the amplifier, and the pipette resistance was monitored by measuring the current response to the square test pulse mentioned above. Contact with the cell membrane was indicated by a rise in pipette resistance (or a decrease in current). When the increase in pipette resistance (or decrease in current) reached 50%, negative pressure was applied to the pipette to facilitate seal formation. A small area of membrane was drawn into the pipette tip, and the seal formed slowly at first and suddenly achieved a high resistance value. Usually, the seal formed between the membrane and the pipette had a resistance of more than 1 gigaohm (G $\Omega$ ), often referred to as a gigaseal, which would significantly reduce the noise and increase the resolution of recordings.

### **2.16 Cell capacitance**

By definition, a cell membrane can be considered as a capacitor since it separates electrical charges between the intracellular and extracellular media. The cell membrane's ability to store charge (Q) at a given potential is defined as capacitance (C). Capacitance is measured in Farads (F) and is the proportionality constant in Equation 2. The charge stored is proportional to the applied voltage (V). This relationship can be described as:

$$Q = C * V \qquad \text{Equation 2}$$

Differentiate the equation with respect to time:

$$\frac{dQ}{dt} = C * \frac{dV}{dt} \quad \text{Equation 3}$$

Since capacitive current,

$$I_{\text{cap}} = \frac{dQ}{dt}$$

$$I_{\text{cap}} = C * \frac{dV}{dt} \quad \text{Equation 4}$$

Capacitive current is the current that flows when charging or discharging a capacitor. In other words, the current flow ( $I_{\text{cap}}$ ) will produce a voltage ramp ( $\frac{dV}{dt}$ ) across the capacitance (C) of the membrane. This occurs when the membrane is stepped from one potential to another. However, once the desired voltage is reached (typically after a few milliseconds), there will be no capacitive current. The concept of voltage clamp is to keep the voltage constant using feedback circuitry. Under such conditions  $dV/dt = 0$ , therefore capacitive current = 0. This allows measurement of the ionic current across the membrane, since:

$$I_{\text{total}} = I_{\text{cap}} + I_{\text{ionic}}$$

Measuring cell capacitance: Worked example

Cell capacitance was calculated by integrating the capacitive current to obtain the charge, Q. This was achieved by measuring the area under the curve of the capacitive transient (passive membrane response) induced when stepping to -80 mV from a holding potential of -100 mV (20 mV difference) (Figure 2.7).

The area under the curve of capacitive transient: 754.6 pA \* ms

$$= 754.6 \times 10^{-12} \times 10^{-3}$$

$$= 754.6 \times 10^{-15}$$

$$C = Q/V$$

$$\begin{aligned}
&= \frac{754.6 \times 10^{-15}}{20 \times 10^{-3}} \\
&= 37.73 \times 10^{-12} \\
&= 37.73 \text{ pF}
\end{aligned}$$

Cell capacitance ( $C_m$ ), calculated for 52 cells, averaged  $37.8 \pm 1$  pF.

Cell capacitance may also be an indication of cell surface/cell size, is used to measure current density. Cell capacitance was not compensated.

## 2.17 Series resistance

During whole-cell recording, current in the pipette ( $I_p$ ) flows through resistance in series with the cell membrane before entering the cell. The sum of all of the resistances between the patch-clamp amplifier input and the cell membrane is termed series resistance ( $R_s$ ). Series resistance may result in a steady-state error, where it causes a potential difference of  $I_p \times R_s$  between the command voltage and the voltage at which the membrane is actually clamped (Ogden and Stanfield, 1994). Thus, a large voltage error may occur when recording a large ionic current if the series resistance is high. Another issue that may arise with high series resistance is a dynamic error, where step changes in command voltage produce membrane potential changes with a lag, making it difficult to measure rapid ionic currents. The time constant of lag due to series resistance can be expressed as:

$$\tau = R_s * C_m \quad \text{Equation 5}$$

Series resistance was calculated by examining the  $\tau$  of capacitive transient (passive membrane response) induced when stepping to -80 mV from a holding potential of -100 mV (20 mV).

Series resistance was calculated for 52 cells by fitting the decay phase of the capacitive transient with an exponential curve using pClamp software. The average  $\tau$  from 52 cells was  $0.34 \pm 0.01$  ms.

Using the cell capacitance calculated above:

$$\begin{aligned}\tau &= R_s * C_m \\ R_s &= \frac{\tau}{C_m} \\ &= \frac{0.34 \times 10^{-3}}{37.8 \times 10^{-12}} \\ &= 8.99 \text{ M}\Omega\end{aligned}$$

As shown above, the value of  $R_s$  obtained was within the quoted series resistance of 5-20  $\text{M}\Omega$  for the whole-cell patch (Rae *et al.*, 1991). Therefore, series resistance was left uncompensated, as sodium currents recorded were generally around 400-600 pA. Assuming  $R_s = 9 \text{ M}\Omega$ , this would only result in a small voltage error of 3 to 5 mV. However, in some experiments, the recorded currents were greater than 600 pA. HEK-293 cells expressing Nav1.5 conduct much bigger currents, so series resistance was electronically compensated by ~70%.

## 2.18 Space clamp

In voltage-clamp experiments, it is assumed that the cell's membrane potential is clamped uniformly at all points distal to the electrode. However, this may not always be the case as injected current will spread radially and decay as an exponential function of distance from the stimulating electrode. This decay is typically expressed as a mathematical constant, the length constant:

$$\lambda = \sqrt{\frac{r_m}{r_i}} \quad \text{Equation 6}$$

Length constant ( $\lambda$ ) is a function of the membrane resistance ( $r_m$ ) and the axial resistance impeding current flow through the cytoplasm ( $r_i$ ). It is defined quantitatively where the steady-state voltage decays to 1/e or 37% of its original value (Boulpaep *et al.*, 2009). Thus, for example, a length constant of 1 mm means that at 1 mm away from the current injection site on the cell, 37% of the voltage magnitude remains.

Commonly, the voltage-clamp is regarded as acceptable if the length of the cell is no more than 1/10 of its length constant. Studies have shown that the length constant for smooth muscle cell is between 1-2 mm (Fry *et al.*, 1999; Casteels *et al.*, 1977; Nagai and Prosser, 1963). Given that the mouse corpus cavernosum smooth muscle cells under study are approximately 45-100  $\mu\text{m}$  in length (Figure 2.8 showing cell on haemocytometer/ruler), artefacts due to inadequate space clamp is unlikely.

Note: Given that the height and length of a CCSM cell is 7.5-10.8  $\mu\text{m}$  (Calculated from Z-slices) and 45-100  $\mu\text{m}$  respectively, the volume of CCSM cell can be estimated. This could be done by assuming the most basic geometrical spindle shape of smooth muscle, which is fundamentally 2 cones stuck together.

Given that the CCSM are typically quite contractile, and that the relationship between cell height and length is inversely proportional, i.e. cell length decrease (contraction) resulting in increased cell height, estimations were made with:

- shortest height x longest length = 1473  $\mu\text{m}^3$
- longest height x shortest length = 1374.3  $\mu\text{m}^3$

Calculations are shown in Figure 2.9.

## **2.19 Leak subtraction**

When whole-cell ionic currents are activated, the measured current is superimposed on a holding or leak current. It is typically caused by current flow from the pipette into the bath through the seal, instead of through the membrane. However, leak channels that are permeable to ions even in an unstimulated or resting state can also contribute to leak current. These leak currents were subtracted from the original traces using Clampfit software.

## 2.20 Statistical analysis

All statistical analysis and curve fitting were performed using GraphPadPrism version 7.0e or version 9.4.1 (GraphPad Software, Inc.) Values are stated as means  $\pm$  SE;  $n$  is the number of animals. All 'n' values quoted refer to individual cells (electrophysiology) or tissue strips (tension) taken from the same number of animals. For data requiring statistical comparisons (electrophysiology and tension) a minimum sample size of  $n = 6$  was chosen, based on previous power calculations and extensive experience. Occasionally, several data points were lost in constructing concentration-effect curves due to loss of the electrical seal, but all points were derived from at least  $n = 5$ . Immunocytochemistry data were not subjected to statistical analysis and were replicated in 5 separate animals for Nav studies and 3 separate animals for TMEM16A studies. Statistical comparisons were made using Student's paired or unpaired  $t$ -test as appropriate, assuming normal distribution of data, on raw (non-normalised) data. The  $V_{1/2}$ 's for activation and inactivation curves for TTX-sensitive and TTX-insensitive currents were compared using extra sum of squares F test in Prism. Multiple comparisons were performed using one way ANOVA for repeated measures with the Dunnett or Tukey post hoc test.  $p < 0.05$  was regarded as statistically significant. All experiments, with the exception of those in Figures 3.4-3.6, employed an *in vitro* within subject (paired samples) experimental model, comparing drug effects with baseline or determining incremental concentration-effect relationships. Randomisation was not considered necessary in such experiments and in some cases would not have been feasible, and not possible as groups were selected based on TTX-sensitivity. Blinding of the operator was not possible because of the knowledge required to run the experimental protocols and because responses observed by the operator to manage the experiment permitted inferences about the treatment. Electrophysiological data were analysed by the operator using pCLAMP software (Molecular Devices) to electronically measure either peak responses found independently by the software or at predetermined time points, therefore blinding was not considered necessary and would have increased the complexity to an extent that could have led to errors. Sigmoidal activation curves were fitted with a Boltzmann equation:  $g/g_{\max} = 1/\{1 + \exp[\pm(V_{1/2} - V_m)/K]\}$ , where  $V_{1/2}$  is membrane potential at which there was half-maximal activation,  $K$  is the slope factor,  $V_m$  is the test potential,  $g$  is conductance, and  $g_{\max}$  is maximal conductance. For Nav currents, conductance ( $g$ ) was

calculated as follows:  $g = I/(V_m - E_{Na})$ , where  $E_{Na}$  is the calculated Nernst potential for  $Na^+$  and  $I$  is the current recorded. Inactivation curves were fitted with a similar Boltzmann function:  $I/I_{max} = 1/\{1 + \exp[\pm(V_{1/2} - V_c)/K]\}$ , where  $I$  is the current recorded at the test step,  $I_{max}$  is the maximal current recorded,  $V_c$  is the conditioning potential (see RESULTS), and  $K$  is the slope factor. Concentration-effect data were fitted with a Hill-Langmuir equation:  $I/I_{control} = 1/\{1 + 10^{(\log[Drug] - \log IC_{50})}\}$ , where  $I$  is the current recorded in the drug,  $I_{control}$  is the current in the absence of drug,  $IC_{50}$  is the half maximal effective concentration, and  $[Drug]$  is the concentration variable. In each case,  $IC_{50}$  is stated, followed by the upper and lower 95% confidence limits (CI, presented in parentheses).

## 2.21 Solutions

Concentrations are stated in millimolar (mM).

- Solution 1: Krebs

NaCl (120), KCl (5.9),  $NaHCO_3$  (25), Glucose (5.5),  $NaH_2PO_4$  (1.2),  $MgCl_2$  (1.2),  $CaCl_2$  (2.5)

pH adjusted to 7.4 using 95%  $O_2$  and 5%  $CO_2$  for 20 minutes.

- Solution 2:  $Ca^{2+}$  free Hanks for cell isolation

NaCl (125), KCl (5.36), Glucose (10), Sucrose (2.9),  $NaHCO_3$  (15.5),  $KH_2PO_4$  (0.44),  $Na_2HPO_4$  (0.33), HEPES (10)

pH adjusted to 7.4 with NaOH.

Osmolarity = 316.49

- Solution 3: Hanks

NaCl (125), KCl (5.36), Glucose (10), Sucrose (2.9),  $NaHCO_3$  (4.17),  $KH_2PO_4$  (0.44),  $Na_2HPO_4$  (0.33),  $MgCl_2 \cdot 6H_2O$  (0.5),  $CaCl_2 \cdot 2H_2O$  (1.8),  $MgSO_4 \cdot 7H_2O$  (0.4), HEPES (10)

pH adjusted to 7.4 with NaOH

Osmolarity = 301.53

- Solution 4: Low  $Na^+$  Hanks

NMDG (116.83), NaCl (8.17), KCl (5.36), Glucose (10), Sucrose (2.9), NaHCO<sub>3</sub> (4.17), KH<sub>2</sub>PO<sub>4</sub> (0.44), Na<sub>2</sub>HPO<sub>4</sub> (0.33), MgCl<sub>2</sub>·6H<sub>2</sub>O (0.5), CaCl<sub>2</sub>·2H<sub>2</sub>O (1.8), MgSO<sub>4</sub>·7H<sub>2</sub>O (0.4), HEPES (10)

pH adjusted to 7.4 with HCL (provides NMDG with 112mM Cl)

Osmolarity = 301.53

Na (13), K (5.8), Cl (134.96), Ca (1.8), Mg (0.9)

- Solution 5: Low Cl Hanks

Na glutamate (86.0), NaCl (39), KCl (5.36), Glucose (10), Sucrose (2.9), NaHCO<sub>3</sub> (4.17), KH<sub>2</sub>PO<sub>4</sub> (0.44), Na<sub>2</sub>HPO<sub>4</sub> (0.33), MgCl<sub>2</sub>·6H<sub>2</sub>O (0.5), CaCl<sub>2</sub>·2H<sub>2</sub>O (1.8), MgSO<sub>4</sub>·7H<sub>2</sub>O (0.4), HEPES (10)

pH adjusted to 7.4 with NaOH.

Na (91.37), Glutamate (86), K (5.8), Cl (48.96)

- Solution 6: Cs<sup>+</sup> whole cell ruptured patch solution ( $E_{Cl}=0$ )

CsCl (132.96), MgCl<sub>2</sub>·6H<sub>2</sub>O (1), EGTA (2), HEPES (10), Na<sub>2</sub>ATP (1), NaGTP (0.1), Na<sub>2</sub>Phosphocreatine (2.5)

pH adjusted to 7.2 with CsOH

Na (7.1), K (132.96), Cl (134.96), Mg (1)

- Solution 7: Cs<sup>+</sup> whole cell perforated patch solution ( $E_{Cl}=0$ )

CsCl (132.96), MgCl<sub>2</sub>·6H<sub>2</sub>O (1), EGTA (0.5), HEPES (10)

pH adjusted to 7.2 with CsOH.

Osmolarity = 279.42

Cs (132.96), Cl (134.96), Mg (1)

- Solution 8: 1xDPBS purchased from Thermofisher Scientific Cat# 14190094
- Solution 9: 4% Paraformaldehyde (PFA): 4 g of PFA (Sigma), 35 mL 5M NaOH, 65 mL 1xDPBS (heated up to 60°C for PFA to dissolve)

## 2.22 Drugs

Drugs were made up in stock solutions, with either water, ethanol, or DMSO. Some drugs were made up fresh daily, while the others were aliquoted and frozen down to maintain stability.

<b>Drugs</b>	<b>Supplier</b>	<b>CAS</b>
2APB	Sigma	524-95-8
4,9-anhydro-TTX	Tocris	13072-89-4
A803467	Abcam	944261-79-4
Ani9	Tocris	356102-14-2
ATP disodium salt hydrate	Sigma	34369-07-8
Atropine	Abcam	51-55-8
CaCCinh-A01	Tocris	407587-33-1
Cyclopiazonic acid	Tocris	18172-33-3
GSK7975A	Sigma	1253186-56-9
ICA-121431	Sigma	313254-51-2
KB-R7943	Tocris	182004-65-5
L-NOARG	Sigma	2149-70-4
NF449	Tocris	627034-85-9
Nifedipine	Tocris	21829-25-4
OD1	SmartTox	NA
PF-05089771	Sigma	1430806-04-4
Phentolamine	Sigma	73-05-2
Phenylephrine	Sigma	61-76-7

Tetracaine	Sigma	94-24-6
TTX	Tocris	18660-81-6
Veratridine	Tocris	71-62-5
$\alpha$ - $\beta$ -methylene-ATP	Tocris	1343364-54-4

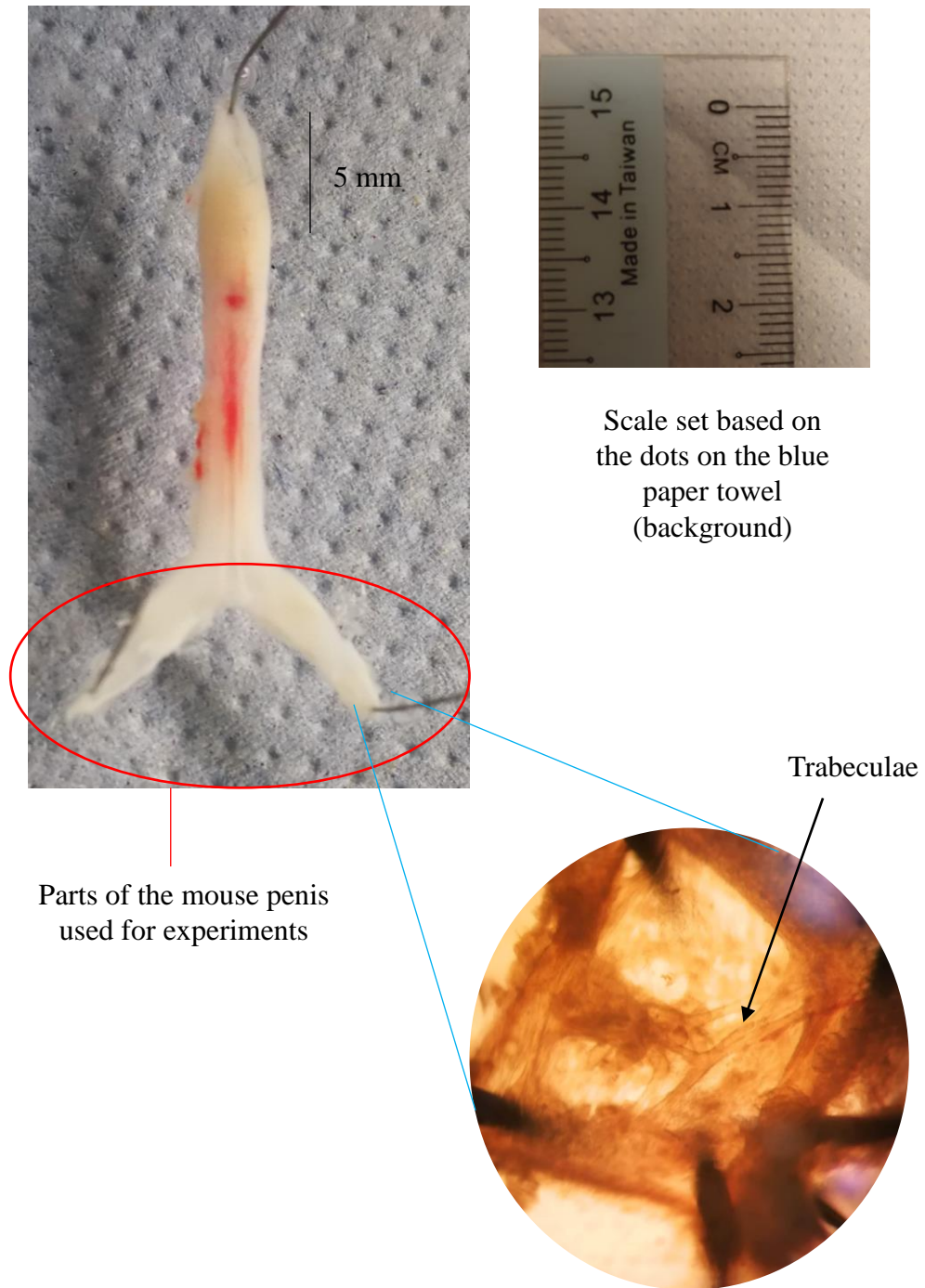


**Figure 2.1: Picture of a mouse penis and the parts used for experiments.** Crura was opened from the proximal end to show trabeculae extending from the surrounding tunica albuginea.

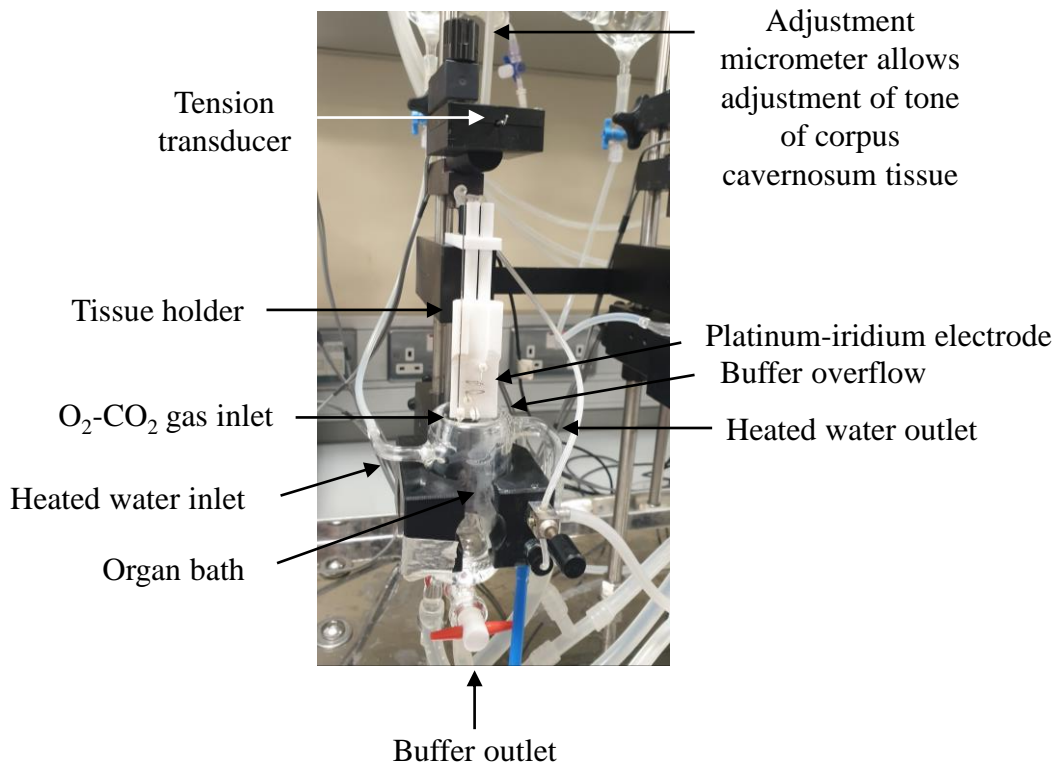
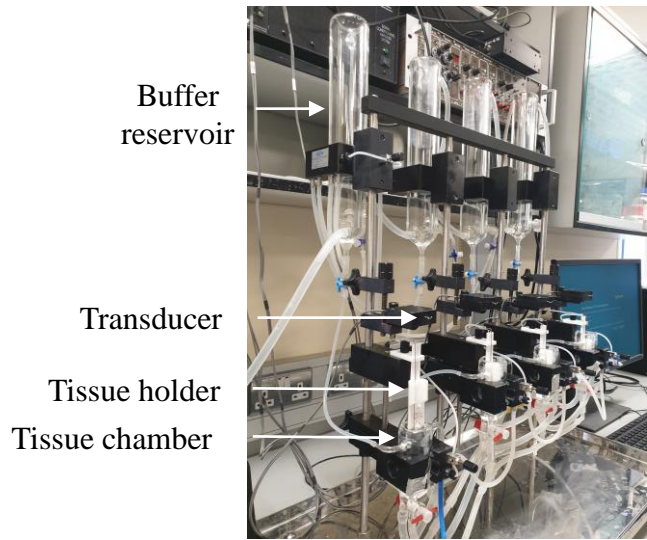


**Figure 2.2: Pictures of isometric tension set-up.**



Example of freshly dispersed corpus cavernosum cell under patching conditions (microscope view)

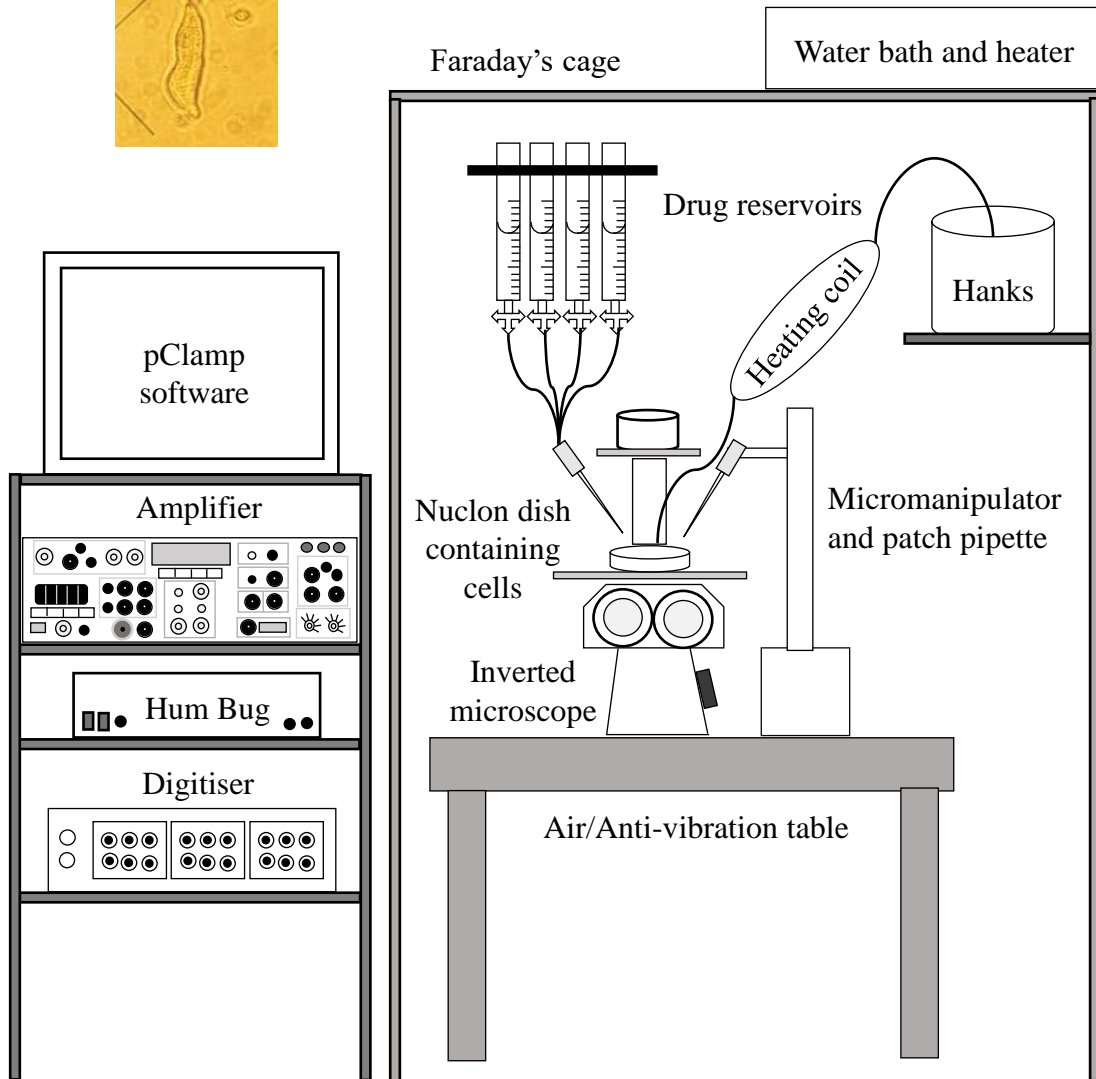


**Figure 2.3: An illustration of apparatus in smooth muscle research centre, DkIT that were used to patch-clamp freshly dispersed mouse corpus cavernosum smooth muscle cells**

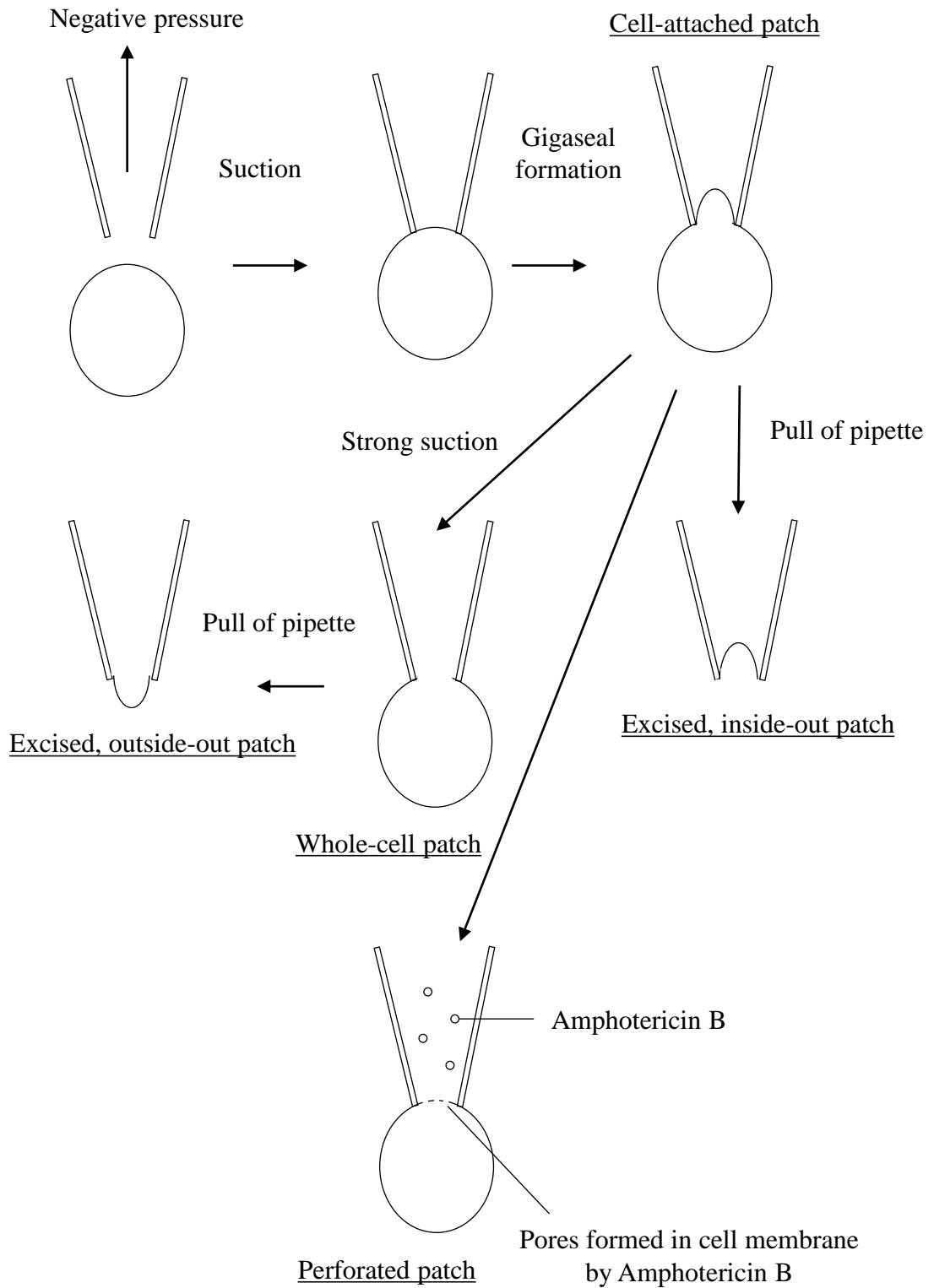


**Figure 2.4: Various patch clamp configurations, indicated with actions needed to progress to each of the configurations.**

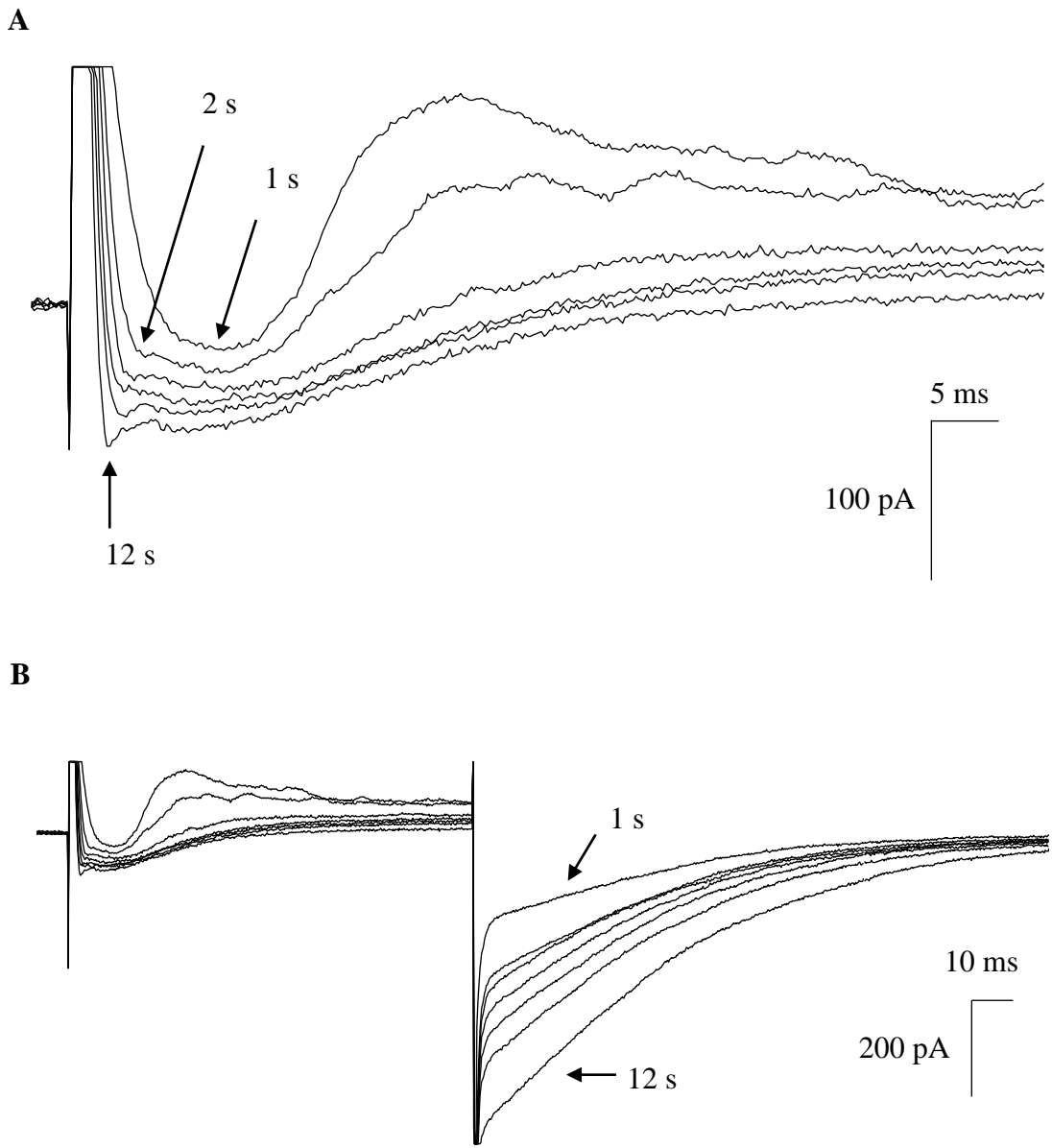


**Figure 2.5: Perforation of the mouse corpus cavernosum smooth muscle cell membrane using amphotericin B in Cs<sup>+</sup> pipette solution. (A)** Traces showing the change from outward current to inward current as electrical access into the cell improves over time. Voltage protocol used was a step from -60 mV to 0 mV for 200 ms. Top trace shows initial outward current 1 s after seal formation. Bottom trace shows a small sharp inward current, followed by a slower inward current 12 s after seal formation **(B)** Traces showing the development of chloride tail current as access improves over time.

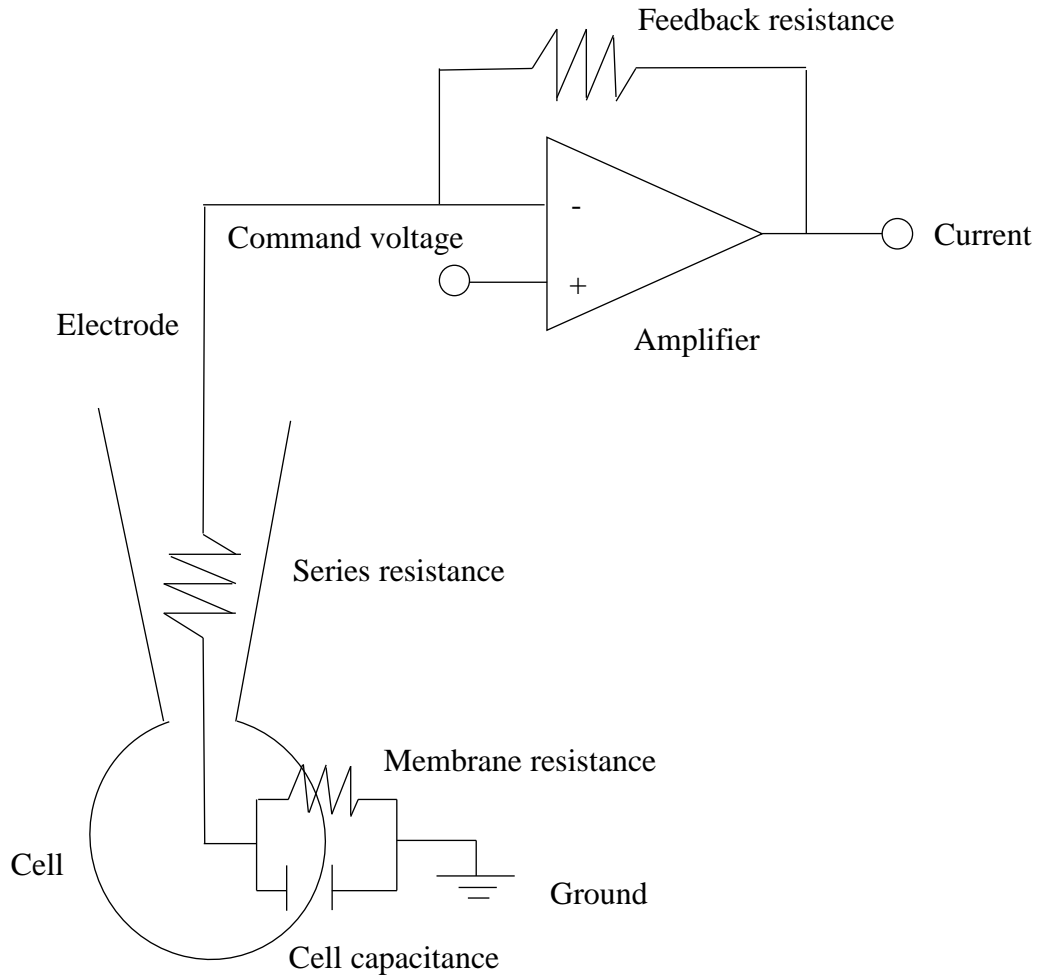


**Figure 2.6: Example of freshly dispersed corpus cavernosum cell under whole cell patch clamp conditions, and its equivalent circuit** (with reference to Ogden and Stanfield, 1994).

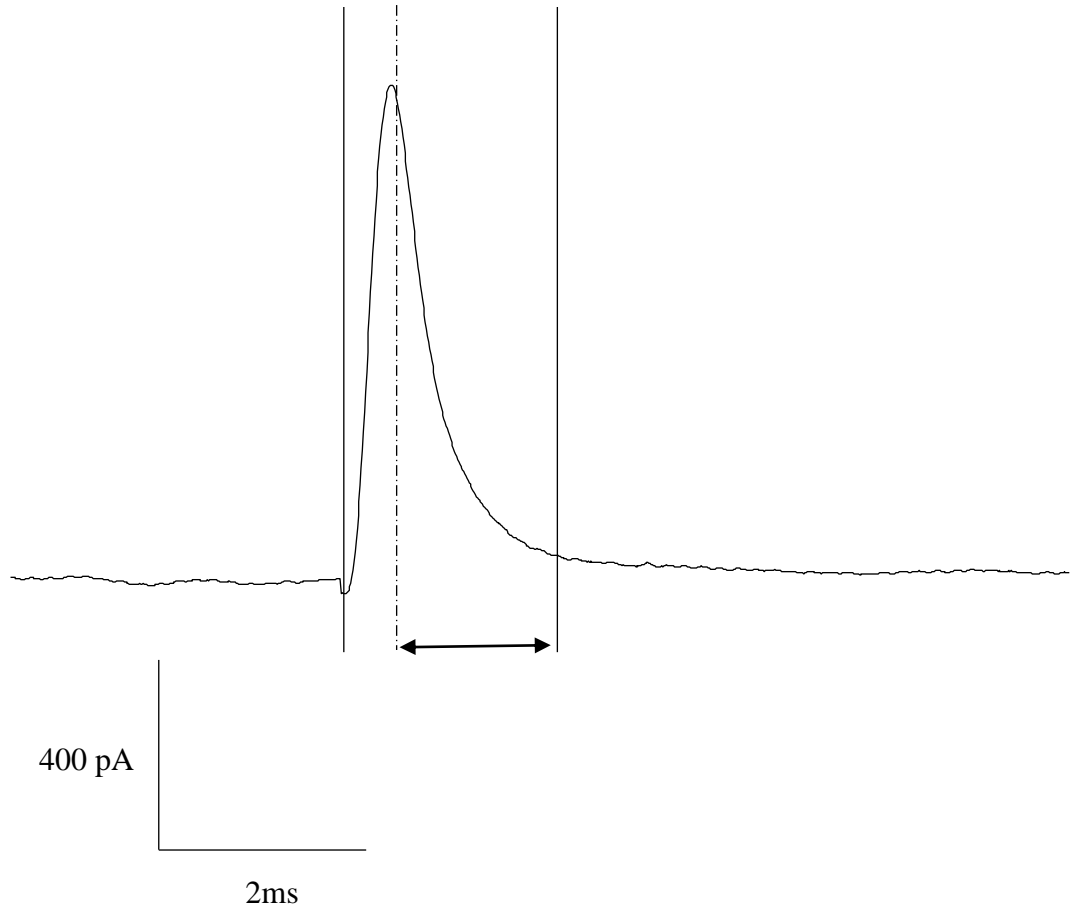
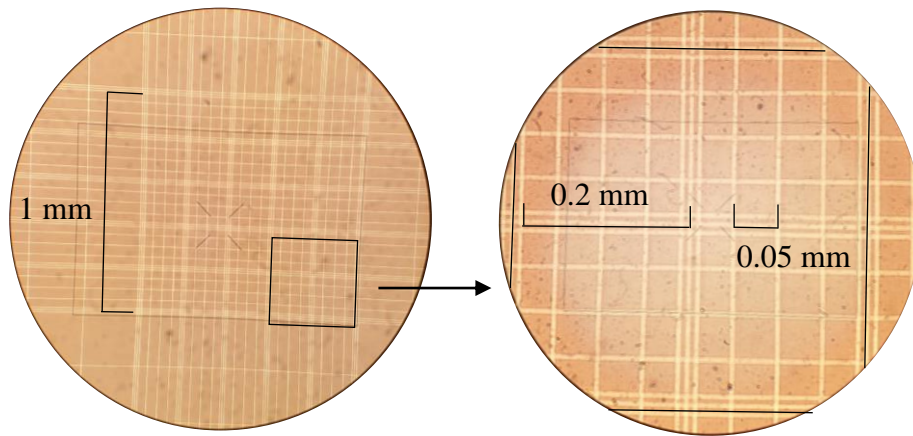


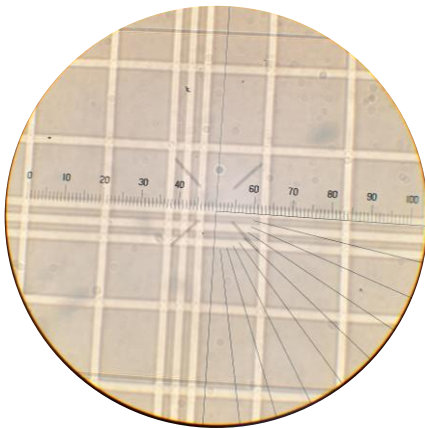
**Figure 2.7: Capacitance transient on a step from -100 to -80 mV from a whole cell ruptured patch recording.** In order to calculate the cell capacitance, the area under the curve was taken between the solid lines. Once the capacitance had been calculated, the exponential part of the same trace was fitted with a tau (between the dotted line and solid line), to calculate the series resistance.

The small initial downward deflection could be an artefact caused by overcompensation of pipette capacitance.

**A**



**Bi**



**Bii**



**Figure 2.8: Length of freshly dispersed, slightly contracted mouse corpus cavernosum smooth muscle cell. (A) Haemocytometer units (Bi) 1 square/0.05 mm is equal to approximately 18 units on ruler scale (Bii) Freshly dispersed mouse corpus cavernosum smooth muscle cells often have slightly contracted morphology. This cell measures to approximately 16 units long, which is approximately 44  $\mu\text{m}$ .**

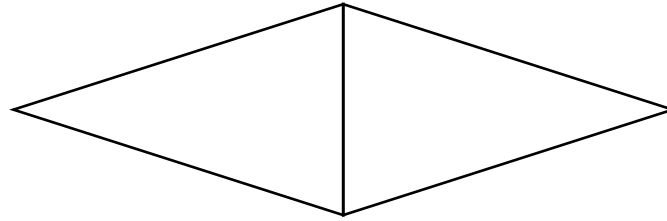


**Figure 2.9: Estimation of CCSM cell volume.**

Assume the most basic geometrical shape of the CCSM: 2 cones.

Assume that the relationship between cell height and length is inversely proportional, i.e. cell length decrease (contraction) results in increased cell height, estimations were made with:

- Volume of shortest height x longest length

$$\begin{aligned}\text{One cone} &= \pi \times r^2 \times h/3 \\ &= \pi \times (7.5/2)^2 \times (50)/3 \\ &= 736.3\end{aligned}$$

$$\begin{aligned}\text{Total volume} &= \text{two cones} \\ &= 736.3 \times 2 \\ &= 1473 \mu\text{m}^3\end{aligned}$$

- Volume of longest height x shortest length

$$\begin{aligned}\text{One cone} &= \pi \times r^2 \times h/3 \\ &= \pi \times (10.8/2)^2 \times (22.5)/3 \\ &= 687.1\end{aligned}$$

$$\begin{aligned}\text{Total volume} &= \text{two cones} \\ &= 687.1 \times 2 \\ &= 1374.3 \mu\text{m}^3\end{aligned}$$

### **Chapter 3: Biophysical properties of Nav currents in CCSM**

### 3.1 Introduction

Failure of the corpus cavernosum to relax results in erectile dysfunction (ED) which, although in the past was largely attributed to psychological factors is now recognised to be due to physical causes in over 80% of cases, with diabetes and vascular disease being the major underlying pathologies (Burnett, 2006). Although phosphodiesterase 5 (PDE5) inhibitors, such as sildenafil, revolutionised the treatment of ED in the 1990s, unfortunately ~30% of cases overall and up to 50% of diabetic patients fail to respond (Costabile, 2009). There is therefore an unmet medical need to identify new treatment targets. One potential starting point is to better understand the physiological processes responsible for the generation of corpus cavernosum contraction and to target these.

CCSM exhibits spontaneous co-ordinated contractions and relaxations, suggesting that the tissue functions as a syncytium. Such phasic activity has been observed in multiple animal models, including the rabbit, cat, and human (Hashitani *et al.*, 2005; Christ *et al.*, 1990; Wagner *et al.*, 1989; Klinge and Sjöstrand, 1977). Mouse and rat corpus cavernosum have been reported as quiescent in some studies (Comerma-Steffensen *et al.*, 2017; Jepps *et al.*, 2016), but phasic contractions have been observed *in vivo* and *in vitro* in other studies (Thornbury *et al.*, 2019; Werner *et al.*, 2005). There is evidence of gap junctions in CCSM (De Carvalho *et al.*, 1993), suggesting that the cells may be electrically coupled to form a single functional unit. Moreover, the rapid spread of excitation observed in tissue slices suggests that the activity may be co-ordinated by membrane depolarisation (Sergeant *et al.*, 2009).

A variety of plasmalemmal ion channels that have the ability to alter membrane potential have been found in corpus cavernosum of a variety of species (for references see Literature Review). The importance of plasmalemmal ion channels in regulating corpus cavernosum contractions has been demonstrated in studies where  $K^+$  channel activators and blockers of L-type  $Ca^{2+}$  channels and  $Ca^{2+}$ -activated  $Cl^-$  channels cause relaxation of phenylephrine-induced and/or spontaneous contractions (Hannigan *et al.*, 2017; Hannigan *et al.*, 2016; Jepps *et al.*, 2016; McCloskey *et al.*, 2009; Kun *et al.*, 2009; Christ *et al.*, 1990). In addition, in transgenic mice, overexpression of endothelial  $K_{Ca2.3}$  channels was found to impair corpus cavernosum contractions, while downregulation of these channels enhanced contractions (Comerma-Steffensen *et al.*, 2017).

Despite the evidence cited above, it is noteworthy that there have been few electrophysiological studies to determine the types of ion channels present in mouse corpus cavernosum, even though the mouse has been widely used as a model for erectile dysfunction in normal and genetically manipulated animals (e.g. Comerma-Steffensen *et al.*, 2017; Luttrell *et al.*, 2008; Werner *et al.*, 2005). We therefore began to characterise the ion channels present in mouse CCSM and were surprised to find voltage-gated sodium ( $\text{Na}_V$ ) currents. Typically,  $\text{Na}_V$  channels are expressed in excitable cells such as cardiac muscle, neurons, and skeletal muscle, where they are involved in action potential generation and propagation. Previously regarded as uncommon in smooth muscle,  $\text{Na}_V$  channels have now been discovered in both spontaneously active ‘phasic’ smooth muscles, as well as some quiescent smooth muscles (see Literature review for references), though they have never previously been found in corpus cavernosum myocytes of any species. Thus, the main aim of this section of the present study was to characterise the biophysical and pharmacological properties of these currents using a combination of patch-clamp electrophysiology and  $\text{Na}_V$ -selective antagonists.

## 3.2 Results

### 3.2.1 Low external sodium abolished the evoked inward current

When freshly dispersed mouse CCSM cells were voltage-clamped at -100 mV and stepped to -20 mV, large transient inward currents, sometimes >600 pA, were obtained (Figure 3.1A). This current peaked within 1-2 ms and then rapidly inactivated. The notion that the transient inward current was carried by Na<sup>+</sup> was affirmed by a 95% reduction in current amplitude when external Na<sup>+</sup> concentration [Na<sup>+</sup>]<sub>o</sub> was reduced from 130 to 13 mM (Figure 3.1B).

### 3.2.2 Reveal of sodium-dependent difference currents

The current-voltage relationship (I-V) of the current was determined by stepping from a holding potential of -60 mV to a 1 s conditioning potential of -100 mV to remove inactivation, followed by a 100 ms test step in the range of -80 mV to -50 mV. This elicited a family of inward currents that activated at voltages positive to -50 mV (Figure 3.2Ai). When [Na<sup>+</sup>]<sub>o</sub> was reduced to 13 mM (solution 4), only the capacitive current and leakage current remained (Figure 3.2Aii). When these were subtracted from the original records, the sodium-dependent difference currents were revealed (Figure 3.2Aiii). A summary of the current-voltage (I-V) relationship of the difference current is shown (Figure 3.2B). The mean peak inward current at -10 mV was  $-601 \pm 204$  pA.

### 3.2.3 Reversal potential of sodium-dependent difference currents

By performing extracellular sodium substitution experiments, it has been shown that the channel was mostly permeable to Na<sup>+</sup> ions. Therefore, it was desirable to demonstrate a reversal potential for the sodium-dependent difference current to authenticate its ionic identity as a Na<sup>+</sup> ion.

The reversal potential ( $V_{eq}$ ) of sodium currents in CCSM cells can be calculated using the Nernst equation (Equation 7), where R is the universal gas constant (J/mol/K), T is the

absolute temperature (K), F is Faraday constant (C/mol),  $[X]_o$  is the extracellular ion concentration, and  $[X]_i$  is the intracellular ion concentration.

$$V_{eq} = \frac{RT}{zF} \ln \frac{[X]_o}{[X]_i} \quad \text{Equation 7}$$

$$V_{eq} = \frac{8.314(295.15)}{1 \times 9.649 \times 10^4} \ln \frac{129.83}{7.1}$$

$$V_{eq} = +74 \text{ mV}$$

This value reasonably corresponds to the membrane potential of +80 mV where there is zero current, based on extrapolation of the I-V plot for the sodium-dependent difference currents in Figure 3.2B. It should, however, be noted that the extrapolation was carried out manually, so the intersection of the curve with the X-axis is an approximation.

Ideally, instead of extrapolation, the voltage protocol could be changed to include more positive steps. However, it is practically very difficult as loss of seal and access are likely to occur. Furthermore, after peaking, the current declined towards the expected reversal potential linearly. Hence, extrapolating is likely to be acceptable.

### 3.2.4 Biophysical properties of the sodium current

Steady-state voltage-dependent inactivation was characterised by subjecting cells to a series of 1 s conditioning pulses from -120 to -20 mV, before stepping to a test potential of -20 mV for 200 ms. Representative traces from one CCSM cell are shown in Figure 3.3A, where inactivation was already evident following conditioning at -100 mV, was approximately half-maximal at -80 mV and complete at -40 mV. The mean steady-state inactivation curve was determined from 11 cells by plotting currents evoked at the test potential, expressed as a function of the maximum available current, against the conditioning potential (Figure 3.3B, filled circles). The mean steady-state activation curve was derived from the I-V protocols in 18 cells by plotting normalised conductance

( $g/g_{max}$ ) against the test potential ( $V_m$ ), also shown in Figure 3.3B (open circles). Data points were fitted with a Boltzmann function, yielding an inactivation  $V_{1/2}$  of  $-75 \pm 1$  mV and an activation  $V_{1/2}$  of  $-35 \pm 1$  mV (Figure 3.3B). The two curves overlapped from -60 to -30 mV, resulting in a small but sustained inward current (window current).

### 3.2.5 TTX sensitivity reveals the presence of $\geq$ two populations of Nav current

In an effort to determine the molecular identity of the Nav  $\alpha$ -subunit that carries the Na<sup>+</sup> current, its sensitivity to TTX was first examined. Currents were evoked at 15 s intervals in cells held at -60 mV, stepped down to -100 mV for 2 s to remove inactivation and then stepped to a test pulse of -20 mV for 100 ms, before repolarising to -80 mV for 30 ms. Interestingly, based on TTX-sensitivity, there were two populations of Nav currents, designated 'TTX-sensitive' and 'TTX-insensitive'.

Since most cells expressed a mixture of these currents, in order to determine the TTX-sensitivity of each component, cells were separated into two groups, based on the effect of 100 nM TTX either blocking  $\geq 70\%$  of current ('TTX-sensitive') or  $\leq 30\%$  of the current ('TTX-insensitive'). Cells that expressed more even proportions of the currents were rejected from the analysis.

TTX reduced the current amplitude in each group in a concentration-dependent manner, albeit over different concentration ranges (Figure 3.4A and B). In the example in Figure 3.4A, approximately half of the current was blocked by 10 nM TTX. In contrast, in the cell in Figure 3.4B, a similar reduction in current was only achieved at 1  $\mu$ M. In Figure 3.4B, there was bunching of the currents recorded at the 30 and 100 nM concentrations, suggesting a biphasic response and that the net current contained two components.

The mean concentration-effect curves for each group are shown in Figure 3.4C. In the 'TTX sensitive group', the mean  $IC_{50}$  was 12 nM (95% CI ranged from 9 to 18 nM), while in the 'TTX-insensitive' group, the curve was best fitted with a biphasic Hill-Langmuir equation, with  $IC_{50}$ s of 14 nM and 650 nM (95% CI ranged from 6 nM to 26 nM and 437 nM to 2.5  $\mu$ M, respectively), respectively.

### 3.2.6 Voltage-dependent kinetics of TTX<sub>sens</sub> and TTX<sub>insens</sub> currents

The possibility that the two populations of cells defined by their TTX-sensitivity had different voltage-dependent kinetics was studied by repeating the activation and inactivation protocols described in Figure 3.2 and 3.3. As described earlier in Section 3.2.5, TTX was first applied to categorise the currents into TTX-sensitive and TTX-insensitive groups. Then, the drug was washed out prior to application of activation and/or inactivation protocols.

To study the activation kinetics of TTX-sensitive and TTX-insensitive currents, I-V protocols described in Figure 3.2 were repeated. A summary of the current-voltage (I-V) relationship of the TTX-sensitive and TTX-insensitive currents is shown (Figure 3.5B). The amplitudes of the TTX-insensitive currents were, on average, larger than those of the TTX-sensitive currents. Their activation  $V_{1/2s}$  were also dissimilar, at  $-28 \pm 1$  mV and  $-39 \pm 1$  mV for the TTX-sensitive and -insensitive currents, respectively (Figure 3.5B). The difference was statistically significant,  $p < 0.05$ . The currents in Figure 3.5 reversed at +30 mV, while in Figure 3.2 they reversed at +80 mV. This is because in Figure 3.2 they were Na<sup>+</sup>-dependent difference currents, uncontaminated by other ion fluxes, especially outward movement of K<sup>+</sup> as they were blocked by Cs.

The inactivation curve for TTX-insensitive current was shifted to the left ( $-78 \pm 1$  mV) compared to TTX-sensitive current ( $-71 \pm 1$  mV; Figure 3.6). The difference was statistically significant,  $p < 0.05$ . However, the time-dependence of inactivation, measured at -20 mV, was similar for the two groups ( $\tau = 1.69 \pm 0.19$  ms and  $1.70 \pm 0.25$  ms for TTX insensitive and TTX-sensitive, respectively,  $n=7$ ).

These findings suggest that the two populations of Nav current can be separated based on their steady-state voltage-dependent activation and inactivation kinetics. The proportions of cells falling into each category with regard to TTX sensitivity were measured in a sample of 48 cells. Of these, 36 expressed Na<sup>+</sup> current, 21 of which were of 'mixed sensitivity', 10 were in the 'TTX-sensitive' group and 5 were in the 'TTX-insensitive' group.

### 3.2.7 Effect of subtype-specific Nav inhibitors on TTX<sub>sens</sub> current

The effect of three Nav  $\alpha$ -subunit-specific blockers (ICA-121431, PF-05089771 and 4,9-anhydro-TTX) on TTX-sensitive currents were examined. ICA-121431 is a potent, state-dependent inhibitor of Nav<sub>v</sub>1.3 (IC<sub>50</sub> 13 nM) and Nav<sub>v</sub>1.1 (IC<sub>50</sub> 23 nM) channels (McCormack *et al.*, 2013). It also blocks Nav<sub>v</sub>1.2 at higher concentrations (IC<sub>50</sub> 240 nM; McCormack *et al.*, 2013). PF-05089771 is a potent, state-dependent, and selective inhibitor of Nav<sub>v</sub>1.7 channels with an IC<sub>50</sub> of 11 nM (Alexandrou *et al.*, 2016) and 4,9-anhydro-TTX is a potent and selective blocker of Nav<sub>v</sub>1.6 with an IC<sub>50</sub> of 7.8 nM (Rosker *et al.*, 2007). Maximal concentrations of these drugs (At least three times the IC<sub>50</sub> of the drugs) were used to screen for the relevant subtypes.

The protocol used to examine the effect of ICA-121431 and PF-05089771 was amended, based on those used by Alexandrou *et al.* (2016) and McCormack *et al.* (2013). CCSM cells were clamped at -100 mV before stepping to -80 mV for 5 seconds to promote compound binding. This was followed by a brief (2 ms) return to -100 mV, before the test step to -20 mV for 20 ms. Both ICA-121431 (1  $\mu$ M) and PF-05089771 (100 nM) caused variable, though usually small, reductions in the amplitude of the TTX-sensitive current, as shown in Figure 3.7A and Figure 3.8A and in summary data in Figure 3.7B and 3.8B. On average, ICA-121431 and PF-05089771 blocked the current by 30% (range 9-52%) and 18% (range 6-50%), respectively.

Application of 30 nM 4,9-anhydro-TTX, which would be expected to block Nav<sub>v</sub>1.6 completely, only produced a 12% (range 0-26%) reduction of the TTX-sensitive currents (Figure 3.9A and B).

Overall, these subtype-specific drugs suggested that several Nav subtypes are responsible for the 'TTX-sensitive current'. To test the possibility that the subtypes Nav<sub>v</sub>1.1, 1.2, 1.3, 1.6, 1.7. all contributed to the TTX-sensitive current, ICA-121431 (1  $\mu$ M), PF-05089771 (100 nM) and 4,9-anhydro-TTX (30 nM) were added cumulatively to 6 cells expressing the 'TTX-sensitive' current. An example is shown in Figure 3.10A, where ICA-121431 reduced the current by 32%. Cumulative addition of PF-05089771 (100 nM), followed by 4,9-anhydro-TTX (30 nM) resulted in an overall block of 48%. Cumulative addition of TTX (100 nM) resulted in almost complete block of the remaining current, confirming

that a substantial proportion of ‘TTX-sensitive’ current was resistant to these blockers. Summary data for 6 cells confirmed this point (Figure 3.10B).

### **3.2.8 Effect of A803467 on CCSM TTX<sub>insens</sub> current and HEK Nav1.5 current**

A803467 is a potent and selective blocker for Nav<sub>v</sub>1.8, a TTX-insensitive Nav<sub>v</sub> subtype (Catterall *et al.* 2005), with an IC<sub>50</sub> of 8 nM (Jarvis *et al.*, 2007). Its effect was tested on TTX-insensitive currents in isolated CCSM cells (Figure 3.11Ai) over the concentration range of 100 nM - 30 μM. Currents were not affected by the application of 100 nM A803467, suggesting that the TTX-insensitive current in CCSM was not mediated by Nav<sub>v</sub>1.8. However, it was noticeable that the currents were reduced by the application of higher concentrations (1-30 μM) of A803467. As the TTX-insensitive Nav<sub>v</sub> in CCSM cells was suspected to be Nav<sub>v</sub>1.5, the effect of A803467 on currents recorded from HEK-293 cells over-expressing Nav<sub>v</sub>1.5 was compared to native TTX-insensitive currents in CCSM cells. Figure 3.11Aii shows that A803467 reduced the Nav<sub>v</sub>1.5 current over a similar concentration range to the native TTX-insensitive current in CCSM cells. Summary data for the effect of A803467 on the TTX-insensitive current in CCSM cells and Nav<sub>v</sub>1.5 current in HEK cells are shown in Figure 3.11B, where A803467 yielded an IC<sub>50</sub> of 1.6 μM in CCSM cells (95% CI range from 978 nM to 2.4 μM) and 1.6 μM for Nav<sub>v</sub>1.5 (95% CI range from 878 nM to 2.8 μM).

### **3.2.9 Effect of OD1 on CCSM TTX<sub>sens</sub> and TTX<sub>insens</sub> current and HEK Nav1.5 current**

The scorpion toxin, OD1, is a potent activator of Nav<sub>v</sub>1.7 and, to a lesser extent, other TTX-sensitive currents (Nav<sub>v</sub>1.4 and Nav<sub>v</sub>1.6), but only weakly affects Nav<sub>v</sub>1.5 (Jalili *et al.* 2005; Durek *et al.* 2013). Therefore, to further differentiate between the currents in CCSM, the effects of OD1 (50 nM) on the TTX-sensitive current, the TTX-insensitive current, and Nav<sub>v</sub>1.5 expressed in HEK-293 cells were compared.

OD1 significantly increased the amplitude of the TTX-sensitive current (Figure 3.12A) but had little effect on the time constant (tau) of inactivation. In 6 cells, the mean

amplitude changed from  $-278.5 \pm 118.9$  pA to  $-398.1 \pm 37.7$  pA in the presence of OD1. The changes in amplitude for the 6 individual cells are shown in Figure 3.12B. The mean tau of inactivation changed only slightly from  $2.1 \pm 0.03$  to  $2.6 \pm 0.7$  ( $p < 0.05$ , paired t test).

OD1 did not affect the amplitude of the TTX-insensitive current or Nav1.5 in HEK-293 (Figure 3.13A and B, summarised for 6 cells in each case in Figure 3.13Ci and Cii). It did, however, prolong the time-dependent inactivation of the latter two currents (Figure 3.13A and B). In the controls, both currents were well fitted with a single exponential ( $\tau = 2.02 \pm 0.2$  and  $0.86 \pm 0.03$  for CCSM and Nav1.5, respectively;  $r > 0.9$ ) [Table 3.1]. In the presence of OD1, the inactivation became biphasic with tau values of  $2.03 \pm 0.3$  ms and  $14.6 \pm 1.4$  ms ( $r > 0.9$ ) for CCSM TTX-insensitive current and  $0.80 \pm 0.03$  ms and  $7.941 \pm 0.3$  ms ( $r > 0.9$ ) ms for Nav1.5 in HEK-293 cells [Table 3.1].

### 3.3 Discussion

The expression of Nav channels has sometimes been found in cultured smooth muscle cells, but not in freshly dispersed cells from the same tissue (see Berra-Romani *et al.*, 2005). However, in freshly dispersed rat mesenteric artery, Nav current was critically dependent upon the enzymatic digestion procedure, where inclusion of papain was severely detrimental (Berra-Romani *et al.*, 2005). In rabbit bronchial myocytes, Nav1.5-mediated currents disappeared after 10-15 min exposure to papain (Bradley *et al.*, 2013). Thus, the relatively gentle dispersal procedure used in the present study may account for the fact that robust Nav currents were preserved in the majority of CCSM cells.

At least two sub-types of Nav currents were distinguished on the basis of TTX sensitivity: 'TTX-sensitive' and 'TTX-insensitive'. In the former, TTX IC<sub>50</sub> was 10 nM, suggesting that it could have been mediated by one or more of the Nav1.1-1.4, 1.6 or 1.7  $\alpha$ -subunits, all of which have a TTX-sensitivity in the nanomolar range (Catterall *et al.*, 2005). In contrast, Nav1.5 has a TTX IC<sub>50</sub> of 1-2  $\mu$ M (Catterall *et al.*, 2005), close to the value of 672 nM obtained for the TTX-insensitive current in the present study, bearing in mind it was contaminated by up to 30% with the TTX-sensitive component. It is, therefore, likely that this current was mediated by Nav1.5 channels.

Indeed, the other two TTX-insensitive Nav subtypes, 1.8 and 1.9, are too insensitive (IC<sub>50</sub>, 40-60  $\mu$ M) to be considered likely candidates. Furthermore, the Nav1.8 specific blocker, A803467, exerted little effect on the TTX-insensitive current, except at high concentrations, where it had a similar effect on Nav1.5 expressed in HEK-293 cells. No specific blocker has yet been developed for Nav1.9, but this channel demonstrates very slow time-dependent inactivation ( $\tau = 10\text{s} - 100\text{s}$ ) compared to the fast inactivation of Na current ( $\tau = 1.3\text{ ms}$ ) seen in the present study (Lin *et al.*, 2016; Catterall *et al.*, 2005).

The above components of current were further characterised by examining their reaction to OD1, which is known to activate several TTX-sensitive Nav subtypes including Nav1.7, Nav1.4 and Nav1.6, while having a weak effect on Nav1.5. In CCSM, 50 nM OD1 increased the amplitude of the TTX-sensitive current but failed to do so for either the TTX-insensitive current in CCSM or for Nav1.5 expressed in HEK-293 cells. For TTX-insensitive current and Nav1.5, the effects were very similar, with the emergence of a slow component of time-dependent inactivation in each case.

We attempted to further characterise the TTX-sensitive component of current in CCSM using three Nav-subtype selective blockers, ICA-121431 (Nav1.1-1.3), 4,9-anhydro-TTX (Nav1.6) and PF-05089771 (Nav1.7). These reduced currents by 30%, 12% and 18%, respectively and, when added together, caused an overall block of ~48%. It seems surprising that PF-05089771 did not exert more effect in CCSM, since Nav1.7 has been commonly found in other vascular myocytes (Rice *et al.*, 2015; Meguro *et al.*, 2009; Saleh *et al.*, 2005). As there is no available Nav1.4 specific blocker, it was not possible to directly evaluate its contribution. Overall, it is likely that the TTX-sensitive component of Nav in our experiments was mediated by a mixture of TTX-sensitive Nav subtypes.

The whole cell Nav current inactivation and activation curves intersected at -50 mV, and the area under the intersection ranged from -60 mV to -30 mV. This range of potentials defines the 'window current', where a small proportion of Nav channels remain continuously open (Doisne *et al.*, 2020). In the heart, several mutations of Nav1.5 result in a negative shift in the 'window current', such that it is generated at the resting potential, leading to hyperexcitability and premature contractions (Doisne *et al.*, 2020). To date, only two studies have recorded the resting membrane potential in CCSM with intracellular microelectrodes (Thornbury *et al.*, 2019; Hashitani *et al.*, 2005), reporting it between -60 and -40 mV, similar to the range of the Nav window current.

To summarise the findings of this chapter, we have demonstrated the presence of at least two components of fast, voltage-dependent sodium current in mouse CCSM myocytes.

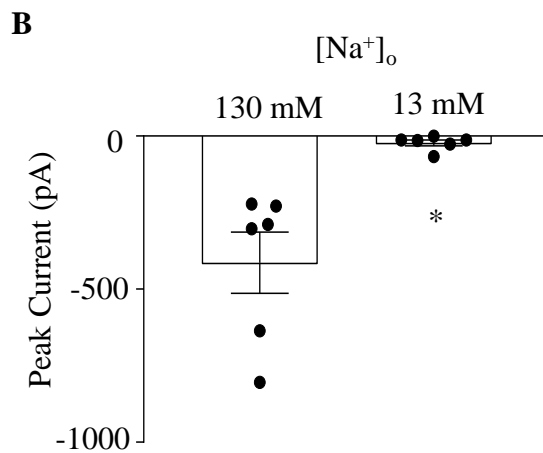
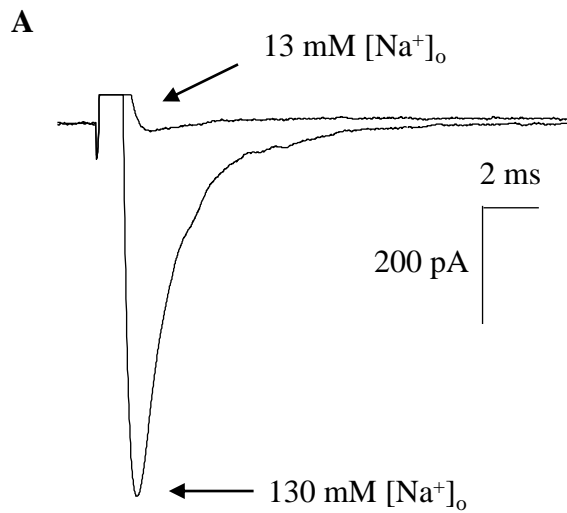


**Figure 3.1: Low external sodium abolished the evoked inward current. (A)** Representative traces showing current evoked on stepping from -100 to -20 mV at extracellular sodium concentrations of 130 and 13 mM. **(B)** Summary data showing 95% current reduction when external sodium concentration was reduced from 130 to 13 mM (n = 6 from 6 animals, \*p<0.05, paired t test).

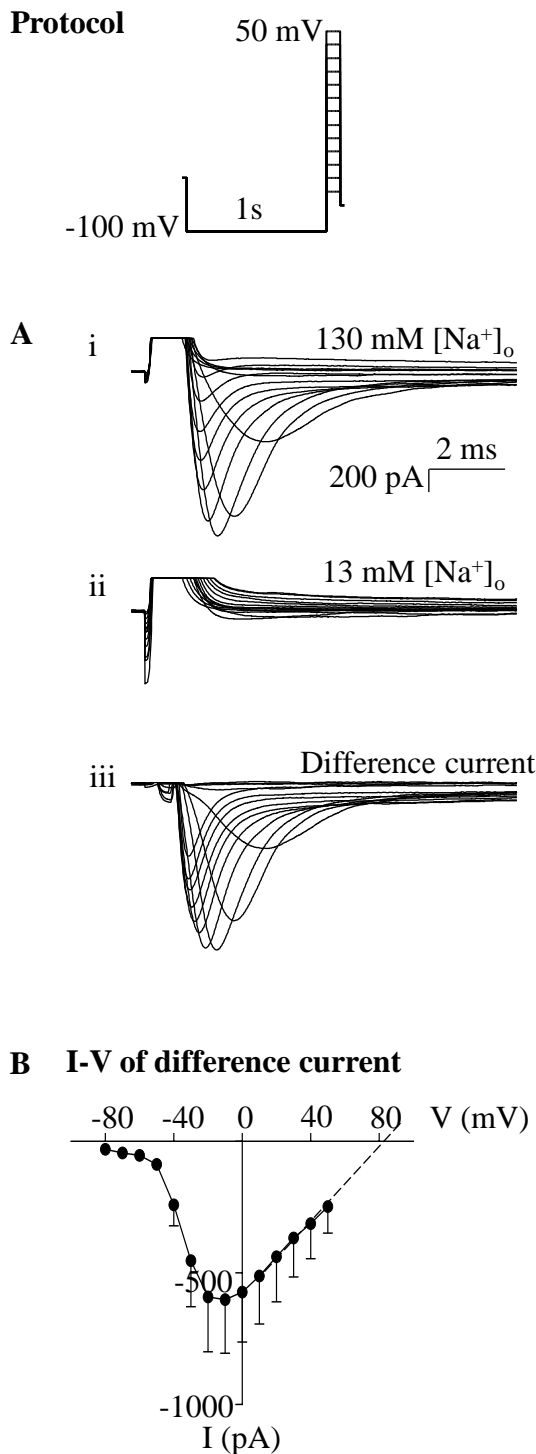


**Figure 3.2: Reveal of sodium-dependent difference currents.** (A) i. Traces showing a family of inward current evoked from -100 mV to test potentials of -80 to +50 mV in 10 mV increments: ii. currents at all voltages were abolished when perfused with 13 mM external sodium; iii. sodium-dependent difference currents revealed through subtraction of currents in ii from i. Inward deflection seen at the beginning of each traces is likely to be an artifact. (B) Summary of current-voltage (I-V) relationship of the sodium-dependent difference currents ( $n = 6$  from 6 animals; shown as mean  $\pm$  SEM, dotted line is extrapolated line).

### Protocol

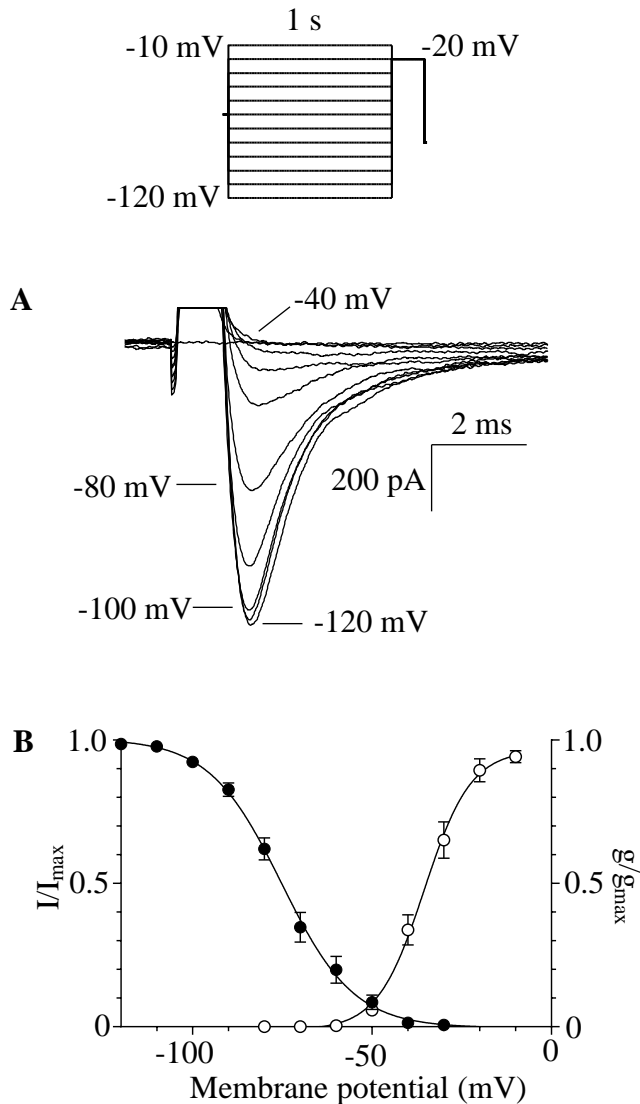


**Figure 3.3: Biophysical properties of the sodium current.** (A) Representative traces showing current obtained from a CCSM cell by stepping from a range of conditioning potentials (-120 to -20 mV) to a -20 mV test potential. Only currents recorded at the test potential are shown. The potentials (-120, -100, -80 & -40 mV) refer to the prior conditioning potential to which the cell was subjected. The current was approximately half-maximally inactivated following a conditioning potential of -80 mV. (B) Summary inactivation and activation curves for CCSM cells. Data points were fitted with the Boltzmann equation and produced an activation  $V_{1/2}$  of  $-35 \pm 1$  mV (white circles,  $n = 18$  from 18 animals) and an inactivation  $V_{1/2}$  of  $-75 \pm 1$  mV (black circles,  $n = 11$  from 11 animals). The curves intersected at -50 mV, allowing a small window current between -60 and -40 mV.

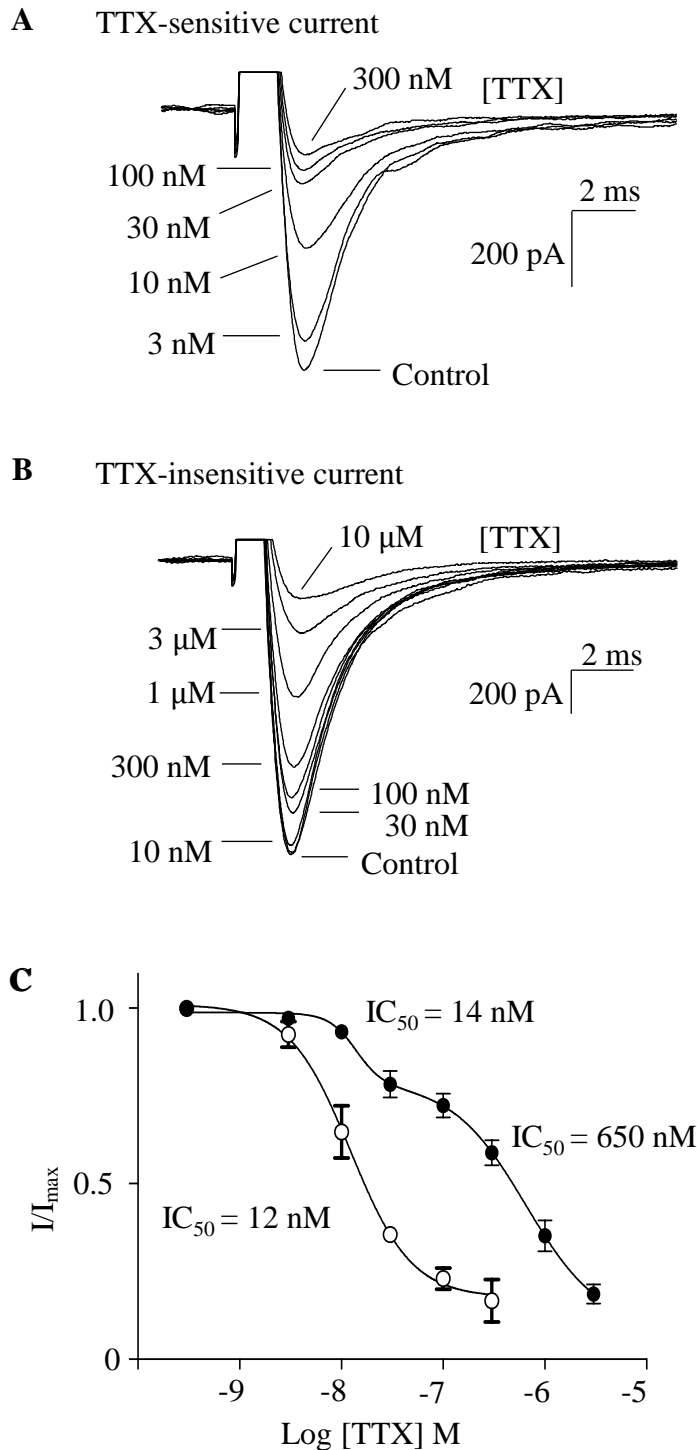


**Figure 3.4: Application of tetrodotoxin (TTX) revealed at least two populations of sodium current.** Representative traces showing (A) TTX-sensitive current and (B) TTX-insensitive current in two different CCSM cells. (C) Cells were categorised (see text) as either TTX-sensitive (open circles,  $n = 6-7$  from 7 animals) or TTX-insensitive (filled circles,  $n = 5-6$  from 6 animals). Solid lines show fits with the Hill-Langmuir equation.

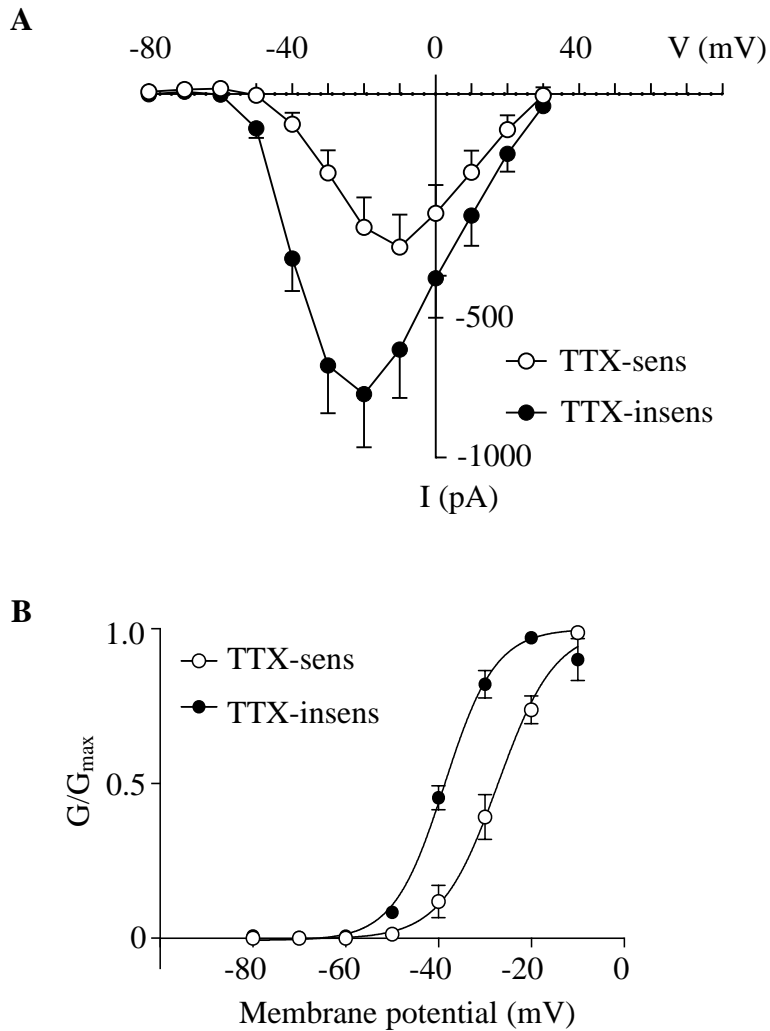


**Figure 3.5: Steady-state voltage-dependence of activation of the two populations of sodium current.** (A) Summary of current-voltage (I-V) relationship of TTX-sensitive ( $n = 10$  from 10 animals) and TTX-insensitive current ( $n = 6$  from 6 animals). (B) The two populations of sodium current had dissimilar activation properties, where TTX-sensitive and TTX-insensitive current had  $V_{1/2}$  of  $-27 \pm 1$  mV ( $n = 10$  from 10 animals) and  $-39 \pm 1$  mV ( $n = 7$  from 7 animals), respectively. This difference was significant ( $*p < 0.05$ , extra sum of squares F test).

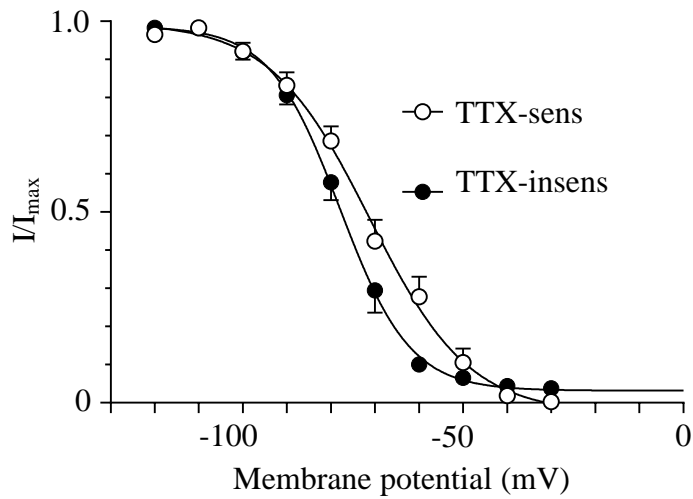


**Figure 3.6: Steady-state voltage-dependence of inactivation of the two populations of sodium current.** The two populations of sodium current had dissimilar inactivation properties, where TTX-sensitive and TTX-insensitive current had  $V_{1/2}$  of  $-71 \pm 1$  mV ( $n = 7$  from 7 animals) and  $-78 \pm 1$  mV ( $n = 7$  from 7 animals), respectively. This difference was significant ( $*p < 0.05$ , extra sum of squares F test).

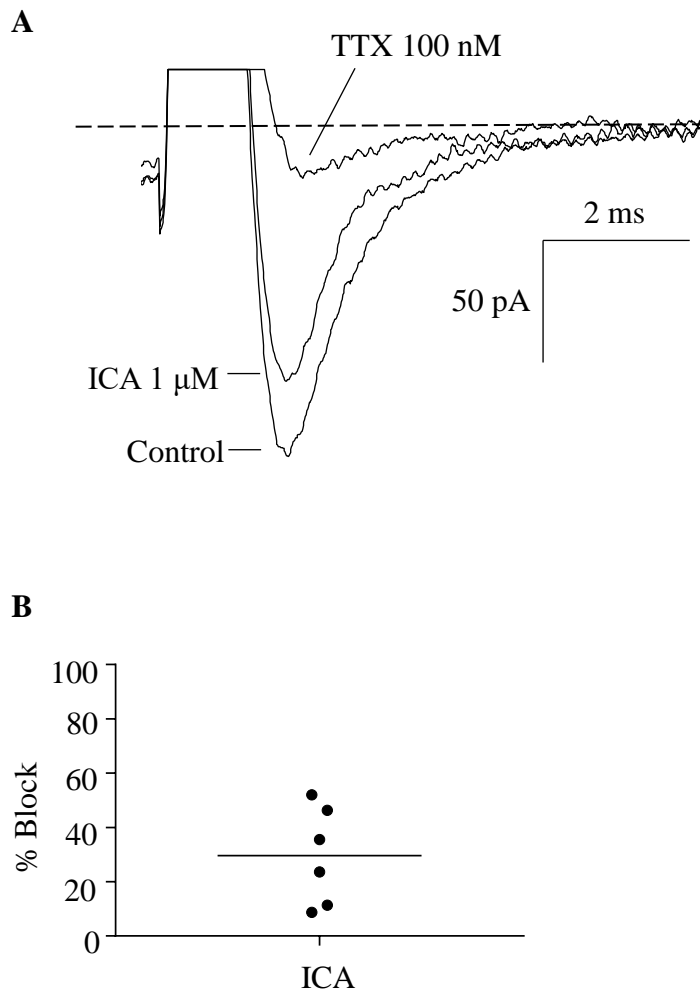


**Figure 3.7: Effect of subtype specific  $\text{Na}_v$  inhibitor, ICA-121431, on TTX-sensitive current. (A)** Representative traces showing the effect of 1  $\mu\text{M}$  ICA-121431 (ICA) on TTX-sensitive current. **(B)** Summary data showing the effect of 1  $\mu\text{M}$  ICA-121431 ( $n = 7$  from 7 animals;  $*p < 0.05$ ).

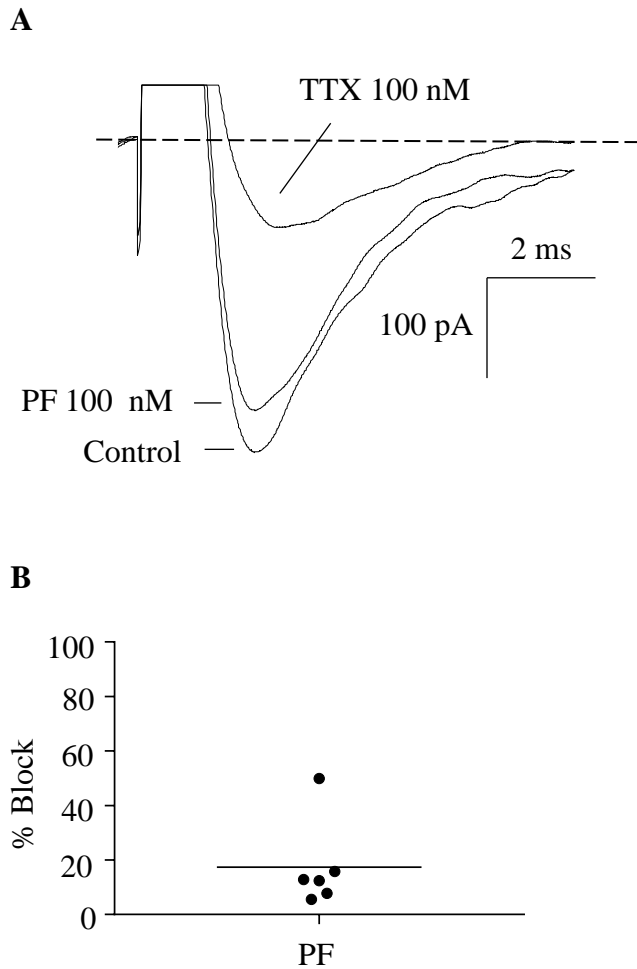


**Figure 3.8: Effect of subtype specific  $\text{Na}_v$  inhibitor, PF-05089771, on TTX-sensitive current. (A)** Representative traces showing the effect of 100 nM PF-05089771 (PF) on TTX-sensitive current. **(B)** Summary data showing the effect of 100 nM PF-05089771 ( $n = 6$  from 6 animals;  $*p < 0.05$ ).

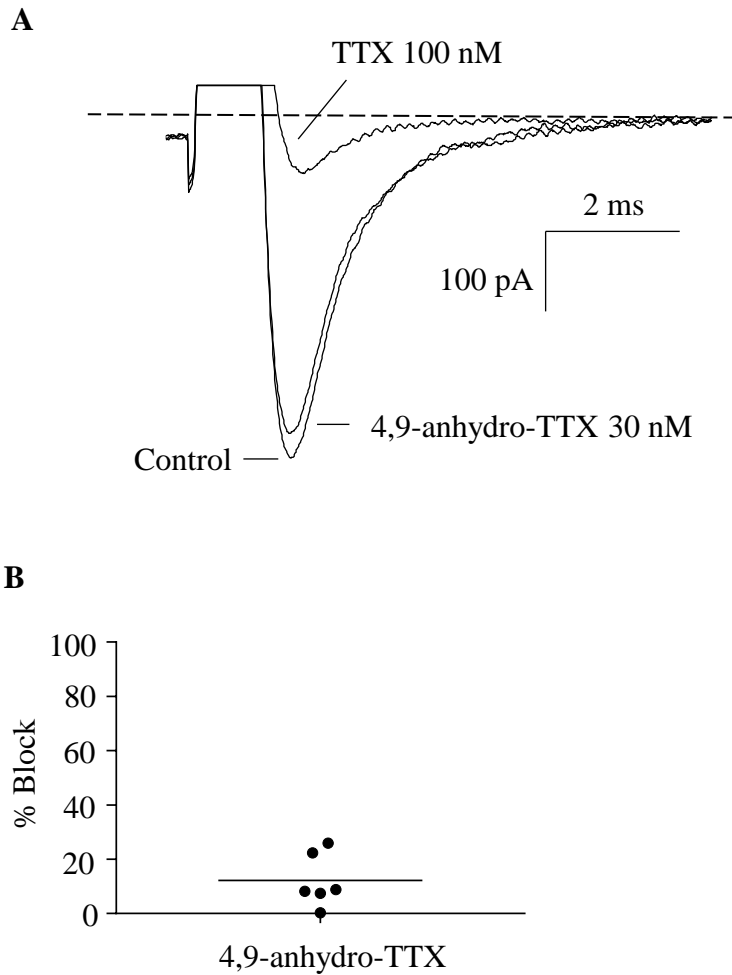


**Figure 3.9: Effect of subtype specific  $\text{Na}_v$  inhibitor, 4,9-anhydro-TTX, on TTX-sensitive current. (A)** Representative traces showing the effect of 30 nM 4,9-anhydro-TTX on TTX-sensitive current. **(B)** Summary data showing the effect of 30 nM 4,9-anhydro-TTX ( $n = 6$  from 6 animals;  $*p < 0.05$ ).

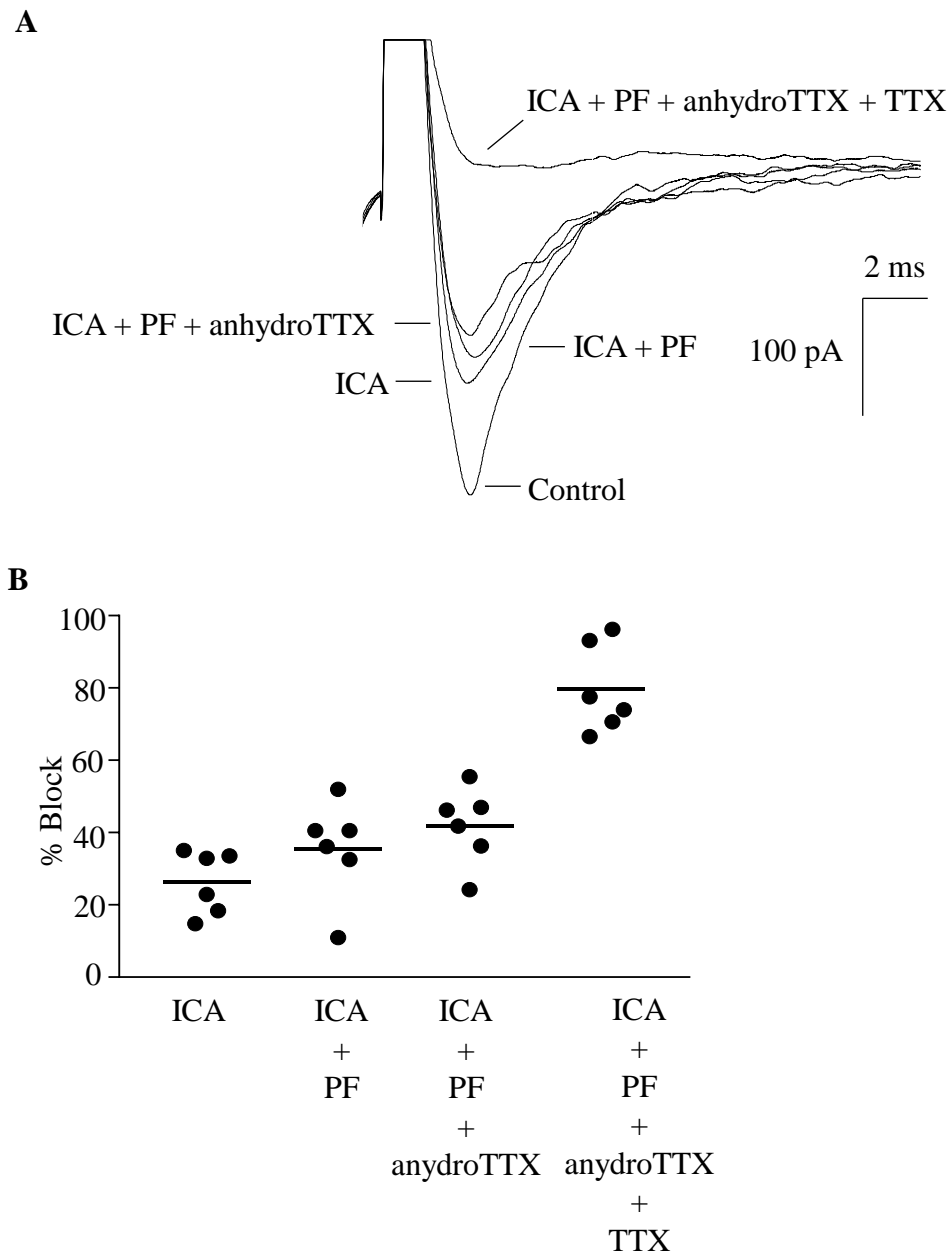


**Figure 3.10: Effect of cumulative addition of subtype-specific  $\text{Na}_v$  inhibitors on TTX-sensitive current.** (A) Representative traces showing the effect of cumulative addition of subtype-specific  $\text{Na}_v$  inhibitors on TTX-sensitive current. (B) Summary data showing the effect of cumulative addition of subtype-specific  $\text{Na}_v$  inhibitors on TTX-sensitive current (n=6 from 6 animals).

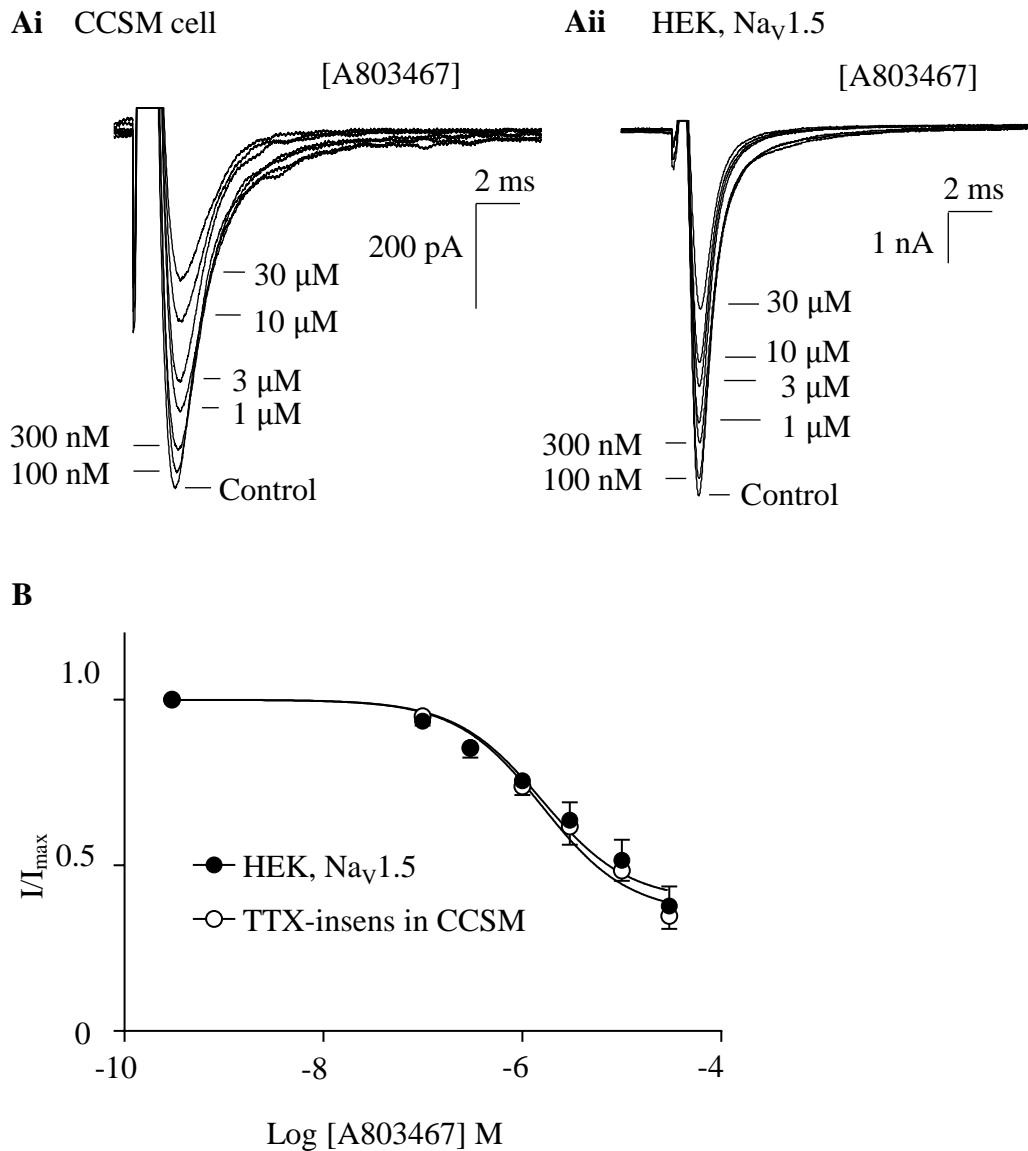


**Figure 3.11: Effect of A803467 on TTX-insensitive current in CCSM cells and in HEK-293 cells expressing Na<sub>v</sub>1.5.** (Ai) Representative traces showing the concentration-effect of A803467 on TTX-insensitive current in CCSM cells. (Aii) Representative traces showing the concentration-effect relationship of A803467 in HEK-293 cells expressing Na<sub>v</sub>1.5. (B) Summary data showing similar dose-responses, where A803467 yielded an IC<sub>50</sub> of 1.5 μM on TTX-insensitive current in CCSM cells (n = 6 from 6 animals) and an IC<sub>50</sub> of 1.6 μM in HEK-293 cells (n = 6 from 6 cells).

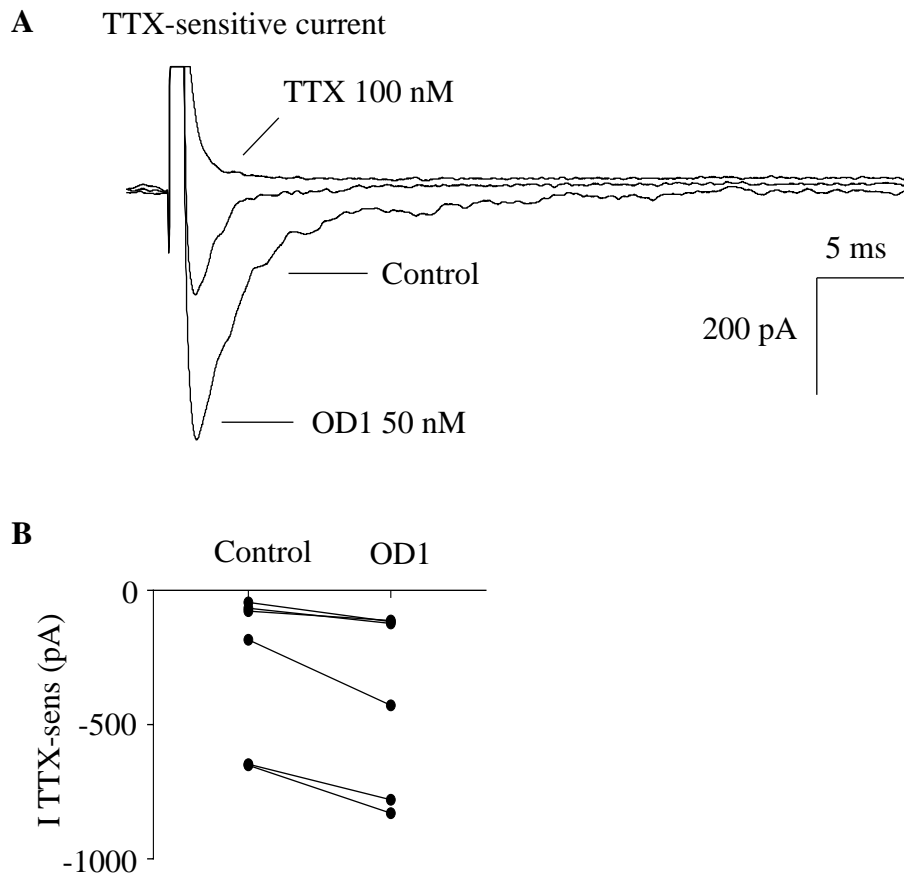


**Figure 3.12: Effect of OD1 on TTX-sensitive current in CCSM cells. (A)** Representative traces showing the effect of 50 nM OD1 on the amplitude of TTX-sensitive current in CCSM cells. **(B)** Summary data showing the effect of 50 nM OD1 on the amplitude of TTX-sensitive current (n = 6 from 6 animals, \*p<0.05, paired t test).

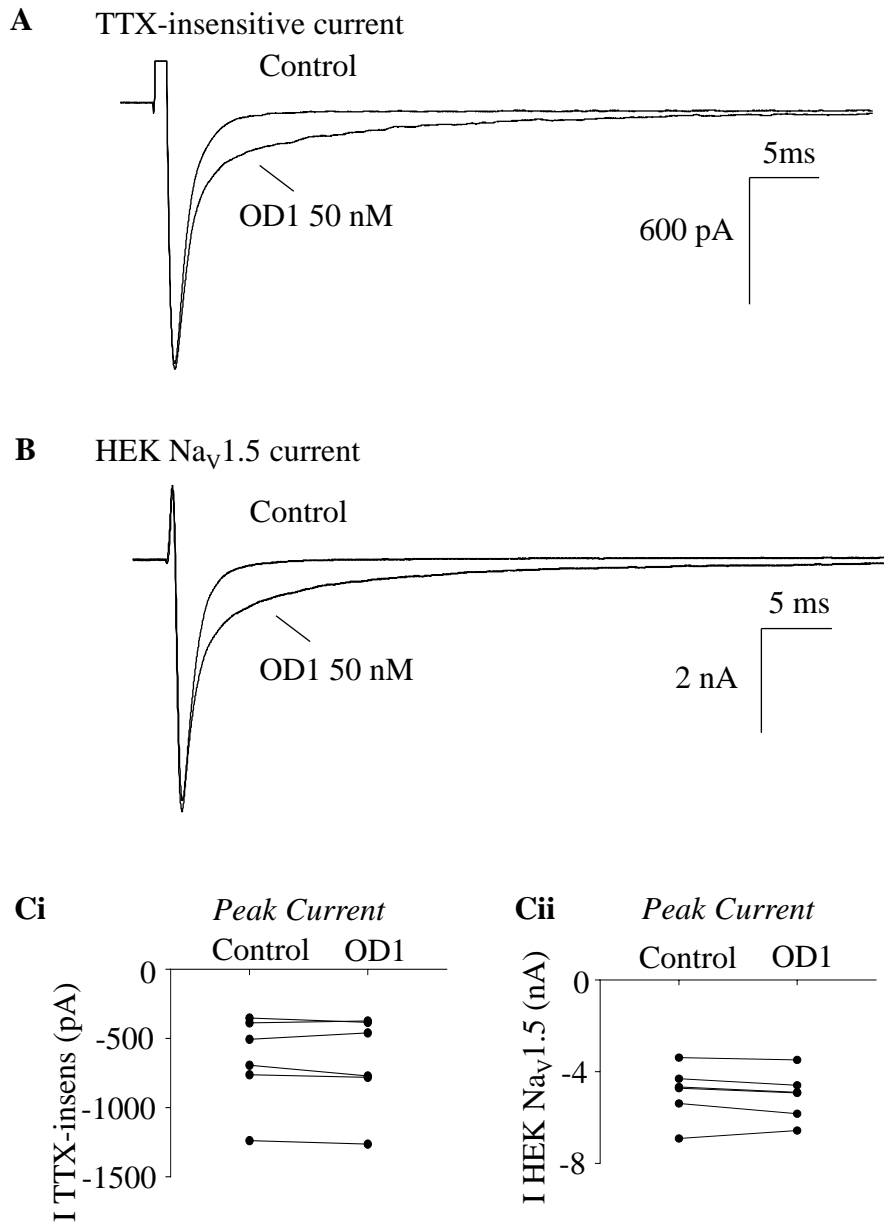


**Figure 3.13: Effect of OD1 on TTX-insensitive current in CCSM cells, and in HEK-293 cells expressing Na<sub>v</sub>1.5.** (A) Representative traces showing the effect of 50 nM OD1 on the amplitude of TTX-insensitive current in CCSM cells and on (B) Na<sub>v</sub>1.5 current expressed in HEK-293 cells. (Ci) Summary data showing the effect of 50 nM OD1 on the amplitude of the TTX-insensitive current (n = 6 from 6 animals, N.S, paired t test). (Cii) Summary data showing the effect of 50 nM OD1 on the amplitude Na<sub>v</sub>1.5 current expressed in HEK-293 cells (n = 6 from 6 cells, N.S, paired t test).

	Inactivation tau (in ms) single fit	
	Control	OD1
TTX sensitive current	2.1 ± 0.3	2.6 ± 0.7

	Inactivation tau (in ms)		
	Control (Single fit)	OD1 Tau 1	OD1 Tau 2
TTX insensitive current	2.02 ± 0.2	2.03 ± 0.3	14.6 ± 1.4
HEK Na <sub>v</sub> 1.5 current	0.86 ± 0.03	0.80 ± 0.03	7.941 ± 0.3

**Table 3.1: Effect of OD1 on the time-dependent inactivation of TTX-sensitive and TTX-insensitive current in CCSM cells and Na<sub>v</sub>1.5 current in HEK293 cells.** Time-dependent inactivation of the currents were fitted with a single exponential function for TTX-sensitive current, and a double exponential function for TTX-insensitive and Na<sub>v</sub>1.5 current.

Equation used for these fits is:  $f(t) = \sum_{i=1}^n A_i e^{-t/\tau_i} + C$

Equation 8

## **Chapter 4: Functional study of Nav in CCSM**

## 4.1 Introduction

The data from Chapter 4 highlighted the novel finding of two populations of Nav currents in CCSM. Nav channels have been discovered in spontaneously active ‘phasic’ smooth muscles, including lymphatics (Telinius *et al.*, 2015; Hollywood *et al.*, 1997), gastrointestinal tract (Neshatian *et al.*, 2015; Deshpande *et al.*, 2002; Holm *et al.*, 2002; Muraki *et al.*, 1991), vas deferens (Teramoto *et al.*, 2012), uterus (Seda *et al.*, 2007; Sperelakis *et al.*, 1992), ureter (Muraki *et al.*, 1991), and portal vein (Saleh *et al.*, 2005). In lymphatics, TTX disrupted spontaneous contractions *in vitro* (Hollywood *et al.*, 1997; Telinius *et al.*, 2015) and mutations of *SCN5A* (encoding Nav1.5) are associated with gastrointestinal motility disorders (Verstraelen *et al.*, 2015; Saito *et al.*, 2008; Locke *et al.*, 2006). Nav currents are also found in ‘quiescent’ smooth muscles, including bronchus (Bradley *et al.*, 2013), systemic arteries (Ho *et al.*, 2013; Bocquet *et al.*, 2010; Fort *et al.*, 2009; Meguro *et al.*, 2009; Berra-Romani *et al.*, 2005), and pulmonary arteries (Okabe *et al.*, 1988). Their role in such tissues is elusive, as tension responses are generally resistant to TTX. However, veratridine, a non-subtype selective Nav channel opener, greatly potentiated tension responses to low concentrations of methoxamine in rat mesenteric artery (Ho *et al.*, 2013) and 6 mM KCl in rat aorta (Fort *et al.*, 2009), suggesting that there is a reserve of ‘silent’ Nav channels that could be recruited under certain circumstances.

Findings from Chapter 3 showed that the whole cell Nav window current ranged from -60 to -30 mV, which is within the resting membrane potential of CCSM (Hashitani *et al.*, 2005), suggesting plausible Nav contribution at resting conditions. Thus, the main aim of this chapter was to investigate the functional role of Nav in CCSM, by examining the effect of veratridine and TTX on electrical activity in cells and on isometric contractions in corpus cavernosum whole tissue strips.

## 4.2 Results

### 4.2.1 Effect of veratridine on CCSM cells

Since Nav window current was reported to be at resting membrane potential [Refer to Chapter 3], it was attractive to examine if contractions could be elicited by veratridine, a non-selective activator that slows inactivation and causes prolonged channel openings (Wang and Wang, 2003). However, the drug's effect must first be examined on cells to ascertain functionality in tissue.

As veratridine activates 'TTX-sensitive' and 'TTX-insensitive' Nav channels regardless of subtype (Catterall *et al.*, 2005), its effect was tested on Nav currents in CCSM cells which had not been selected on the basis of TTX-sensitivity. Interestingly, veratridine has previously been found to cause persistent openings but reduce channel conductance by up to 75% (Wang and Wang, 2003).

A typical example is shown in Figure 4.1A, where veratridine (10  $\mu$ M) reduced the peak current (measured at point indicated) but induced a sustained current (measured at point indicated). Overall, in 6 cells, veratridine decreased peak current from  $-289 \pm 43$  to  $-253 \pm 36$  pA and increased sustained current from  $-10 \pm 3$  to  $-76 \pm 13$  pA (Figure 4.1B). Similar effects were obtained with 30  $\mu$ M veratridine in 6 different cells (Figure 4.2), where it reduced the peak current by 20% ( $-730 \pm 186$  to  $-590 \pm 173$  pA), and increased the sustained current amplitude by 7-fold ( $-20 \pm 12$  to  $-145 \pm 41$  pA).

### 4.2.2 Effect of veratridine on evoked action potential (AP)

By dialling in current, the baseline potential was set to -100 mV to remove Nav inactivation. Action potentials were evoked from isolated CCSM cells via a brief (25 ms) injection of depolarising current. The representative traces in Figure 4.3A shows that veratridine (30  $\mu$ M, 30s application) increased action potential duration and that this effect was reversed by TTX (10  $\mu$ M, 30s application). Summary data in Figure 4.3B shows that the mean duration of action potentials (time from half maximum amplitude to half minimum amplitude) was increased from  $0.2 \pm 0.1$  s to  $1.2 \pm 0.3$  s by 30  $\mu$ M

veratridine, and this was reduced to  $0.1 \pm 0.02$  s by 10  $\mu$ M TTX. Depolarisation spikes were commonly seen to escape TTX block.

#### **4.2.3 Effect of veratridine and TTX On CCSM cells**

In current clamp mode, even though the incubation of CCSM cells in veratridine causes depolarisations, the time required for the event to occur varies (10 seconds to 5 mins). An example in Figure 4.4A shows that veratridine (30  $\mu$ M) induced depolarisations like STDs in a mouse CCSM cell under current-clamp conditions (observed  $n = 8$  from 6 animals). However, due to the variability in depolarisation shape, and sometimes fluctuations in baseline, the data are not summarised.

Often, 10  $\mu$ M TTX failed to inhibit STDs in CCSM cells (~90%). An example of the rare occasion when it did is shown in Figure 4.4B. TTX (10  $\mu$ M) reduced spontaneous depolarisations in a mouse CCSM cell, in which the responses returned upon washout of TTX ( $n=3$  from 3 animals). Most of the time, incubation of quiescent CCSM cells in veratridine induced singular depolarising event. In the rarer occasions where multiple and continuous depolarising events were observed, TTX (10  $\mu$ M) readily blocked those events, which returned upon washout of TTX back into veratridine ( $n=3$  from 3 animals) (Figure 4.4C).

#### **4.2.4 Effect of KB-R7943 on currents in CCSM**

In vascular myocytes, veratridine has been shown to modulate tension responses to agonists. These effects were blocked by KB-R7943, a blocker of reverse mode  $\text{Na}^+/\text{Ca}^{2+}$  exchange (NCX), suggesting that they were due to  $\text{Na}^+$  accumulation followed by  $\text{Ca}^{2+}$  influx by NCX (Ho *et al.*, 2013; Saleh *et al.*, 2005). However, KB-R7943 has been shown to block  $\text{Na}_v$  channels (Wongcharoen *et al.*, 2006; Watano *et al.*, 1996). As its effects on tension were to be examined, its effects on  $\text{Na}_v$  in CCSM were first determined. As there is no indication that its effects on  $\text{Na}_v$  are subtype-specific, it was applied to  $\text{Na}_v$  currents without categorising cells on the basis of their TTX-sensitivity. Figure 4.5A shows a typical effect of KB-R7943, which blocked current dose-dependently at 1, 3 and 10  $\mu$ M.

Summary data in Figure 4.5B shows that significant reductions were obtained at all three concentrations, with >50% reduction obtained at 3  $\mu\text{M}$  and complete inhibition at 10  $\mu\text{M}$ . However, despite these effects, KB-R7943 was not as effective at blocking the sustained current induced by veratridine. Figure 4.6A and B show that there was no significant block of the sustained current at 1 or 3  $\mu\text{M}$  KB-R7943, though 10  $\mu\text{M}$  still completely blocked the current.

#### **4.2.5 Veratridine evokes contractions in mouse corpus cavernosum tissue**

Next, we examined if veratridine could induce contractions of corpus cavernosum tissue. At first, we looked at veratridine (10  $\mu\text{M}$ ) without any other drugs present. In 10 quiescent tissues, veratridine induced phasic contractions as shown in Figure 4.7. These contractions were well maintained and gradually increased in amplitude over a period of 45 min. Overall, in 6 tissues, the contractions had a mean amplitude of  $1.07 \pm 0.08$  mN, duration of  $10.4 \pm 0.2$  s, and frequency of  $136 \pm 12$  per hr (measured at the end of 45 min).

Because veratridine can stimulate nerves and therefore release neurotransmitters, the remaining experiments were performed in the presence of the nitric oxide synthase inhibitor L-NO-ARG (100  $\mu\text{M}$ ), adrenergic receptor antagonist phentolamine (3  $\mu\text{M}$ ), cholinergic receptor antagonist atropine (1  $\mu\text{M}$ ), and the P2X receptor-desensitising agonist  $\alpha,\beta$ -MeATP (10  $\mu\text{M}$ ). Despite the presence of these blockers, veratridine (10  $\mu\text{M}$ ) induced a series of phasic, oscillatory contractions similar to those in the absence of blockers (Figure 4.8). These were abolished by 100 nM TTX (Figure 4.8A). These effects of veratridine, and its reversal by TTX, were observed in all 6 tissues tested and are summarised in Figure 4.8Bi and Bii.

Approximately 10% of the strips used in the present study developed spontaneous contractions, although these generally did not last long enough to comprehensively study. An example is shown in Figure 4.9 for comparison to veratridine-induced activity, which in contrast was consistent and long lasting. In 6 strips that developed spontaneous contractions the mean amplitude, frequency and duration of the contractions were  $0.3 \pm 0.1$  mN,  $3.4 \pm 0.3$  s, and  $18 \pm 9$  per hr, respectively.

Finally, to test the possibility that the veratridine-induced contractions were due to  $\text{Ca}^{2+}$  influx due to reverse mode NCX, as a result of intracellular  $[\text{Na}^+]$  accumulation, we examined the effect of KB-R7943. In the example shown in Figure 4.10A, veratridine-induced phasic contractions were unaffected by either 1 or 3  $\mu\text{M}$  KB-R7943, but were abolished by nifedipine (1  $\mu\text{M}$ ), indicating that they were dependent upon  $\text{Ca}^{2+}$  influx via L-type  $\text{Ca}^{2+}$  channels. Similar results were obtained in a total of 6 cells, summarised in Figure 4.10Bi and Bii.

In the above experiments, veratridine induced phasic contractions in all of 22 tissues tested (10 with no blockers, and 12 with the cocktail of L-NO-ARG, phentolamine, atropine and  $\alpha,\beta$ -MeATP). In an additional six experiments, veratridine was still able to induce phasic contractions, reversible by TTX, when indomethacin (10  $\mu\text{M}$ ) was added to the above cocktail of blockers (Figure 4.11).

#### **4.2.6 TTX inhibited PE-induced transient depolarisations**

Since the main excitatory component in CC is adrenergic, it was therefore of interest to examine if  $\text{Nav}$  channels play a role in adrenergic responses in CCSM cells. In six CCSM cells, studied under current clamp, with resting membrane potential adjusted between -50 to -60 mV by current injection, the mean amplitude of 300 nM phenylephrine-evoked depolarisations was decreased from  $44.92 \pm 3.692$  mV to  $20.05 \pm 5.786$  mV by TTX (Figure 4.12). The effect of TTX was reversible by washing back into 300 nM phenylephrine, suggesting that the diminishing depolarisations were not time-dependent, but were in fact due to TTX.

#### **4.2.7 TTX reduced the frequency of PE-induced contractions in CCSM tissue**

To examine the functional role of  $\text{Nav}$  channels in CCSM contractility, we examined if phenylephrine-induced contractions of CCSM strips were affected by TTX. Figure 4.13 shows that 300 nM phenylephrine induced a series of phasic contractions, where its frequency was reduced from  $268 \pm 46$  to  $78 \pm 33$  contractions per hour by 10  $\mu\text{M}$  TTX ( $p < 0.05$ , paired t-test,  $n=6$  from 6 animals). Without TTX, the frequency

of phasic contractions was slightly affected over a similar length of time (30 min) ( $242 \pm 35$  to  $184 \pm 27$  contractions per hour) ( $p < 0.05$ , paired t-test,  $n=6$  from 6 animals). It should be noted that the time-dependent decrease in frequency was approximately 25% but statistically significant. The greater reduction in the TTX experiments suggests that Nav channels may play a role in phenylephrine-induced contractions in CCSM tissue. Note: TTX was not tested spontaneous contractions because they were not robust.

### 4.3 Discussion

Given that the whole cell  $\text{Na}_V$  window current intersected at resting membrane potential, it was of interest to examine if tissue contractions could be elicited by veratridine, which increased the amplitude of sustained sodium current. Veratridine elicited contractions that were susceptible to blockade by TTX. The fact that these developed gradually (typically over 15-30 min), might possibly be explained if few  $\text{Na}_V$  channels were activated at the resting membrane potential. Since veratridine binds preferentially to activated  $\text{Na}_V$  channels (Ulbricht, 2005) and then prevents inactivation, it might require some time to act as more  $\text{Na}_V$  channels gradually open. This may lead to depolarisation, causing secondary effects such as calcium entry, calcium oscillations, and activation of calcium-activated chloride channels (Sergeant *et al.*, 2009).

However, Blaustein and colleagues, using NCX knockout mice, have provided strong evidence of a role for reverse mode NCX in the generation of vascular tone and development of salt-sensitive hypertension (Zhang *et al.*, 2010; Iwamoto *et al.*, 2004). Hence, intracellular  $\text{Na}^+$  accumulation due to activation of  $\text{Na}_V$  channels might result in myogenic activity due to reverse mode NCX. Indeed, in murine portal vein and rat mesenteric artery, effects of veratridine on tension were reversed by KB-R7943 (Ho *et al.*, 2013; Saleh *et al.*, 2005). Since this drug has been reported to directly block  $\text{Na}_V$  channels (Wongcharoen *et al.*, 2006; Watano *et al.*, 1996), we examined its effect on the  $\text{Na}_V$  currents in CCSM cells. It caused a concentration-dependent block of the current, but up to 3  $\mu\text{M}$  failed to block the sustained  $\text{Na}_V$  current induced by veratridine. The  $\text{IC}_{50}$  values for KB-R7943 block of reverse mode NCX ranges from 0.32 - 2.4  $\mu\text{M}$  in ventricular myocytes and vascular smooth muscle cells (Iwamoto *et al.*, 1996; Watano *et al.*, 1996) and 3  $\mu\text{M}$  was sufficient to block veratridine-induced contractures of lymphatic vessels (Telinius *et al.*, 2015).

Surprisingly, KB-R7943 (1- 3  $\mu\text{M}$ ) had no effect on veratridine-induced phasic contractions in whole CCSM, suggesting that reverse mode NCX was not involved. In contrast, nifedipine abolished the contractions, consistent with a direct depolarising effect of the sustained sodium current induced by veratridine causing activation of L-type  $\text{Ca}^{2+}$  channels.

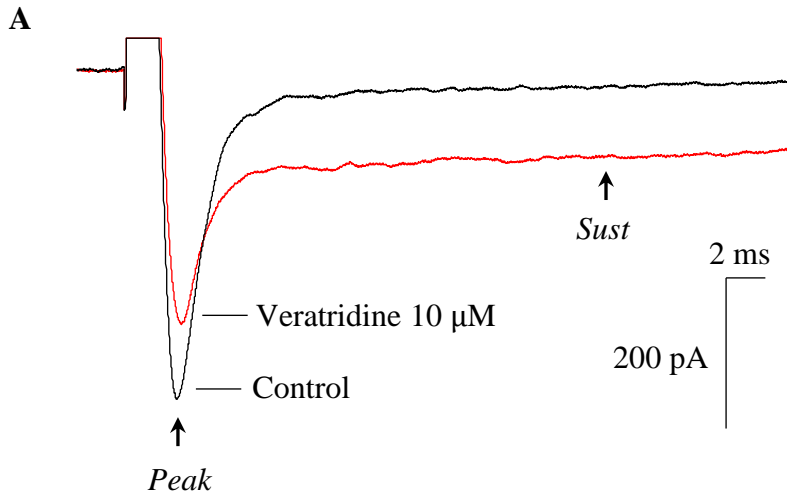
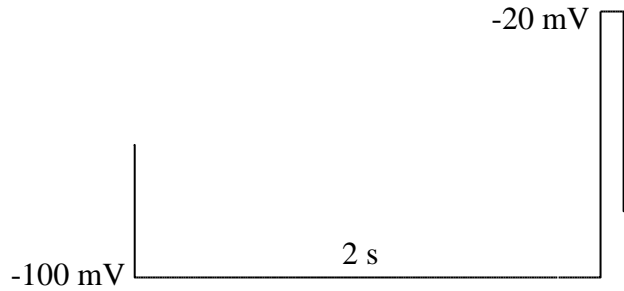
Nav channel activators have been previously shown to cause relaxations of human and rabbit corpus cavernosum due to nitric oxide release from nerves (Teixeira *et al.*, 2004; Fernandes de Oliveira *et al.*, 2003; Teixeira *et al.*, 1998). Another possible source of nitric oxide (or other mediators) is the endothelium, which sometimes express Nav channels (e.g. see Bocquet *et al.*, 2010). Thus, we cannot completely exclude the possibility that the veratridine-induced effects were indirect, due to release of mediators from endothelium, although we attempted to minimise any such effects with a cocktail of blockers, including phentolamine, atropine, L-NO-Arg,  $\alpha$ - $\beta$ -methylene-ATP and indomethacin.

The fact that 100 nM TTX abolished all veratridine-induced contractions suggests that these responses were wholly mediated by 'TTX-sensitive' Nav channels. Interestingly, the voltage-dependent kinetics of the 'TTX-insensitive current' were shifted slightly to the left compared to the TTX-sensitive current and it is noteworthy that the voltage-dependent kinetics of Nav1.5 are highly mechano-sensitive, with stretch causing a further marked leftward shift in the window current (Beyder *et al.*, 2010). It is possible that stretch resulted in Nav becoming unavailable under our *in vitro* recording conditions. This also raises the intriguing possibility that mechanical effects *in vivo* during tumescence or detumescence change the availability Nav1.5, and therefore its contribution to contractile activity.

To assess whether Nav channels contribute adrenergic excitation in CCSM, TTX was applied to phenylephrine-induced depolarisations in current-clamped cells. Interestingly, TTX reversibly inhibited phenylephrine-induced depolarisations. Similarly in tissue, TTX also significantly disrupted phenylephrine-induced phasic contractions, suggesting a role for Nav channels in the regulation of CCSM contractility by the sympathetic nerves. However, difficulty presented in the blocking of spontaneous depolarisations by TTX suggests that Nav channels are not involved in myogenic depolarisations. Interestingly, spontaneous depolarisations in CCSM were susceptible to blockade by Ca<sup>2+</sup>-activated Cl channel antagonist, Ani9, which will be presented and discussed in detail in Chapter 6.

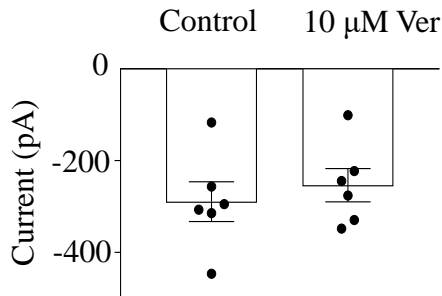
To summarise, we have demonstrated the role of Nav channels in veratridine-induced and phenylephrine-induced excitations in the mouse CCSM.

### Protocol



### Bi

Amplitude



### Bii

Sustained current

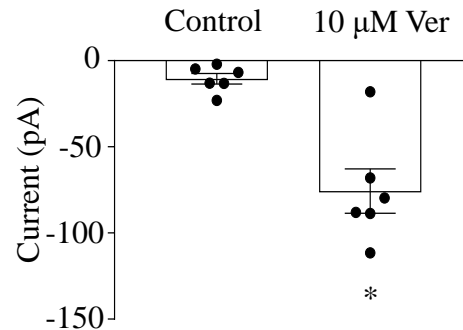
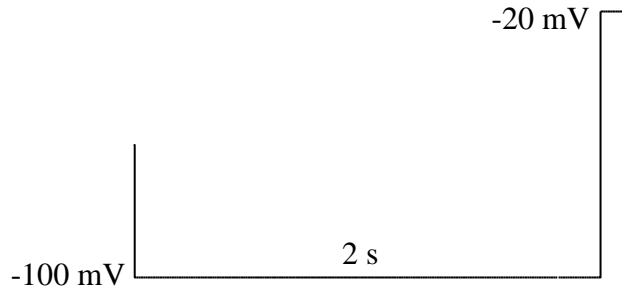


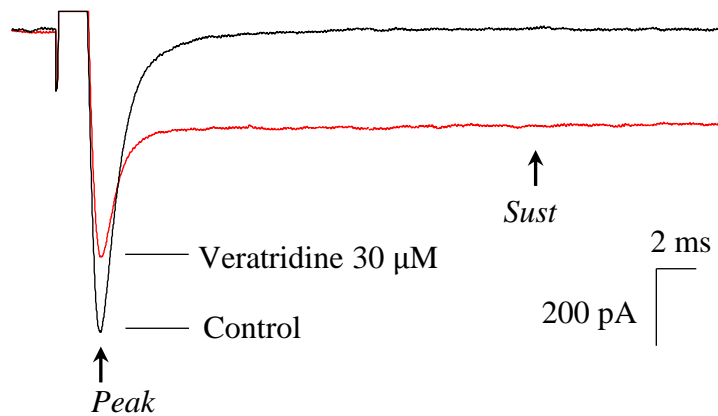
### Figure 4.1: Effect of 10 μM veratridine on sodium current in CCSM cells. (A)

Representative traces showing the effect of 10 μM veratridine (Ver, red) on evoked current. Currents were evoked at 15 s intervals in cells held at -60 mV, stepped down to -100 mV for 2 s to remove inactivation and then stepped to a test pulse of -20 mV for 100 ms. **(Bi)** Summary data showing the effect of veratridine on peak current measured at the point indicated ( $I_{Peak}$ ,  $n = 6$  from 6 animals,  $*p < 0.05$ , paired t test), and on **(Bii)** sustained current measured at the point indicated ( $I_{Sust}$ ,  $n = 6$  from 6 animals,  $*p < 0.05$ , paired t test).

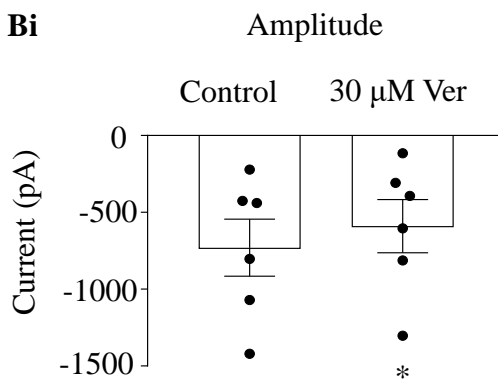
### Protocol



### A



### Bi



### Bii

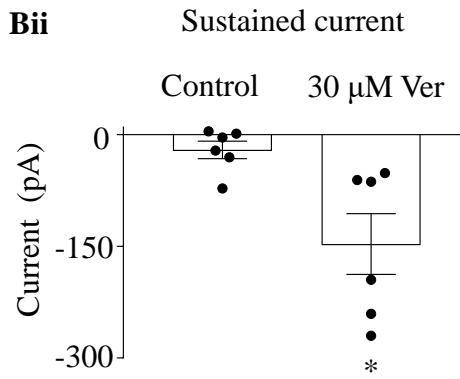


**Figure 4.2: Effect of 30  $\mu\text{M}$  veratridine on sodium current in CCSM cells. (A)** Representative traces showing the effect of 30  $\mu\text{M}$  veratridine (Ver, red) on evoked current. **(Bi)** Summary data showing the effect of veratridine on peak current measured at the point indicated ( $I_{\text{Peak}}$ ,  $n = 6$  from 6 animals,  $*p < 0.05$ , paired t test), and on **(Bii)** sustained current measured at the point indicated ( $I_{\text{Sust}}$ ,  $n = 6$  from 6 animals,  $*p < 0.05$ , paired t test).

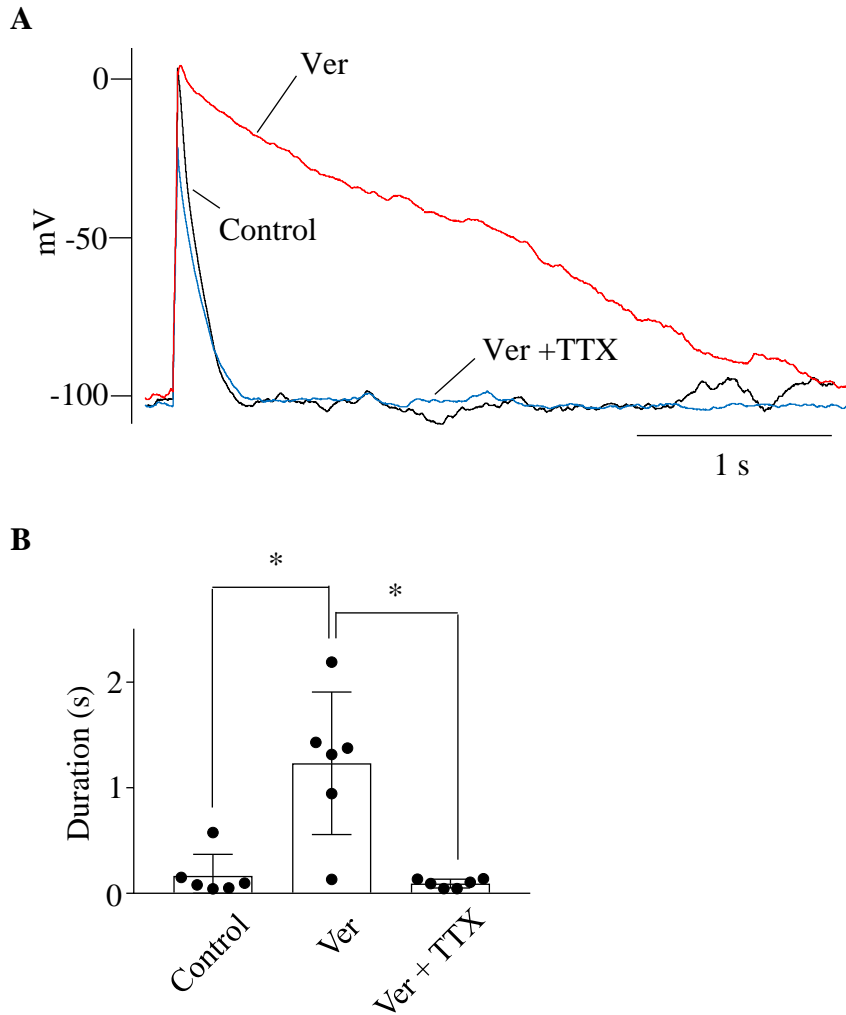


**Figure 4.3: Effect of veratridine on evoked action potential (AP).** After setting the baseline potential at -100 mV, sufficient current was injected to evoke an AP. **(A)** Representative traces showing that the evoked action potential duration was increased by 30  $\mu$ M veratridine (Ver, red trace) and reduced by 10  $\mu$ M TTX (blue trace). **(B)** Summary of the effect of 30  $\mu$ M veratridine (Ver,  $n = 6$  from 6 animals) and veratridine + TTX (10  $\mu$ M) on action potential duration ( $n = 6$  from 6 animals,  $*p < 0.05$ , ANOVA).

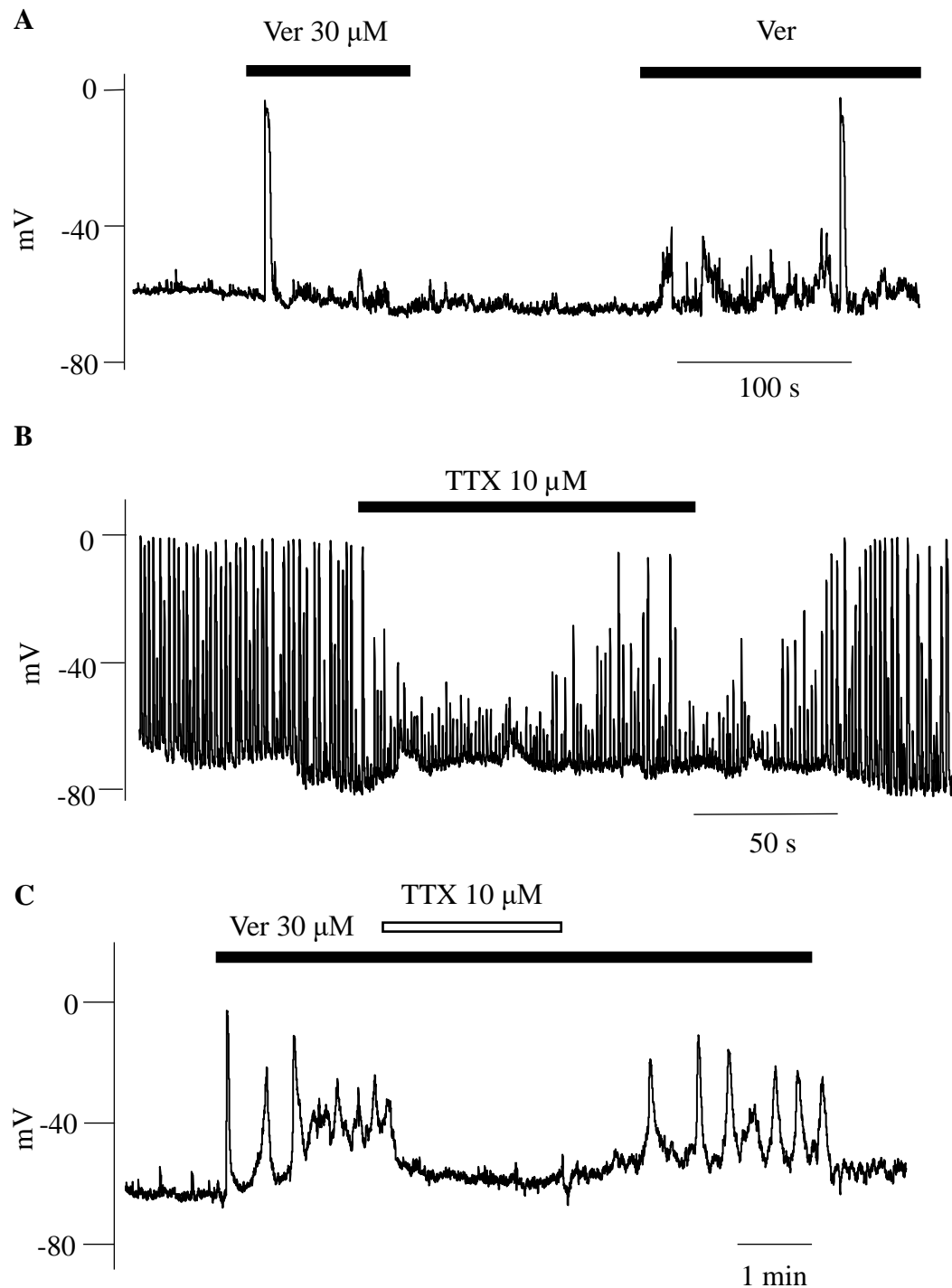
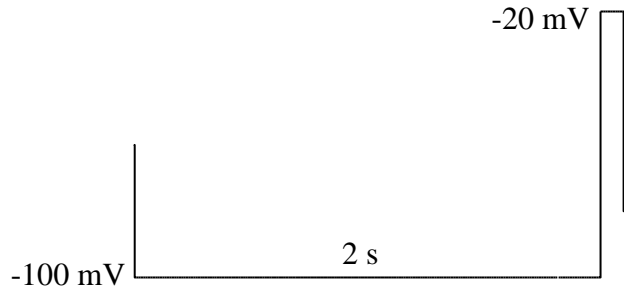
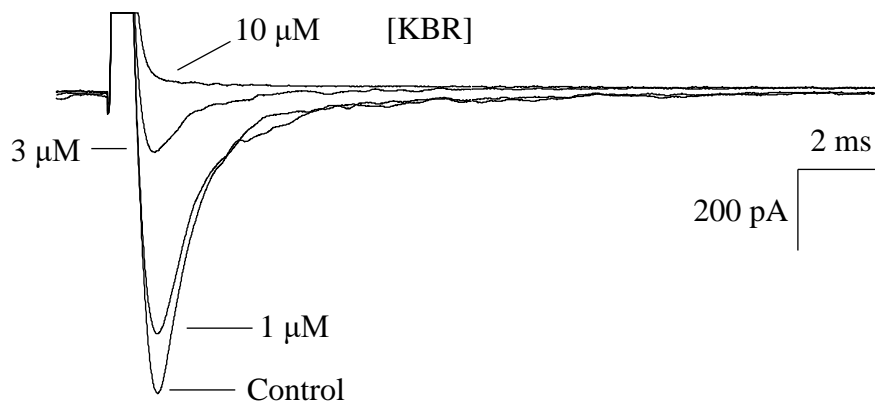


**Figure 4.4: Effect of veratridine and TTX on CCSM cells.** (A) Traces showing veratridine (30  $\mu$ M) induced depolarisations similar to AP in CCSM cells under current clamp conditions (n = 8 from 6 animals). (B) An example of the effect of TTX on spontaneous depolarisations in CCSM cells. (C) An example of the effect of veratridine and veratridine + TTX on CCSM cells.

### Protocol



### A



### B

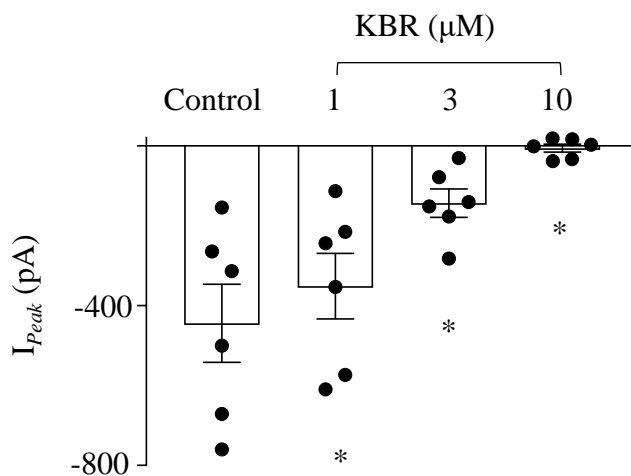


**Figure 4.5: Effect of KB-R7943 on sodium peak current in CCSM cells. (A)** Representative traces showing the concentration-effect of KB-R7943 (KBR) on sodium peak current. **(B)** Summary data showing the concentration-effect relationship of KB-R7943 on sodium peak current ( $n = 6$  from 6 animals,  $*p < 0.05$  when compared to control, ANOVA).

### Protocol

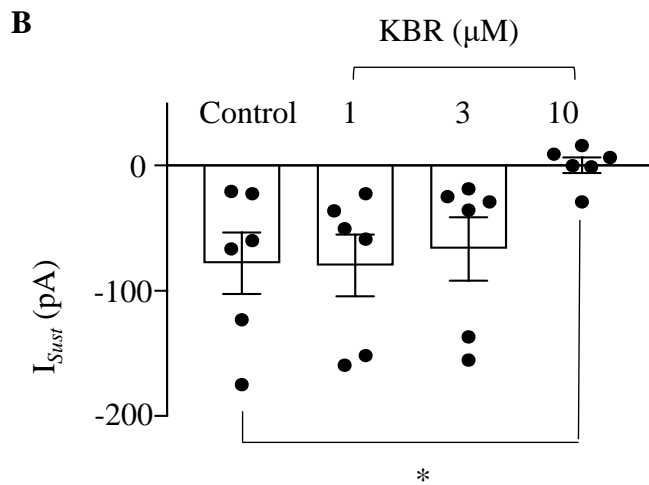
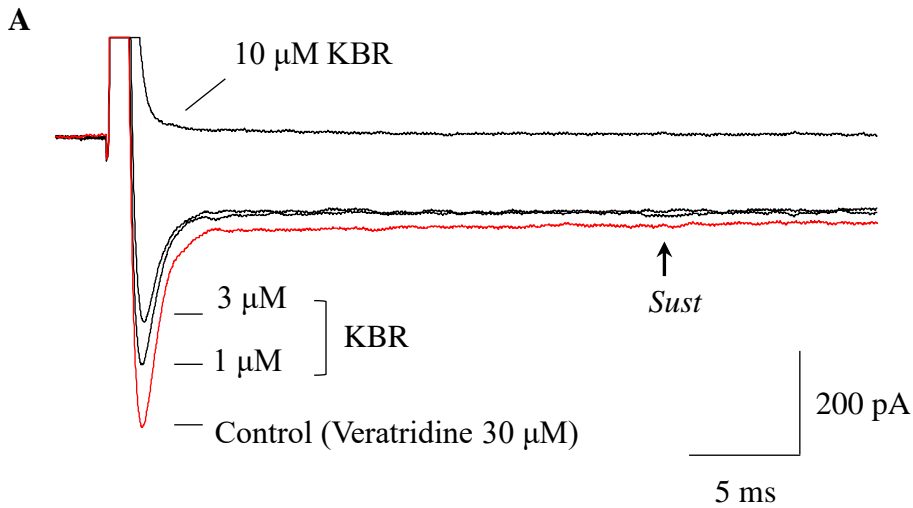
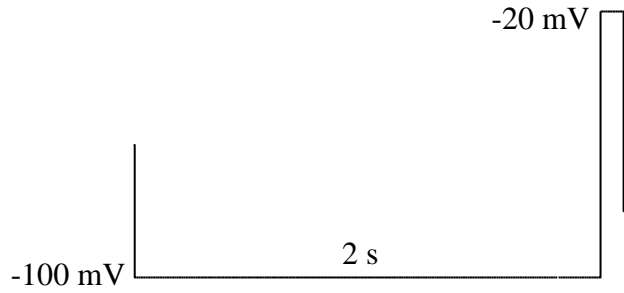


**Figure 4.6: Effect of KB-R7943 on veratridine-induced sustained current in CCSM cells.** (A) Representative traces showing the concentration-effect of KB-R7943 on sustained current evoked by veratridine. (B) Summary data showing the concentration-effect relationship of KB-R7943 on veratridine-evoked sustained current, measured at the point indicated ( $n = 6$  from 6 animals,  $*p < 0.05$ , ANOVA).

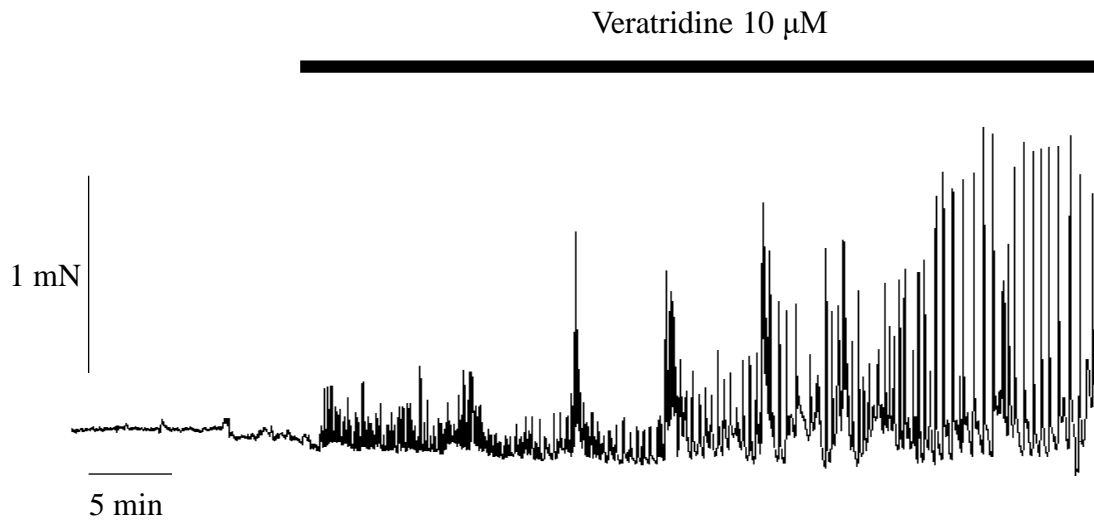
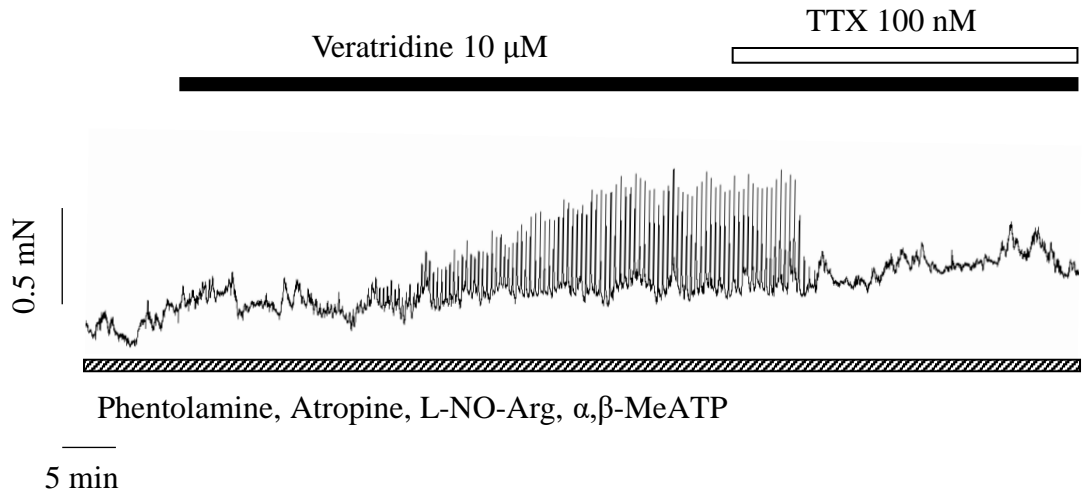
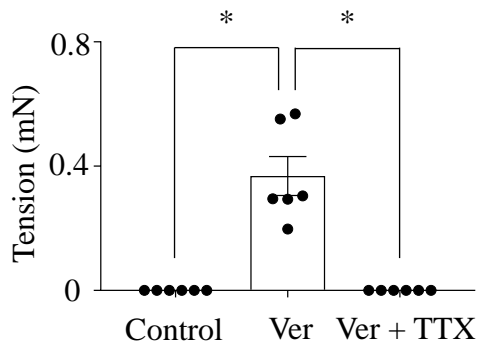


**Figure 4.7: Veratridine-evoked contractions in CCSM tissue strips on basal conditions.** Representative traces showing contractions evoked by 10  $\mu$ M veratridine under basal conditions [no blocker present] (typical of n=6 from 6 animals).

A



Bi



Bii

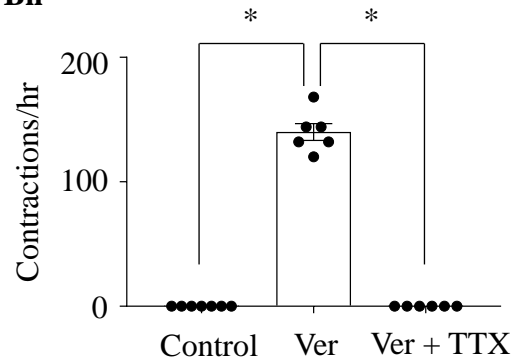
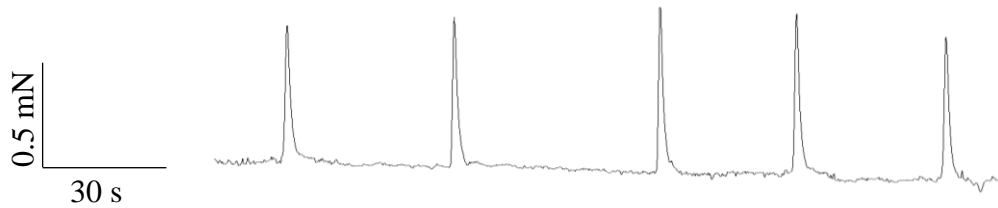


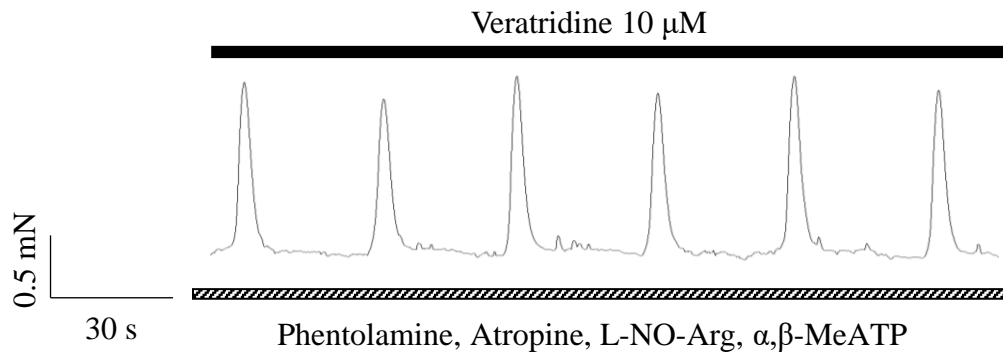
**Figure 4.8: Veratridine evokes contractions in mouse corpus cavernosum tissue.**

(A) Representative traces showing contractions evoked by 10  $\mu\text{M}$  veratridine in the presence of NO-ARG (100  $\mu\text{M}$ ), phentolamine (3  $\mu\text{M}$ ), atropine (1  $\mu\text{M}$ ), and  $\alpha,\beta$ -MeATP (10  $\mu\text{M}$ ). The effect of veratridine was reversed by 100 nM TTX. (Bi) Summary data showing mean contraction amplitude evoked by veratridine ( $n = 6$  from 6 animals,  $*p < 0.05$ , ANOVA) and (Bii) evoked contraction events per hour ( $n = 6$  from 6 animals,  $*p < 0.05$ , ANOVA).

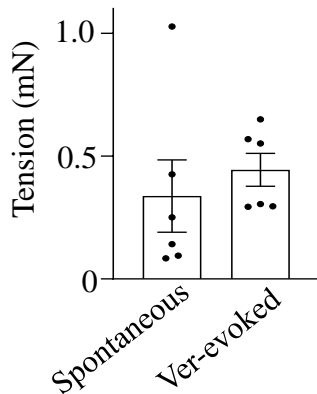
### A Spontaneous contractions



### B Veratridine-evoked contractions



### Ci



### Cii

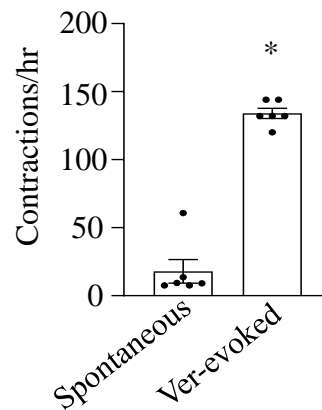


**Figure 4.9: Spontaneous and veratridine-evoked contractions in CCSM tissue strips.** (A) Spontaneous contractions in mouse CCSM tissue strips. (B) Veratridine-evoked contractions in mouse CCSM tissue strips. (Ci) Summary data showing mean spontaneous and veratridine-evoked contractions amplitude (n = 6 from 6 animals, \*p>0.05, unpaired t test) and (Cii) Mean spontaneous and veratridine-evoked contraction events per hour (n = 6 from 6 animals, \*p<0.05, unpaired t test).

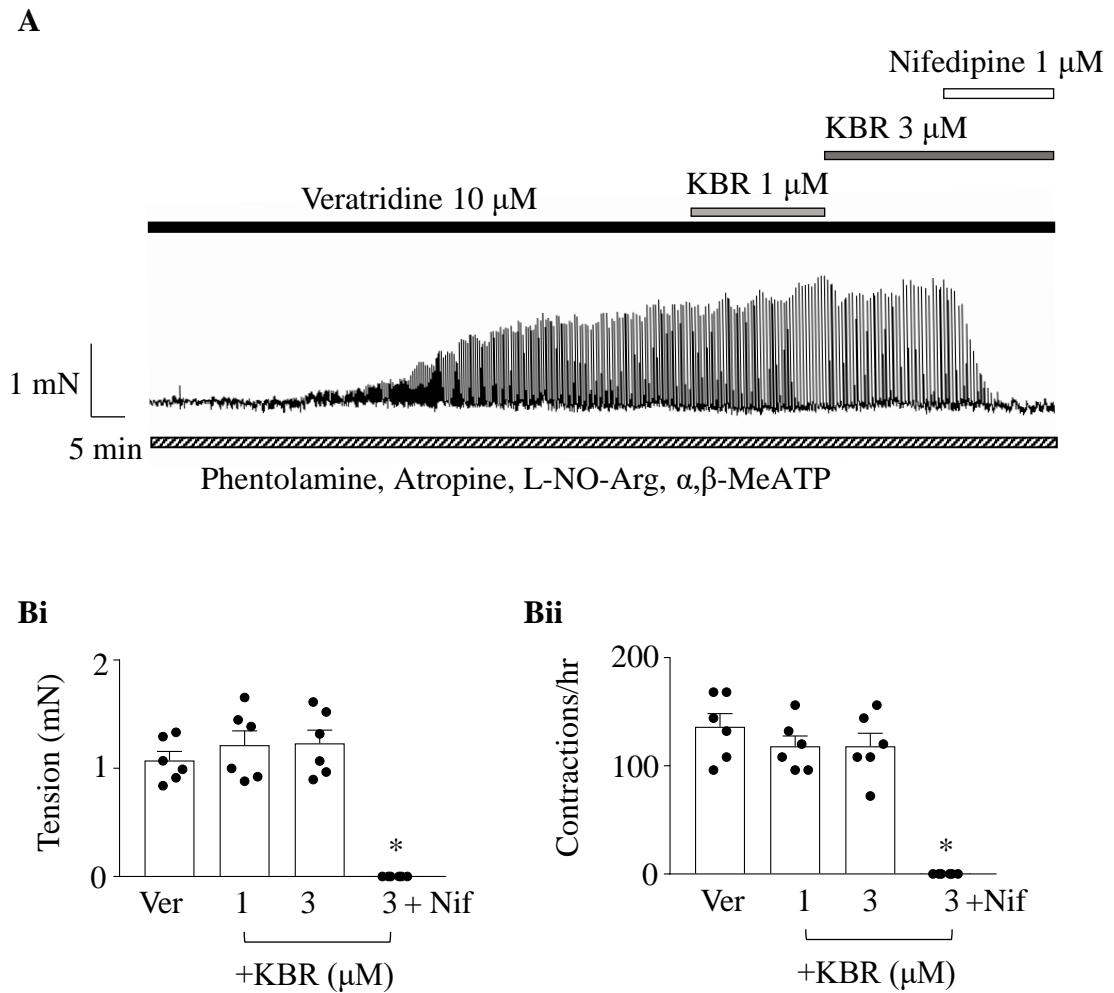


**Figure 4.10: Veratridine-evoked contractions can be blocked by nifedipine but not by KB-R7943. (A)** Veratridine-evoked contractions are not susceptible to blockade by KB-R7943 (KBR 1  $\mu\text{M}$  and 3  $\mu\text{M}$ ) but are effectively blocked by nifedipine (1  $\mu\text{M}$ ). **(Bi)** Summary data showing mean evoked contraction amplitude ( $n = 6$  from 6 animals,  $*p < 0.05$ , ANOVA) and **(Bii)** evoked contraction events per hour ( $n = 6$  from 6 animals,  $*p < 0.05$ , ANOVA). Ver = veratridine 10  $\mu\text{M}$ ; KBR = KB-R7943; Nif = nifedipine 1  $\mu\text{M}$ .

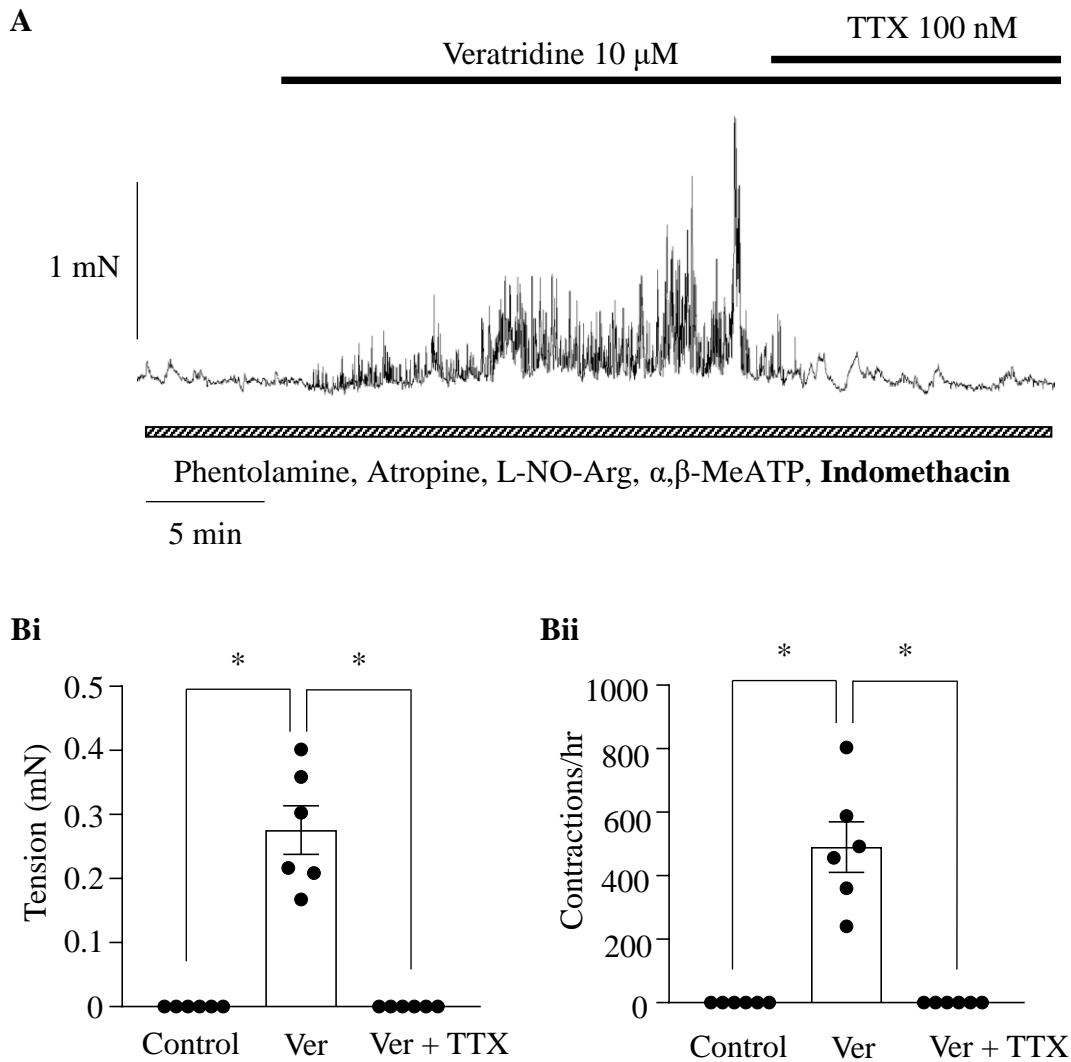


**Figure 4.11: Veratridine evokes contractions in the presence of COX-inhibitor.**

Representative traces showing contractions evoked by 10  $\mu$ M veratridine in the presence of COX-inhibitor, indomethacin, and blockers of the effects of neurotransmitter release [Phentolamine, Atropine, L-NO-Arg,  $\alpha,\beta$ -MeATP] (n = 6 from 6 animals). **(Bi)** Summary data showing mean evoked contraction amplitude (n = 6 from 6 animals, \*p<0.05, ANOVA) and **(Bii)** evoked contraction events per hour (n = 6 from 6 animals, \*p<0.05, ANOVA). Ver = veratridine 10  $\mu$ M.

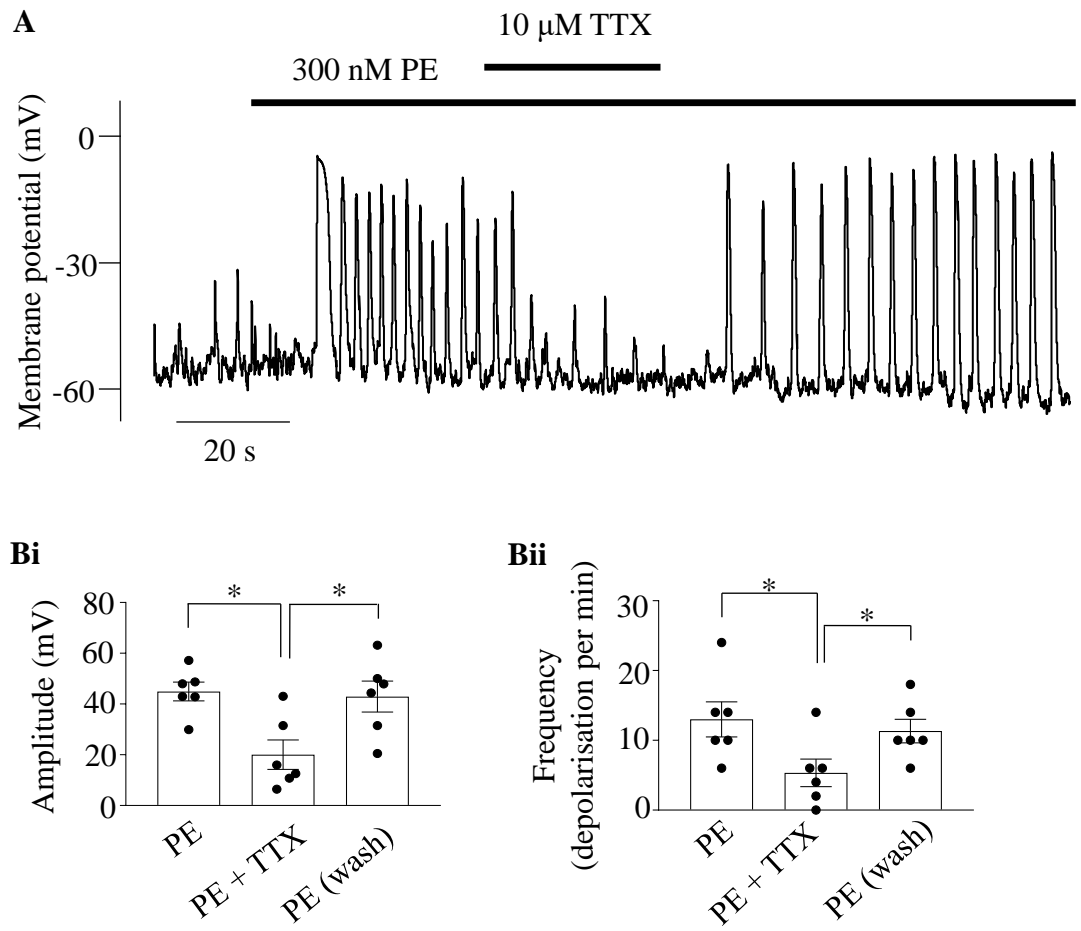


**Figure 4.12: The effect of TTX on phenylephrine-induced electrical activity. (A)** Single-cell current clamp recording showing that 300 nM phenylephrine-induced depolarisations were reversibly blocked by 10  $\mu$ M TTX. **(Bi)** Summary of the effect of TTX on the amplitude and **(Bii)** frequency of phenylephrine-induced depolarisations (n=6 from 6 animals, \*p<0.05, ANOVA and Dunnett's multiple comparison test).

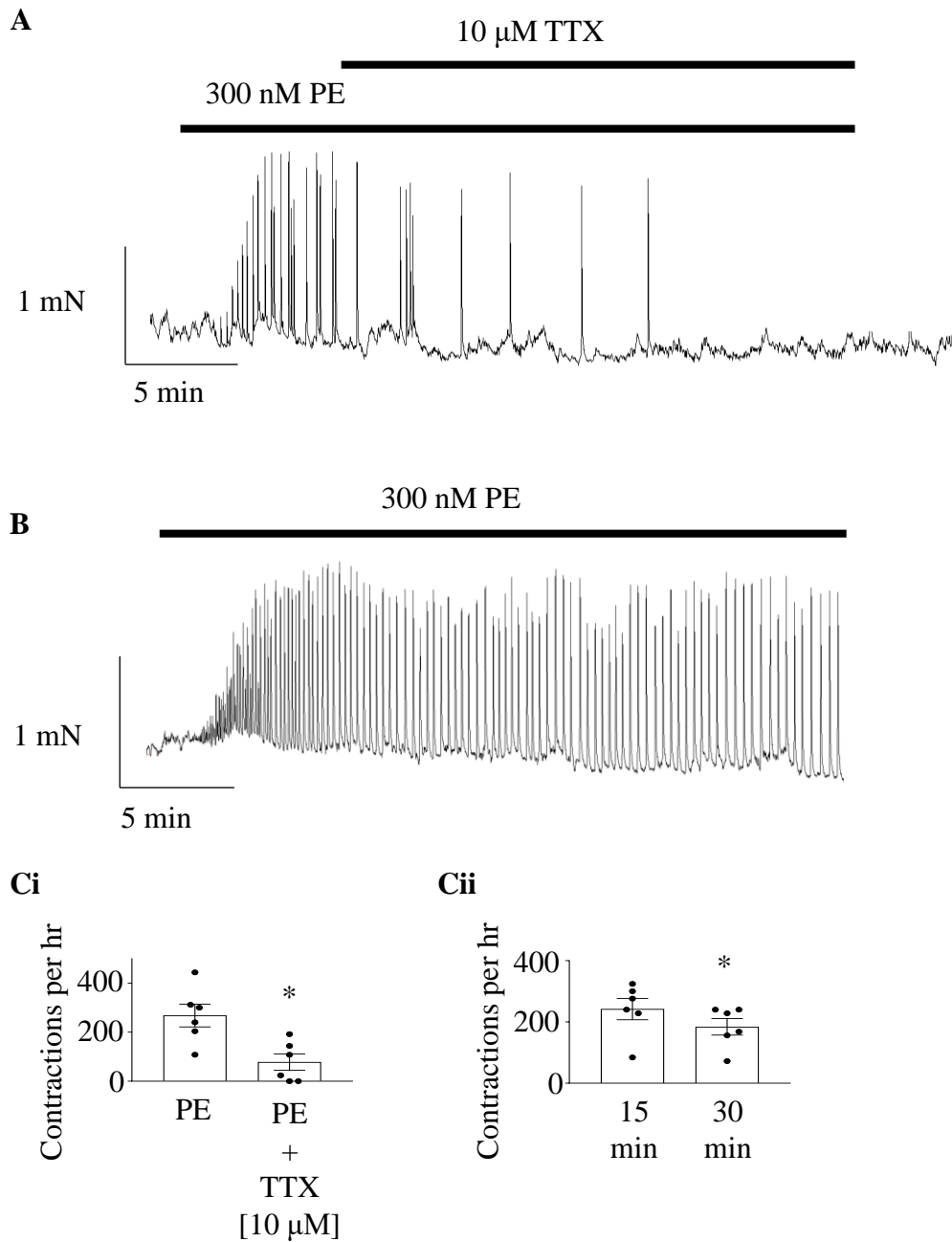


**Figure 4.13: The effect of TTX on phenylephrine-induced contractions in CCSM tissue slices.** (A) Traces showing 300 nM phenylephrine-induced phasic contractions in CCSM tissue, and (B) its time control. (Ci) Summary of the effect of TTX on the frequency of phenylephrine-induced contractions (n = 6 from 6 animals; \*p<0.05, paired t test). (Cii) Summary of the time control for the frequency of phenylephrine-induced contractions (n = 6 from 6 animals; \*p<0.05, paired t test).

## **Chapter 5: Transcriptional and immunocytochemistry study of Nav in CCSM**

## 5.1 Introduction

Nav channels have been identified in some smooth muscle types: Nav1.2 in longitudinal smooth muscle tissue of non-pregnant rat myometrium (Seda *et al.*, 2007); Nav1.3 in human lymphatic vessel tissue (Telinius *et al.*, 2015); Nav1.4 in cultured human oesophageal smooth muscle cells (Deshpande *et al.*, 2002); Nav1.5 in freshly dispersed human jejunal circular smooth muscle cells (Strege *et al.*, 2003; Holm *et al.*, 2002); Nav1.6 in mouse vas deferens (Teramoto *et al.*, 2012; Zhu *et al.*, 2008); and Nav1.7 in cultured human bronchial, coronary arterial, and pulmonary arterial smooth muscle cells (Jo *et al.*, 2004). However, the molecular identity of Nav channels in CCSM has not been explored thus far. Based on the Nav channels' biophysical and pharmacological properties shown in Chapter 3 and 4, TTX-insensitive current is likely to be Nav1.5, whereas different subtypes may contribute to TTX-sensitive current. Our data has narrowed down some possible candidates for the two populations of Nav currents in CCSM but has yet to provide direct evidence of their identity. Hence the main aims of this chapter are to investigate the transcriptional expression and protein expression of Nav channels in mouse CCSM.

## **5.2 Results**

### **5.2.1 Transcriptional expression of Nav channels in CCSM tissue**

In an effort to narrow down the identity of Nav channels, transcriptional expression of Nav channels in CCSM tissue was first examined with end-point PCR. Using primers designed for Nav channels (Table 2.3), PCR was performed on cDNA from mouse CCSM strips. Sybersafe–stained 2% agarose gel (Figure 5.1) showed that all Nav channels were transcriptionally expressed in CCSM tissue (n=5 from 5 animals). Mouse brain was included as a positive control. PCR was also performed on reaction mixtures in which template cDNA was omitted (NTC), to control for contamination and non-specific amplification.

### **5.2.2 Relative transcriptional expression of Nav channels in CCSM tissue**

Following end-point PCR, qPCR experiments were also performed to quantify mRNA transcripts encoding Nav channel subtypes in whole corpus cavernosum tissue. First, the efficacy of each of the Nav  $\alpha$ -subunit primers for Nav1.1–1.9 was confirmed using RNA extracted from mouse brain (Nav1.1, 1.2, 1.3, 1.6 and 1.7), dorsal root ganglion (Nav1.8 and 1.9), skeletal muscle (Nav1.4), and cardiac tissues (Nav1.5).

Performance of qPCR (Figure 5.2) showed most prominent expression of Nav1.1 (*SCN1A*), Nav1.2 (*SCN2A*), and Nav1.4 (*SCN4A*), with Nav1.5 (*SCN5A*) and Nav1.7 (*SCN9A*) next. Interestingly, there was relatively little expression of Nav1.6 (*SCN8A*), which would correspond to the low sensitivity to 4,9-anhydro-TTX shown in Figure 3.9 [Chapter 3].

### **5.2.3 Expression of Nav1.5 and Nav1.4 in CCSM cells**

The representative confocal photomicrographs in Figures 5.3 and 5.4 confirm that freshly isolated CCSM cells were immunoreactive for Nav1.5 and Nav1.4 respectively, which were demonstrated by strong immunofluorescence. Staining shown in Figures 5.3 and 5.4

was similar in 5 procedures carried out on cells dispersed from 5 animals. Figure 5.3 (Nav1.5) shows staining in a punctate pattern located around the periphery of the cell (arrows). Figure 5.4 (Nav1.4) shows punctate staining (arrows), though not confined to the periphery. This might indicate a lack of specificity of the antibody; therefore, it would be worth testing the effect of several alternative Nav1.4 antibodies in the future.

Positive control for anti-Nav1.5 antibody revealed staining for both HEK Nav1.5 cells and untransfected HEK cells (Figure 5.5), although the fluorescence was brighter in Nav1.5 overexpressed cells than in untransfected cells. Secondary antibody-only control in HEK Nav1.5 cells showed no immunoreactivity (Figure 5.6). Positive control for anti-Nav1.4 antibody on skeletal muscle tissue slice showed clear staining, especially at striations of the muscle (Figure 5.7A). On the other hand, negative control showed that both anti-Nav1.4 antibody and anti-Nav1.5 antibody were not immunoreactive to mouse detrusor smooth muscle cells, suggesting antibody specificity (Figures 5.7Bi, 5.7Bii, 5.8A, and 5.8B). Staining shown in these figures was similar in three procedures carried out on cells dispersed from three animals. We also carried out staining for smooth muscle myosin heavy chain 11 (Figure 5.9A). In this case, dense staining was observed throughout the cells. Figure 5.9Bi and 5.9Bii show a secondary antibody-only control in CCSM cells, demonstrating that no immunofluorescence was observed in the absence of smooth muscle myosin heavy chain 11 antibody.

### 5.3 Discussion

Data in Chapter 4 suggests that the TTX-insensitive current was not carried by Nav1.8 or Nav1.9, leaving Nav1.5 as the most likely candidate. To confirm this, immunocytochemistry experiments were performed to examine if Nav1.5 was present in isolated CCSM cells. As shown in Figure 5.3, localised punctate staining, distributed peripherally at the cell membrane, was seen with an antibody targeting Nav1.5, confirming plasmalemmal expression of Nav1.5. However, untransfected HEK cells also immuno-stained for Nav1.5, albeit less intense. Negative control preparations (incubated with secondary antibody only) did not show any fluorescence. This eliminates the possibility of autofluorescence from solutions or fixation, so the staining in untransfected cells would be caused by either non-specific antibody binding or endogenous expression of Nav1.5 in untransfected cells.

Interestingly, Cummins *et al.* (1999) showed that HEK-293 cells endogenously express Nav1.5. Using whole-cell patch clamp technique, they showed that the endogenous currents have kinetics and TTX pharmacology similar to cardiac Nav1.5. He and Soderlund (2010) also provided evidence of endogenous Nav currents, where Nav1.5 detected in RT-PCR could contribute to the endogenous currents in the cells. Although endogenous expression of Navs may be attributed by HEK lineage, passage number, and culture conditions, it is plausible that any expression of Nav1.5 channel, however minute, would cause antibody binding. Importantly, the fact remains that the Ghovanloo *et al.* (2018) has validated the antibody in Nav1.5 knockout mice, suggesting antibody specificity.

In fact, transcriptional studies corroborated with the expression of Nav1.5 in CCSM, as qPCR experiments show that Nav1.5 expression was the highest among the TTX-insensitive subtypes present. Meanwhile for TTX-sensitive current, qPCR experiments pointed to relatively high expression of Nav1.4 (along with Nav1.1 and 1.2, consistent with the effects of ICA-121431). Expression of Nav1.4 was confirmed in immunofluorescence staining in isolated cells. Taken together, these experiments suggest that ~80% of the 'TTX-sensitive' current can be accounted for by a combination of Nav1.1, 1.2 and 1.4. Although Nav1.4 is mainly expressed in skeletal muscle, it has also been found in oesophageal smooth muscle (Deshpande *et al.*, 2002).

It should be noted that the transcriptional expression of Nav1.1 and Nav1.2 was also detected, and, given that ICA-121431 exerted 30% inhibition on the TTX-sensitive currents (Chapter 3), future experiments should include immunocytochemical staining for these channels, to ascertain if they are also expressed at protein level.

In summary, this chapter demonstrated the molecular identity of Nav channels in CCSM. It provides novel evidence that the TTX-insensitive and TTX-sensitive Nav channels expressed in CCSM are mainly composed of Nav1.5 and Nav1.4 respectively.

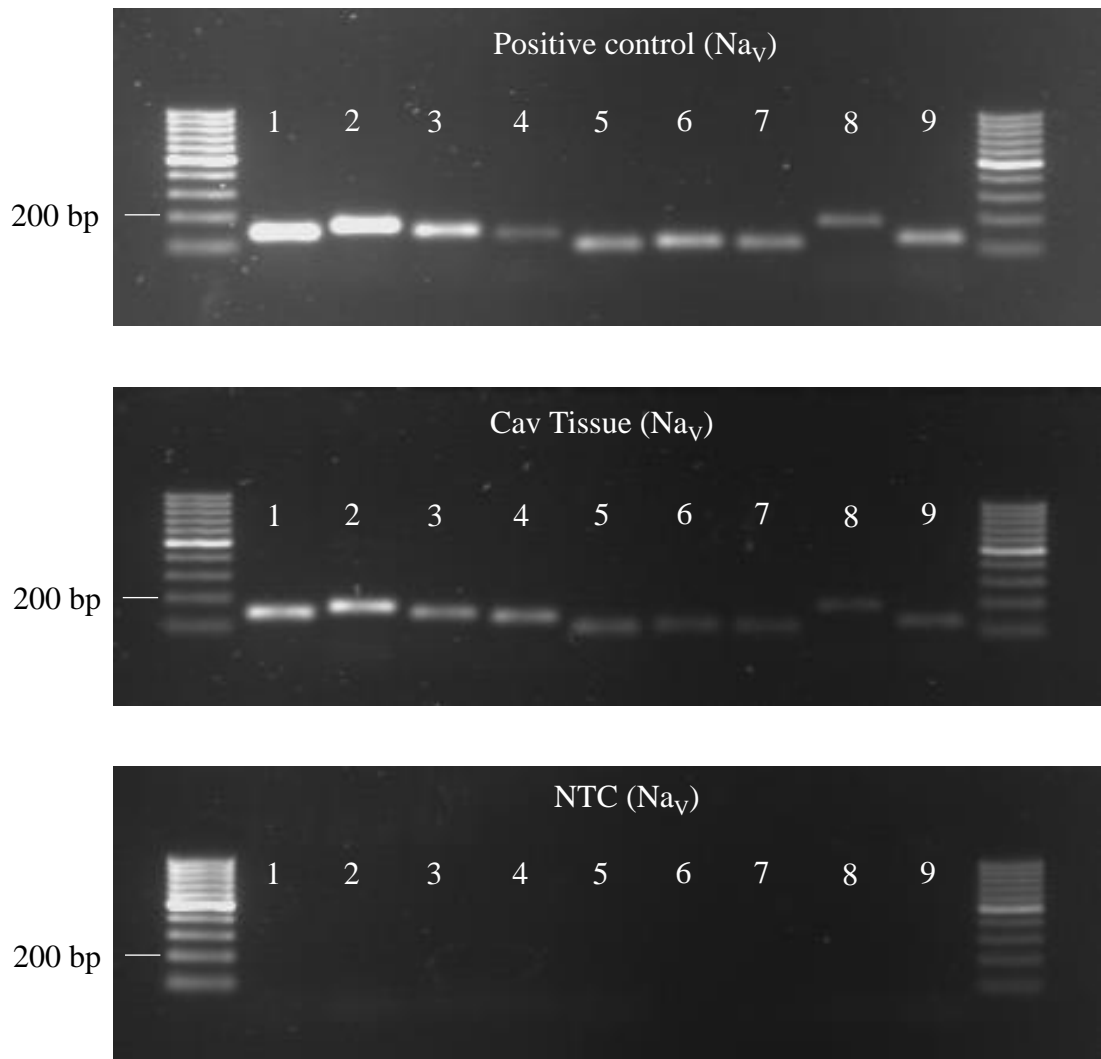


**Figure 5.1: Transcriptional expression of Na<sub>v</sub> channels in mouse CCSM tissue.** Syber safe–stained 2% agarose gel showing that mouse CCSM tissue was positive for every Na<sub>v</sub> channels (n=5 from 5 animals). Band sizes in positive control (brain) and in CCSM tissue were similar. Bands of expected sizes were present in positive control and absent in non-template control (NTC).

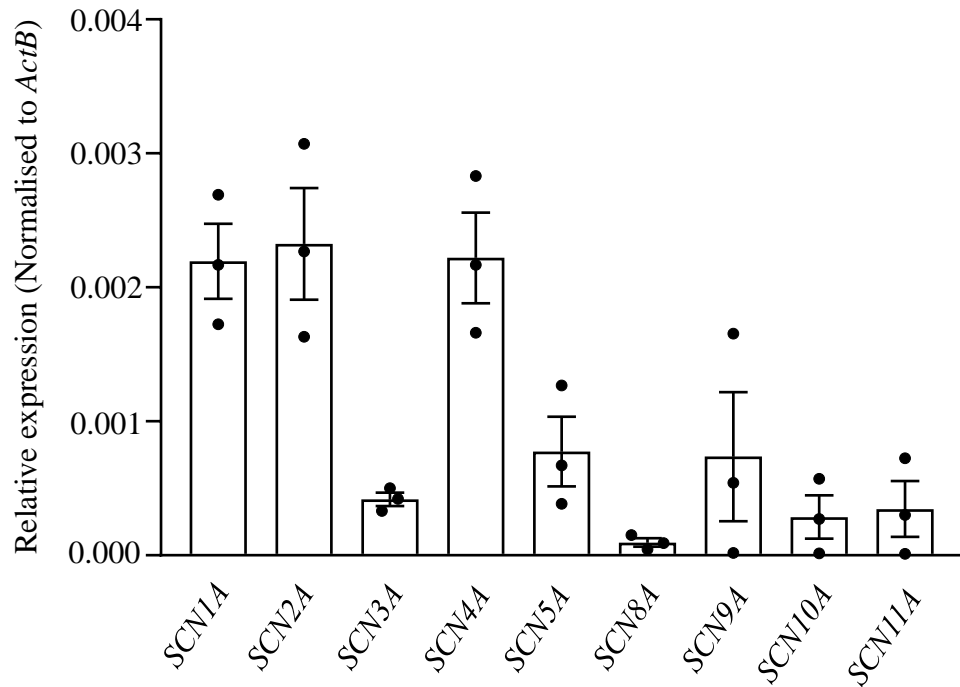


**Figure 5.2: Summary data of quantitative RT-PCR experiments.** Summary data of quantitative RT-PCR experiments showing the relative mRNA expression levels of *SCN1A* ( $\text{Na}_v1.1$ ), *SCN2A* ( $\text{Na}_v1.2$ ), *SCN3A* ( $\text{Na}_v1.3$ ), *SCN4A* ( $\text{Na}_v1.4$ ), *SCN5A* ( $\text{Na}_v1.5$ ), *SCN8A* ( $\text{Na}_v1.6$ ), *SCN9A* ( $\text{Na}_v1.7$ ), *SCN10A* ( $\text{Na}_v1.8$ ), and *SCN11A* ( $\text{Na}_v1.9$ ) in CCSM tissues (n=3 from 6 animals).

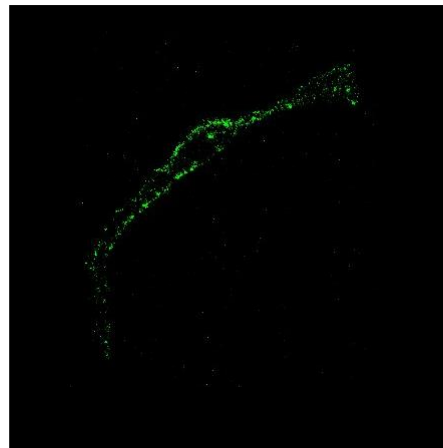
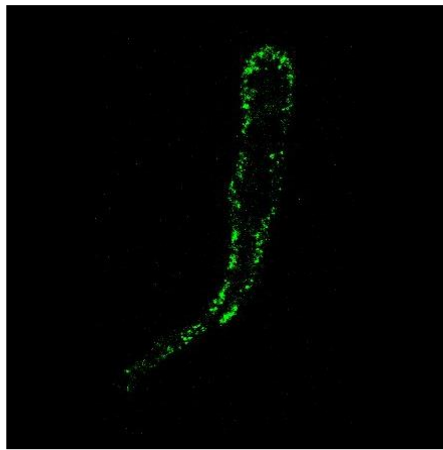
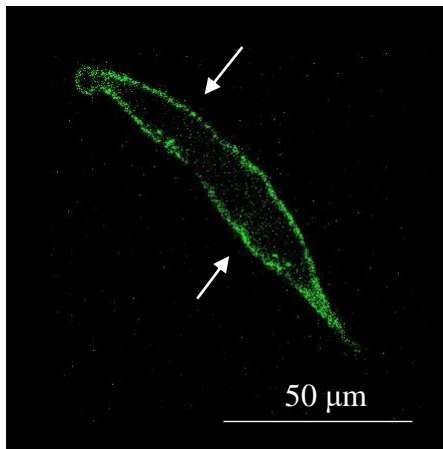


**Figure 5.3: Immunofluorescence staining for  $\text{Na}_v1.5$  on CCSM cells.** Representative confocal photomicrographs showing that freshly isolated mouse CCSM cells were immunoreactive to a selective anti- $\text{Na}_v1.5$  antibody [green] (n=5 from 5 animals).

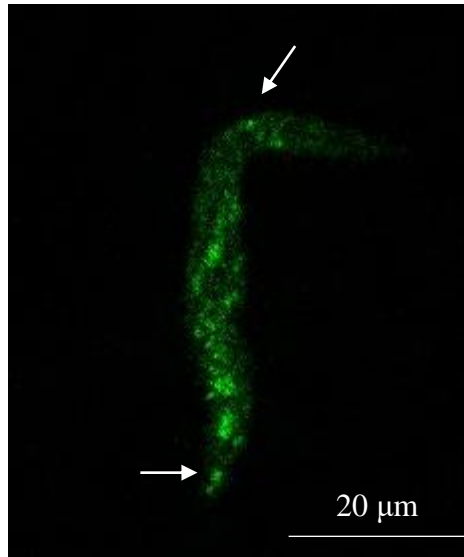
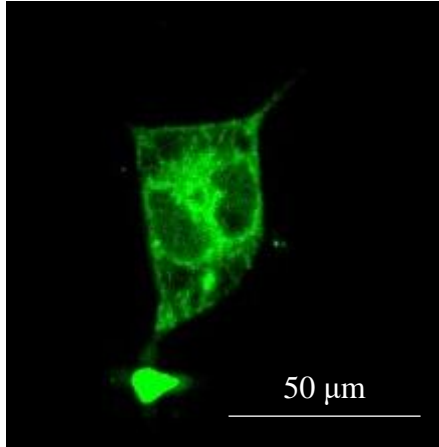


**Figure 5.4: Immunofluorescence staining for Na<sub>v</sub>1.4 on CCSM cell.** Representative confocal photomicrographs showing that freshly isolated mouse CCSM cells were immunoreactive to a selective anti-Na<sub>v</sub>1.4 antibody [green] (n=5 from 5 animals).

**A** HEK293 cells expressing Na<sub>v</sub>1.5



**B** Untransfected HEK293 cells

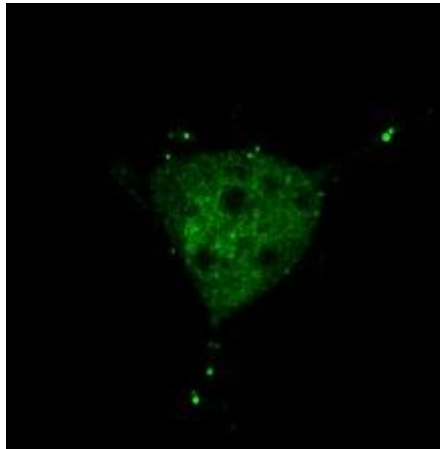
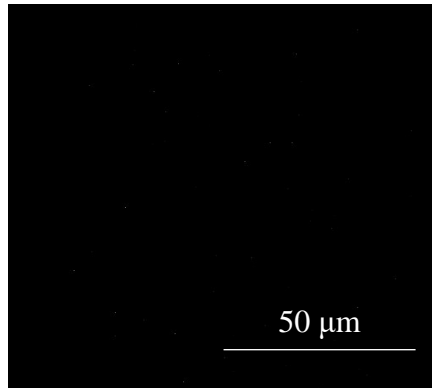


**Figure 5.5: Immunofluorescence staining for Na<sub>v</sub>1.5 on HEK293 cells (Positive control).** (A) Representative confocal photomicrographs showing that HEK293 cells expressing Na<sub>v</sub>1.5 were immunoreactive to a selective anti-Na<sub>v</sub>1.5 antibody [green] (n=3). (B) Representative confocal photomicrographs showing that untransfected HEK293 cells were immunoreactive to a selective anti-Na<sub>v</sub>1.5 antibody [green] (n=3).

**A**



**B**

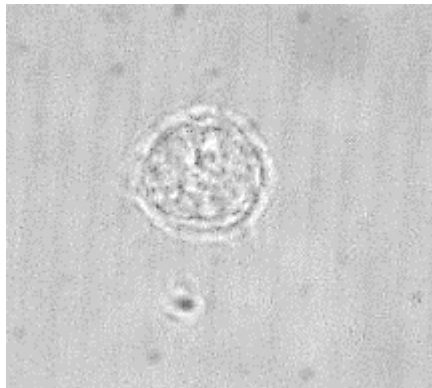
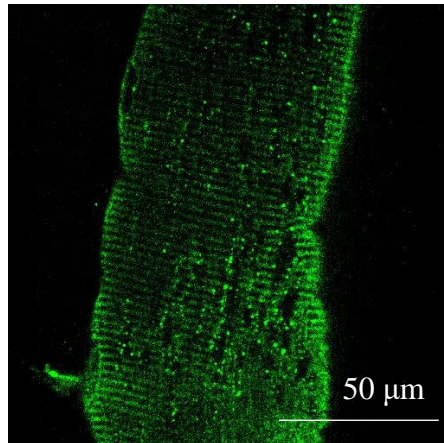
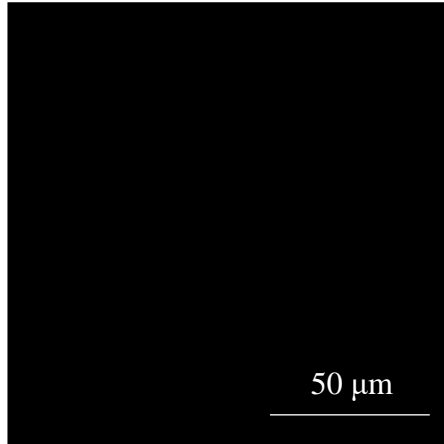


**Figure 5.6: Immunofluorescence staining for Na<sub>v</sub>1.5 on HEK293 cells (Secondary antibody-only control).** (A) Representative confocal photomicrographs showing that HEK293 cells expressing Na<sub>v</sub>1.5 were not immunoreactive to secondary antibody (n=3). (B) Brightfield image of the same cell in A.

**A**



**Bi**



**Bii**

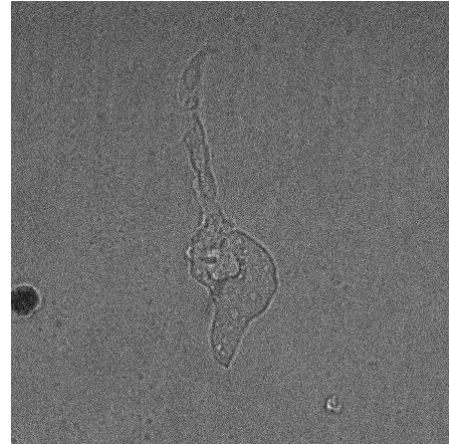
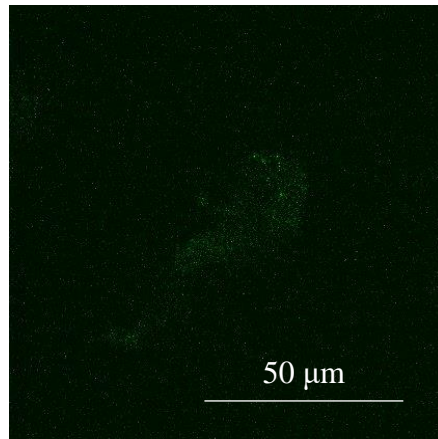


**Figure 5.7: Immunofluorescence staining for Na<sub>v</sub>1.4 on skeletal muscle tissue slice and on bladder SM cell.** (A) Representative confocal photomicrographs showing that skeletal muscle tissue slice were immunoreactive to a selective anti-Na<sub>v</sub>1.4 antibody [green] (n=4 from 4 animals). (Bi) Representative confocal photomicrographs showing that freshly isolated mouse bladder smooth muscle cells were not immunoreactive to a selective anti-Na<sub>v</sub>1.4 antibody [green] (n=3 from 3 animals). (Bii) Brightfield image of the same cell in Bi.

**A**



**B**

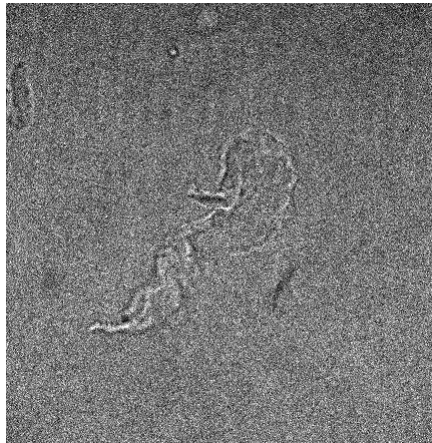
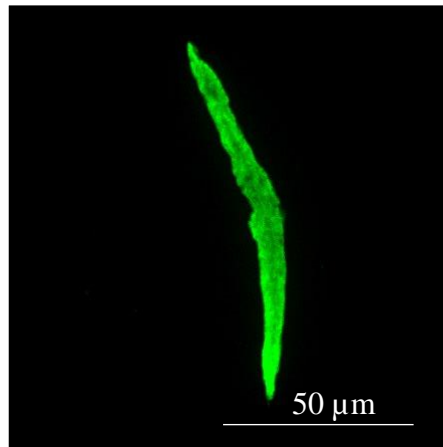
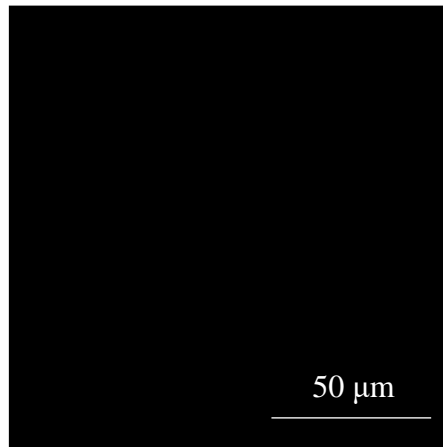


**Figure 5.8: Immunofluorescence staining for Na<sub>v</sub>1.5 on bladder SM cells (Negative control).** (A) Representative confocal photomicrographs showing that mouse bladder cells were not immunoreactive to a selective anti-Na<sub>v</sub>1.5 antibody [green] (n=3 from 3 animals). (B) Brightfield image of the same cell in A.

**A**



**Bi**



**Bii**

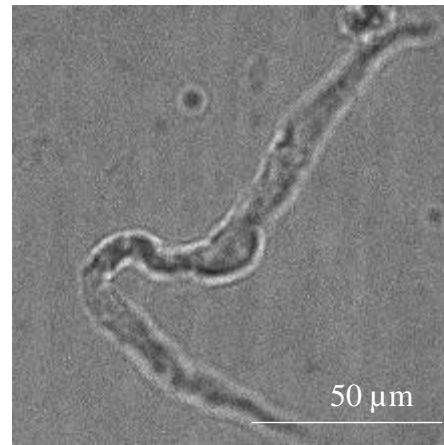


**Figure 5.9: Immunofluorescence staining for smooth muscle myosin. (A)** Smooth muscle cells were identified by smooth muscle myosin positive immunoreactivity [green] (n=5 from 5 animals). **(Bi)** Secondary antibody (Ab) only control, showing no immunofluorescence in the absence of primary antibody. (Scale bars: 50  $\mu\text{m}$ .) (Replicated in n = 5 from 5 animals). **(Bii)** Brightfield image of the same cell in **Bi**.

## **Chapter 6: Ca<sup>2+</sup>-activated Cl<sup>-</sup> channels in CCSM**

## 6.1 Introduction

Contraction of CCSM is determined by the intracellular  $\text{Ca}^{2+}$  concentration, which facilitates the actin-myosin complex.  $\text{Ca}^{2+}$  release from intracellular stores, and/or the influx of extracellular  $\text{Ca}^{2+}$  can contribute to the rise in intracellular  $\text{Ca}^{2+}$  (Hill-Eubanks *et al.*, 2011). Importantly, L-type  $\text{Ca}^{2+}$  channel blockers have been shown to reduce the amplitude of both spontaneous and agonist-induced contractions in CCSM, suggesting that depolarisation of membrane potential plays an important role in maintaining detumescent tone (McCloskey *et al.*, 2009; Hashitani *et al.*, 2005; Höppner *et al.*, 1996). However, the cellular mechanisms that regulate membrane potential in CCSMC are still unclear.

$\text{Ca}^{2+}$ -activated  $\text{Cl}^-$  channels are one of the many ion channels expressed in the CCSM (Hannigan *et al.*, 2017; Williams and Sims, 2007; Craven *et al.*, 2004; Karkanis *et al.*, 2003). In 2008, the molecular identity of  $\text{Ca}^{2+}$ -activated  $\text{Cl}^-$  channels was shown to be TMEM16A (Yang *et al.*, 2008; Caputo *et al.*, 2008; Schroeder *et al.*, 2008) and transcripts for *ANO1*, the gene encoding TMEM16A, have been detected in rabbit CCSM (Hannigan *et al.*, 2017). The resting membrane potential (RMP) of rabbit CCSM lies within the range -50 mV to -41 mV (Hashitani *et al.*, 2005), while the  $\text{Cl}^-$  equilibrium potential ( $E_{\text{Cl}}$ ) in various smooth muscle types falls in the range -38 mV to -19 mV (Chipperfield and Harper, 2000). Thus, activation of  $\text{Ca}^{2+}$ -activated  $\text{Cl}^-$  channels in CCSM cells at the RMP would be expected to result in an efflux of  $\text{Cl}^-$  ions, generating an inward current and membrane depolarisation and resultant opening L-type  $\text{Ca}^{2+}$  channels (Bulley *et al.*, 2012; Jones *et al.*, 2004; Large and Wang, 1996).

It is important to characterise this activity in murine tissues as murine models are commonly used to study erectile dysfunction (Xie *et al.*, 2007; Werner *et al.*, 2005; Hedlund *et al.*, 2000). Also, Low Density Lipid (LDL) receptor-knockout (KO) mice, db/db mice, and TallyHo mice have also been developed to study the effects of type II diabetes and obesity (Leong *et al.*, 2015; Luttrell *et al.*, 2008; Didion *et al.*, 2007; Staprans 2000), which are associated with erectile dysfunction (Burnett, 2006). Although  $\text{Ca}^{2+}$ -activated  $\text{Cl}^-$  channels have been found in CCSM in the species mentioned above, to date, no evidence has been presented to show that they are expressed in mouse CCSM. The main aims of this part of the study were: i) to determine if  $\text{Ca}^{2+}$ -activated  $\text{Cl}^-$  currents are present within this species; ii) if so, to characterise them; iii) to determine if TMEM16A

is expressed; iv) to examine the mechanisms underlying activation of these currents and, finally; v) determine if they participate in mediating contractions in the whole tissue.

## **6.2 Results**

### **6.2.1 Protein expression of TMEM16A in CCSM cells**

The representative confocal photomicrograph in Figure 6.1Ai confirm that freshly isolated CCSM cells were immunoreactive for TMEM16A, demonstrated by the strong immunofluorescence in cells treated with anti-TMEM16A antibody. Staining shown in Figure 6.1Ai was similar in three procedures carried out on cells dispersed from three animals. Figure 6.1Aii shows a bright field image of the same cell. The anti-TMEM16A antibody was validated with negative and positive controls. Figure 6.1Bi shows a negative control, demonstrating that immunofluorescence was not observed in the vast majority of murine detrusor SM cells, while weak immunofluorescence was observed in < 2% of the detrusor cells. Figure 6.1Bii shows a bright field image of the same cell. Since interstitial cells of Cajal (ICCs) in murine jejunum are known to express TMEM16A proteins (Gomez-Pinilla, 2009), we used the same antibody on jejunum smooth muscle tissue strips as a positive control. Figure 6.2A shows immunofluorescence on myenteric ICC located in between the longitudinal and circular muscle layers of the jejunum. We also carried out staining for smooth muscle myosin (SMM) heavy chain 11 in CCSM cells. In this case, dense staining was observed throughout the cells (Figure 6.2B). Therefore, spindle shaped cells dispersed from mouse CCSM were immunoreactive to SMM heavy chain and TMEM16A antibodies, confirming the protein expression of TMEM16A in CCSM cells.

### **6.2.2 Two different TMEM16A specific blockers inhibited chloride tail currents**

Having confirmed the expression of TMEM16A in mouse CCSM, we next evaluated the effects of specific TMEM16A antagonists on CCSM electrical activity. First, we examined the effects of the TMEM16A antagonists, Ani9 and CaCC (inh)-A01, on evoked tail current in isolated CCSM cells using patch clamp techniques. Cells were held at -60 mV and currents were evoked by a step from -60 mV to 0 mV. Tail currents were then evoked by a step down to -80 mV for 600 ms. Figures 6.3Ai and Bi are representative traces which show that 1  $\mu$ M Ani9 and 3  $\mu$ M CaCC(inh)-A01 inhibited tail current

amplitude, suggesting that the tail current was conducted through TMEM16A channels. Summary data for the effects of the two TMEM16A blockers on peak tail current amplitude are shown in Figures 6.3Aii and Bii.

### 6.2.3 The effect of low Cl<sup>-</sup> Hanks on tail current

Next, to confirm that the tail current was carried by chloride ions, we examined the effect of reducing the external Cl<sup>-</sup> concentration on tail current reversal potential. Cells were initially stepped to a test potential of -20 mV for 500 ms followed by a 150 ms voltage ramp from -50 to +50 (Figure 6.4A). The step duration was sometimes varied depending on the rate of current activation. The procedure was then repeated a few seconds after reducing [Cl]<sub>o</sub> to 49 mM (solution 5). This had the effect of shifting the reversal potential of the tail current in the positive direction. Both sweeps were then corrected for capacitance and leakage currents by subtracting a 'null' trace evoked in the presence of nifedipine. Nifedipine was previously shown to abolish Ca<sup>2+</sup>-activated Cl<sup>-</sup> currents evoked by voltage steps by blocking Ca<sup>2+</sup> influx via L-type Ca<sup>2+</sup> channels (Craven *et al.*, 2004). In control (135 mM external Cl<sup>-</sup>, calculated E<sub>Cl</sub> = 0 mV), the difference current reversed at 0 mV (+3 mV when corrected for a junction potential of +3 mV), while in low external Cl<sup>-</sup> solution (49 mM external Cl<sup>-</sup>, calculated E<sub>Cl</sub> = +27 mV) it shifted to +17 mV (+19 mV when corrected for +2 mV junction potential). In the example shown in Figure 6.4A, the amplitude of the inward current during the step to -20 mV also increased in the presence of low external Cl<sup>-</sup>. In six experiments, the mean reversal potential was +1 ± 3 mV for 135 mM external Cl<sup>-</sup> and +24 ± 4 mV for 49 mM external Cl<sup>-</sup> (corrected for junction potentials, p<0.05, Figure 6.4B). Based on the reversal of tail current at the Cl<sup>-</sup> equilibrium potential, and its susceptibility to external Cl<sup>-</sup> concentration, it is very likely that the tail currents were carried mainly by chloride ions.

### 6.2.4 Two different TMEM16A specific blockers abolished STICs and STDs

In voltage-clamp mode, 141 out of 298 (47%) mouse CCSM cells studied fired STICs when held at -60 mV. To determine if STICs were carried by Ca<sup>2+</sup>-activated Cl<sup>-</sup> currents, two different TMEM16A-specific blockers, Ani9 and CaCC(inh)-A01, were tested on

these spontaneous currents (Figures 6.5 and 6.6). For the purposes of summarising these data, the average STIC amplitude in each cell was calculated for the 30 s period immediately before application of each drug, and again for 30 s after the drug had exerted its maximal effect. The average values were then used to calculate the means.

Ani9 and CaCC(inh)-A01 both greatly reduced STIC amplitude, but had less effect on frequency (Figures 6.5 and 6.6). Overall, Ani9 (1  $\mu$ M) and CaCC(inh)-A01 (3  $\mu$ M) reduced mean STIC amplitude by 95% and 83%, respectively (Figures 6.5Bi and Bii) and frequency by 61 % and 60 %, respectively (Figures 6.6Bi and Bii).

Cells were also studied in current clamp mode to observe changes in membrane potential. In these experiments, the resting membrane potential was adjusted to between -50 mV and -60 mV by injecting small hyperpolarising currents. The majority of cells (72 of 111) displayed regular depolarisations of membrane potential, referred to as STDs. These STDs were sensitive to Ani9 and CaCC(inh)-A01 (Figures 6.7 and 6.8). 1  $\mu$ M Ani9 reduced STD amplitude by 87% and frequency by 53% (Figures 6.7Bi and Bii), while 3  $\mu$ M CaCC reduced STD amplitude by 84% and frequency by 74% (Figures 6.8Bi and Bii).

### **6.2.5 Contribution of Ca<sup>2+</sup> stores to STICs and STDs in CCSMC**

Ca<sup>2+</sup>-release-activated Ca<sup>2+</sup> (CRAC) channels are known to be involved in SR refilling (Putney *et al.*, 2017). We investigated if CRAC channels were involved in the generation of STICs and STDs in CCSM cells by examining the effects of GSK7975A, an ORAI channel blocker. GSK7975A had a marked inhibitory effect on STICs (Figure 6.9) and on STDs (Figure 6.10) in CCSM cells. Summary data showing the effect of GSK7975A on STICs and STDs in 6 cells are presented in Figures 6.9 Bi and Bii and Figures 6.10 Bi and Bii, respectively. It would be interesting to try GSK7975A on Cl<sup>-</sup> tail current for future experiments, as it could act as a control that it did not block TMEM16A channel.

The effect of cyclopiazonic acid (CPA, 10  $\mu$ M), a blocker of the sarcoplasmic Ca<sup>2+</sup>-ATPase, was also studied on STICs and STDs. CPA (10  $\mu$ M) abolished these events (Figures 6.11 and 6.12), while in 1 cell out of 6 it also caused a depolarisation (Figure 6.13). Summary data for the effect of CPA on STICs and STDs are summarised in Figures 6.11Bi and Bii and 6.12Bi and Bii, respectively.

### **6.2.6 Involvement of both RyR and IP<sub>3</sub>R in the activation of STICs and STDs**

Previous studies on rabbit CC tissue slices suggested that ryanodine receptors (RyRs) and inositol 1,4,5-trisphosphate (IP<sub>3</sub>) receptors (IP<sub>3</sub>Rs) were involved in the generation of Ca<sup>2+</sup> waves (Sergeant *et al.* 2009), which presumably contribute to the activation of TMEM16A channels, generating STICs and STDs. Hence, we tested the relative contributions of RyRs and IP<sub>3</sub>Rs to mouse CCSM electrical activity using tetracaine, an inhibitor of RyRs and 2APB, a blocker of IP<sub>3</sub>Rs. Figures 6.14A and 6.15A show an example where tetracaine (100 μM) and 2APB (100 μM) reversibly inhibited STICs. Summary data for these effects are shown in Figures 6.14Bi and Bii and 6.15Bi and Bii, where the STICs were effectively inhibited; tetracaine exerted 100% block for both amplitude and frequency, while 2APB exerted 98% block for amplitude and 88% reduction in frequency. Tetracaine (100 μM) and 2APB (100 μM) also reversibly blocked STDs (Figures 6.16 and 6.17) as evidenced by the 93% reduction in amplitude and 94% decrease in frequency, while 2APB caused a 96% block in amplitude and 92% reduction in frequency. Taken together, these results suggest that Ca<sup>2+</sup> release from both RyRs and IP<sub>3</sub>Rs are required for STICs and STDs in CCSM cells.

### **6.2.7 Involvement of L-type Ca<sup>2+</sup> channel in the activation of STICs and STDs**

To find out if Ca<sup>2+</sup> entry through L-type calcium channels was involved in the activation of STICs or STDs, the effect of nifedipine was tested on these events. Nifedipine (1 μM) failed to diminish the amplitude or frequency of STICs (Figure 6.18). Nifedipine also failed to diminish the amplitude and frequency of STDs (Figure 6.19), however, it was apparent that the mean duration of the STDs was reduced (Figure 6.20). Summary data in Figure 6.20B shows that the mean duration of depolarisations (time from half maximum voltage to half minimum voltage) was reduced in the presence of 1 μM nifedipine.

### **6.2.8 Ani9 inhibited PE-induced transient inward currents and transient depolarisations.**

Since the main excitatory innervation in CC is adrenergic, it was of interest to examine if TMEM16A contributed to adrenergic responses in CCSM cells. In voltage-clamped CCSM cells, addition of the adrenergic  $\alpha$ 1-receptor agonist phenylephrine (300 nM), caused a large transient inward current, followed by smaller, oscillating transient inward currents (Figure 6.21). Ani9 was then used to examine the contribution of  $\text{Ca}^{2+}$ -activated  $\text{Cl}^-$  channels in phenylephrine-induced inward currents. Addition of Ani9 (1  $\mu\text{M}$ ) significantly reduced both the amplitude (Figure 6.21Bi) and frequency (Figure 6.21Bii) of the oscillating currents. The effect of phenylephrine was partially restored upon wash-out of the blocker. In current clamp mode, 300 nM phenylephrine evoked a series of phasic depolarisations (Figure 6.22A) that were susceptible to blockade by 1  $\mu\text{M}$  Ani9 (Figures 6.22A, Bi and Bii). These suggest that TMEM16A may be involved in adrenergic excitatory responses in CCSM cells.

### **6.2.9 Ani9 reduced the frequency of PE-induced contractions in CCSM tissue**

To investigate the functional role of TMEM16A channels in CCSM contractility we examined if phenylephrine-induced contractions of CCSM strips were affected by Ani9. The representative trace in Figure 6.23A shows that phenylephrine induced a series of phasic contractions. Ani9 (10  $\mu\text{M}$ ) reduced the frequency, but not the amplitude, of these events (Figures 6.23A,Bi and Bii ). Summary data in Figure 6.23Bii shows that Ani9 significantly reduced the mean frequency of the phenylephrine-induced contractions from  $244 \pm 35$  to  $38 \pm 10$  contractions per hour.

Since  $\alpha$ -adrenoceptor-induced contractions in corpus cavernosum can be antagonized by L-type  $\text{Ca}^{2+}$  channel blockers (McCloskey *et al.*, 2009), it was important to ensure that Ani9 did not have a non-specific blocking effect on these channels. Patch clamp experiments confirmed that Ani9 (10  $\mu\text{M}$ ) had very little effect on L-type  $\text{Ca}^{2+}$  current (Figure 6.24). These experiments suggest that TMEM16A may have a functional role in adrenergic responses in CC tissue.

### 6.3 Discussion

$\text{Ca}^{2+}$ -activated  $\text{Cl}^-$  channels regulate many physiological functions, including cell excitability (Cotton *et al.*, 1997), osmotic balance, and fluid secretion (Eggermont, 2004). In smooth muscle, activation of these channels is usually excitatory because the  $\text{Cl}^-$  equilibrium potential ( $E_{\text{Cl}}$ ) in smooth muscles is believed to be within the range of  $-38$  mV to  $-19$  mV (Chipperfield and Harper, 2000; Aickin and Brading, 1982), whereas the resting membrane potential is usually more hyperpolarised than this. For example, in rabbit CCSM, the resting membrane potential is within the range of  $-50$  mV to  $-41$  mV (Hashitani *et al.*, 2005) and consequently, opening  $\text{Cl}^-$  channels in this tissue will induce depolarisation and opening of L-type  $\text{Ca}^{2+}$  channels, which will result in  $\text{Ca}^{2+}$ -influx and contraction (Sanders, 2008). Intracellular recordings from rabbit corpus cavernosum show that the tissue develops spontaneous depolarisations that are blocked by niflumic acid, a  $\text{Ca}^{2+}$ -activated chloride channel blocker and dihydropyridines, blockers of L-type  $\text{Ca}^{2+}$  channels (Thornbury *et al.*, 2019; Hashitani *et al.*, 2005). The presence and/or physiological relevance of  $\text{Cl}^-$  channels in the CCSM of the mouse species is unknown, and therefore forms the focus of this Chapter.

TMEM16A was identified as a  $\text{Ca}^{2+}$ -activated chloride channel (CaCC) in 2008 (Yang *et al.*, 2008; Caputo *et al.*, 2008; Schroeder *et al.*, 2008) and was proposed as the molecular identity of  $\text{Ca}^{2+}$ -activated  $\text{Cl}^-$  channels in rabbit CCSM (Hannigan *et al.*, 2017). In the present study, we present evidence based on immunocytochemistry,  $[\text{Cl}^-]_o$ -dependence, and pharmacology, that TMEM16A is functionally expressed in mouse CCSM cells. Inhibition of chloride tail currents using two different  $\text{Ca}^{2+}$ -activated  $\text{Cl}^-$  channel blockers, combined with the shift in the reversal potential of the tail current in ion substitution experiments, verified the presence of  $\text{Ca}^{2+}$ -activated  $\text{Cl}^-$  currents in isolated CC myocytes. Furthermore, the molecular identity of  $\text{Ca}^{2+}$ -activated  $\text{Cl}^-$  channels was confirmed to be TMEM16A via CCSM single-cell immunofluorescence staining.

In the present study, both STICs and STDs in murine CCSMC were inhibited by CPA, consistent with a role for  $\text{Ca}^{2+}$  release from the SR in the generation of this activity (Craven *et al.*, 2004). STICs and STDs were also abolished by tetracaine and 2APB, antagonists of ryanodine receptors (Laver and van Helden, 2011) and  $\text{IP}_3$  receptors (Maruyama *et al.*, 1997), respectively. Therefore, it appears that the spontaneous activation of TMEM16A channels in murine CCSMC relies on a combination of  $\text{Ca}^{2+}$

release from both RyRs and IP<sub>3</sub>Rs. It should be noted however, that both tetracaine and 2-APB may also have off-target effects. Tetracaine can block Nav channels (Li *et al.*, 1999). Although Nav1.5 are present in mouse CCSM, most of the Nav channels would be inactivated at resting membrane potential (-50 mV to -60 mV), suggesting little contribution to myogenic activity at these potentials, under normal circumstances (Lim *et al.*, 2022). This is supported by the frequent inability of TTX to inhibit STDs [Refer to Chapter 4]. However, their contribution during excitatory stimulation, for example, veratridine-induced or  $\alpha$ -adrenoreceptor agonist-induced excitation, cannot be overlooked [Refer to Chapters 3 and 4]. In the context where spontaneous electrical activities are being studied in single CCSM cells, using tetracaine should not pose as a problem.

The IP<sub>3</sub>R inhibitor, 2APB has been shown to inhibit store operated Ca<sup>2+</sup> (SOC) entry (Peinelt *et al.*, 2006; Peppiatt *et al.*, 2003). Unfortunately, almost every IP<sub>3</sub>R antagonist has limitations and their selectivity has been questioned. For example, heparin has low tissue penetration (Saleem *et al.*, 2014) and Xestospongin C blocks L-type Ca<sup>2+</sup> channels and K<sup>+</sup> channels (Ozaki *et al.*, 2002), both of which contribute to CCSM phasic contractions (Hannigan *et al.*, 2017; 2016). Although 2APB may have unwanted off-target effects in some cell types, we previously found that it was able to consistently and reversibly inhibit IP<sub>3</sub>-mediated Ca<sup>2+</sup> signals (Morgan *et al.*, 2022; Drumm *et al.*, 2018; Griffin *et al.*, 2016; Drumm *et al.*, 2015; Johnston *et al.*, 2005; Sergeant *et al.*, 2001), without affecting caffeine-induced Ca<sup>2+</sup>-entry (Drumm *et al.*, 2015), sarcoplasmic reticulum refilling (Sergeant *et al.*, 2001), or capacitive Ca<sup>2+</sup> entry (Bradley *et al.*, 2005). Therefore, we chose 2APB as the antagonist of IP<sub>3</sub>Rs in this study.

Vascular diseases like diabetes and hypertension can impair neurogenic and endothelium-mediated relaxation of penile smooth muscle (Ledda, 2000). A survey involving 7,689 patients found that ED was prevalent (>50%) among those with diabetes and/or hypertension (Giuliano *et al.*, 2004). Alterations in STIM and ORAI activity has been highlighted in injured or diseased blood vessels (Zhang *et al.*, 2011) and Giachini *et al.* (2009) showed that the transcriptional and proteomic expression, as well as the function of both STIM and ORAI were upregulated in the aorta of hypertensive rats. Since vascular dysfunction can compromise cavernosal function (Lue *et al.*, 2000), we investigated the effect of GSK-7975A, a selective store-operated calcium channel inhibitor, on STICs and STDs recorded from murine CCSM. A low concentration (3  $\mu$ M) of GSK-7975A

inhibited these events, suggesting that they are reliant on store-operated calcium entry, assuming specificity at blocking ORAI channel.

In contrast, the L-type  $\text{Ca}^{2+}$  channel blocker, nifedipine had no effect on STICs, or the amplitude and frequency of the STDs, suggesting that  $\text{Ca}^{2+}$  entry via L-type  $\text{Ca}^{2+}$  channels was not involved in the initiation of these events. However, nifedipine shortened the duration of the STDs, suggesting that influx via L-type  $\text{Ca}^{2+}$  currents contributes to the STD plateau potential. This is similar to findings in sheep urethral smooth muscle cells, where nifedipine reduced STD plateau duration, but did not reduce STD frequency (Cotton *et al.*, 1997). However, Cotton *et al.* (1997) found that nifedipine also reduced STD amplitude, possibly as a result of larger L-type  $\text{Ca}^{2+}$  currents expressed in these urethral cells.

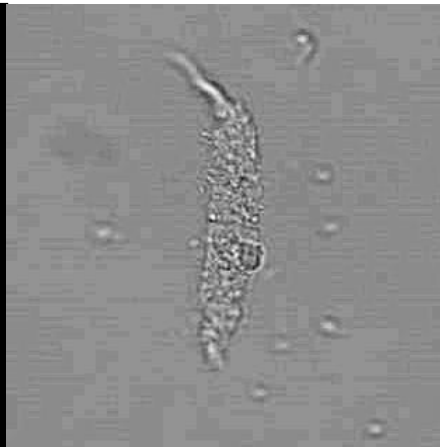
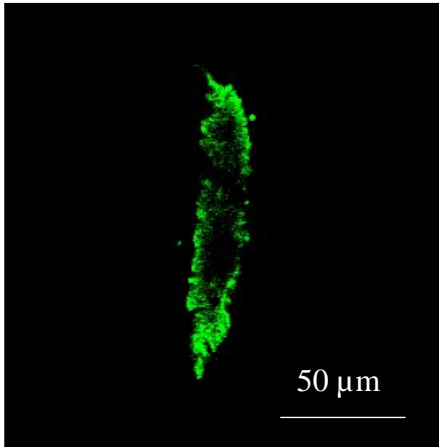
The functional role of TMEM16A in intact CCSM tissue strips was investigated using Ani9, a selective TMEM16A blocker (Seo *et al.*, 2016). Phenylephrine (300 nM) induced phasic contractions, which were significantly disrupted by Ani9, suggesting a role for TMEM16A in the regulation of CCSM contractility by the sympathetic nerves.

Some TMEM16A blockers are known to also block L-type  $\text{Ca}^{2+}$  current (Hannigan *et al.*, 2017), hence it was important to check that the effects of Ani9 were not attributable to an off-target effect on L-type  $\text{Ca}^{2+}$  channels. We found that Ani9 (10  $\mu\text{M}$ ) did not inhibit L-type  $\text{Ca}^{2+}$  currents, therefore its inhibitory effect on phasic contractions of mouse CCSM tissue strips is not due to an effect on L-type  $\text{Ca}^{2+}$  channels, as may be the case with other CaCC blockers (Liu *et al.*, 2021). Furthermore, previous work done in our lab has shown that Ani9 did not inhibit  $\text{Ca}^{2+}$  waves in airway SM cells, suggesting little effect on  $\text{Ca}^{2+}$  release from the store. However, similar experiments should be performed in CCSM cells to ascertain drug specificity.

In summary, the present study provides direct evidence that the mouse CCSM exhibits spontaneous TMEM16A currents that are activated by  $\text{Ca}^{2+}$  released from the sarcoplasmic reticulum. Furthermore, these channels contribute to the contractile state of the CCSM and therefore are likely to help maintain penile detumescence.

**Ai** TMEM16A antibody

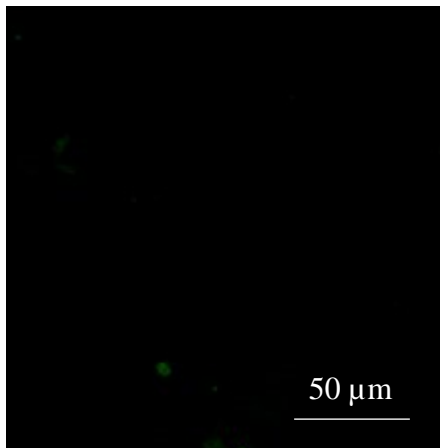
**Aii** Bright field image



CCSMC

**Bi** TMEM16A antibody

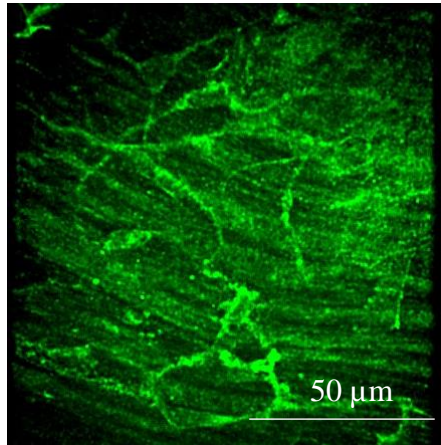
**Bii** Bright field image



Detrusor  
SMC

**Figure 6.1: Immunofluorescence staining for (A) TMEM16A in CCSM cells [green] (n = 3 from 3 animals). (B) TMEM16A in detrusor SM cell [Negative control] (n = 3 from 3 animals).**

**A** Mouse Jejunum tissue



**B** Smooth muscle myosin

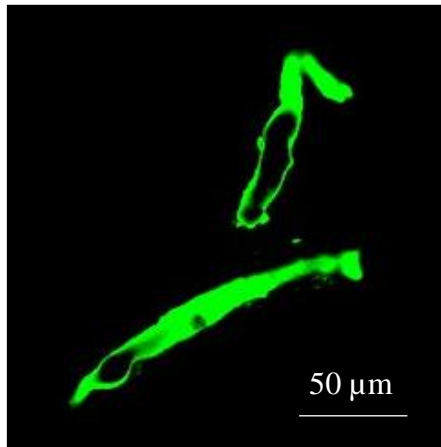


**Figure 6.2: Immunofluorescence staining for (A) TMEM16A in mouse jejunum tissue strip [positive control, green] (n = 3 from N= 3 animals). (B) Smooth muscle myosin in CCSM cells [green] (n = 3 from N = 3 animals).**

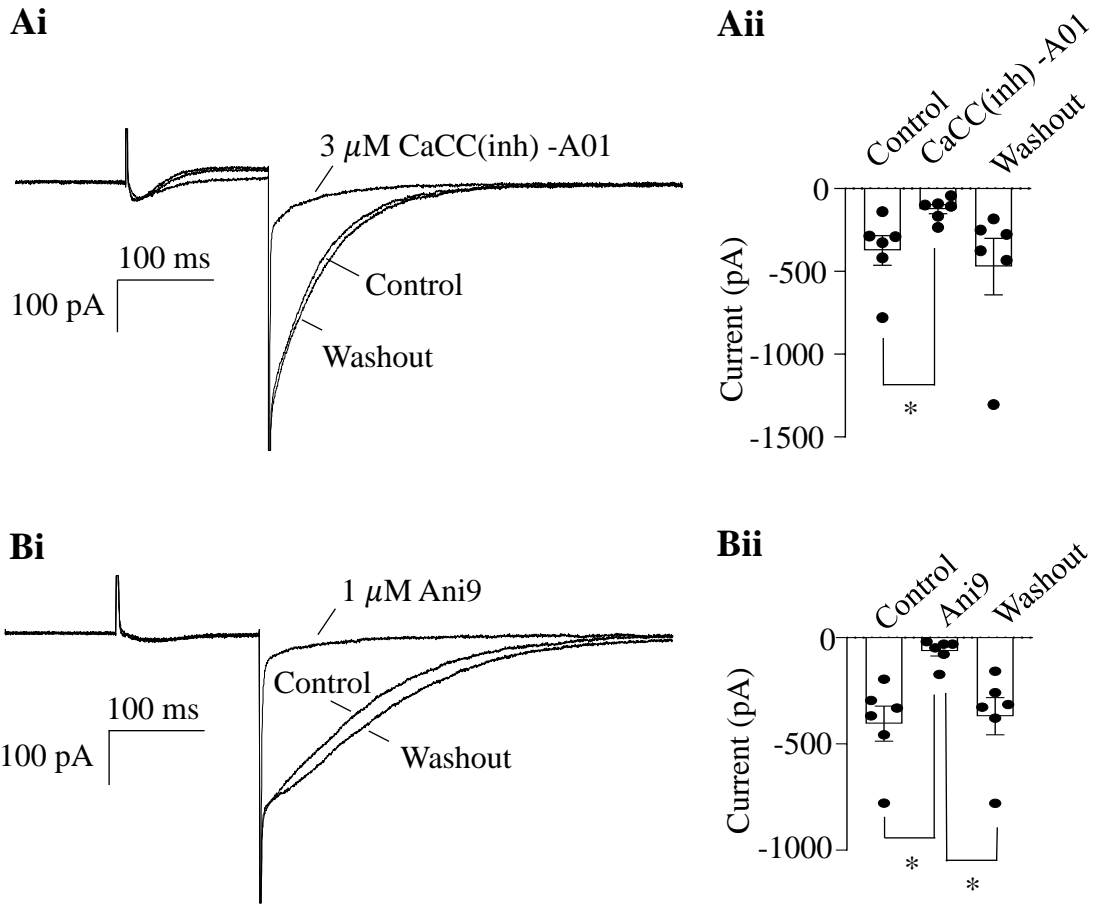


**Figure 6.3: Effect of CaCC(inh)-A01 and Ani9 on chloride tail.** (Ai) Cell was held at -60 mV and stepped to 0 mV. It was then stepped down to -80 mV to evoke a tail current. Representative traces showing the reversible effect of 3  $\mu\text{M}$  CaCC(inh)-A01 on tail current. (Aii) Summary data showing the effect of 3  $\mu\text{M}$  CaCC(inh)-A01 on tail current ( $n = 6$  from 6 animals,  $*p < 0.05$ , one way ANOVA). (Bi) Representative traces showing the reversible effect of 1  $\mu\text{M}$  Ani9 on tail current. (Bii) Summary data showing the effect of 3  $\mu\text{M}$  Ani9 on tail current ( $n = 6$  from 6 animals,  $*p < 0.05$ , one way ANOVA).

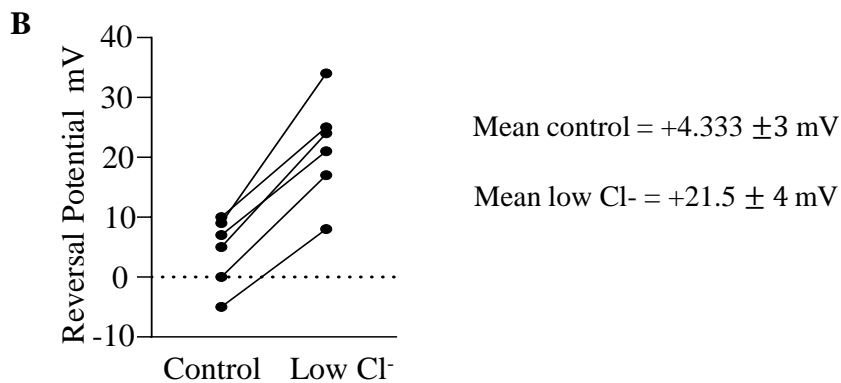
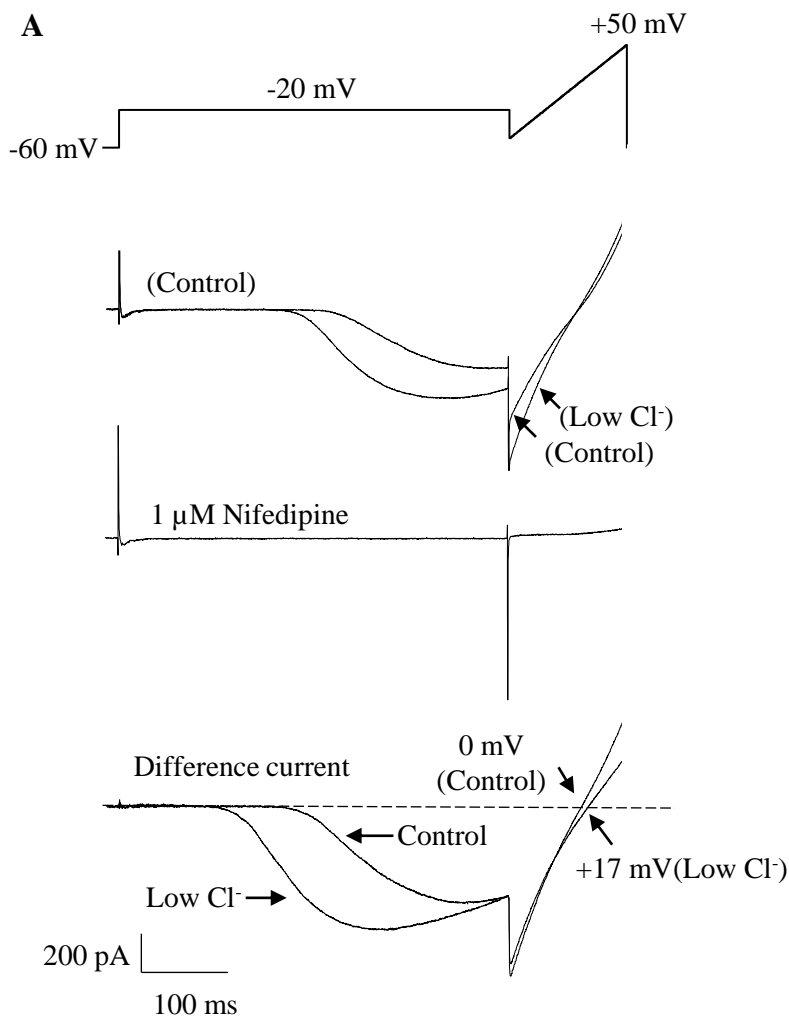


**Figure 6.4: The effect of low Cl<sup>-</sup> Hanks on tail current.** (A) Cell was held at -60 mV and stepped to -20 mV to load the cell with Ca<sup>2+</sup>. It was then ramped from -50 to +50 mV to record the reversal potential of the tail current. Recordings were made in 135 mM Cl<sup>-</sup> (Control) and 49 mM Cl<sup>-</sup> (low Cl<sup>-</sup>). (B) The shift in each case is consistent with the current being carried through TMEM16A channels (n = 6 from 6 animals; \*p<0.05, paired t test).

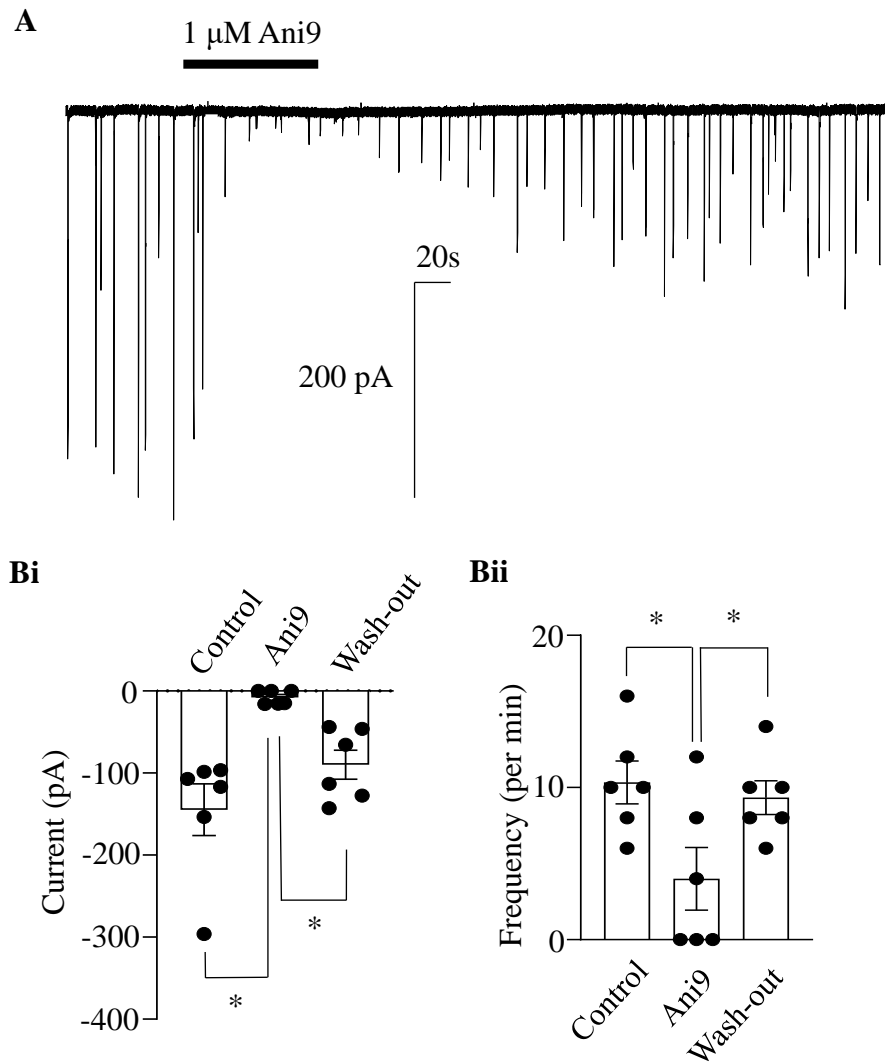


**Figure 6.5: TMEM16A specific blocker Ani9 abolished STICs.** (A) An example showing the effect of 1  $\mu$ M Ani9 on STICs when a CCSM cell was held under voltage clamp at -60 mV. (Bi) Summary of the effect of 1  $\mu$ M Ani9 on STICs amplitude (n = 6 from 6 animals; \*p<0.05, one way ANOVA) and (Bii) STICs frequency (n = 6 from 6 animals; \*p<0.05, one way ANOVA).

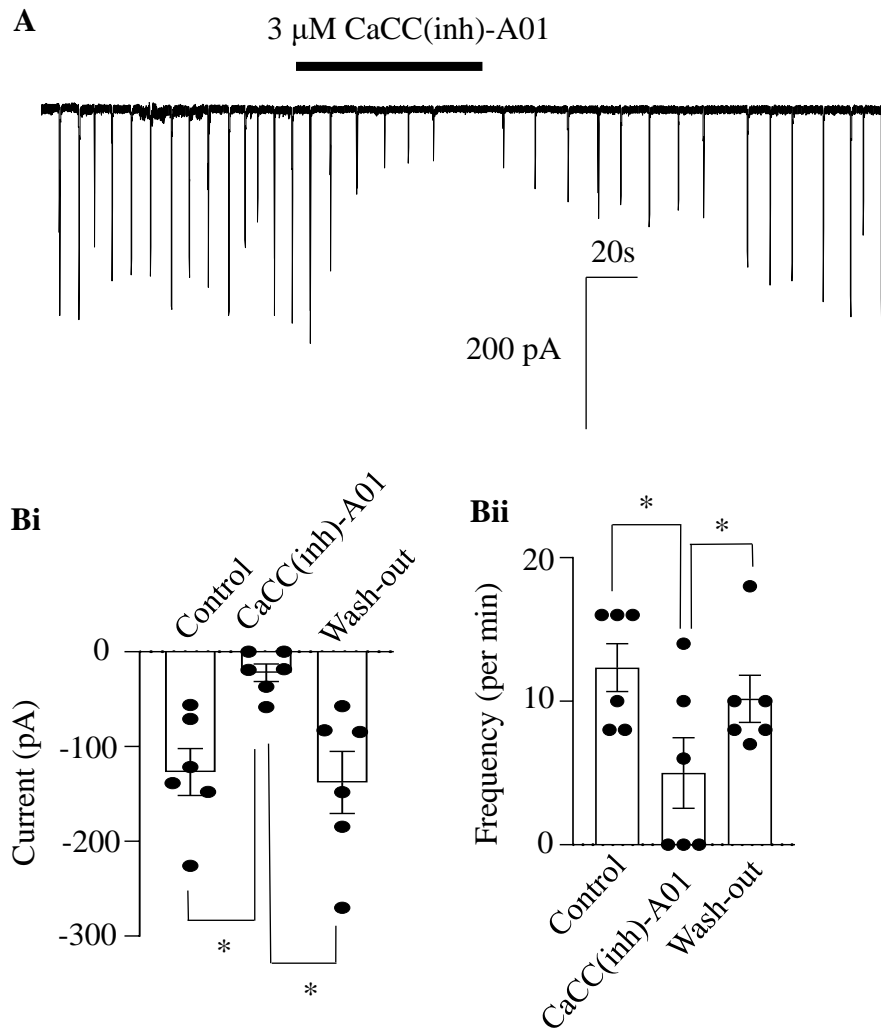


**Figure 6.6: TMEM16A specific blocker CaCC(inh)-A01 abolished STICs. (A)** An example showing the effect of 3  $\mu$ M CaCC(inh)-A01 on STICs when a CCSM cell was held under voltage clamp at -60 mV. **(Bi)** Summary of the effect of 3  $\mu$ M CaCC(inh)-A01 on STICs amplitude (n = 6 from 6 animals; \*p<0.05, one way ANOVA) and **(Bii)** STICs frequency (n = 6 from 6 animals; \*p<0.05, one way ANOVA).

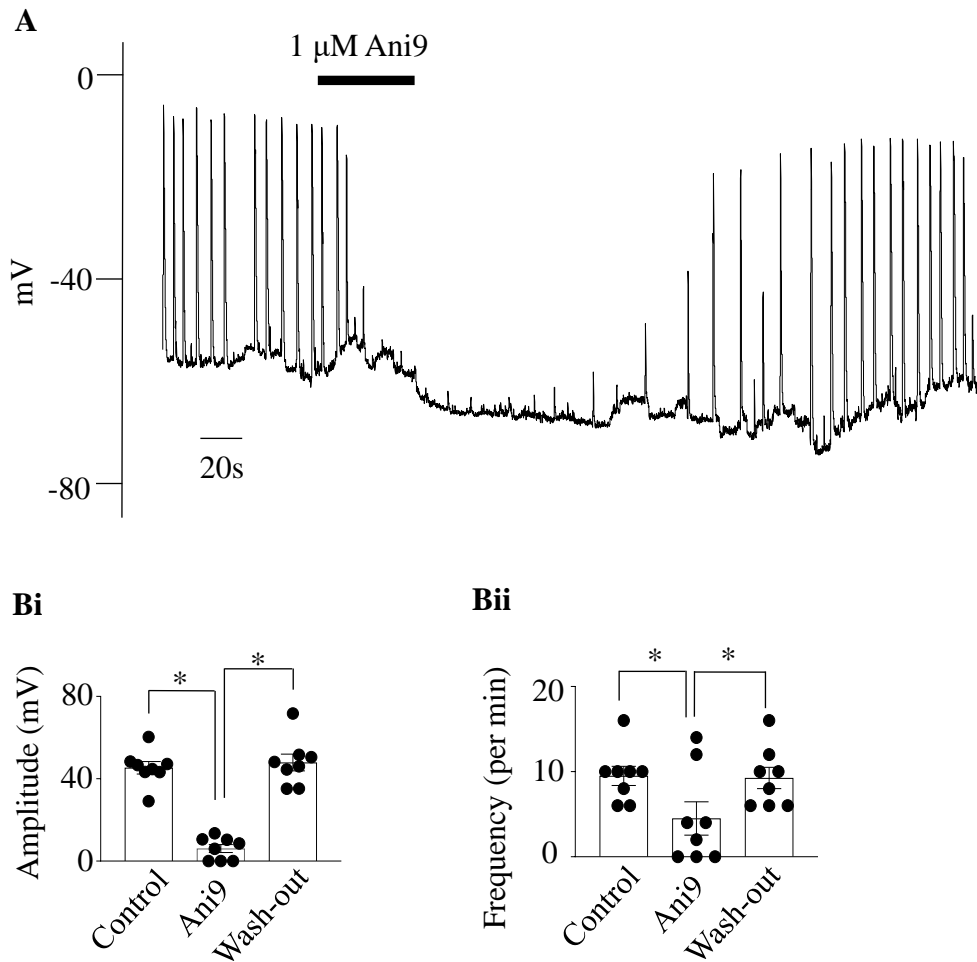


**Figure 6.7: TMEM16A specific blocker Ani9 abolished STDs.** (A) An example showing the effect of 1  $\mu$ M Ani9 on STDs in current clamp mode. (Bi) Summary of the effect of 1  $\mu$ M Ani9 on STDs amplitude (n = 6 from 6 animals; \*p<0.05, one way ANOVA) and (Bii) STDs frequency (n = 6 from 6 animals; \*p<0.05, one way ANOVA).

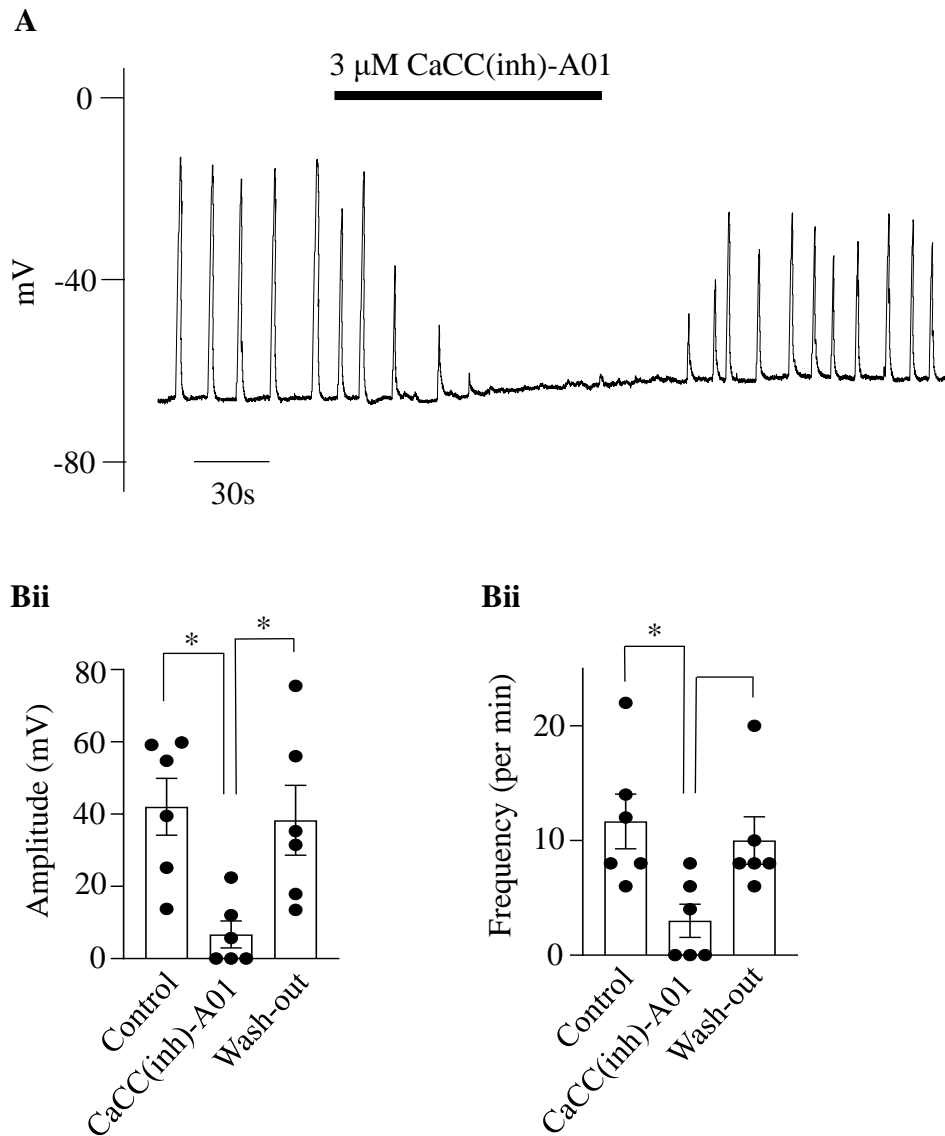


**Figure 6.8: TMEM16A specific blocker CaCC(inh)-A01 abolished STDs.** (A) An example showing the effect of 3  $\mu$ M CaCC(inh)-A01 on STDs in current clamp mode. (Bi) Summary of the effect of 3  $\mu$ M CaCC(inh)-A01 on STDs amplitude (n = 6 from 6 animals; \*p<0.05, one way ANOVA) and (Bii) STDs frequency (n = 6 from 6 animals; \*p<0.05, one way ANOVA).



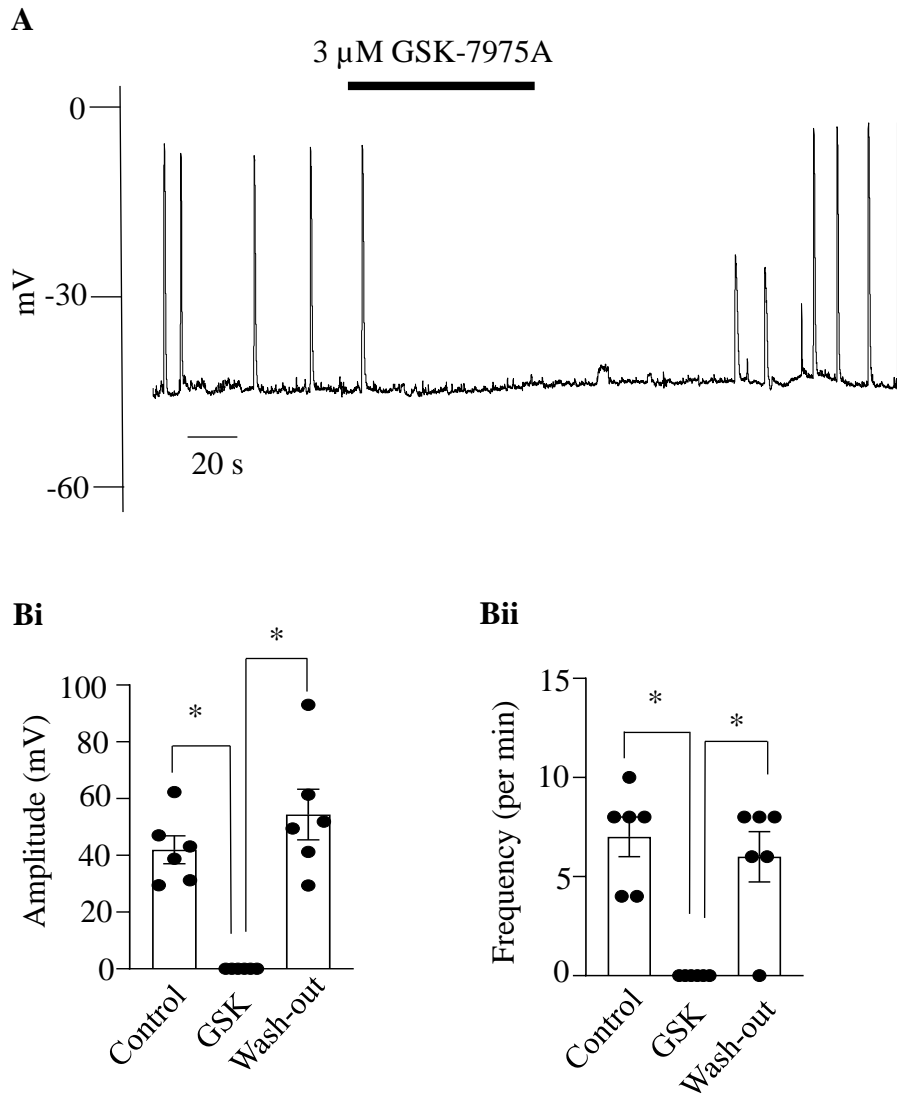


**Figure 6.10: ORAI is involved in mechanism of activation of STDs.** (A) An example showing the effect of 3  $\mu$ M GSK-7975A on STDs in current clamp mode. (Bi) Summary of the effect of 3  $\mu$ M GSK-7975A on STDs amplitude (n = 6 from 6 animals; \*p<0.05, one way ANOVA) and (Bii) STDs frequency (n = 6 from 6 animals; \*p<0.05, one way ANOVA).

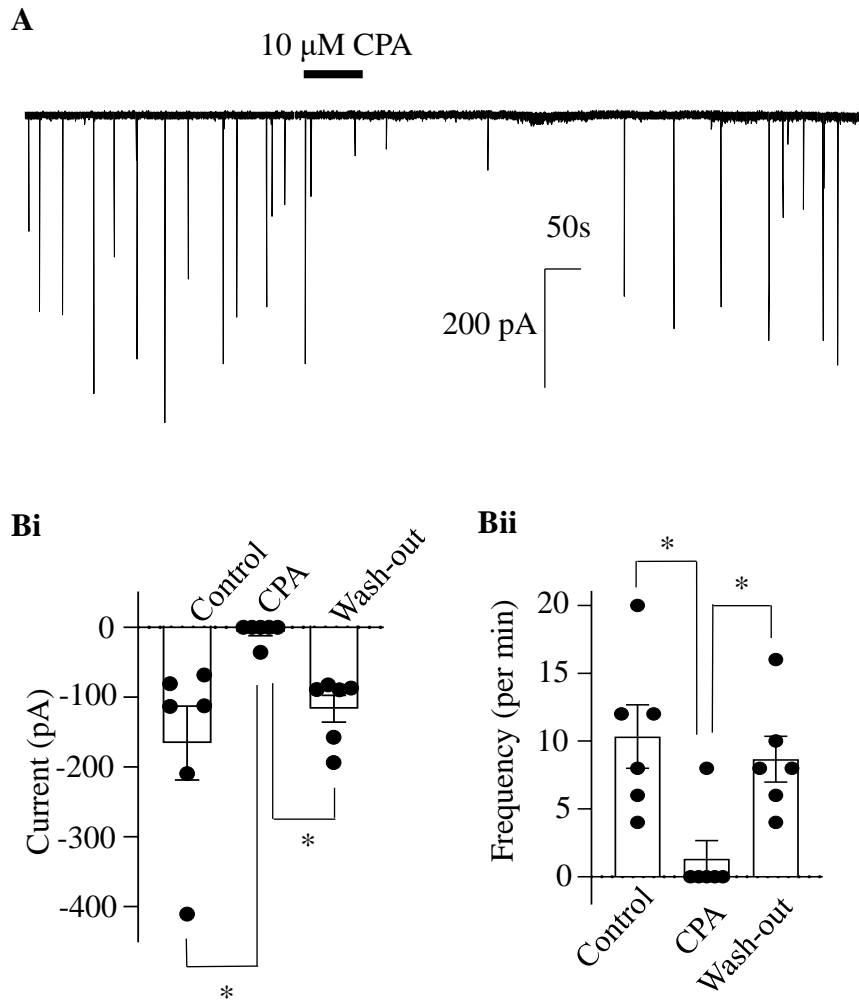


**Figure 6.11: Sarcoplasmic reticulum  $\text{Ca}^{2+}$ -ATPase is involved in the mechanism of activation of STICs. (A)** An example showing the effect of 10  $\mu\text{M}$  CPA on STICs when a CCSM cell was held under voltage clamp at -60 mV. **(Bi)** Summary of the effect of 10  $\mu\text{M}$  CPA on STICs amplitude ( $n = 6$  from 6 animals;  $*p < 0.05$ , one way ANOVA) and **(Bii)** STICs frequency ( $n = 6$  from 6 animals;  $*p < 0.05$ , one way ANOVA).

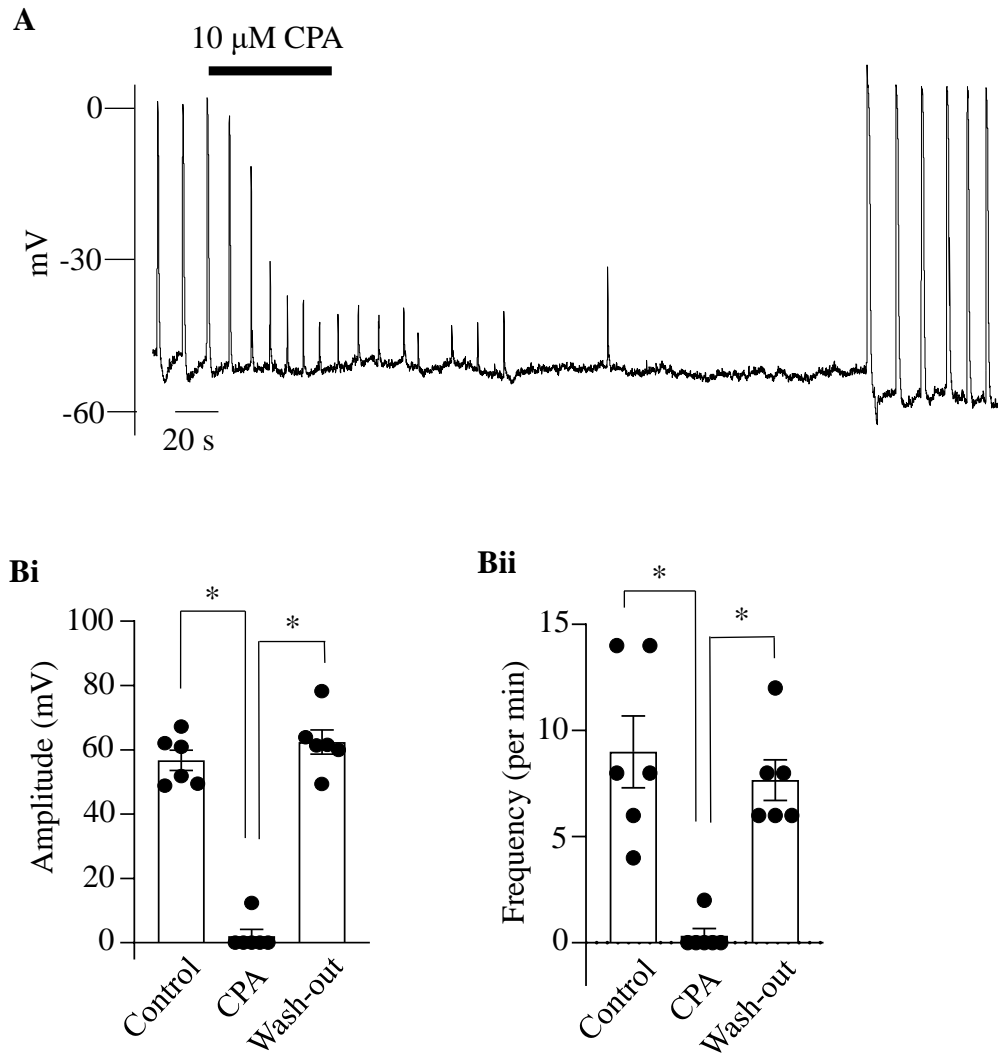


**Figure 6.12: Sarcoplasmic reticulum  $\text{Ca}^{2+}$ -ATPase is involved in the mechanism of activation of STDs. (A)** An example showing the effect of 10  $\mu$ M CPA on STDs in current clamp mode. **(Bi)** Summary of the effect of 10  $\mu$ M CPA on STDs amplitude (n = 6 from 6 animals; \*p<0.05, one way ANOVA) and **(Bii)** STDs frequency (n = 6 from 6 animals; \*p<0.05, one way ANOVA).

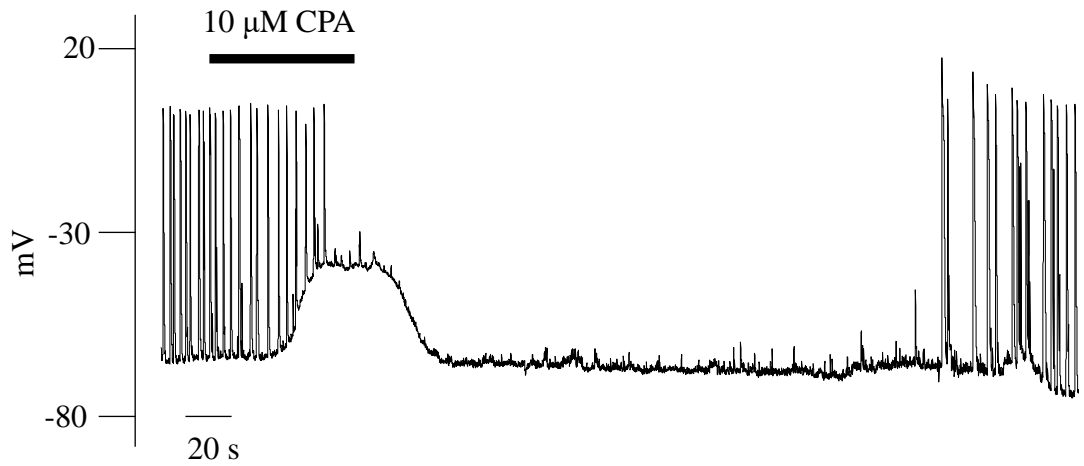


**Figure 6.13: Blockade of sarcoplasmic reticulum  $\text{Ca}^{2+}$ -ATPase may lead to cellular depolarisation.** On the rare occasion, incubation of CCSM cell in 10  $\mu\text{M}$  CPA can induce depolarisation [observed in 1 out of 6 cells]. The membrane potential returned to baseline upon wash-out.

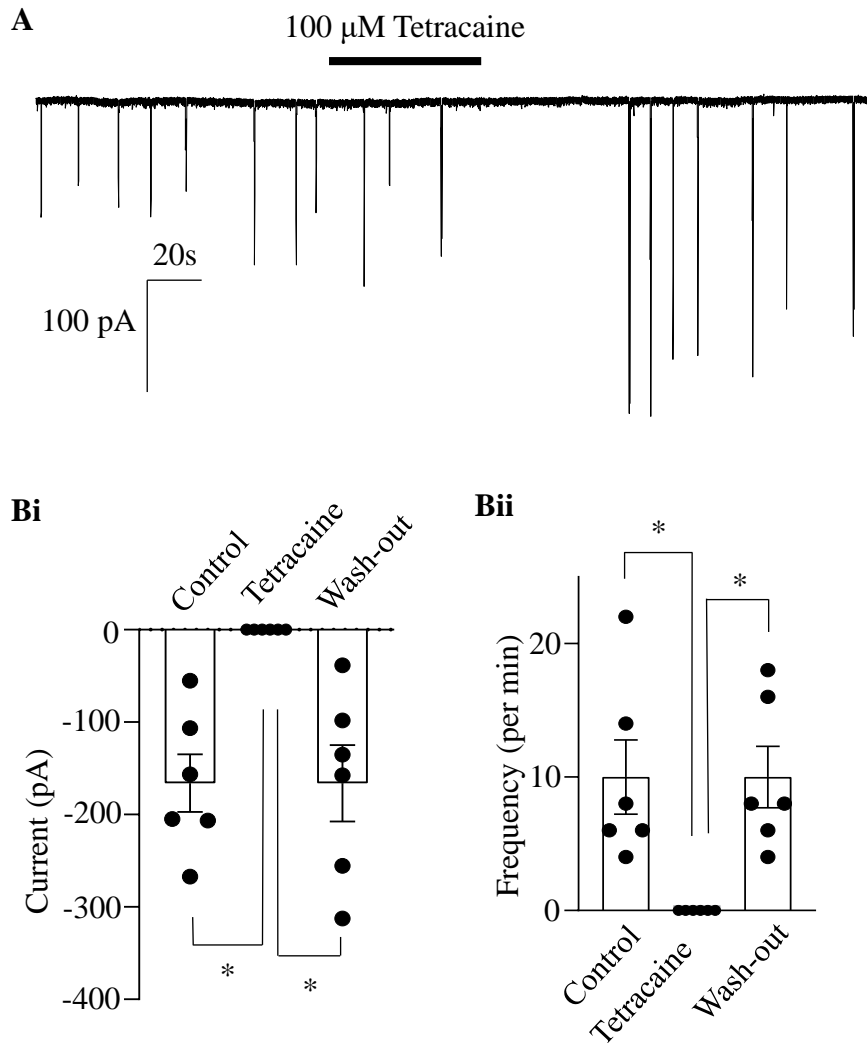


**Figure 6.14: Ryanodine-receptor is involved in the mechanism of activation of STICs.** (A) An example showing the effect of 100  $\mu$ M tetracaine on STICs when a CCSM cell was held under voltage clamp at -60 mV. (Bi) Summary of the effect of 100  $\mu$ M tetracaine on STICs amplitude (n = 6 from 6 animals; \*p<0.05, one way ANOVA) and (Bii) STICs frequency (n = 6 from 6 animals; \*p<0.05, one way ANOVA).

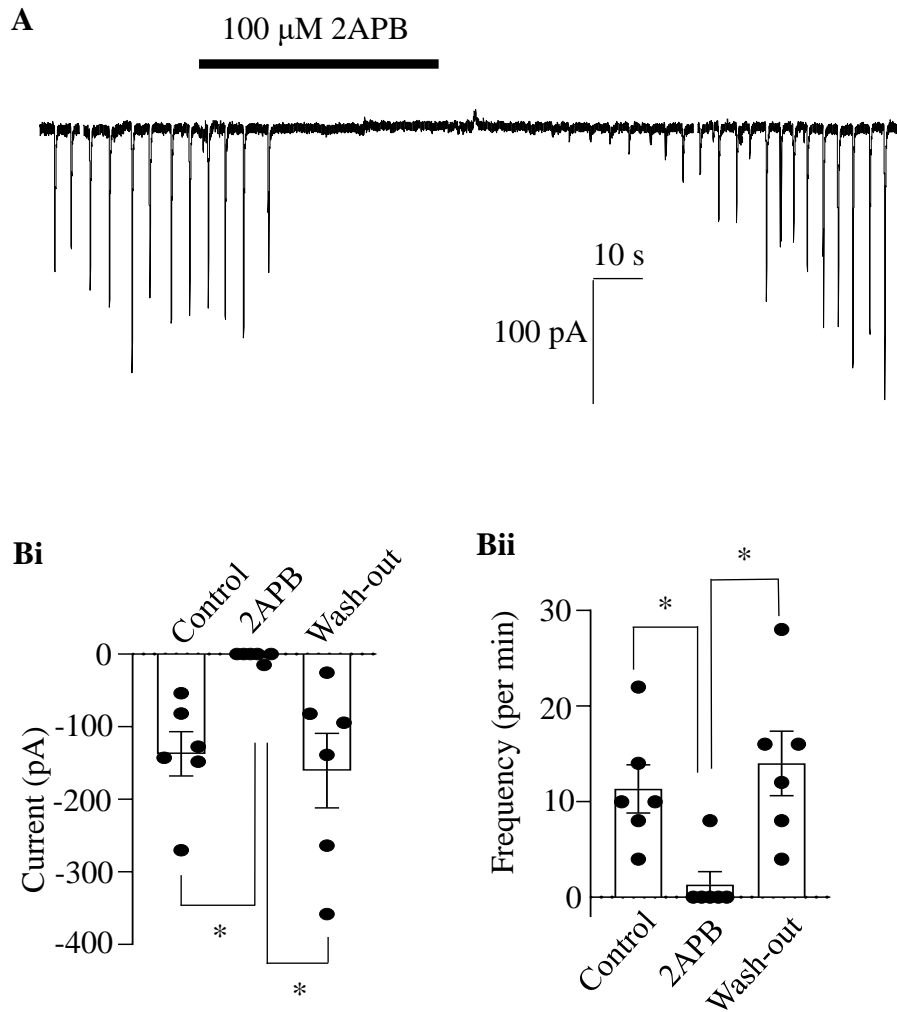


**Figure 6.15:  $IP_3$ -receptor is involved in the mechanism of activation of STICs.**

(A) An example showing the effect of 100  $\mu$ M 2APB on STICs when a CCSM cell was held under voltage clamp at -60 mV. (Bi) Summary of the effect of 100  $\mu$ M 2APB on STICs amplitude (n = 6 from 6 animals; \* $p$ <0.05, one way ANOVA) and (Bii) STICs frequency (n = 6 from 6 animals; \* $p$ <0.05, one way ANOVA).

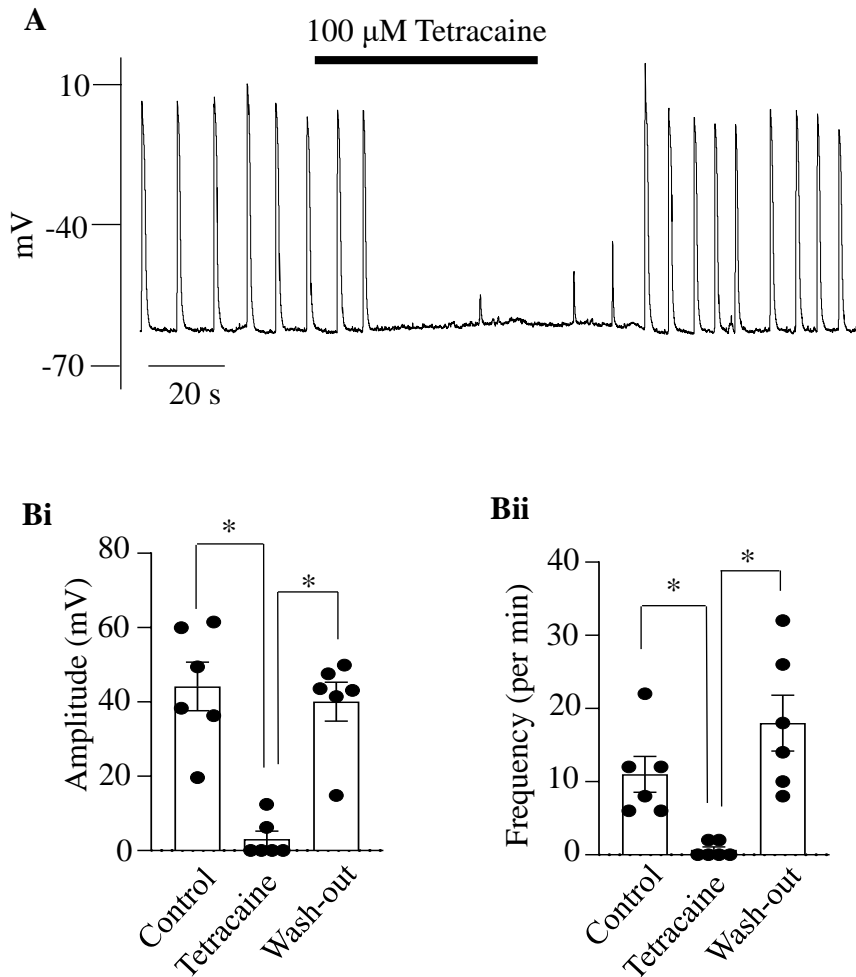


**Figure 6.16: Ryanodine receptor is involved in the mechanism of activation of STDs.** (A) An example showing the effect of 100  $\mu$ M tetracaine on STDs in current clamp mode. (Bi) Summary of the effect of 100  $\mu$ M tetracaine on STDs amplitude ( $n = 6$  from 6 animals;  $*p < 0.05$ , one way ANOVA) and (Bii) STDs frequency ( $n = 6$  from 6 animals;  $*p < 0.05$ , one way ANOVA).

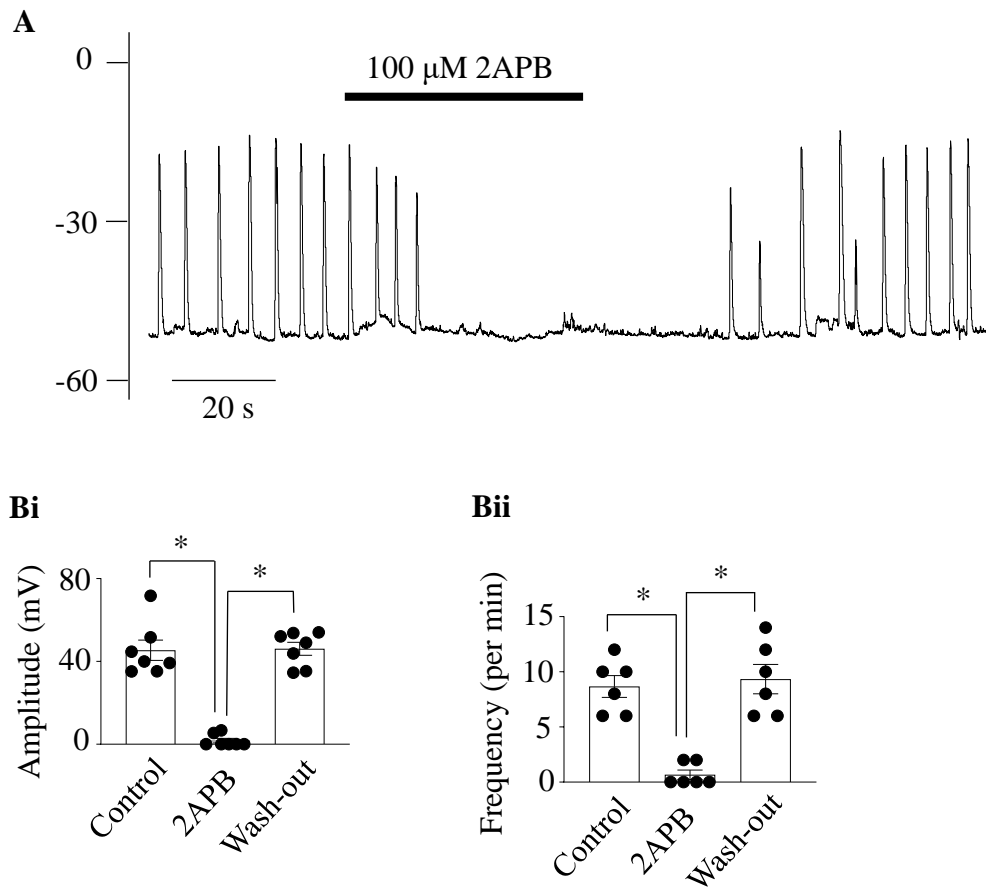


**Figure 6.17:  $IP_3$ -receptor is involved in the mechanism of activation of STDs.**

(A) An example showing the effect of 100  $\mu$ M 2APB on STDs in current clamp mode. (Bi) Summary of the effect of 100  $\mu$ M 2APB on STDs amplitude (n = 6 from 6 animals; \* $p$ <0.05, one way ANOVA) and (Bii) STDs frequency (n = 6 from 6 animals; \* $p$ <0.05, one way ANOVA).

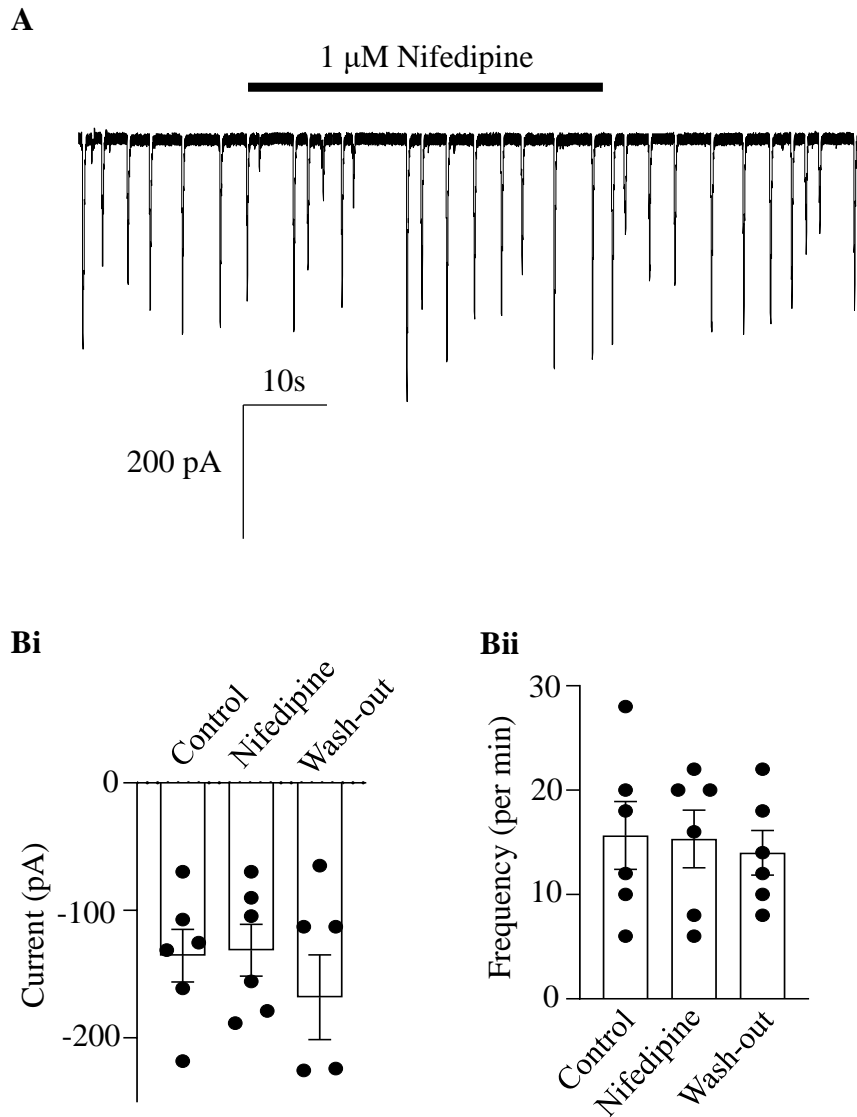


**Figure 6.18: L-type  $\text{Ca}^{2+}$  channel blocker failed to inhibit STICs.** (A) An example showing the effect of 1  $\mu\text{M}$  nifedipine on STICs when a CCSM cell was held under voltage clamp at -60 mV. (Bi) Summary of the effect of 1  $\mu\text{M}$  nifedipine on STICs amplitude ( $n = 6$  from 6 animals;  $*p > 0.05$ , one way ANOVA) and (Bii) STICs frequency ( $n = 6$  from 6 animals;  $*p > 0.05$ , one way ANOVA).

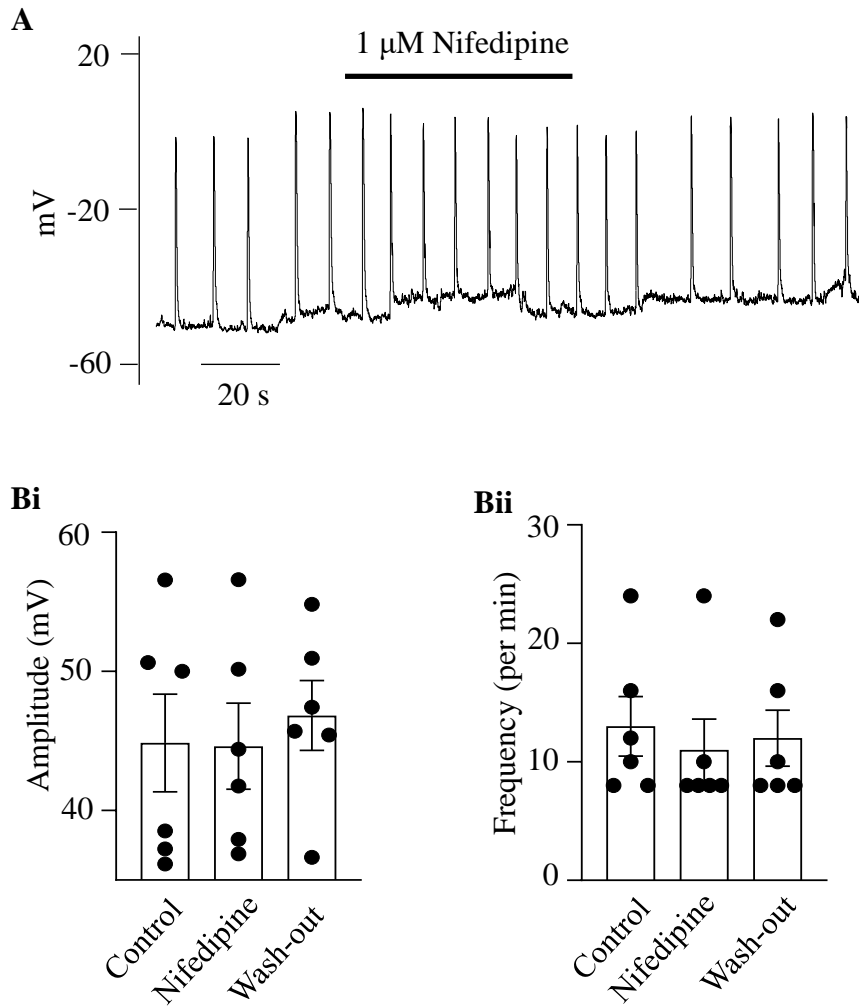


**Figure 6.19: L-type  $\text{Ca}^{2+}$  channel blocker failed to inhibit STDs.** (A) An example showing the effect of 1  $\mu\text{M}$  nifedipine on STDs in current clamp mode. (Bi) Summary of the effect of 1  $\mu\text{M}$  nifedipine on STDs amplitude ( $n = 6$  from 6 animals;  $*p > 0.05$ , one way ANOVA) and (Bii) STDs frequency ( $n = 6$  from 6 animals;  $*p > 0.05$ , one way ANOVA).

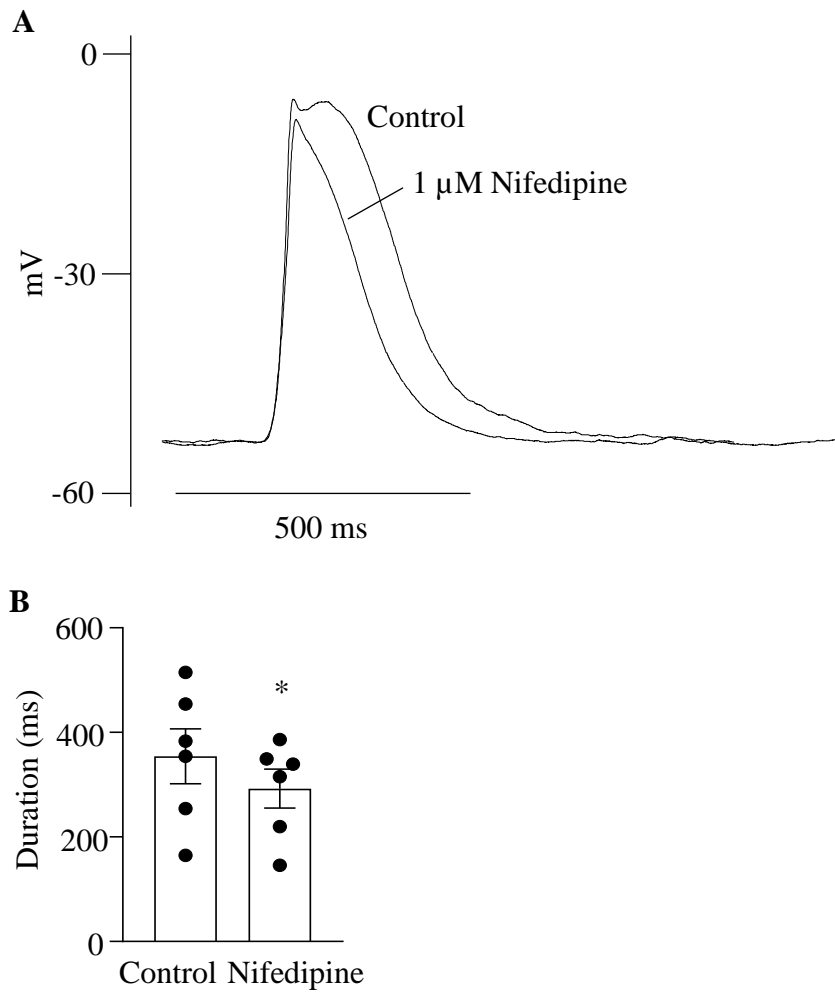


**Figure 6.20: L-type  $\text{Ca}^{2+}$  channel blocker reduced the duration of STDs.** (A) An example showing the effect of 1  $\mu\text{M}$  nifedipine on STD duration in CCSM cells. (B) Summary of the effect of 1  $\mu\text{M}$  nifedipine on STD duration (n = 6 from 6 animals; \* $p < 0.05$ , paired t test).

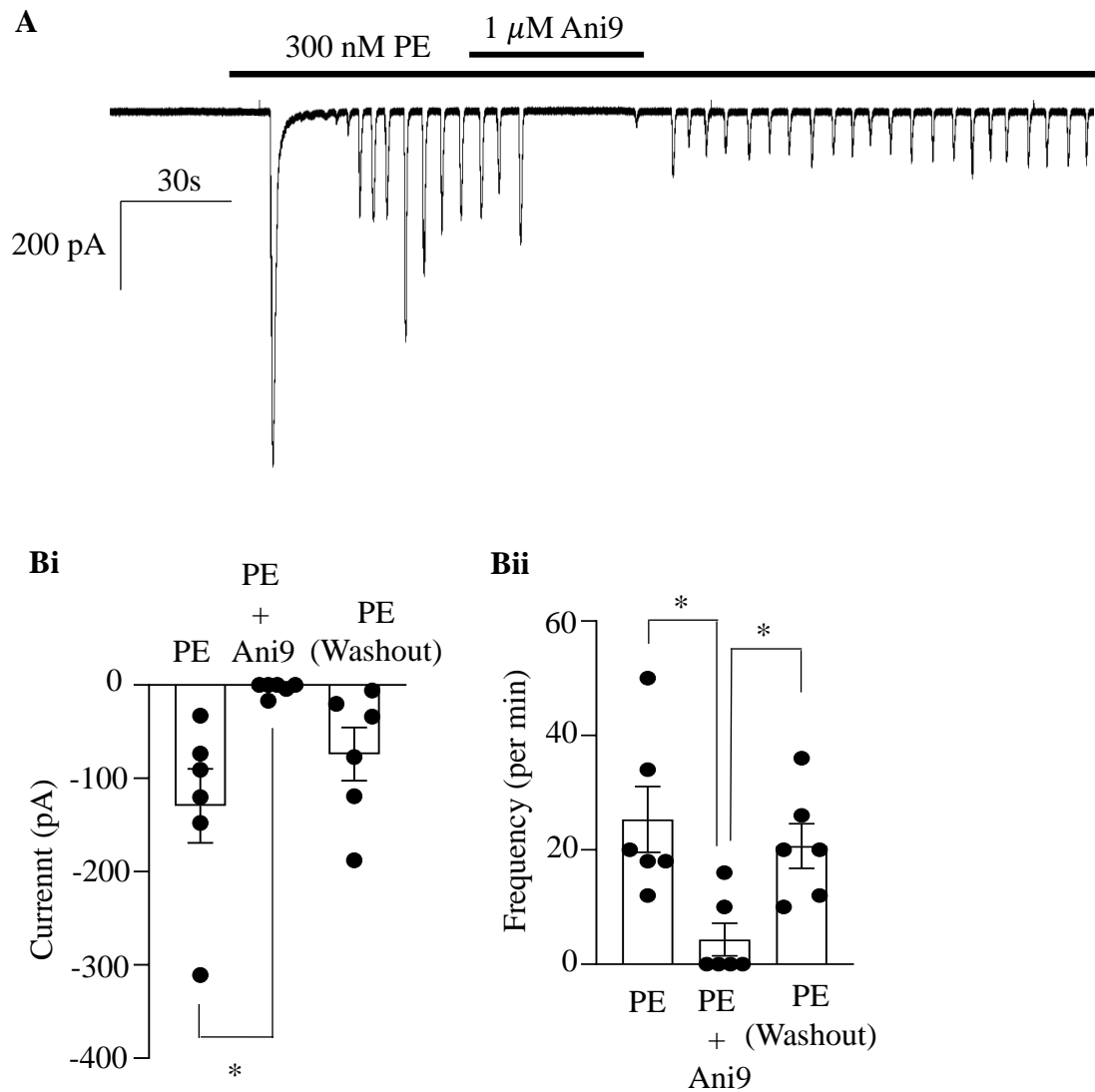


**Figure 6.21: Anil9 inhibited phenylephrine-induced transient inward currents.**

(A) 300 nM phenylephrine evoked a large, transient inward current, followed by oscillatory transient inward currents which were susceptible to blockade by 1  $\mu$ M Anil9. There was only partial return of phenylephrine response after washout from Anil9 (Bi) Summary data showing the effect of Anil9 on the amplitude (n = 6 from 6 animals; \*p<0.05, one way ANOVA) and (Bii) frequency of phenylephrine-induced inward currents (n = 6 from 6 animals; \*P<0.05, one way ANOVA).

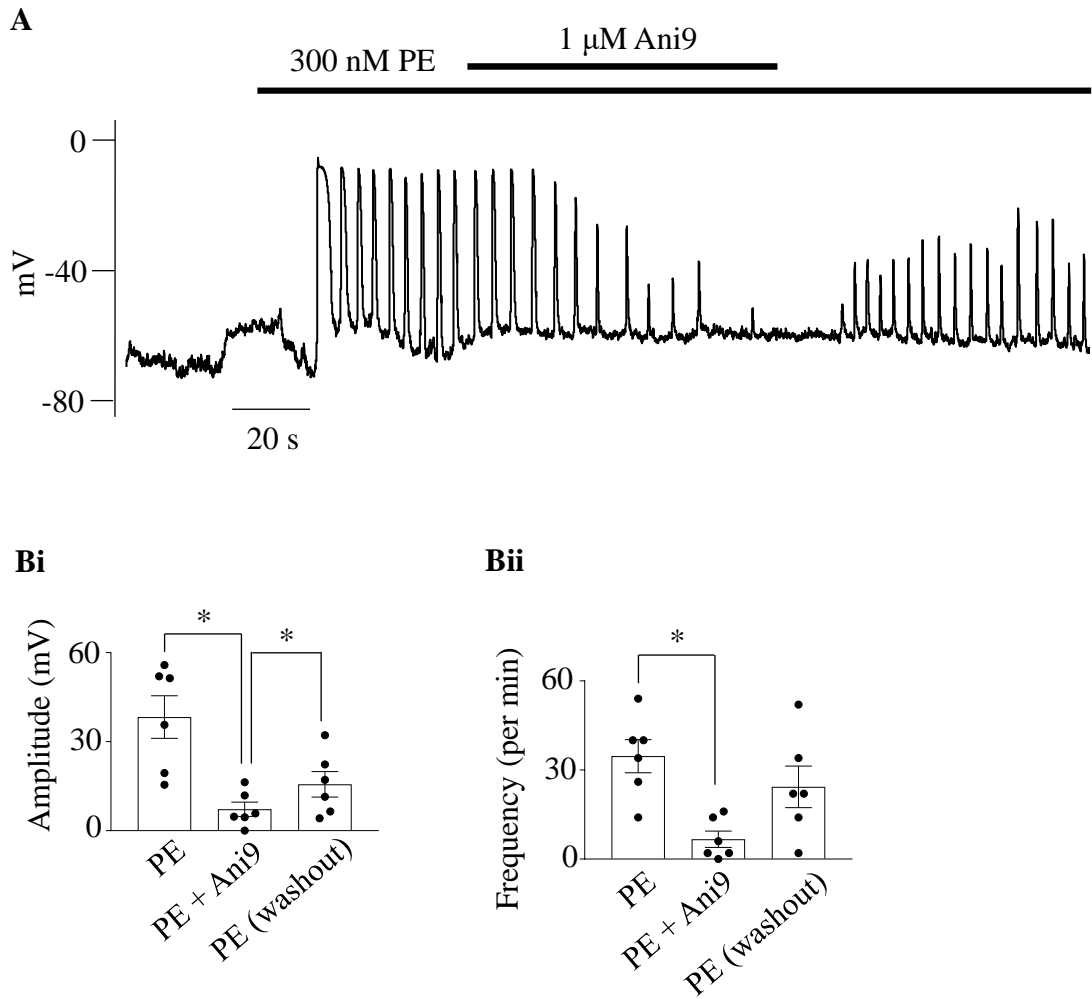


**Figure 6.22: Effect of 1  $\mu$ M Ani9 on 300 nM PE-induced transient depolarisations.** (A) 300 nM phenylephrine evoked regular, oscillating transient depolarisations, which were susceptible to blockade by 1  $\mu$ M Ani9. (Bi) Summary data showing the effect of Ani9 on the amplitude ( $n = 6$  from 6 animals;  $*p < 0.05$ , one way ANOVA) and (Bii) frequency of phenylephrine-induced transient depolarisations ( $n = 6$  from 6 animals;  $*p < 0.05$ , one way ANOVA).

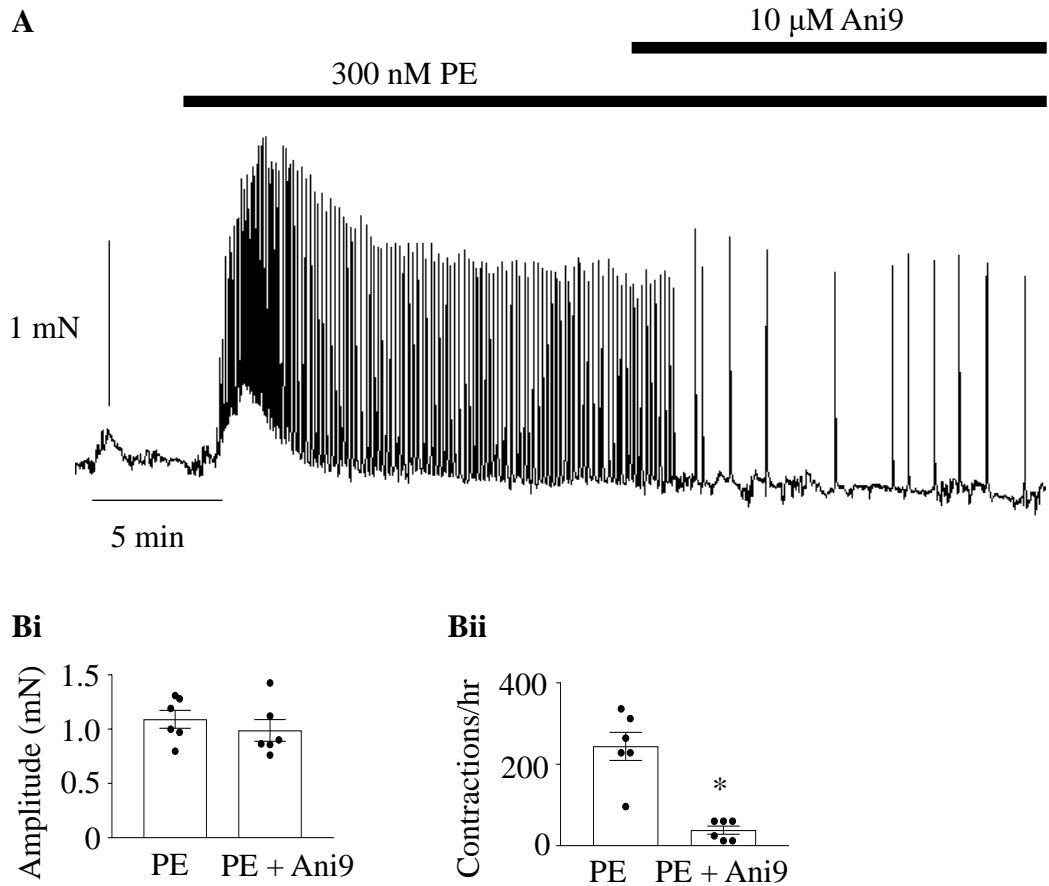


**Figure 6.23: Effect of 10  $\mu$ M Ani9 on 300 nM PE-evoked phasic contractions.**

(A) Phenylephrine-evoked contractions were susceptible to blockade by high concentration of Ani9 (10  $\mu$ M). (Bi) Summary data showing the effect of Ani9 on the mean evoked contraction amplitude (n = 6 from 6 animals, \*p>0.05, paired t test) and (Bii) evoked contraction events per hour (n = 6 from 6 animals, \*p<0.05, paired t test).

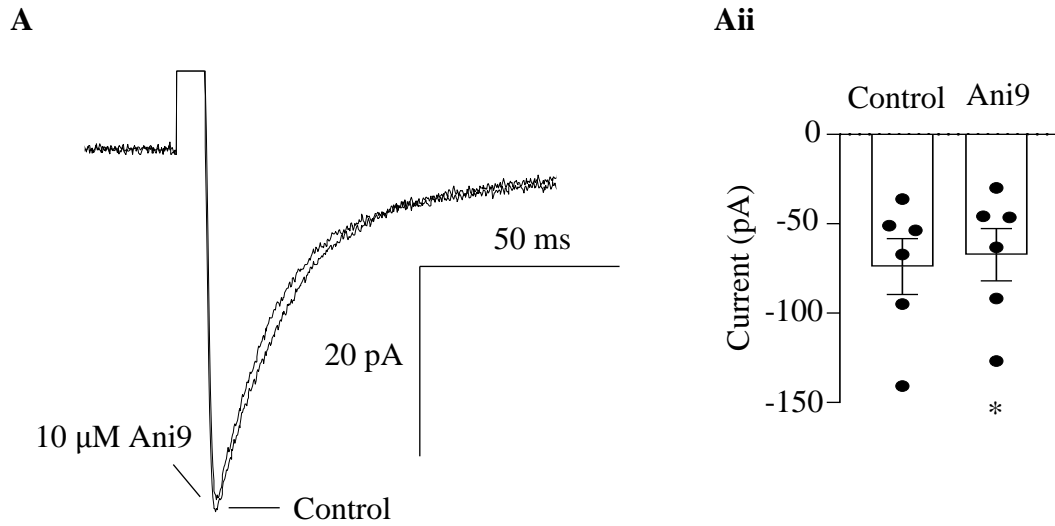


**Figure 6.24: Effect of 10  $\mu\text{M}$  Ani9 on L-type  $\text{Ca}^{2+}$  current.** (Ai) Representative traces showing L-type  $\text{Ca}^{2+}$  current, which 10  $\mu\text{M}$  Ani9 had little effect on. L-type  $\text{Ca}^{2+}$  current was evoked by stepping from a holding potential of -60 mV to 0 mV for 100 ms. (Aii) Summary data showing the effect of 10  $\mu\text{M}$  Ani9 on L-type  $\text{Ca}^{2+}$  current (n = 6 from 6 animals; \*p<0.05, paired t test).

## Chapter 7: General discussion and future work

The present study is the first to confirm the functional expression of fast voltage-gated sodium (Nav) channels and Ca<sup>2+</sup>-activated Cl<sup>-</sup> channels in CCSM of the mouse, achieved using the patch-clamp technique, pharmacological methods, tension recording experiments, as well as transcriptional and immunocytological studies. As Nav channels have never been found in the CCSM, a thorough characterisation was carried out. The novel Nav current was discovered to be made up from two populations of channels: TTX-sensitive and TTX-insensitive. They have different activation and inactivation kinetics, with TTX-insensitive channels having more negative values for both. A number of pharmacological agonists and antagonists were used to examine their properties. The effect of ICA-121431 (Nav1.1, 1.2, 1.3 antagonist), PF-05089771 (Nav1.7 antagonist), anhydro-TTX (Nav1.6 antagonist), and OD1 (Nav1.7 agonist) on TTX-sensitive currents were studied. Cumulative addition of all the antagonists did not achieve complete block, indicating the presence of a mixture of TTX-sensitive subtypes. On the other hand, the effect of A803467 (Nav1.8 blocker) on TTX-insensitive channels were also studied. The results eliminate Nav1.8 as the TTX-insensitive channel. The identity of the Nav channels was confirmed with transcriptional and immunocytochemical studies, where the TTX-insensitive channels were confirmed to be Nav1.5, and the TTX-sensitive channels were made up of a mixture of subtypes, with Nav1.4 being the more prominent.

Incubation of CCSM tissue with the Nav agonist, veratridine, gradually induced phasic contractions that were susceptible to blockade by a low concentration of TTX, suggesting the involvement of TTX-sensitive channels. The slow onset of veratridine could plausibly be attributed to a small population Nav channels being active at resting conditions (Nav window current is between -60 mV to -40 mV). Since veratridine binds favourably to activated Nav channels (Ulbricht, 2005) and then prevents inactivation, it might take a while to work as more Nav channels gradually open. Veratridine-induced phasic contractions could be blocked by an L-type Ca<sup>2+</sup> channel blocker but not by a NCX blocker, suggesting a direct depolarising effect of the sustained sodium current induced by veratridine. Nav channels are involved in adrenergic-mediated excitation in CCSM, as TTX disrupted phenylephrine-induced depolarisations in cells and phenylephrine-

induced contractions in tissues. This suggests a role of Nav channels in the regulation of tissue contractility by the sympathetic nerves.

Since  $E_{Cl}$  is positive (Chipperfield and Harper, 2000; Aickin and Brading, 1982) to the resting membrane potential of CCSM (Hashitani *et al.*, 2005), activation of  $Ca^{2+}$ -activated  $Cl^-$  currents would cause  $Cl^-$  efflux, resulting in membrane depolarisation and contributes towards excitation in CCSM. Transcripts for TMEM16A have been identified in rabbit CCSM (Hannigan *et al.*, 2017), but neither  $Ca^{2+}$ -activated  $Cl^-$  currents nor TMEM16A channels have been studied in mouse CCSM. The findings of this study describe the first account of  $Ca^{2+}$ -activated  $Cl^-$  current in the CCSM of the mouse species. First and foremost, the protein expression of TMEM16A channels was confirmed with immunocytochemistry experiments. Then, the reversal potential of  $Ca^{2+}$ -activated  $Cl^-$  tail current was found to be shifted in the positive direction in the presence of low  $Cl^-$  extracellular solution, identifying  $Cl^-$  as the ions going through those channels.

Spontaneous electrical activity in CCSM myocytes was investigated next, as  $Ca^{2+}$ -activated  $Cl^-$  currents have been implicated in the activation of STICs and STDs in the rabbit species (Craven *et al.*, 2004). Similarly in the mouse CCSM, both STICs and STDs were blocked by two different TMEM16A specific antagonists, Ani9 and CaCC(inh)-A01, confirming that these events were carried by  $Ca^{2+}$ -activated  $Cl^-$  currents. STICs and STDs were also inhibited by CPA, tetracaine, and 2APB, consistent with a role for  $Ca^{2+}$  release from the SR involving RyR and  $IP_3R$  in the generation of this activity. Furthermore, low concentration of ORAI inhibitor, GSK-7975A inhibited both STICs and STDs, suggesting that they were reliant on store operated  $Ca^{2+}$  entry. In contrast, the L-type  $Ca^{2+}$  channel blocker, nifedipine did not affect the amplitude and frequency of STICs or STDs, but it shortened the duration of the STDs. These data suggest that  $Ca^{2+}$ -influx through L-type  $Ca^{2+}$  channels contributed to the STD plateau potential. In the mouse CCSM tissue, Ani9 disrupted phenylephrine-induced phasic contractions, demonstrating the physiological relevance of TMEM16A in modulating CCSM contractility by sympathetic innervation.

Based on the results presented, a basic scheme is proposed whereby spontaneous depolarisations are initiated by TMEM16A as a result of spontaneous  $Ca^{2+}$  release from stores that depends on both RyR and  $IP_3R$ , while refilling of the stores depends on both the SERCA pump and external  $Ca^{2+}$  influx via STIM/Orai store operated  $Ca^{2+}$  entry. In

turn, the depolarisations result in activation of L-type  $\text{Ca}^{2+}$  currents, leading to voltage-dependent  $\text{Ca}^{2+}$  influx and contraction. This underlying mechanism is upregulated upon  $\alpha$ -adrenoceptor stimulation, most likely via stimulation of phospholipase C (PLC) and  $\text{IP}_3$  generation, thus pushing the balance towards penile detumescence.

The findings presented in this thesis imply that both  $\text{Nav}$  channels and  $\text{Ca}^{2+}$ -activated  $\text{Cl}^-$  channels contribute towards CCSM excitation. Both inward currents play a role in activator- and/or agonist-induced contractions in tissues, suggesting physiological importance. The importance of  $\text{Nav}$  channels in regulating CCSM contraction is highlighted by the fact that activation of  $\text{Nav}$  channels caused  $\text{Ca}^{2+}$ -influx, as evidenced by blockade of veratridine-induced contractions with nifedipine. Furthermore, from a physiological standpoint, its involvement in adrenergic-induced excitation warrants further investigations as this channel could be a potential target for erectile dysfunction treatment. However, since the presence of a similar current in humans is not yet known, it is too early to say if this current contributes to the flaccid state, or if it remains 'silent', but can become available in certain disease states, such as diabetes or vascular disease. Certainly, there is a large reserve of  $\text{Nav}$  channels that could potentially become available under, as yet undetermined circumstances. Nevertheless, it is essential to fully characterise the mouse corpus cavernosum, as it is widely used as a model to study both normal and abnormal erectile function (Luttrell *et al.*, 2008; Werner *et al.*, 2005).

Diabetes is associated with ED (Lue, 2000), and 30 to 40% of ED patients with diabetes are resistant to Viagra<sup>TM</sup> (De Tejada, 2004). Interestingly, mRNA and protein expression of TMEM16A was found to be upregulated in the CCSM of diabetic rats, suggesting the association of TMEM16A with diabetic erectile dysfunction (Ruan *et al.*, 2016). Moreover, in 2004, Craven *et al.* showed that nitric oxide-cGMP pathway suppresses the intrinsic  $\text{Ca}^{2+}$ -activated  $\text{Cl}^-$  currents in rabbit CCSM myocytes. Hence, it is conceivable that diminished nitric oxide production in diabetes may lead to increased  $\text{Ca}^{2+}$ -activated  $\text{Cl}^-$  currents, thereby leading to high penile contractile tone in erectile dysfunction. Findings from Lau and Adaikan (2014) supports this hypothesis as they demonstrated heightened  $\text{Ca}^{2+}$ -activated  $\text{Cl}^-$  channel sensitivity to A9C in diabetic CC tissue. It is crucial to note that  $\text{Ca}^{2+}$ -activated  $\text{Cl}^-$  currents are expressed in human CCSM cells, as demonstrated by Karkanis and colleagues (Karkanis *et al.*, 2003). Hence, targeting the  $\text{Ca}^{2+}$ -activated  $\text{Cl}^-$  channel to achieve erection might be a viable alternative treatment to

alleviate dependence on the cavernosal nitric oxide synthase-cGMP pathway, which is invariably impaired in diabetes.

In summary, this thesis describes a novel  $\text{Na}_v$  current, as well as TMEM16A current in the mouse CCSM. A graphical abstract describing these channels and their activities is detailed in Figure I (page 5).

Even though they have been shown to regulate mouse CCSM excitability, much work needs to be done in human to establish clinical application. Nevertheless, electromechanical coupling is believed to play an important role in the human corpus cavernosum contractility. Indeed, EMG recordings from human volunteers showed characteristic electrical potential patterns during tumescence, detumescence, and flaccidity (Jiang *et al.*, 2005), and abnormal electrical activity has been implicated in patients suffering from several types of erectile dysfunction (Shafik *et al.*, 2004). For example, in comparison with controls, EMG patterns were ‘silent’ in neurogenic ED; ‘bradyarrhythmic’ in arteriogenic ED, ‘normal’ in venogenic ED, and ‘overactive’ in psychogenic ED (Shafik *et al.*, 2004). Future work will determine if the  $\text{Na}_v$  current or  $\text{Ca}^{2+}$ -activated  $\text{Cl}^-$  current play a part in evoking or coordinating activity at whole organ level in human, and therefore has a role in erectile dysfunction.

## **Future Work**

The present study has unearthed novel findings of the functional expression of voltage-gated sodium ( $\text{Na}_v$ ) channels in CCSM, and that  $\text{Ca}^{2+}$ -activated  $\text{Cl}^-$  channels (TMEM16A) underlie spontaneous electrical activity in isolated mouse CCSM cells. However, much remains to be uncovered regarding the precise role of  $\text{Na}_v$  and TMEM16A in the mouse CCSM. Below are some experiments that may further expand on these findings and contribute to our understanding of the mechanisms underlying penile contraction/ED:

1. Determine the expression, electrophysiological characteristics, and pharmacology of the following channels in normal mouse CC:
  - Calcium-activated  $\text{K}^+$  ( $\text{BK}_{\text{Ca}}$ ) channel

- K<sub>V</sub>7 channel
  - K<sub>ATP</sub> channel
  - T-type Ca<sup>2+</sup> channel
  - P2X1 receptor
2. Perform intracellular recordings [Methods detailed in Appendix] to characterise the electrical activity in the syncytium.

Preliminary data (Figure App.1, Appendix) was obtained in collaboration with electrophysiologists from University of Reno, Nevada. Interestingly, different patterns of spontaneous depolarisations were recorded in mouse CCSM tissues. Note that its resting membrane potential is at approximately -50 mV.

The preliminary data obtained in the mouse was different from other studies in the rabbit. Hashitani *et al.* (2005) showed intracellular recordings consisting of either 1) bursts of spontaneous depolarisations consisting of an initial spike, followed by oscillations, or 2) more commonly, continuous bursting depolarisations. On the other hand, Professor Sean Ward (Thornbury *et al.*, 2019: unpublished observations) demonstrated more discrete, yet regular depolarisations than described in the Hashitani study and the membrane potential was more negative at -60 mV.

Given the disparity observed in intra- and inter-species, there would need to be much more work done, though this technique is challenging, as impalements are hard to maintain due to tissue mobility.

3. Having done 1 and 2, try modulators of the currents identified in the mouse CCSM on the shape and patterns of the electrical activity using intracellular recordings.

For example, TTX (Na<sub>V</sub> inhibitor), veratridine (Na<sub>V</sub> activator), Ani9 (TMEM16A inhibitor), iberiotoxin (BK<sub>Ca</sub> inhibitor), TEA (Non-selective K<sub>V</sub> inhibitor), XE911 (K<sub>V</sub>7 inhibitor), pinacidil (K<sub>ATP</sub> activator), mibefradil (T-type Ca<sup>2+</sup>-channel inhibitor), and NF449 (P2X1 receptor inhibitor).

4. Ideally, perform intracellular and tension recordings in relevant KO animals.

BK<sub>Ca</sub> knock-out mouse lacking the *Slo* gene (*Slo*<sup>-/-</sup>) used in Werner *et al.* (2005) should be studied further, as these authors only measured tension.

Inducible TMEM16A knock-out in adult mice might be achievable by crossing floxed TMEM16A<sup>fl/fl</sup> mice, whose generation has been described in detail (Schreiber *et al.*, 2015), with mice expressing Cre recombinase under the control of the smooth muscle myosin heavy chain protein (smMHC) promoter.

5. Perform similar experiments to those in point 3 on tissue slices from normal, wild-type and GCaMP mice using Ca<sup>2+</sup>-imaging technique [Methods detailed in Appendix].

The Ca<sup>2+</sup>-imaging technique has an advantage over intracellular recording and tension by showing the spatiotemporal spread of excitation and potential pacemaker sites. Preliminary Ca<sup>2+</sup>-imaging data obtained in the wild-type mice are shown in Figure App.2 (Appendix), where spontaneous Ca<sup>2+</sup> events can be seen travelling across the smooth muscle of a cavernosal sinus.

To improve Ca<sup>2+</sup>-imaging data acquisition, GCaMP mice may be utilised. Acta2-GCaMP8.1-mVermilion mice have a genetically encoded calcium indicator, under the control of the acta2 promoter, that directs expression only in smooth muscle cells. One advantage of using these mice includes bypassing the mandatory calcium-sensitive indicator (fluorophore) loading step that is often harsh on the cells and may be taken up by non-smooth muscle cell types. However, the tissue may be susceptible to the effects of Ca<sup>2+</sup>-buffering and exposure to phototoxicity.

6. Investigate the role of Na<sub>v</sub> and TMEM16A in animal models of ED and diabetes. For example, db/db, a monogenic diabetic mouse with well characterised ED

(Luttrell *et al.*, 2008) or TALLYHO/JngJ, a polygenic type II diabetic mouse expressing vascular disorders (Didion *et al.*, 2007).

Investigate the expression and function of Nav channels and TMEM16A channels using the patch clamp technique, tension recordings, Ca<sup>2+</sup>-imaging, intracellular recording, and immunocytochemistry. Ideally, perform tension recording with Ca<sup>2+</sup>-imaging simultaneously in diabetic/ED mice models, with aims to establish impaired cavernosal function, perhaps due to diminished propagation of Ca<sup>2+</sup>-signals by dysfunctional ion channels or diminished channel expression, and investigate if these can be rescued with channel activators.

7. Finally (knowing all of the above), investigate if similar mechanisms apply to 1) healthy human tissue or 2) tissue from ED patients.

## References

- Abriel, H. and Kass, R. (2005). Regulation of the Voltage-Gated Cardiac Sodium Channel Nav1.5 by Interacting Proteins. *Trends in Cardiovascular Medicine*, 15(1), pp.35-40.
- Ahern, C. (2013). What activates inactivation? *The Journal of General Physiology*, 142(2), pp.97-100.
- Ahern, C.A., Payandeh, J., Bosmans, F., and Chanda, B. (2016). The hitchhiker's guide to the voltage-gated sodium channel galaxy. *Journal of General Physiology*, 147(1), pp.1-24.
- Aickin C.C. and Brading A.F. (1984). The role of chloride-bicarbonate exchange in the regulation of intracellular chloride in guinea-pig vas deferens. *The Journal of Physiology*, 349, p.587-606.
- Aickin, C.C. and Brading, A.F. (1982). Measurement of intracellular chloride in guinea-pig vas deferens by ion analysis, <sup>36</sup>chloride and micro-electrodes. *The Journal of Physiology*, 326(1), pp.139-154.
- Aickin, C.C. and Brading, A.F. (1990). Effect of Na<sup>+</sup> and K<sup>+</sup> on Cl<sup>-</sup> distribution in guinea-pig vas deferens smooth muscle: evidence for Na<sup>+</sup>, K<sup>+</sup>, Cl<sup>-</sup> co-transport. *The Journal of Physiology*, 421(1), pp.13-32.
- Alexandrou, A.J., Brown, A.R., Chapman, M.L., Estacion, M., Turner, J., Mis, M.A., Wilbrey, A., Payne, E.C., Gutteridge, A., Cox, P.J., and Doyle, R. (2016). Subtype-selective small molecule inhibitors reveal a fundamental role for Nav1.7 in nociceptor electrogenesis, axonal conduction and presynaptic release. *PloS one*, 11(4), p.e0152405.
- Amano, M., Fukata, Y., and Kaibuchi, K. (2000). Regulation and functions of Rho-associated kinase. *Experimental Cell Research*, 261(1), pp.44-51.
- Andersson, K.E. (2001). Pharmacology of penile erection. *Pharmacological Reviews*, 53(3), pp.417-450.
- Andersson, K.E. (2011). Mechanisms of penile erection and basis for pharmacological treatment of erectile dysfunction. *Pharmacological Reviews*, 63(4), pp.811-859.

- Andrikopoulos, P., Fraser, S.P., Patterson, L., Ahmad, Z., Burcu, H., Ottaviani, D., Diss, J.K., Box, C., Eccles, S.A., and Djamgoz, M.B. (2011). Angiogenic Functions of Voltage-gated Na<sup>+</sup> Channels in Human Endothelial Cells Modulation of Vascular Endothelial Growth Factor (VEGF) Signaling. *Journal of Biological Chemistry*, 286(19), p.16846-16860.
- Armstrong, C.M. (2006). Na<sup>+</sup> channel inactivation from open and closed states. *Proceedings of the National Academy of Sciences*, 103(47), pp.17991-17996.
- Armstrong, C.M. and Bezanilla, F. (1977). Inactivation of the sodium channel. II. Gating current experiments. *The Journal of General Physiology*, 70(5), pp.567-590.
- Armstrong, C.M. and Gilly, W.F. (1979). Fast and slow steps in the activation of sodium channels. *The Journal of General Physiology*, 74(6), pp.691-711.
- Bader, C.R., Bertrand, D., and Schwartz, E.A. (1982). Voltage-activated and calcium-activated currents studied in solitary rod inner segments from the salamander retina. *The Journal of Physiology*, 331(1), pp.253-284.
- Balsler, J.R., Nuss, H.B., Chiamvimonvat, N., Pérez-García, M.T., Marban, E., and Tomaselli, G.F. (1996). External pore residue mediates slow inactivation in mu 1 rat skeletal muscle sodium channels. *The Journal of Physiology*, 494(2), pp.431-442.
- Bant, J.S. and Raman, I.M. (2010). Control of transient, resurgent, and persistent current by open-channel block by Na<sup>+</sup> channel  $\beta$ 4 in cultured cerebellar granule neurons. *Proceedings of the National Academy of Sciences*, 107(27), pp.12357-12362.
- Barish, M.E. (1983). A transient calcium-dependent chloride current in the immature *Xenopus* oocyte. *The Journal of Physiology*, 342(1), pp.309-325.
- Benson, D.W., Wang, D.W., Dymont, M., Knilans, T.K., Fish, F.A., Strieper, M.J., Rhodes, T.H., and George, A.L. (2003). Congenital sick sinus syndrome caused by recessive mutations in the cardiac sodium channel gene (SCN5A). *The Journal of Clinical Investigation*, 112(7), pp.1019-1028.
- Berra-Romani, R., Blaustein, M. P., and Matteson, D. R. (2005). TTX-sensitive voltage-gated Na<sup>+</sup> channels are expressed in mesenteric artery smooth muscle cells. *American Journal of Physiology. Heart and Circulatory Physiology*, 289(1), H137-H145.

- Berridge, M.J. (2008). Smooth muscle cell calcium activation mechanisms. *The Journal of Physiology*, 586(21), pp.5047-5061.
- Beyder, A., Rae, J. L., Bernard, C., Strege, P. R., Sachs, F., and Farrugia, G. (2010). Mechanosensitivity of Nav1.5, a voltage-sensitive sodium channel. *The Journal of Physiology*, 588(24), 4969-4985.
- Bezanilla, F. and Armstrong, C.M. (1977). Inactivation of the sodium channel. I. Sodium current experiments. *The Journal of General Physiology*, 70(5), pp.549-566.
- Bezprozvanny, I.B., Ondrias, K., Kaftan, E., Stoyanovsky, D.A., and Ehrlich, B.E. (1993). Activation of the calcium release channel (ryanodine receptor) by heparin and other polyanions is calcium dependent. *Molecular Biology of the Cell*, 4(3), pp.347-352.
- Bitsch, M., Kromann-Andersen, B., Schou, J., and Sjøntoft, E. (1990). The Elasticity and the Tensile Strength of Tunica Albuginea of the Corpora Cavernosa. *The Journal of Urology*, 143(3), pp.642-645.
- Bocquet, A., Sablayrolles, S., Vacher, B., and Le Grand, B. (2010). F 15845, a new blocker of the persistent sodium current prevents consequences of hypoxia in rat femoral artery. *British Journal of Pharmacology*, 161(2), pp.405-415.
- Boedtkjer, D.M.B., Kim, S., Jensen, A.B., Matchkov, V.M., and Andersson, K.E. (2015). New selective inhibitors of calcium-activated chloride channels-T16Ainh-A 01, CaCC inh-A 01 and MONNA—what do they inhibit?. *British Journal of Pharmacology*, 172(16), pp.4158-4172.
- Bootman, M.D. (2012). Calcium signaling. *Cold Spring Harbor perspectives in biology*, 4(7), p.a011171.
- Boulpaep, E.L., Boron, W.F., Caplan, M.J., Cantley, L., Igarashi, P., Aronson, P.S., and Moczydlowski, E. (2009). Medical physiology a cellular and molecular approach. *Signal Transduct*, 48, pp.398-400.
- Bozkurt, N.B., Vural, I.M., Sarioglu, Y., and Pekiner, C. (2007). Nicotine potentiates the nitrenergic relaxation responses of rabbit corpus cavernosum tissue via nicotinic acetylcholine receptors. *European Journal of Pharmacology*, 558(1-3), pp.172-178.
- Brackenbury, W.J. (2012). Voltage-gated sodium channels and metastatic disease. *Channels*, 6(5), p.352-361.

Brackenbury, W.J. and Isom, L.L. (2011). Na<sup>+</sup> channel  $\beta$  subunits: overachievers of the ion channel family. *Frontiers in Pharmacology*, 2, p.53.

Bradley, E., Fedigan, S., Webb, T., Hollywood, M.A., Thornbury, K.D., McHale, N.G., and Sergeant, G.P. (2014). Pharmacological characterization of TMEM16A currents. *Channels*, 8(4), pp.308-320.

Bradley, E., Hollywood, M.A., McHale, N.G., Thornbury, K.D., and Sergeant, G.P. (2005). Pacemaker activity in urethral interstitial cells is not dependent on capacitative calcium entry. *American Journal of Physiology-Cell Physiology*, 289(3), pp.C625-C632.

Bradley, E., Webb, T.I., Hollywood, M.A., Sergeant, G.P., McHale, N.G., and Thornbury, K.D. (2013). The cardiac sodium current Nav1.5 is functionally expressed in rabbit bronchial smooth muscle cells. *American Journal of Physiology. Cell Physiology*, 305(4):C427-C435.

Browne, L.E., Blaney, F.E., Yusaf, S.P., Clare, J.J., and Wray, D. (2009). Structural determinants of drugs acting on the Nav1.8 channel. *Journal of Biological Chemistry*, 284(16), pp.10523-10536.

Bulley, S., Neeb, Z.P., Burris, S.K., Bannister, J.P., Thomas-Gatewood, C.M., Jangsangthong, W., and Jaggar, J.H. (2012). TMEM16A/ANO1 channels contribute to the myogenic response in cerebral arteries. *Circulation Research*, 111(8), pp.1027-1036

Burnett A.L. (2006) Erectile dysfunction. *Journal of Urology*, 175(3 Pt 2):S25-31.

Burnstock, G. (2018). Purine and purinergic receptors. *Brain and Neuroscience Advances*, 2, p.2398212818817494.

Byerly L. and Yazejian B. (1986) Intracellular factors for maintenance of Ca<sup>2+</sup> currents in internally perfused neurones of the snail *Lymnaea Stagnalis*. *Journal of Physiology*, 370(1), pp.631-651

Cannon, S.C. (2011). Channelopathies of skeletal muscle excitability. *Comprehensive Physiology*, 5(2), pp.761-790.

Capes, D.L., Arcisio-Miranda, M., Jarecki, B.W., French, R.J., and Chanda, B. (2012). Gating transitions in the selectivity filter region of a sodium channel are coupled to the domain IV voltage sensor. *Proceedings of the National Academy of Sciences*, 109(7), pp.2648-2653.

- Caputo, A., Caci, E., Ferrera, L., Pedemonte, N., Barsanti, C., Sondo, E., Pfeffer, U., Ravazzolo, R., Zegarra-Moran, O., and Galletta, L.J. (2008). TMEM16A, a membrane protein associated with calcium-dependent chloride channel activity. *Science*, 322(5901), pp.590-594.
- Carmeliet, E. (1987). Voltage-dependent block by tetrodotoxin of the sodium channel in rabbit cardiac Purkinje fibers. *Biophysical Journal*, 51(1), pp.109-114.
- Casteels, R., Kitamura, K., Kuriyama, H., and Suzuki, H. (1977). The membrane properties of the smooth muscle cells of the rabbit main pulmonary artery. *The Journal of Physiology*, 271(1), pp.41-61.
- Castro, M.J., Stam, A.H., Lemos, C., De Vries, B., Vanmolkot, K.R.J., Barros, J., Terwindt, G.M., Frants, R.R., Sequeiros, J., Ferrari, M.D., and Pereira-Monteiro, J.M. (2009). First mutation in the voltage-gated Nav1.1 subunit gene SCN1A with co-occurring familial hemiplegic migraine and epilepsy. *Cephalalgia*, 29(3), pp.308-313.
- Catterall, W.A. (2000). From Ionic Currents to Molecular Mechanisms. *Neuron*, 26(1), pp.13-25.
- Catterall, W.A. (2014). Structure and function of voltage-gated sodium channels at atomic resolution. *Experimental Physiology*, 99(1), pp.35-51.
- Catterall, W.A., Goldin, A.L., and Waxman, S.G. (2005). International Union of Pharmacology. XLVII. Nomenclature and structure-function relationships of voltage-gated sodium channels. *Pharmacological Reviews*, 57(4), pp.397-409.
- Centeio, R., Cabrita, I., Benedetto, R., Talbi, K., Ousingawat, J., Schreiber, R., Sullivan, J.K., Kunzelmann, K. (2020). Pharmacological inhibition and activation of the Ca<sup>2+</sup> activated Cl<sup>-</sup> channel TMEM16A. *International Journal of Molecular Science*, 21(7), p.2557.
- Cestèle, S. and Catterall, W.A. (2000). Molecular mechanisms of neurotoxin action on voltage-gated sodium channels. *Biochimie*, 82(9-10), pp.883-892.
- Cestèle, S., Qu, Y., Rogers, J.C., Rochat, H., Scheuer, T., and Catterall, W.A. (1998). Voltage sensor-trapping: enhanced activation of sodium channels by  $\beta$ -scorpion toxin bound to the S3-S4 loop in domain II. *Neuron*, 21(4), pp.919-931.

- Cha, A., Ruben, P.P.C., George Jr, A.L., Fujimoto, E., and Bezanilla, F. (1999). Voltage sensors in domains III and IV, but not I and II, are immobilised by Na<sup>+</sup> channel fast inactivation. *Neuron*, 22(1), pp.73-87.
- Chanda, B. and Bezanilla, F. (2002). Tracking Voltage-dependent Conformational Changes in Skeletal Muscle Sodium Channel during Activation. *Journal of General Physiology*, 120(5), pp.629-645.
- Chatelier, A., Mercier, A., Tremblier, B., Thériault, O., Moubarak, M., Benamer, N., Corbi, P., Bois, P., Chahine, M., and Faivre, J. F. (2012). A distinct de novo expression of Nav1.5 sodium channels in human atrial fibroblasts differentiated into myofibroblasts. *The Journal of Physiology*, 590(17), p.4307-4319.
- Chatterjee, S., Vyas, R., Chalamalasetti, S.V., Sahu, I.D., Clatot, J., Wan, X., Lorigan, G.A., Deschênes, I., and Chakrapani, S. (2018). The voltage-gated sodium channel pore exhibits conformational flexibility during slow inactivation. *Journal of General Physiology*, 150(9), pp.1333-1347.
- Chen, C., Bharucha, V., Chen, Y., Westenbroek, R.E., Brown, A., Malhotra, J.D., Jones, D., Avery, C., Gillespie, P.J., Kazen-Gillespie, K.A., and Kazarinova-Noyes, K. (2002). Reduced sodium channel density, altered voltage dependence of inactivation, and increased susceptibility to seizures in mice lacking sodium channel  $\beta$ 2-subunits. *Proceedings of the National Academy of Sciences*, 99(26), pp.17072-17077.
- Chen, L., Staubli, S.E., Schneider, M.P., Kessels, A.G., Ivic, S., Bachmann, L.M., and Kessler, T.M. (2015). Phosphodiesterase 5 inhibitors for the treatment of erectile dysfunction: a trade-off network meta-analysis. *European Urology*, 68(4), pp.674-680.
- Chen, Q., Kirsch, G.E., Zhang, D., Brugada, R., Brugada, J., Brugada, P., Potenza, D., Moya, A., Borggrefe, M., Breithardt, G., and Ortiz-Lopez, R. (1998). Genetic basis and molecular mechanism for idiopathic ventricular fibrillation. *Nature*, 392(6673), pp.293-296.
- Chen, Y., Frank, H.Y., Surmeier, D.J., Scheuer, T., and Catterall, W.A. (2006). Neuromodulation of Na<sup>+</sup> channel slow inactivation via cAMP-dependent protein kinase and protein kinase C. *Neuron*, 49(3), pp.409-420.
- Chipperfield, A.R. and Harper, A.A. (2000). Chloride in smooth muscle. *Progress In Biophysics and Molecular Biology*, 74(3-5), pp.175-221.

Chipperfield, A.R., Davis, J.P.L., and Harper, A.A. (1993). An acetazolamide-sensitive inward chloride pump in vascular smooth muscle. *Biochemical and Biophysical Research Communications*, 194(1), pp.407-412.

Chopra, S., Watanabe, H., Zhong, T., and Roden, D. (2007). Molecular cloning and analysis of zebrafish voltage-gated sodium channel beta subunit genes: implications for the evolution of electrical signaling in vertebrates. *BMC Evolutionary Biology*, 7(1).

Christ, G.J. (2000). Gap junctions and ion channels: relevance to erectile dysfunction. *International Journal of Impotence Research*, 12(4), pp.S15-S25.

Christ, G.J., Maayani, S., Valcic, M., and Melman, A. (1990). Pharmacological studies of human erectile tissue: characteristics of spontaneous contractions and alterations in  $\alpha$ -adrenoceptor responsiveness with age and disease in isolated tissues. *British Journal of Pharmacology*, 101(2), pp. 375-381.

Christ, G.J., Moreno, A., Melman, A., and Spray, D. (1992). Gap junction-mediated intercellular diffusion of  $Ca^{2+}$  in cultured human corporal smooth muscle cells. *American Journal of Physiology-Cell Physiology*, 263(2), pp.C373-C383.

Christ, G.J., Moreno, A., Parker, M., Gondre, C., Valcic, M., Melman, A., and Spray, D. (1991). Intercellular communication through gap junctions: A potential role in pharmacomechanical coupling and syncytial tissue contraction in vascular smooth muscle isolated from the human corpus cavernosum. *Life Sciences*, 49(24), pp.PL195-PL200.

Chu, L.L. and Adaikan, P.G. (2008). Role of chloride channels in the regulation of corpus cavernosum tone: a potential therapeutic target for erectile dysfunction. *The Journal of Sexual Medicine*, 5(4), pp.813-821.

Cil, O., Chen, X., Askew, P.H.R., Baldwin, S.N., Jordan, M.C., Myat The, P., Anderson, M.O., Haggie, P.M., Greenwood, I.A., Roos, K.P., Alan, S.V. (2021). A small molecule inhibitor of the chloride channel TMEM16A blocks vascular smooth muscle contraction and lowers blood pressure in spontaneously hypertensive rats. *Kidney International*, 100, pp.311-320

Claes, L.R., Deprez, L., Suls, A., Baets, J., Smets, K., Van Dyck, T., Deconinck, T., Jordanova, A., and De Jonghe, P. (2009). The SCN1A variant database: a novel research and diagnostic tool. *Human Mutation*, 30(10), pp.E904-E920.

Comerma-Steffensen, S.G., Carvacho, I., Hedegaard, E.R., and Simonsen, U. (2017). Small and intermediate calcium-activated potassium channel openers improve rat endothelial and erectile function. *Frontiers in Pharmacology*, 8, p.660.

Consensus, N.I.H. (1993). Development Panel on Impotence. NIH Consensus Conference. Impotence. *Jama*, 270, pp.83-90.

Corona, G., Mondaini, N., Ungar, A., Razzoli, E., Rossi, A., and Fusco, F. (2011). Phosphodiesterase type 5 (PDE5) inhibitors in erectile dysfunction: the proper drug for the proper patient. *The Journal of Sexual Medicine*, 8(12), pp.3418-3432.

Costa, W., Carrerete, F., Horta, W., and Sampaio, F. (2006). Comparative analysis of the penis corpora cavernosa in controls and patients with erectile dysfunction. *BJU International*, 97(3), pp.567-569.

Costabile, R.A. (2008). Pharmacological Therapy for the Treatment of Sexual Dysfunction-Are We There Yet?. *The Journal of Urology*, 179(3), pp.819-820.

Cotton, K.D., Hollywood, M.A., McHale, N.G., and Thornbury, K.D. (1997).  $Ca^{2+}$  current and  $Ca^{2+}$ -activated chloride current in isolated smooth muscle cells of the sheep urethra. *The Journal of Physiology*, 505(1), pp.121-131.

Craven, M. (2006). Regulation of rabbit corpus cavernosum smooth muscle. (Ph.D.) thesis, Queen's University, Belfast.

Craven, M., Sergeant, G.P., Hollywood, M.A., McHale, N.G., and Thornbury, K.D. (2004). Modulation of spontaneous  $Ca^{2+}$ -activated  $Cl^{-}$  currents in the rabbit corpus cavernosum by the nitric oxide–cGMP pathway. *The Journal of Physiology*, 556(2), pp.495-506.

Crottès, D. and Jan, L.Y. (2019). The multifaceted role of TMEM16A in cancer. *Cell Calcium*, 82, p.102050.

Cummins, T.R., Dib-Hajj, S.D., Black, J.A., Akopian, A.N., Wood, J.N., and Waxman, S.G. (1999). A novel persistent tetrodotoxin-resistant sodium current in SNS-null and wild-type small primary sensory neurons. *Journal of Neuroscience*, 19(24), pp.RC43-RC43.

Danahay, H.L., Lilley, S., Fox, R., Charlton, H., Sabater, J., Button, B., McCarthy, C., Collingwood, S.P., and Gosling, M. (2020). TMEM16A potentiation: a novel therapeutic

approach for the treatment of cystic fibrosis. *American Journal of Respiratory and Critical Care Medicine*, 201(8), pp.946-954.

Davis, A.J., Forrest, A.S., Jepps, T.A., Valencik, M.L., Wiwchar, M., Singer, C.A., Sones, W.R., Greenwood, I.A., and Leblanc, N. (2010). Expression profile and protein translation of TMEM16A in murine smooth muscle. *American Journal of Physiology-Cell Physiology*, 299(5), pp.C948-C959.

Davis, A.J., Shi, J., Pritchard, H.A., Chadha, P.S., Leblanc, N., Vasilikostas, G., Yao, Z., Verkman, A.S., Albert, A.P., and Greenwood, I.A. (2013). Potent vasorelaxant activity of the TMEM16A inhibitor T16Ainh-A01. *British Journal of Pharmacology*, 168(3), pp.773-784.

Davis, J.P., Harper, A.A., and Chipperfield, A.R. (1997). Stimulation of intracellular chloride accumulation by noradrenaline and hence potentiation of its depolarization of rat arterial smooth muscle in vitro. *British Journal of Pharmacology*, 122(4), p.639.

De Carvalho, A.C., Roy, C., Moreno, A.P., Melman, A., Hertzberg, E.L., Christ, G.J., and Spray, D.C. (1993). Gap junctions formed of connexin43 are found between smooth muscle cells of human corpus cavernosum. *The Journal of Urology*, 149(6), p.1568-1575.

De Lera Ruiz, M. and Kraus, R.L. (2015). Voltage-gated sodium channels: structure, function, pharmacology, and clinical indications. *Journal of Medicinal Chemistry*, 58(18), pp.7093-7118.

De Tejada, I.S. (2004). Therapeutic strategies for optimising PDE-5 inhibitor therapy in patients with erectile dysfunction considered difficult or challenging to treat. *International Journal of Impotence Research*, 16(1), pp.S40-S42.

De Tejada, I.S., Kim, N., Lagan, I., Krane, R.J., and Goldstein, I. (1989). Regulation of adrenergic activity in penile corpus cavernosum. *The Journal of Urology*, 142(4), pp.1117-1121.

Dean, R. and Lue, T. (2005). Physiology of Penile Erection and Pathophysiology of Erectile Dysfunction. *Urologic Clinics of North America*, 32(4), pp.379-395.

DeFeo, T.T. and Morgan, K.G. (1985). Calcium-force relationships as detected with aequorin in two different vascular smooth muscles of the ferret. *The Journal of Physiology*, 369(1), pp.269-282.

- Denac, H., Mevissen, M., and Scholtysik, G. (2000). Structure, function and pharmacology of voltage-gated sodium channels. *Naunyn-Schmiedeberg's Archives of Pharmacology*, 362(6), pp.453-479.
- Deshpande, M. A., Wang, J., Preiksaitis, H. G., Laurier, L. G., and Sims, S. M. (2002). Characterization of a voltage-dependent Na<sup>+</sup> current in human esophageal smooth muscle. *The American Journal of Physiology*, 283(4), C1045-C1055.
- Devigili, G., Eleopra, R., Pierro, T., Lombardi, R., Rinaldo, S., Lettieri, C., Faber, C.G., Merkies, I.S., Waxman, S.G., and Lauria, G. (2014). Paroxysmal itch caused by gain-of-function Nav1.7 mutation. *PAIN®*, 155(9), pp.1702-1707.
- Dhabuwala, C.B., Ramakrishna, C.V., and Anderson, G.F. (1985). Beta adrenergic receptors in human cavernous tissue. *The Journal of Urology*, 133(4), pp.721-723.
- Dib-Hajj, S.D., Rush, A.M., Cummins, T.R., Hisama, F.M., Novella, S., Tyrrell, L., Marshall, L., and Waxman, S.G. (2005). Gain-of-function mutation in Nav1.7 in familial erythromelalgia induces bursting of sensory neurons. *Brain*, 128(8), pp.1847-1854.
- Didion, S.P., Lynch, C.M., and Faraci, F.M. (2007). Cerebral vascular dysfunction in TallyHo mice: a new model of Type II diabetes. *American Journal of Physiology-Heart and Circulatory Physiology*, 292(3), pp.H1579-H1583.
- DiSanto, M.E., Wang, Z., Menon, C., Zheng, Y., Chacko, T., Hypolite, J., Broderick, G., Wein, A.J., and Chacko, S. (1998). Expression of myosin isoforms in smooth muscle cells in the corpus cavernosum penis. *American Journal of Physiology-Cell Physiology*, 275(4), pp.C976-C987.
- Doisne, N., Waldmann, V., Redheuil, A., Waintraub, X., Fressart, V., Ader, F., Fossé, L., Hidden-Lucet, F., Gandjbakhch, E., and Neyroud, N. (2020). A novel gain-of-function mutation in SCN5A responsible for multifocal ectopic Purkinje-related premature contractions. *Human Mutation*, 41(4), 850-859.
- Doyle, C., Sergeant, G.P., Hollywood, M.A., McHale, N.G., and Thornbury, K.D. (2014). ATP evokes inward currents in corpus cavernosum myocytes. *The Journal of Sexual Medicine*, 11(1), pp.64-74.
- Drake, R., Gray, H., Mitchell, A., and Vogl, W. (2015). Gray's anatomy for students. 4th ed. Philadelphia, Pa.: *Churchill Livingstone Elsevier*, pp.281, 425-428, 516-518.

- Drenth, J.P. and Waxman, S.G. (2007). Mutations in sodium-channel gene SCN9A cause a spectrum of human genetic pain disorders. *The Journal of Clinical Investigation*, 117(12), pp.3603-3609.
- Drumm, B.T., Large, R.J., Hollywood, M.A., Thornbury, K.D., Baker, S.A., Harvey, B.J., McHale, N.G., and Sergeant, G.P. (2015). The role of Ca<sup>2+</sup> influx in spontaneous Ca<sup>2+</sup> wave propagation in interstitial cells of Cajal from the rabbit urethra. *The Journal of Physiology*, 593, 3333-3350.
- Drumm, B.T., Rembetski, B.E., Cobine, C.A., Baker, S.A., Sergeant, G.P., Hollywood, M.A., Thornbury, K.D., and Sanders, K.M. (2018). Ca<sup>2+</sup> signalling in mouse urethral smooth muscle in situ: role of Ca<sup>2+</sup> stores and Ca<sup>2+</sup> influx mechanisms. *Journal of Physiology*, 596, 1433-1466.
- Dudem, S., Sergeant, G.P., Thornbury, K.D., and Hollywood, M.A. (2021). Calcium-activated K<sup>+</sup> channels (K<sub>Ca</sub>) and therapeutic implications. In *Pharmacology of Potassium Channels* (pp. 379-416). Springer, Cham.
- Durek, T., Vetter, I., Wang, C.I.A., Motin, L., Knapp, O., Adams, D.J., Lewis, R.J., and Alewood, P.F. (2013). Chemical engineering and structural and pharmacological characterisation of the  $\alpha$ -scorpion toxin OD1. *ACS Chemical Biology*, 8(6), pp.1215-1222.
- Eggermont, J. (2004). Calcium-activated Chloride Channels: (Un) known,(Un) loved?. *Proceedings of the American Thoracic Society*, 1(1), pp.22-27.
- Emrich, S.M., Yoast, R.E., Xin, P., Arige, V., Wagner, L.E., Hempel, N., Gill, D.L., Sneyd, J., Yule, D.I., and Trebak, M. (2021). Omnitemporal choreographies of all five STIM/Orai and IP3Rs underlie the complexity of mammalian Ca<sup>2+</sup> signaling. *Cell reports*, 34(9), p.108760.
- Escayg, A. and Goldin, A.L. (2010). Sodium channel SCN1A and epilepsy: mutations and mechanisms. *Epilepsia*, 51(9), pp.1650-1658.
- Fernandes de Oliveira, J., Teixeira, C. E., Arantes, E. C., de Nucci, G., and Antunes, E. (2003). Relaxation of rabbit corpus cavernosum by selective activators of voltage-gated sodium channels: Role of nitric oxide/cyclic guanosine monophosphate pathway. *Urology*, 62(3), 581-588.

- Ferrera, L., Caputo, A., Ubbly, I., Bussani, E., Zegarra-Moran, O., Ravazzolo, R., Pagani, F., and Galletta, L.J. (2009). Regulation of TMEM16A chloride channel properties by alternative splicing. *Journal of Biological Chemistry*, 284(48), pp.33360-33368.
- Forrest, A.S., Joyce, T.C., Huebner, M.L., Ayon, R.J., Wiwchar, M., Joyce, J., Freitas, N., Davis, A.J., Ye, L., Duan, D.D., and Singer, C.A. (2012). Increased TMEM16A-encoded calcium-activated chloride channel activity is associated with pulmonary hypertension. *American Journal of Physiology-Cell Physiology*, 303(12), pp.C1229-C1243.
- Fort, A., Cordaillat, M., Thollon, C., Salazar, G., Mechaly, I., Villeneuve, N., Vilaine, J. P., Richard, S., and Virsolvy, A. (2009). New insights in the contribution of voltage-gated Nav channels to rat aorta contraction. *PLoS ONE*, 4, e7360.
- French, R.J., Worley 3rd, J.F., and Krueger, B.K. (1984). Voltage-dependent block by saxitoxin of sodium channels incorporated into planar lipid bilayers. *Biophysical Journal*, 45(1), pp.301-310.
- Fry, C.H., Cooklin, M., Birns, J., and Mundy, A.R. (1999). Measurement of intercellular electrical coupling in guinea-pig detrusor smooth muscle. *The Journal of Urology*, 161(2), pp.660-664.
- Gardill, B.R., Rivera-Acevedo, R.E., Tung, C.C., Okon, M., McIntosh, L.P., and Van Petegem, F. (2018). The voltage-gated sodium channel EF-hands form an interaction with the III-IV linker that is disturbed by disease-causing mutations. *Scientific Reports*, 8(1), pp.1-13.
- Gelbard, M. (1982). The Disposition and function of Elastic and Collagenous Fibers in the Tunic of the Corpus Cavernosum. *The Journal of Urology*, 128(4), pp.850-851.
- Ghovanloo, M.R., Abdelsayed, M., Peters, C.H., and Ruben, P.C. (2018). A mixed periodic paralysis and myotonia mutant, P1158S, imparts pH-sensitivity in skeletal muscle voltage-gated sodium channels. *Scientific Reports*, 8(1), pp.1-13.
- Giachini, F.R., Chiao, C.W., Carneiro, F.S., Lima, V.V., Carneiro, Z.N., Dorrance, A.M., Tostes, R.C., and Webb, R.C. (2009). Increased activation of stromal interaction molecule-1/Orai-1 in aorta from hypertensive rats: a novel insight into vascular dysfunction. *Hypertension*, 53(2), pp.409-416.

- Giachini, F.R., Lima, V.V., Hannan, J.L., Carneiro, F.S., Webb, R.C., and Tostes, R.C. (2011). STIM1/Orai1-mediated store-operated Ca<sup>2+</sup> entry: the tip of the iceberg. *Brazilian Journal of Medical and Biological Research*, 44, pp.1080-1087.
- Giuliano, F.A., Leriche, A., Jaudinot, E.O., and de Gendre, A.S. (2004). Prevalence of erectile dysfunction among 7689 patients with diabetes or hypertension, or both. *Urology*, 64(6), pp.1196-1201.
- Goldfarb, M. (2012). Voltage-gated sodium channel-associated proteins and alternative mechanisms of inactivation and block. *Cellular and Molecular Life Sciences*, 69(7), pp.1067-1076.
- Goldin, A.L. (2003). Mechanisms of sodium channel inactivation. *Current Opinion in Neurobiology*, 13(3), pp.284-290.
- Goldstein, A. and Padma-Nathan, H. (1990). The Microarchitecture of the Intracavernosal Smooth Muscle and the Cavernosal Fibrous Skeleton. *The Journal of Urology*, 144(5), pp.1144-1146.
- Gomez-Pinilla, P.J., Gibbons, S.J., Bardsley, M.R., Lorincz, A., Pozo, M.J., Pasricha, P.J., de Rijn, M.V., West, R.B., Sarr, M.G., Kendrick, M.L., and Cima, R.R. (2009). Ano1 is a selective marker of interstitial cells of Cajal in the human and mouse gastrointestinal tract. *American Journal of Physiology-Gastrointestinal and Liver Physiology*, 296(6), pp.G1370-G1381.
- Gonoi, T., Sherman, S.J., and Catterall, W.A. (1985). Voltage clamp analysis of tetrodotoxin-sensitive and-insensitive sodium channels in rat muscle cells developing in vitro. *Journal of Neuroscience*, 5(9), pp.2559-2564.
- Gordon, J.L. (1986). Extracellular ATP: effects, sources and fate. *Biochemical Journal*, 233(2), pp.309-319.
- Grann, M., Comerma-Steffensen, S., Arcanjo, D.D., and Simonsen, U. (2016). Mechanisms involved in thromboxane A<sub>2</sub>-induced vasoconstriction of rat intracavernous small penile arteries. *Basic and Clinical Pharmacology and Toxicology*, 119, pp.86-95.
- Griffin, C.S., Bradley, E., Dudem, S., Hollywood, M.A., McHale, N.G., Thornbury, K.D., and Sergeant, G.P. (2016). Muscarinic Receptor Induced Contractions of the Detrusor are Mediated by Activation of TRPC4 Channels. *Journal of Urology*, 196, 1796-1808.

Groenewegen, W.A., Firouzi, M., Bezzina, C.R., Vliex, S., van Langen, I.M., Sandkuijl, L., Smits, J.P., Hulsbeek, M., Rook, M.B., Jongsma, H.J., and Wilde, A.A. (2003). A cardiac sodium channel mutation cosegregates with a rare connexin40 genotype in familial atrial standstill. *Circulation Research*, 92(1), pp.14-22.

Groome, J., Lehmann-Horn, F., and Holzherr, B. (2011). Open-and closed-state fast inactivation in sodium channels: differential effects of a site-3 anemone toxin. *Channels*, 5(1), pp.65-78.

Guidone, G., Müller, D., Vogt, K., and Mukhopadhyay, A.K. (2002). Characterisation of VIP and PACAP receptors in cultured rat penis corpus cavernosum smooth muscle cells and their interaction with guanylate cyclase-B receptors. *Regulatory Peptides*, 108(2-3), pp.63-72.

Guo, S., Chen, Y., Pang, C., Wang, X., Qi, J., Mo, L., Zhang, H., An, H., and Zhan, Y. (2017). Ginsenoside Rb1, a novel activator of the TMEM16A chloride channel, augments the contraction of guinea pig ileum. *Pflügers Archiv-European Journal of Physiology*, 469(5), pp.681-692.

Gur, S., Kadowitz, P.J., Abdel-Mageed, A.B., Kendirci, M., Sikka, S.C., Burnstock, G., and Hellstrom, W.J. (2009). Management of erectile function by penile purinergic p2 receptors in the diabetic rat. *The Journal of Urology*, 181(5), pp.2375-2382.

Habbout, K., Poulin, H., Rivier, F., Giuliano, S., Sternberg, D., Fontaine, B., Eymard, B., Morales, R.J., Echenne, B., King, L., and Hanna, M.G. (2016). A recessive Nav1.4 mutation underlies congenital myasthenic syndrome with periodic paralysis. *Neurology*, 86(2), pp.161-169.

Hains, B.C., Klein, J.P., Saab, C.Y., Craner, M.J., Black, J.A., and Waxman, S.G. (2003). Upregulation of sodium channel Nav1.3 and functional involvement in neuronal hyperexcitability associated with central neuropathic pain after spinal cord injury. *Journal of Neuroscience*, 23(26), pp.8881-8892.

Hammond, C. (2014). Cellular and molecular neurophysiology. *Academic Press*.

Hannigan, K.I., Griffin, C.S., Large, R.J., Sergeant, G.P., Hollywood, M.A., McHale, N.G., and Thornbury, K.D. (2017). The role of Ca<sup>2+</sup>-activated Cl<sup>-</sup> current in tone generation in the rabbit corpus cavernosum. *American Journal of Physiology-Cell Physiology*, 313(5), pp.C475-C486.

- Hannigan, K.I., Large, R.J., Bradley, E., Hollywood, M.A., Sergeant, G.P., McHale, N.G., and Thornbury, K.D. (2016). Effect of a novel BK<sub>Ca</sub> opener on BK<sub>Ca</sub> currents and contractility of the rabbit corpus cavernosum. *American Journal of Physiology-Cell Physiology*, 310(4), pp.C284-C292.
- Hartzell, C., Putzier, I., and Arreola, J. (2005). Calcium-activated chloride channels. *Annual Review of Physiology*, 67, pp.719-758.
- Hashitani, H., Fukuta, H., Dickens, E.J., and Suzuki, H. (2002). Cellular mechanisms of nitric oxide-induced relaxation of corporeal smooth muscle in the guinea-pig. *The Journal of Physiology*, 538(2), pp.573-581.
- Hashitani, H., Yanai, Y., Shirasawa, N., Soji, T., Tomita, A., Kohri, K., and Suzuki, H. (2005). Interaction between spontaneous and neurally mediated regulation of smooth muscle tone in the rabbit corpus cavernosum. *The Journal of Physiology*, 569(3), pp.723-735.
- Hawn, M.B., Akin, E., Hartzell, H.C., Greenwood, I.A., and Leblanc, N. (2021). Molecular mechanisms of activation and regulation of ANO1-Encoded Ca<sup>2+</sup>-Activated Cl<sup>-</sup> channels. *Channels*, 15(1), pp.569-603.
- He, B. and Soderlund, D.M. (2010). Human embryonic kidney (HEK293) cells express endogenous voltage-gated sodium currents and Nav1.7 sodium channels. *Neuroscience Letters*, 469(2), pp.268-272.
- Hedlund, H. and Andersson, K.E. (1985). Comparison of the responses to adrenoreceptor and muscarinic receptor active drugs in isolated human corpus cavernosum and cavernous artery. *Journal of Autonomic Pharmacology*, 5, pp.81-88.
- Hedlund, P., Aszódi, A., Pfeifer, A., Alm, P., Hofmann, F., Ahmad, M., Fässler, R., and Andersson, K.E. (2000). Erectile dysfunction in cyclic GMP-dependent kinase I-deficient mice. *Proceedings of the National Academy of Sciences*, 97(5), pp.2349-2354.
- Heinze, C., Seniuk, A., Sokolov, M.V., Huebner, A.K., Klementowicz, A.E., Szijártó, I.A., Schleifenbaum, J., Vitzthum, H., Gollasch, M., Ehmke, H., and Schroeder, B.C. (2014). Disruption of vascular Ca<sup>2+</sup>-activated chloride currents lowers blood pressure. *The Journal of clinical investigation*, 124(2), pp.675-686.

- Higgins, A., Nash, M., and Lynch, A.M. (2010). Antidepressant-associated sexual dysfunction: impact, effects, and treatment. *Drug, Healthcare and Patient Safety*, 2, p.141.
- Hilber, K., Sandtner, W., Kudlacek, O., Schreiner, B., Glaaser, I., Schütz, W., Fozzard, H.A., Dudley, S.C., and Todt, H. (2002). Interaction between fast and ultra-slow inactivation in the voltage-gated sodium channel does the inactivation gate stabilise the channel structure? *Journal of Biological Chemistry*, 277(40), pp.37105-37115.
- Hille, B. (1977). Local anesthetics: hydrophilic and hydrophobic pathways for the drug-receptor reaction. *The Journal of General Physiology*, 69(4), pp.497-515.
- Hille, B. (2001). *Ion Channels of Excitable Membranes*, 3rd Edn, Sunderland: Sinauer Associates.
- Hill-Eubanks, D.C., Werner, M.E., Heppner, T.J., and Nelson, M.T. (2011). Calcium signaling in smooth muscle. *Cold Spring Harbor Perspectives in Biology*, 3(9), p.a004549.
- Ho, W. S. V., Davis, A. J., Chadha, P. S., and Greenwood, I. A. (2013). Effective contractile response to voltage-gated Na<sup>+</sup> channels revealed by a channel activator. *The American Journal of Physiology*, 304(8), C739-C747.
- Hodgkin, A.L. and Huxley, A.F. (1952). The components of membrane conductance in the giant axon of *Loligo*. *The Journal of Physiology*, 116(4), pp.473.
- Hogg, R.C., Wang, Q., and Large, W.A. (1994). Effects of Cl channel blockers on Ca-activated chloride and potassium currents in smooth muscle cells from rabbit portal vein. *British Journal of Pharmacology*, 111(4), pp.1333-1341.
- Holland, K.D., Kearney, J.A., Glauser, T.A., Buck, G., Keddache, M., Blankston, J.R., Glaaser, I.W., Kass, R.S., and Meisler, M.H. (2008). Mutation of sodium channel SCN3A in a patient with cryptogenic pediatric partial epilepsy. *Neuroscience Letters*, 433(1), pp.65-70.
- Hollywood, M. A., Cotton, K. D., Thornbury, K. D., and McHale, N. G. (1997). Tetrodotoxin-sensitive sodium current in sheep lymphatic smooth muscle. *The Journal of Physiology*, 503(Pt 1), 13.

- Holm, A.N., Rich, A., Miller, S.M., Strege, P., Ou, Y., Gibbons, S.J., Sarr, M.G., Szurszewski, J.H., Rae, J.L., and Farrugia, G. (2002). Sodium current in human jejunal circular smooth muscle cells. *Gastroenterology*, 122(1), p.178-187
- Holz, R. and Finkelstein, A. (1970). The water and nonelectrolyte permeability induced in thin lipid membranes by the polyene antibiotics nystatin and amphotericin B. *The Journal of General Physiology*, 56(1), pp.125-145.
- Höppner, C.K., Stief, C.G., Jonas, U., Mandrek, K., Noack, T., and Golenhofen, K. (1996). Electrical and chemical control of smooth muscle activity of rabbit corpus cavernosum in vitro. *Urology*, 48(3), pp.512-518.
- Horn, R. and Marty, A. (1988). Muscarinic activation of ionic currents measured by a new whole-cell recording method. *The Journal of General Physiology*, 92(2), pp.145-159.
- Horn, R., Ding, S., and Gruber, H.J. (2000). Immobilising the Moving Parts of Voltage-Gated Ion Channels. *Journal of General Physiology*, 116(3), pp.461-476.
- Horn, R., Patlak, J., and Stevens, C.F. (1981). Sodium channels need not open before they inactivate. *Nature*, 291(5814), pp.426-427.
- Hsu, G., Brock, G., Martinez-Pineiro, L., Nunes, L., Heyden, B., and Lue, T. (1992). The three-dimensional structure of the human tunica albuginea: anatomical and ultrastructural levels. *International Journal of Impotence Research*, 4, pp.117-129.
- Hsu, G., Hsieh, C., Wen, H., Chen, Y., Chen, S., and Mok, M. (2003). Penile Venous Anatomy: An Additional Description and Its Clinical Implication. *Journal of Andrology*, 24(6), pp.921-927.
- Huang, F., Rock, J.R., Harfe, B.D., Cheng, T., Huang, X., Jan, Y.N., and Jan, L.Y. (2009). Studies on expression and function of the TMEM16A calcium-activated chloride channel. *Proceedings of the National Academy of Sciences*, 106(50), pp.21413-21418.
- Huang, Y., Zhou, Y., Wong, H.C., Chen, Y., Chen, Y., Wang, S., Castiblanco, A., Liu, A., and Yang, J.J. (2009). A single EF-hand isolated from STIM1 forms dimer in the absence and presence of Ca<sup>2+</sup>. *The FEBS journal*, 276(19), pp.5589-5597.
- Iacono, F., Barra, S., and Lotti, T. (1995). Elastic fibre concentration in the tunica albuginea of corpora cavernosa and nocturnal tumescence monitoring. *International Journal of Impotence Research*, 7(2), pp.63-70.

Isom, L., De Jongh, K., Patton, D., Reber, B., Offord, J., Charbonneau, H., Walsh, K., Goldin, A., and Catterall, W. (1992). Primary structure and functional expression of the beta 1 subunit of the rat brain sodium channel. *Science*, 256(5058), pp.839-842.

Isom, L., Ragsdale, D., De Jongh, K., Westenbroek, R., Reber, B., Scheuer, T., and Catterall, W. (1995). Structure and function of the  $\beta 2$  subunit of brain sodium channels, a transmembrane glycoprotein with a CAM motif. *Cell*, 83(3), pp.433-442.

Iwamoto, T., Kita, S., Zhang, J., Blaustein, M.P., Arai, Y., Yoshida, S., Wakimoto, K., Komuro, I., Katsuragi, T. (2004). Salt-sensitive hypertension is triggered by  $\text{Ca}^{2+}$  entry via  $\text{Na}^+/\text{Ca}^{2+}$  exchanger type-1 in vascular smooth muscle. *Nature Medicine*. 10: 1193-1199

Iwamoto, T., Watano, T., and Shigekawa, M. (1996). A novel isothiourea derivative selectively inhibits the reverse mode of  $\text{Na}^+/\text{Ca}^{2+}$  exchange in cells expressing NCX1. *Journal of Biological Chemistry*, 271(37):22391-7.

Iwamoto, Y., Song, K., Takai, S., Yamada, M., Jin, D., Sakaguchi, M., Ueda, H., Katsuoka, Y., and Miyazaki, M. (2001). Multiple pathways of angiotensin I conversion and their functional role in the canine penile corpus cavernosum. *Journal of Pharmacology and Experimental Therapeutics*, 298(1), pp.43-48.

Jalali, A., Bosmans, F., Amininasab, M., Clynen, E., Cuypers, E., Zaremirakabadi, A., Sarbolouki, M.N., Schoofs, L., Vatanpour, H., and Tytgat, J. (2005). OD1, the first toxin isolated from the venom of the scorpion *Odonthobuthus doriae* active on voltage-gated  $\text{Na}^+$  channels. *FEBS letters*, 579(19), pp.4181-4186.

Jarvis, M.F., Honore, P., Shieh, C.C., Chapman, M., Joshi, S., Zhang, X.F., Kort, M., Carroll, W., Marron, B., Atkinson, R., and Thomas, J. (2007). A-803467, a potent and selective  $\text{Na}_v1.8$  sodium channel blocker, attenuates neuropathic and inflammatory pain in the rat. *Proceedings of the National Academy of Sciences*, 104(20), pp.8520-8525.

Jepps, T.A., Olesen, S.P., Greenwood, I.A., and Dalsgaard, T. (2016). Molecular and functional characterisation of  $\text{K}_v7$  channels in penile arteries and corpus cavernosum of healthy and metabolic syndrome rats. *British Journal of Pharmacology*, 173(9), pp.1478-1490.

- Ji, Q., Guo, S., Wang, X., Pang, C., Zhan, Y., Chen, Y., and An, H. (2019). Recent advances in TMEM16A: Structure, function, and disease. *Journal of Cellular Physiology*, 234(6), pp.7856-7873.
- Ji, S., George Jr, A.L., Horn, R., and Barchi, R.L. (1996). Paramyotonia congenita mutations reveal different roles for segments S3 and S4 of domain D4 in hSkM1 sodium channel gating. *The Journal of General Physiology*, 107(2), pp.183-194.
- Jiang, X., Meuleman, E.J., Wijkstra, H., and Wagner, G. (2005). Corpus cavernosum electromyography during morning naps in healthy volunteers: further evidence that corpus cavernosum potentials reflect sympathetically mediated activity. *The Journal of Urology*, 174(5), pp.1917-1920.
- Jo, T., Nagata, T., Iida, H., Imuta, H., Iwasawa, K., Ma, J., Hara, K., Omata, M., Nagai, R., Takizawa, H., and Nagase, T. (2004). Voltage-gated sodium channel expressed in cultured human smooth muscle cells: involvement of SCN9A. *FEBS letters*, 567(2-3), pp.339-343.
- Johnston, L., Sergeant, G.P., Hollywood, M.A., Thornbury, K.D., and McHale, N.G. (2005). Calcium oscillations in interstitial cells of the rabbit urethra. *Journal of Physiology* 565, 449-461.
- Jones, K., Shmygol, A., Kupittayanant, S., and Wray, S. (2004). Electrophysiological characterization and functional importance of calcium-activated chloride channel in rat uterine myocytes. *Pflügers Archiv*, 448(1), pp.36-43.
- Juskiewenski, S., Vaysse, P., Moscovici, J., Hammoudi, S., and Bouissou, E. (1982). A study of the arterial blood supply to the penis. *Anatomia Clinica*, 4(2), pp.101-107.
- Kalienkova, V., Mosina, V.C., and Paulino, C. (2021). The groovy TMEM16 family: molecular mechanisms of lipid scrambling and ion conduction. *Journal of Molecular Biology*, 433(16), p.166941.
- Karaki, H., Ozaki, H., Hori, M., Mitsui-Saito, M., Amano, K.I., Harada, K.I., Miyamoto, S., Nakazawa, H., Won, K.J., and Sato, K. (1997). Calcium movements, distribution, and functions in smooth muscle. *Pharmacological Reviews*, 49(2), pp.157-230.

Karkanis, T., DeYoung, L., Brock, G.B., and Sims, S.M. (2003).  $\text{Ca}^{2+}$ -activated  $\text{Cl}^-$  channels in corpus cavernosum smooth muscle: a novel mechanism for control of penile erection. *Journal of Applied Physiology*, 94(1), pp.301-313.

Karoly, R., Lenkey, N., Juhasz, A.O., Vizi, E.S., and Mike, A. (2010). Fast-or slow-inactivated state preference of  $\text{Na}^+$  channel inhibitors: a simulation and experimental study. *PLoS Comput Biol*, 6(6), p.e1000818.

Kifor, I., Williams, G.H., Vickers, M.A., Sullivan, M.P., Jodbert, P., and Dluhy, R.G. (1997). Tissue angiotensin II as a modulator of erectile function. I. Angiotensin peptide content, secretion and effects in the corpus cavernosum. *The Journal of Urology*, 157(5), pp.1920-1925.

Kim, Y.C., Choi, H.K., Ahn, Y.S., Kim, K.H., Hagen, P.O., and Carson III, C.C. (1994). The effect of vasoactive intestinal polypeptide (VIP) on rabbit cavernosal smooth muscle contractility. *Journal of Andrology*, 15(5), pp.392-397.

Klinge, E. and Sjöstrand, N.O. (1977). Comparative study of some isolated mammalian smooth muscle effectors of penile erection. *Acta Physiologica Scandinavica*, 100(3):354-67.

Kontis, K.J. and Goldin, A.L. (1997). Sodium channel inactivation is altered by substitution of voltage sensor positive charges. *The Journal of General Physiology*, 110(4), pp.403-413.

Kreye, V.A., Bauer, P.K., and Villhauer, I. (1981). Evidence for furosemide-sensitive active chloride transport in vascular smooth muscle. *European Journal of Pharmacology*, 73(1), pp.91-95.

Kun, A., Matchkov, V.V., Stankevicius, E., Nardi, A., Hughes, A.D., Kirkeby, H.J., Demnitz, J., and Simonsen, U. (2009). NS11021, a novel opener of large-conductance  $\text{Ca}^{2+}$ -activated  $\text{K}^+$  channels, enhances erectile responses in rats. *British Journal of Pharmacology*, 158(6), pp.1465-1476.

Kuo, Y.C., Chung, S.D., Liu, S.P., Chang, H.C., Yu, H.J., and Hsieh, J.T. (2009). The role of chloride channels in rat corpus cavernosum: in vivo study. *The Journal of Sexual Medicine*, 6(3), pp.708-716.

- Kuruma, A. and Hartzell, H.C. (2000). Bimodal control of a  $\text{Ca}^{2+}$ -activated  $\text{Cl}^-$  channel by different  $\text{Ca}^{2+}$  signals. *The Journal of General Physiology*, 115(1), pp.59-80.
- Lam, A.K., Rheinberger, J., Paulino, C., and Dutzler, R. (2021). Gating the pore of the calcium-activated chloride channel TMEM16A. *Nature Communications*, 12(1), pp.1-13.
- Large, R.J., Kshatri, A., Webb, T.I., Roy, S., Akande, A., Bradley, E., Sergeant, G.P., Thornbury, K.D., McHale, N.G., and Hollywood, M.A. (2015). Effects of the novel BK ( $\text{K}_{\text{Ca}1.1}$ ) channel opener GoSlo-SR-5-130 are dependent on the presence of BK  $\beta$  subunits. *British Journal of Pharmacology*, 172(10), pp.2544-2556.
- Large, W.A. and Wang, Q. (1996). Characteristics and physiological role of the  $\text{Ca}^{2+}$ -activated  $\text{Cl}^-$  conductance in smooth muscle. *American Journal of Physiology-Cell Physiology*, 271(2), pp.C435-C454.
- Lau, L.C. and Adaikan, P.G. (2014). Possibility of inhibition of calcium-activated chloride channel rescuing erectile failures in diabetes. *International Journal of Impotence Research*, 26(4), pp.151-155.
- Laver, D.R. and van Helden, D.F. (2011). Three independent mechanisms contribute to tetracaine inhibition of cardiac calcium release channels. *Journal of Molecular and Cellular Cardiology*, 51(3), pp.357-369.
- Ledda, A. (2000). Diabetes, hypertension and erectile dysfunction. *Current Medical Research And Opinion*, 16(sup1), pp.s17-s20.
- Lee, S.W., Wang, H.Z., Zhao, W., Ney, P., Brink, P.R., and Christ, G.J. (1999). Prostaglandin E1 activates the large-conductance  $\text{K}_{\text{Ca}}$  channel in human corporal smooth muscle cells. *International Journal of Impotence Research*, 11(4), pp.189-199.
- Lenaeus, M.J., El-Din, T.M.G., Ing, C., Ramanadane, K., Pomès, R., Zheng, N., and Catterall, W.A. (2017). Structures of closed and open states of a voltage-gated sodium channel. *Proceedings of the National Academy of Sciences*, 114(15), pp.E3051-E3060.
- Leong, X.F., Ng, C.Y., and Jaarin, K. (2015). Animal models in cardiovascular research: hypertension and atherosclerosis. *BioMed research international*, 2015.
- Li, H.L., Galue, A., Meadows, L., and Ragsdale, D.S. (1999). A molecular basis for the different local anesthetic affinities of resting versus open and inactivated states of the sodium channel. *Molecular Pharmacology*, 55(1), pp.134-141.

- Li, L., Ma, K.T., Zhao, L., and Si, J.Q. (2008). Niflumic acid hyperpolarizes the smooth muscle cells by opening BK<sub>Ca</sub> channels through ryanodine-sensitive Ca<sup>2+</sup> release in spiral modiolar artery. *Acta Physiologica Sinica*, 60(6), pp.743-750.
- Lim, X.R., Bradley, E., Griffin, C.S., Hollywood, M.A., Sergeant, G.P., and Thornbury, K.D. (2022). Fast voltage-dependent sodium (Nav) currents are functionally expressed in mouse corpus cavernosum smooth muscle cells. *British Journal of Pharmacology*, 179(5), pp.1082-1101.
- Liu, Y., Liu, Z., and Wang, K. (2021). The Ca<sup>2+</sup>-activated chloride channel ANO1/TMEM16A: An emerging therapeutic target for epithelium-originated diseases?. *Acta Pharmaceutica Sinica B*, 11(6), pp.1412-1433.
- Livak, K.J. and Schmittgen, T.D. (2001) Analysis of relative gene expression data using real-time quantitative PCR and the 2<sup>-</sup>ΔΔCT method. *Methods* 25, 402-408.
- Locke, G. R., Ackerman, M. J., Zinsmeister, A. R., Thapa, P., and Farrugia, G. (2006). Gastrointestinal symptoms in families of patients with an SCN5A-encoded cardiac channelopathy: Evidence of an intestinal channelopathy. *The American Journal of Gastroenterology*, 101(6), 1299-1304.
- Lossin, C., Shi, X., Rogawski, M.A., and Hirose, S. (2012). Compromised function in the Nav1.2 Dravet syndrome mutation R1312T. *Neurobiology of Disease*, 47(3), pp.378-384.
- Luangkhot, R., Rutchik, S., Agarwal, V., Puglia, K., Bhargava, G., and Melman, A. (1992). Collagen Alterations in the Corpus Cavernosum of Men With Sexual Dysfunction. *The Journal of Urology*, 148(2), pp.467-471.
- Lue, T.F. (2000). Erectile Dysfunction. *New England Journal of Medicine*, 342(24), pp.1802-1813.
- Lue, T.F., Zeineh, S.J., Schmidt, R.A., and Tanagho, E.A. (1984). Neuroanatomy of penile erection: its relevance to iatrogenic impotence. *The Journal of Urology*, 131(2), pp.273-280.
- Luttrell, I.P., Swee, M., Starcher, B., Parks, W.C., and Chitale, K. (2008). Erectile dysfunction in the type II diabetic db/db mouse: impaired venoocclusion with altered cavernosal vasoreactivity and matrix. *American Journal of Physiology-Heart and Circulatory Physiology*, 294(5), pp.H2204-H2211.

- MacLennan, G., Hinman, F., and Stempen, P. (2012). Hinman's atlas of urosurgical anatomy. Philadelphia, PA: Elsevier Saunders, p.325.
- Malysz, J., Farrugia, G., Ou, Y., Szurszewski, J.H., Nehra, A., and Gibbons, S.J. (2002). The K<sub>v</sub>2.2  $\alpha$  subunit contributes to delayed rectifier K<sup>+</sup> currents in myocytes from rabbit corpus cavernosum. *Journal of Andrology*, 23(6), pp.899-910. PMID: 12399537
- Malysz, J., Gibbons, S.J., Miller, S.M., Gettman, M., Nehra, A., Szurszewski, J.H., and Farrugia, G. (2001). Potassium outward currents in freshly dissociated rabbit corpus cavernosum myocytes. *The Journal of Urology*, 166(3), pp.1167-1177. PMID: 11490317
- Männikkö, R., Wong, L., Tester, D.J., Thor, M.G., Sud, R., Kullmann, D.M., Sweeney, M.G., Leu, C., Sisodiya, S.M., FitzPatrick, D.R., and Evans, M.J. (2018). Dysfunction of Nav1.4, a skeletal muscle voltage-gated sodium channel, in sudden infant death syndrome: a case-control study. *The Lancet*, 391(10129), pp.1483-1492.
- Manoury, B., Tamuleviciute, A., and Tammaro, P. (2010). TMEM16A/anoctamin 1 protein mediates calcium-activated chloride currents in pulmonary arterial smooth muscle cells. *The Journal of Physiology*, 588(13), pp.2305-2314.
- Maruyama, T., Kanaji, T., Nakade, S., Kanno, T., and Mikoshiba, K. (1997). 2APB, 2-aminoethoxydiphenyl borate, a membrane-penetrable modulator of Ins (1, 4, 5) P<sub>3</sub>-induced Ca<sup>2+</sup> release. *The Journal of Biochemistry*, 122(3), pp.498-505.
- Masterson, L.R., Yu, T., Shi, L., Wang, Y., Gustavsson, M., Mueller, M.M., and Veglia, G. (2011). cAMP-dependent protein kinase A selects the excited state of the membrane substrate phospholamban. *Journal of Molecular Biology*, 412(2), pp.155-164.
- Matthews, R.M., Bradley, E., Griffin, C.S., Lim, X.R., Mullins, N.D., Hollywood, M.A., Lundy, F.T., McGarvey, L.P., Sergeant, G.P., and Thornbury, K.D. (2022). Functional expression of Nav1.7 channels in freshly dispersed mouse bronchial smooth muscle cells. *American Journal of Physiology-Cell Physiology*.
- Mazzone, A., Bernard, C.E., Strege, P.R., Beyder, A., Galietta, L.J., Pasricha, P.J., Rae, J.L., Parkman, H.P., Linden, D.R., Szurszewski, J.H. and Ördög, T. (2011). Altered expression of Anol1 variants in human diabetic gastroparesis. *Journal of Biological Chemistry*, 286(15), pp.13393-13403.

Mazzone, A., Gibbons, S.J., Bernard, C.E., Nowsheen, S., Middha, S., Almada, L.L., Ordog, T., Kendrick, M.L., Lombardo, K.R., Shen, K.R., and Galiotta, L.J. (2015). Identification and characterization of a novel promoter for the human ANO1 gene regulated by the transcription factor signal transducer and activator of transcription 6 (STAT6). *The FASEB Journal*, 29(1), pp.152-163.

McCloskey, C., Cagney, V., Large, R., Hollywood, M., Sergeant, G., McHale, N., and Thornbury K. (2009) Voltage-dependent  $Ca^{2+}$  currents contribute to spontaneous  $Ca^{2+}$  waves in rabbit corpus cavernosum myocytes. *Journal of Sexual Medicine*; 6, pp.3019-3031.

McCormack, K., Santos, S., Chapman, M.L., Krafte, D.S., Marron, B.E., West, C.W., Krambis, M.J., Antonio, B.M., Zellmer, S.G., Printzenhoff, D., and Padilla, K.M. (2013). Voltage sensor interaction site for selective small molecule inhibitors of voltage-gated sodium channels. *Proceedings of the National Academy of Sciences*, 110(29), pp.E2724-E2732.

McMahon, C.G. (2014). Erectile dysfunction. *Internal medicine journal*, 44(1), pp.18-26.

Meguro, K., Iida, H., Takano, H., Morita, T., Sata, M., Nagai, R., and Nakajima, T. (2009). Function and role of voltage-gated sodium channel  $Na_v1.7$  expressed in aortic smooth muscle cells. *American Journal of Physiology-Heart and Circulatory Physiology*, 296(1), pp.H211-H219.

Miledi, R. (1982). A calcium-dependent transient outward current in *Xenopus laevis* oocytes. *Proceedings of the Royal Society of London. Series B. Biological Sciences*, 215(1201), pp.491-497.

Milenkovic, V.M., Brockmann, M., Stöhr, H., Weber, B.H., and Strauss, O. (2010). Evolution and functional divergence of the anoctamin family of membrane proteins. *BMC Evolutionary Biology*, 10(1), pp.1-9.

Miner, K., Labitzke, K., Liu, B., Wang, P., Henckels, K., Gaida, K., Elliott, R., Chen, J.J., Liu, L., Leith, A., and Trueblood, E. (2019). Drug repurposing: the anthelmintics niclosamide and nitazoxanide are potent TMEM16A antagonists that fully bronchodilate airways. *Frontiers in pharmacology*, p.51.

Mitri, C., Sharma, H., Corvol, H., and Tabary, O. (2021). TMEM16A/ANO1: current strategies and novel drug approaches for cystic fibrosis. *Cells*, 10(11), p.2867.

- Moreau, A., Gosselin-Badaroudine, P., Delemotte, L., Klein, M.L., and Chahine, M. (2015). Gating pore currents are defects in common with two Nav1.5 mutations in patients with mixed arrhythmias and dilated cardiomyopathy. *Journal of General Physiology*, 145(2), pp.93-106.
- Moreland, R.B., Kim, N., Nehra, A., Goldstein, I., and Traish, A. (2003). Functional prostaglandin E (EP) receptors in human penile corpus cavernosum. *International Journal of Impotence Research*, 15(5), pp.362-368.
- Moreland, R.B., Kim, N.N., Nehra, A., Parulkar, B.G., and Traish, A. (2000). Misoprostol induces relaxation of human corpus cavernosum smooth muscle: comparison to prostaglandin E 1. *International Journal of Impotence Research*, 12(2), pp.107-110.
- Morgan, L.M., Martin, S.L., Mullins, N.D., Hollywood, M.A., Thornbury, K.D., and Sergeant, G.P. (2022). Modulation of carbachol-induced Ca<sup>2+</sup> oscillations in airway smooth muscle cells by PGE2. *Cell Calcium*, 103, 102547.
- Moslehi, R., Langlois, S., Yam, I., and Friedman, J.M. (1998). Linkage of malignant hyperthermia and hyperkalemic periodic paralysis to the adult skeletal muscle sodium channel (SCN4A) gene in a large pedigree. *American Journal of Medical Genetics*, 76(1), pp.21-27.
- Muraki, K., Imaizumi, Y., and Watanabe, M. (1991). Sodium currents in smooth muscle cells freshly isolated from stomach fundus of the rat and ureter of the guinea-pig. *The Journal of Physiology*, 442, 351-375.
- Nagai, T. and Prosser, C.L. (1963). Electrical parameters of smooth muscle cells. *American Journal of Physiology-Legacy Content*, 204(5), pp.915-924.
- Nakano, T. (1995). Three-Dimensional Architecture of Collagen Fibrils in the Mouse Corpus cavernosum penis. *Cells Tissues Organs*, 152(3), pp.215-223.
- Namadurai, S., Yereddi, N., Cusdin, F., Huang, C., Chirgadze, D., and Jackson, A. (2015). A new look at sodium channel subunits. *Open Biology*, 5(1), pp.140192-140192.
- Namkung, W., Phuan, P.W., and Verkman, A.S. (2011). TMEM16A inhibitors reveal TMEM16A as a minor component of calcium-activated chloride channel conductance in airway and intestinal epithelial cells. *Journal of Biological Chemistry*, 286(3), pp.2365-2374.

- Namkung, W., Thiagarajah, J.R., Phuan, P.W., and Verkman, A.S. (2010). Inhibition of  $\text{Ca}^{2+}$ -activated  $\text{Cl}^-$  channels by gallotannins as a possible molecular basis for health benefits of red wine and green tea. *The FASEB Journal*, 24(11), pp.4178-4186.
- Neshatian, L., Strege, P.R., Rhee, P.L., Kraichely, R.E., Mazzone, A., Bernard, C.E., Cima, R.R., Larson, D.W., Dozois, E.J., Kline, C.F., and Mohler, P.J. (2015). Ranolazine inhibits voltage-gated mechanosensitive sodium channels in human colon circular smooth muscle cells. *American Journal of Physiology-Gastrointestinal and Liver Physiology*, 309(6), p.G506-G512.
- Ni, Y.L., Kuan, A.S., and Chen, T.Y. (2014). Activation and inhibition of TMEM16A calcium-activated chloride channels. *PloS one*, 9(1), p.e86734.
- Nimmegeers, S., Sips, P., Buys, E., Decaluwé, K., Brouckaert, P., and Van de Voorde, J. (2008). Role of the soluble guanylyl cyclase  $\alpha 1$ -subunit in mice corpus cavernosum smooth muscle relaxation. *International Journal of Impotence Research*, 20(3), pp.278-284.
- Noda, M., Shimizu, S., Tanabe, T., Takai, T., Kayano, T., Ikeda, T., Takahashi, H., Nakayama, H., Kanaoka, Y., Minamino, N., Kangawa, K., Matsuo, H., Raftery, M., Hirose, T., Inayama, S., Hayashida, H., Miyata, T., and Numa, S. (1984). Primary structure of *Electrophorus electricus* sodium channel deduced from cDNA sequence. *Nature*, 312(5990), pp.121-127.
- Noda, M., Suzuki, H., Numa, S., and Stühmer, W. (1989). A single point mutation confers tetrodotoxin and saxitoxin insensitivity on the sodium channel II. *FEBS letters*, 259(1), pp.213-216.
- O'Brien, J.E. and Meisler, M.H. (2013). Sodium channel SCN8A (Nav1.6): properties and de novo mutations in epileptic encephalopathy and intellectual disability. *Frontiers In Genetics*, 4, p.213.
- Ogden D. and Stanfield P. (1994). Patch clamp techniques for single channel and whole cell recording. *Microelectrode techniques: the Plymouth workshop handbook, 2nd edn. The Company of Biologists, Cambridge*, pp. 53-78.
- Oh, S.J., Hwang, S.J., Jung, J., Yu, K., Kim, J., Choi, J.Y., Hartzell, H.C., Roh, E.J., and Lee, C.J. (2013). MONNA, a potent and selective blocker for transmembrane protein with unknown function 16/anoctamin-1. *Molecular Pharmacology*, 84(5), pp.726-735.

- Ohmori, I., Ouchida, M., Kobayashi, K., Jitsumori, Y., Inoue, T., Shimizu, K., Matsui, H., Ohtsuka, Y., and Maegaki, Y. (2008). Rasmussen encephalitis associated with SCN1A mutation. *Epilepsia*, 49(3), pp.521-526.
- Okabe, K., Kitamura, K., and Kuriyama, H. (1988). The existence of a highly tetrodotoxin sensitive Na channel in freshly dispersed smooth muscle cells of the rabbit main pulmonary artery. *Pflügers Archiv*, 411(4), p.423-428.
- Okuda, H., Noguchi, A., Kobayashi, H., Kondo, D., Harada, K.H., Youssefian, S., Shioi, H., Kabata, R., Domon, Y., Kubota, K., and Kitano, Y. (2016). Infantile pain episodes associated with novel Nav1.9 mutations in familial episodic pain syndrome in Japanese families. *PLoS One*, 11(5), p.e0154827.
- Ozaki, H., Hori, M., Kim, Y.S., Kwon, S.C., Ahn, D.S., Nakazawa, H., Kobayashi, M., and Karaki, H. (2002). Inhibitory mechanism of xestospongine-C on contraction and ion channels in the intestinal smooth muscle. *British Journal of Pharmacology*, 137(8), pp.1207-1212.
- Palmer, L.S., Valcic, M., Melman, A., Giraldi, A., Wagner, G., and Christ, G.J. (1994). Characterisation of cyclic AMP accumulation in cultured human corpus cavernosum smooth muscle cells. *The Journal of Urology*, 152(4), pp.1308-1314.
- Papp, R., Nagaraj, C., Zabini, D., Nagy, B.M., Lengyel, M., Maurer, D.S., Sharma, N., Egemnazarov, B., Kovacs, G., Kwapiszewska, G., and Marsh, L.M. (2019). Targeting TMEM16A to reverse vasoconstriction and remodelling in idiopathic pulmonary arterial hypertension. *European Respiratory Journal*, 53(6).
- Park, J.K., Kim, S.Z., Kim, S.H., Park, Y.K., and Cho, K.W. (1997). Renin angiotensin system in rabbit corpus cavernosum: functional characterisation of angiotensin II receptors. *The Journal of Urology*, 158(2), pp.653-658.
- Patino, G., Brackenbury, W., Bao, Y., Lopez-Santiago, L., O'Malley, H., Chen, C., Calhoun, J., Lafreniere, R., Cossette, P.P., Rouleau, G., and Isom, L. (2011). Voltage-Gated Na<sup>+</sup> Channel 1B: A Secreted Cell Adhesion Molecule Involved in Human Epilepsy. *Journal of Neuroscience*, 31(41), pp.14577-14591.
- Paulino, C., Kalienkova, V., Lam, A.K., Neldner, Y., and Dutzler, R. (2017). Activation mechanism of the calcium-activated chloride channel TMEM16A revealed by cryo-EM. *Nature*, 552(7685), pp.421-425.

- Peinelt, C., Vig, M., Koomoa, D.L., Beck, A., Nadler, M.J., Koblan-Huberson, M., Lis, A., Fleig, A., Penner, R., and Kinet, J.P. (2006). Amplification of CRAC current by STIM1 and CRACM1 (Orai1). *Nature Cell Biology*, 8(7), pp.771-773.
- Penzotti, J.L., Fozzard, H.A., Lipkind, G.M., and Dudley Jr, S.C. (1998). Differences in saxitoxin and tetrodotoxin binding revealed by mutagenesis of the Na<sup>+</sup> channel outer vestibule. *Biophysical Journal*, 75(6), pp.2647-2657.
- Peppiatt, C.M., Collins, T.J., Mackenzie, L., Conway, S.J., Holmes, A.B., Bootman, M.D., Berridge, M.J., Seo, J.T., and Roderick, H.L. (2003). 2-Aminoethoxydiphenyl borate (2-APB) antagonises inositol 1, 4, 5-trisphosphate-induced calcium release, inhibits calcium pumps and has a use-dependent and slowly reversible action on store-operated calcium entry channels. *Cell Calcium*, 34(1), pp.97-108.
- Perez-Reyes, E. (2003). Molecular physiology of low-voltage-activated T-type calcium channels. *Physiological Reviews*, 83(1), pp.117-161.
- Peters, C.J., Yu, H., Tien, J., Jan, Y.N., Li, M., and Jan, L.Y. (2015). Four basic residues critical for the ion selectivity and pore blocker sensitivity of TMEM16A calcium-activated chloride channels. *Proceedings of the National Academy of Sciences*, 112(11), pp.3547-3552.
- Phatarpekar, P.V., Wen, J., and Xia, Y. (2010). Role of adenosine signalling in penile erection and erectile disorders. *The Journal of Sexual Medicine*, 7(11), pp.3553-3564.
- Pifferi, S., Dibattista, M., and Menini, A. (2009). TMEM16B induces chloride currents activated by calcium in mammalian cells. *Pflügers Archiv-European Journal of Physiology*, 458(6), pp.1023-1038.
- Plant, L.D., Bowers, P.N., Liu, Q., Morgan, T., Zhang, T., Chen, W., Kittles, R.A., and Goldstein, S.A. (2006). A common cardiac sodium channel variant associated with sudden infant death in African Americans, SCN5A S1103Y. *The Journal of Clinical Investigation*, 116(2), pp.430-435.
- Pretorius, E., Siegelman, E., Ramchandani, P., and Banner, M. (2001). MR Imaging of the Penis. *RadioGraphics*, 21(suppl\_1), pp.S283-S298.
- Prieto, D. (2008). Physiological regulation of penile arteries and veins. *International Journal of Impotence Research*, 20(1), pp.17-29.

- Putney, J.W., Steinckwich-Besançon, N., Numaga-Tomita, T., Davis, F.M., Desai, P.N., D'Agostin, D.M., Wu, S., and Bird, G.S. (2017). The functions of store-operated calcium channels. *Biochimica et Biophysica Acta (BBA)-Molecular Cell Research*, 1864(6), pp.900-906.
- Rae, J., Cooper, K., Gates, P., and Watsky, M. (1991). Low access resistance perforated patch recordings using amphotericin B. *Journal of Neuroscience Methods*, 37(1), pp.15-26.
- Rasband, W.S. (2011). Imagej, us national institutes of health, bethesda, maryland, usa. <http://imagej.nih.gov/ij/>.
- Rice, F. L., Albrecht, P. J., Wymer, J. P., Black, J. A., Merkies, I. S., Faber, C. G., and Waxman, S. G. (2015). Sodium channel Nav1.7 in vascular myocytes, endothelium, and innervating axons in human skin. *Molecular Pain*, 11, s12990-s12015.
- Rogers, J.C., Qu, Y., Tanada, T.N., Scheuer, T., and Catterall, W.A. (1996). Molecular determinants of high affinity binding of  $\alpha$ -scorpion toxin and sea anemone toxin in the S3-S4 extracellular loop in domain IV of the Na<sup>+</sup> channel  $\alpha$  subunit. *Journal of Biological Chemistry*, 271(27), pp.15950-15962.
- Rosker, C., Lohberger, B., Hofer, D., Steinecker, B., Quasthoff, S., and Schreiber, W. (2007). The TTX metabolite 4,9-anhydro-TTX is a highly specific blocker of the Nav1.6 voltage-dependent sodium channel. *American Journal of Physiology-Cell Physiology*, 293(2), pp.C783-C789.
- Ruan, Y., Chen, Y., Li, M., Wang, T., Yang, J., Rao, K., Wang, S., Yang, W., Liu, J., and Ye, Z. (2016). AB095. Increased expression of TMEM16A/Ano1 chloride channel associated with diabetic erectile dysfunction. *Translational Andrology and Urology*, 5(Suppl 1).
- Saito, Y. A., Strege, P. R., Tester, D. J., Locke, G. R., Talley, N. J., Bernard, C. E., Rae, J. L., Makielski, J. C., Ackerman, M. J., and Farrugia, G. (2009). Sodium channel mutation in irritable bowel syndrome: Evidence for an ion channelopathy. *The American Journal of Physiology*, 296, G211-G218.
- Saleem, H., Tovey, S.C., Molinski, T.F., and Taylor, C.W. (2014). Interactions of antagonists with subtypes of inositol 1,4,5-trisphosphate (IP<sub>3</sub>) receptor. *British Journal of Pharmacology*, 171(13), pp.3298-3312.

- Saleh, S., Yeung, S.Y.M., Prestwich, S., Pucovský, V., and Greenwood, I. (2005). Electrophysiological and molecular identification of voltage-gated sodium channels in murine vascular myocytes. *The Journal of Physiology*, 568(1), p.155-169.
- Sam, P. and LaGrange, C. A. (2018). Anatomy, Abdomen and Pelvis, Penis, StatPearls. StatPearls Publishing. Available at: <http://www.ncbi.nlm.nih.gov/pubmed/29489230> (Accessed: 29 December 2018).
- Sancho, M., García-Pascual, A., and Triguero, D. (2012). Presence of the Ca<sup>2+</sup>-activated chloride channel anoctamin 1 in the urethra and its role in excitatory neurotransmission. *American Journal of Physiology-Renal Physiology*, 302(3), pp.F390-F400.
- Sanders, K.M. (2008). Regulation of smooth muscle excitation and contraction. *Neurogastroenterology and Motility*, 20, pp.39-53.
- Savio Galimberti, E., Gollob, M., and Darbar, D. (2012). Voltage-gated sodium channels: biophysics, pharmacology, and related channelopathies. *Frontiers in Pharmacology*, 3, p.124.
- Schreiber, R., Faria, D., Skryabin, B.V., Wanitchakool, P., Rock, J.R., and Kunzelmann, K. (2015). Anoctamins support calcium-dependent chloride secretion by facilitating calcium signaling in adult mouse intestine. *Pflügers Archiv-European Journal of Physiology*, 467(6), pp.1203-1213.
- Schroeder, B.C., Cheng, T., Jan, Y.N., and Jan, L.Y. (2008). Expression cloning of TMEM16A as a calcium-activated chloride channel subunit. *Cell*, 134(6), pp.1019-1029.
- Scudieri, P., Sondo, E., Ferrera, L., and Galletta, L.J. (2012). The anoctamin family: TMEM16A and TMEM16B as calcium-activated chloride channels. *Experimental Physiology*, 97(2), pp.177-183.
- Seda, M., Pinto, F.M., Wray, S., Cintado, C.G., Noheda, P., Buschmann, H., and Candenas, L. (2007). Functional and molecular characterisation of voltage-gated sodium channels in uteri from nonpregnant rats. *Biology of Reproduction*, 77(5), p.855-863.
- Segura-Covarrubias, G., Aréchiga-Figueroa, I.A., Jesús-Pérez, D., José, J., Sánchez-Solano, A., Pérez-Cornejo, P., and Arreola, J. (2020). Voltage-dependent protonation of

the calcium pocket enable activation of the calcium-activated chloride channel Anoctamin-1 (TMEM16A). *Scientific Reports*, 10(1), pp.1-12.

Selmer, K.K., Lund, C., Brandal, K., Undlien, D.E., and Brodtkorb, E. (2009). SCN1A mutation screening in adult patients with Lennox–Gastaut syndrome features. *Epilepsy and Behavior*, 16(3), pp.555-557.

Seo, Y., Lee, H.K., Park, J., Jeon, D.K., Jo, S., Jo, M., and Namkung, W. (2016). Ani9, a novel potent small-molecule ANO1 inhibitor with negligible effect on ANO2. *PloS one*, 11(5), p.e0155771.

Sergeant, G.P., Craven, M., Hollywood, M.A., McHale, N.G., and Thornbury, K.D. (2009). Spontaneous Ca<sup>2+</sup> waves in rabbit corpus cavernosum: Modulation by nitric oxide and cGMP. *The Journal of Sexual Medicine*, 6(4), pp.958-966.

Sergeant, G.P., Hollywood, M.A., McCloskey, K.D., McHale, N.G., and Thornbury, K.D. (2001). Role of IP<sub>3</sub> in modulation of spontaneous activity in pacemaker cells of rabbit urethra. *American Journal of Physiology Cell Physiology*, 280, C1349-C1356.

Sevilleja-Ortiz, A., El Assar, M., García-Rojo, E., Romero-Otero, J., García-Gómez, B., Medina-Polo, J., La Fuente, J.M., Rodríguez-Mañas, L., and Angulo, J. (2020). Enhanced contribution of orai channels to contractility of human penile smooth muscle in erectile dysfunction. *The Journal of Sexual Medicine*, 17(5), pp.881-891.

Shafik, A., Shafik, A.A., El-Sibai, O., and Ahmed, I. (2004). Electrocavernosogram in erectile dysfunction: A diagnostic tool. *Archives of Andrology*, 50(5), pp.317-325.

Shalev, M., Staerman, F., Allain, H., Lobel, B., and Saiag, B. (1999). Stimulation of P2y purinoceptors induces, via nitric oxide production, endothelium-dependent relaxation of human isolated corpus cavernosum. *The Journal of Urology*, 161(3), pp.955-959.

Shields, S.D., Cheng, X., Gasser, A., Saab, C.Y., Tyrrell, L., Eastman, E.M., Iwata, M., Zwinger, P.J., Black, J.A., Dib-Hajj, S.D., and Waxman, S.G. (2012). A channelopathy contributes to cerebellar dysfunction in a model of multiple sclerosis. *Annals of Neurology*, 71(2), pp.186-194.

Silva, J.R. and Goldstein, S.A. (2013). Voltage-sensor movements describe slow inactivation of voltage-gated sodium channels I: Wild-type skeletal muscle Nav1.4. *Journal of General Physiology*, 141(3), pp.309-321.

- Soderlund, D.M., Gilbert, L.I., Iatrou, K., and Gill, S.S. (2010). Sodium channels. *Comprehensive insect science. Pharmacology*, 5.
- Sopko, N.A., Hannan, J.L., and Bivalacqua, T.J. (2014). Understanding and targeting the Rho kinase pathway in erectile dysfunction. *Nature Reviews Urology*, 11(11), pp.622-628.
- Sorota, S. (1999). Insights into the structure, distribution, and function of the cardiac chloride channels. *Cardiovascular Research*, 42(2), pp.361-376.
- Sperelakis, N., Inoue, Y., and Ohya, Y. (1992). Fast Na<sup>+</sup> channels in smooth muscle from pregnant rat uterus. *Canadian Journal of Physiology and Pharmacology*, 70(4), p.491-500.
- Staprans, I., Pan, X.M., Rapp, J.H., Grunfeld, C., and Feingold, K.R. (2000). Oxidized cholesterol in the diet accelerates the development of atherosclerosis in LDL receptor- and apolipoprotein E-deficient mice. *Arteriosclerosis, Thrombosis, and Vascular Biology*, 20(3), pp.708-714.
- Steers, W.D. (2002). Pharmacologic treatment of erectile dysfunction. *Reviews in Urology*, 4(Suppl 3), p.S17.
- Strege, P.R., Holm, A.N., Rich, A., Miller, S.M., Ou, Y., Sarr, M.G., and Farrugia, G. (2003). Cytoskeletal modulation of sodium current in human jejunal circular smooth muscle cells. *American Journal of Physiology-Cell Physiology*, 284(1), pp.C60-C66.
- Struyk, A.F., Markin, V.S., Francis, D., and Cannon, S.C. (2008). Gating pore currents in DIIS4 mutations of Nav1.4 associated with periodic paralysis: saturation of ion flux and implications for disease pathogenesis. *The Journal of General Physiology*, 132(4), pp.447-464.
- Stühmer, W., Conti, F., Suzuki, H., Wang, X., Noda, M., Yahagi, N., Kubo, H., and Numa, S. (1989). Structural parts involved in activation and inactivation of the sodium channel. *Nature*, 339(6226), pp.597-603.
- Suadicaní, S.O., Urban-Maldonado, M., Tar, M.T., Melman, A., and Spray, D.C. (2009). Effects of ageing and streptozotocin-induced diabetes on connexin43 and P2 purinoceptor expression in the rat corpora cavernosa and urinary bladder. *BJU International*, 103(12), p.1686.

Sugawara, T., Tsurubuchi, Y., Agarwala, K.L., Ito, M., Fukuma, G., Mazaki-Miyazaki, E., Nagafuji, H., Noda, M., Imoto, K., Wada, K., and Mitsudome, A., (2001). A missense mutation of the Na<sup>+</sup> channel  $\alpha$ II subunit gene Nav1.2 in a patient with febrile and afebrile seizures causes channel dysfunction. *Proceedings of the National Academy of Sciences*, 98(11), pp.6384-6389.

Sun, H., Jiang, J., Gong, L., Li, X., Yang, Y., Luo, Y., Guo, Z., Lu, R., Li, H., Li, J., and Zhao, J. (2019). Voltage-gated sodium channel inhibitor reduces atherosclerosis by modulating monocyte/macrophage subsets and suppressing macrophage proliferation. *Biomedicine and Pharmacotherapy*, 120, p.109352.

Sun, H., Xia, Y., Paudel, O., Yang, X.R., and Sham, J.S. (2012). Chronic hypoxia-induced upregulation of Ca<sup>2+</sup>-activated Cl<sup>-</sup> channel in pulmonary arterial myocytes: a mechanism contributing to enhanced vasoreactivity. *The Journal of Physiology*, 590(15), pp.3507-3521.

Szendroedi, J., Sandtner, W., Zarrabi, T., Zebedin, E., Hilber, K., Dudley Jr, S.C., Fozzard, H.A., and Todt, H. (2007). Speeding the recovery from ultraslow inactivation of voltage-gated Na<sup>+</sup> channels by metal ion binding to the selectivity filter: a foot-on-the-door? *Biophysical Journal*, 93(12), pp.4209-4224.

Takahashi, R., Nishimura, J., Hirano, K., Naito, S., and Kanaide, H. (2003). Modulation of Ca<sup>2+</sup> sensitivity regulates contractility of rabbit corpus cavernosum smooth muscle. *The Journal of Urology*, 169(6), pp.2412-2416.

Tank, P., Grant, J., and Sauerland, E. (2005). Grant's dissector. 15th ed. Baltimore: Lippincott Williams and Wilkins, p.135.

Teixeira, C. E., Bento, A. C., Lopes-Martins, R. A., Teixeira, S. A., von Eickestedt, V., Muscará, M. N., Arantes, E. C., Giglio, J. R., Antunes, E., and de Nucci, G. (1998). Effect of Tityus serrulatus scorpion venom on the rabbit isolated corpus cavernosum and the involvement of NANC nitreergic nerve fibres. *British Journal of Pharmacology*, 123(3), 435-442.

Teixeira, C. E., de Oliveira, J. F., Baracat, J. S., Priviero, F. B., Okuyama, C. E., Rodrigues Netto, N. Jr., Fregonesi, A., Antunes, E., and De Nucci, G. (2004). Nitric oxide release from human corpus cavernosum induced by a purified scorpion toxin. *Urology*, 63(1), 184-189.

- Telinius, N., Majgaard, J., Kim, S., Katballe, N., Pahle, E., Nielsen, J., Hjortdal, V., Aalkjaer, C., and Boedtkjer, D.B. (2015). Voltage-gated sodium channels contribute to action potentials and spontaneous contractility in isolated human lymphatic vessels. *The Journal of Physiology*, 593(14), p.3109-3122.
- Teramoto, N., Zhu, H.L., Yotsu-Yamashita, M., Inai, T., and Cunnane, T.C. (2012). Resurgent-like currents in mouse vas deferens myocytes are mediated by Nav1.6 voltage-gated sodium channels. *Pflügers Archiv-European Journal of Physiology*, 464(5), p.493-502.
- Terlau, H., Heinemann, S.H., Stühmer, W., Pusch, M., Conti, F., Imoto, K., and Numa, S. (1991). Mapping the site of block by tetrodotoxin and saxitoxin of sodium channel II. *FEBS letters*, 293(1-2), pp.93-96.
- Thomas-Gatewood, C., Neeb, Z.P., Bulley, S., Adebisi, A., Bannister, J.P., Leo, M.D., and Jaggar, J.H. (2011). TMEM16A channels generate Ca<sup>2+</sup>-activated Cl<sup>-</sup> currents in cerebral artery smooth muscle cells. *American Journal of Physiology-Heart and Circulatory Physiology*, 301(5), pp.H1819-H1827.
- Thornbury, K. D., Hollywood, M. A., and Sergeant, G. P. (2019). Ion channels and intracellular calcium signalling in corpus cavernosum. Book chapter in “Smooth muscle spontaneous activity” Eds H Hashitani and RJ Lange, published by Springer Nature, Singapore. *Advances in Experimental Medicine and Biology*, 1124, 171-194.
- Tien, J., Peters, C.J., Wong, X.M., Cheng, T., Jan, Y.N., Jan, L.Y., and Yang, H. (2014). A comprehensive search for calcium binding sites critical for TMEM16A calcium-activated chloride channel activity. *Elife*, 3, p.e02772.
- Traish, A.M., Palmer, M.S., Goldstein, I., and Moreland, R.B. (1995). Expression of functional muscarinic acetylcholine receptor subtypes in human corpus cavernosum and in cultured smooth muscle cells. *Receptor*, 5(3), pp.159-176.
- Triggle, D.J., Gopalakrishnan, M., Rampe, D., Zheng, W., Mannhold, R., Kubinyi, H., and Folkers, G. eds. (2006). Voltage-gated ion channels as drug targets (Vol. 29). Weinheim, Germany: Wiley-VCH.
- Ulbricht, W. (2005). Sodium channel inactivation: molecular determinants and modulation. *Physiological Reviews*, 85(4), pp.1271-1301.

- Van Helden, D.F. (1993). Pacemaker potentials in lymphatic smooth muscle of the guinea-pig mesentery. *The Journal of Physiology*, 471(1), pp.465-479.
- Vein, C. (2003). Anatomy and Physiology of erection: pathophysiology of erectile dysfunction. *International Journal of Impotence Research*, 15(7), pp.S5-S8.
- Verstraelen, T. E., Ter Bekke, R. M., Volders, P. G., Masclee, A. A., and Kruimel, J. W. (2015). The role of the SCN5A-encoded channelopathy in irritable bowel syndrome and other gastrointestinal disorders. *Neurogastroenterology and Motility*, 27(7), 906-913.
- Vocke, K., Dauner, K., Hahn, A., Ulbrich, A., Broecker, J., Keller, S., Frings, S., and Möhrlen, F. (2013). Calmodulin-dependent activation and inactivation of anoctamin calcium-gated chloride channels. *Journal of General Physiology*, 142(4), pp.381-404.
- Wagner, G., Gerstenberg, T., and Levin, R.J. (1989). Electrical activity of corpus cavernosum during flaccidity and erection of the human penis: a new diagnostic method?. *The Journal of Urology*, 142(3), pp.723-725.
- Wagner, S., Dybkova, N., Rasenack, E.C., Jacobshagen, C., Fabritz, L., Kirchhof, P., Maier, S.K., Zhang, T., Hasenfuss, G., Brown, J.H., and Bers, D.M. (2006). Ca<sup>2+</sup>/calmodulin-dependent protein kinase II regulates cardiac Na<sup>+</sup> channels. *The Journal of Clinical Investigation*, 116(12), pp.3127-3138.
- Wang, G.K. and Wang, S.Y. (2003). Veratridine block of rat skeletal muscle Nav1.4 sodium channels in the inner vestibule. *The Journal of Physiology*, 548(3), pp.667-675.
- Wang, H.S., Dixon, J.E., and McKinnon, D. (1997). Unexpected and Differential Effects of Cl<sup>-</sup> Channel Blockers on the Kv4.3 and Kv4.2 K<sup>+</sup> Channels: Implications for the Study of the I<sub>to2</sub> Current. *Circulation Research*, 81(5), pp.711-718.
- Wang, H.Z., Lee, S.W., and Christ, G.J. (2000). Comparative studies of the maxi-K (K<sub>Ca</sub>) channel in freshly isolated myocytes of human and rat corpora. *International Journal of Impotence Research*, 12(1), pp.9-18.
- Wang, M., Yang, H., Zheng, L.Y., Zhang, Z., Tang, Y.B., Wang, G.L., Du, Y.H., Lv, X.F., Liu, J., Zhou, J.G., and Guan, Y.Y. (2012). Downregulation of TMEM16A calcium-activated chloride channel contributes to cerebrovascular remodeling during hypertension by promoting basilar smooth muscle cell proliferation. *Circulation*, 125(5), pp.697-707.

- Wang, Q., Shen, J., Splawski, I., Atkinson, D., Li, Z., Robinson, J.L., Moss, A.J., Towbin, J.A., and Keating, M.T. (1995). SCN5A mutations associated with an inherited cardiac arrhythmia, long QT syndrome. *Cell*, 80(5), pp.805-811.
- Watano, T., Kimura, J., Morita, T., and Nakanishi, H. (1996). A novel antagonist, No. 7943, of the Na<sup>+</sup>/Ca<sup>2+</sup> exchange current in guinea-pig cardiac ventricular cells. *British Journal of Pharmacology*, 119(3), 555-563.
- Waxman, S. (2012). Sodium channels, the electrogenosome and the electrogenistat: lessons and questions from the clinic. *The Journal of Physiology*, 590(11), pp.2601-2612.
- Weiss, J., Pyrski, M., Jacobi, E., Bufe, B., Willnecker, V., Schick, B., Zizzari, P., Gossage, S.J., Greer, C.A., Leinders-Zufall, T., and Woods, C.G. (2011). Loss-of-function mutations in sodium channel Nav1.7 cause anosmia. *Nature*, 472(7342), pp.186-190.
- Weiss, L.A., Escayg, A., Kearney, J.A., Trudeau, M., MacDonald, B.T., Mori, M., Reichert, J., Buxbaum, J.D., and Meisler, M.H. (2003). Sodium channels SCN1A, SCN2A and SCN3A in familial autism. *Molecular Psychiatry*, 8(2), pp.186-194.
- Weiss, R.E. and Horn, R. (1986). Functional differences between two classes of sodium channels in developing rat skeletal muscle. *Science*, 233(4761), pp.361-364.
- Werner, M.E., Zvara, P., Meredith, A.L., Aldrich, R.W., and Nelson, M.T. (2005). Erectile dysfunction in mice lacking the large-conductance calcium-activated potassium (BK) channel. *The Journal of Physiology*, 567(2), pp.545-556.
- West, R.B., Corless, C.L., Chen, X., Rubin, B.P., Subramanian, S., Montgomery, K., Zhu, S., Ball, C.A., Nielsen, T.O., Patel, R., and Goldblum, J.R. (2004). The novel marker, DOG1, is expressed ubiquitously in gastrointestinal stromal tumors irrespective of KIT or PDGFRA mutation status. *The American Journal of Pathology*, 165(1), pp.107-113.
- Williams, B.A. and Sims, S.M. (2007). Calcium sparks activate calcium-dependent Cl<sup>-</sup> current in rat corpus cavernosum smooth muscle cells. *American Journal of Physiology-Cell Physiology*, 293(4), pp.C1239-C1251.
- Wongcharoen, W., Chen, Y. C., Chen, Y. J., Chang, C. M., Yeh, H. J., Lin, C. I., and Chen, S. A. (2006). Effects of a Na<sup>+</sup>/Ca<sup>2+</sup> exchanger inhibitor on pulmonary vein electrical activity and ouabain-induced arrhythmogenicity. *Cardiovascular Research*, 70(3), 497-508.

- Wu, H.Y., Broderick, G.A., Suh, J.K., Hypolite, J.A., and Levin, R.M. (1993). Effects of purines on rabbit corpus cavernosum contractile activity. *International Journal of Impotence Research*, 5(3), pp.161-167.
- Xiao, Q., Yu, K., Perez-Cornejo, P., Cui, Y., Arreola, J., and Hartzell, H.C. (2011). Voltage-and calcium-dependent gating of TMEM16A/Ano1 chloride channels are physically coupled by the first intracellular loop. *Proceedings of the National Academy of Sciences*, 108(21), pp.8891-8896.
- Xie, D., Odronic, S.I., Wu, F., Pippen, A., Donatucci, C.F., and Annex, B.H. (2007). Mouse model of erectile dysfunction due to diet-induced diabetes mellitus. *Urology*, 70(1), pp.196-201.
- Xu, L., Ding, X., Wang, T., Mou, S., Sun, H., and Hou, T. (2019). Voltage-gated sodium channels: structures, functions, and molecular modeling. *Drug Discovery Today*, 24(7), pp.1389-1397.
- Yang, N., George, A.L., and Horn, R. (1996). Molecular basis of charge movement in voltage-gated sodium channels. *Neuron*, 16(1), pp. 113-122.
- Yang, Y.D., Cho, H., Koo, J.Y., Tak, M.H., Cho, Y., Shim, W.S., Park, S.P., Lee, J., Lee, B., Kim, B.M., and Raouf, R. (2008). TMEM16A confers receptor-activated calcium-dependent chloride conductance. *Nature*, 455(7217), pp.1210-1215.
- Yarov-Yarovoy, V., DeCaen, P.P., Westbroek, R.E., Pan, C.Y., Scheuer, T., Baker, D., and Catterall, W.A. (2012). Structural basis for gating charge movement in the voltage sensor of a sodium channel. *Proceedings of the National Academy of Sciences*, 109(2), pp.93-102.
- Yordanova, I., Todorov, T., Dimova, P., Hristova, D., Tincheva, R., Litvinenko, I., Yotovska, O., Kremensky, I., and Todorova, A. (2011). One novel Dravet syndrome causing mutation and one recurrent MAE causing mutation in SCN1A gene. *Neuroscience Letters*, 494(2), pp.180-183.
- Yoshida, S. (1994). Tetrodotoxin-resistant sodium channels. *Cellular and Molecular Neurobiology*, 14(3), pp.227-244.
- Yu, F., Westbroek, R., Silos-Santiago, I., McCormick, K., Lawson, D., Ge, P.P., Ferreria, H., Lilly, J., DiStefano, P.P., Catterall, W., Scheuer, T., and Curtis, R. (2003).

Sodium Channel  $\beta 4$ , a New Disulfide-Linked Auxiliary Subunit with Similarity to  $\beta 2$ . *The Journal of Neuroscience*, 23(20), pp.7577-7585.

Yu, K., Duran, C., Qu, Z., Cui, Y.Y., and Hartzell, H.C. (2012). Explaining calcium-dependent gating of anoctamin-1 chloride channels requires a revised topology. *Circulation Research*, 110(7), pp.990-999.

Yu, K., Zhu, J., Qu, Z., Cui, Y.Y., and Hartzell, H.C. (2014). Activation of the Ano1 (TMEM16A) chloride channel by calcium is not mediated by calmodulin. *Journal of General Physiology*, 143(2), pp.253-267.

Zhang, C.H., Li, Y., Zhao, W., Lifshitz, L.M., Li, H., Harfe, B.D., Zhu, M.S., and ZhuGe, R. (2013). The transmembrane protein 16A  $\text{Ca}^{2+}$ -activated  $\text{Cl}^-$  channel in airway smooth muscle contributes to airway hyperresponsiveness. *American Journal of Respiratory and Critical Care Medicine*, 187(4), pp.374-381.

Zhang, J.Z., Yarov-Yarovoy, V., Scheuer, T., Karbat, I., Cohen, L., Gordon, D., Gurevitz, M., and Catterall, W.A. (2012). Mapping the interaction site for a  $\beta$ -scorpion toxin in the pore module of domain III of voltage-gated  $\text{Na}^+$  channels. *Journal of Biological Chemistry*, 287(36), pp.30719-30728.

Zhang, W., Halligan, K.E., Zhang, X., Bisailon, J.M., Gonzalez-Cobos, J.C., Motiani, R.K., Hu, G., Vincent, P.A., Zhou, J., Barroso, M., and Singer, H.A. (2011). Orai1-mediated ICRAC is essential for neointima formation after vascular injury. *Circulation Research*, 109(5), pp.534-542.

Zhang, X., Du, X.N., Zhang, G.H., Jia, Z.F., Chen, X.J., Huang, D.Y., Liu, B.Y., and Zhang, H.L. (2012). Agonist-dependent potentiation of vanilloid receptor transient receptor potential vanilloid type 1 function by stilbene derivatives. *Molecular Pharmacology*, 81(5), pp.689-700.

Zhou, X.B., Arntz, C., Kamm, S., Motejlek, K., Sausbier, U., Wang, G.X., Ruth, P., and Korth, M. (2001). A molecular switch for specific stimulation of the  $\text{BK}_{\text{Ca}}$  channel by cGMP and cAMP kinase. *Journal of Biological Chemistry*, 276(46), pp.43239-43245.

Zhu, H.L., Aishima, M., Morinaga, H., Wassall, R.D., Shibata, A., Iwasa, K., Nomura, M., Nagao, M., Sueishi, K., Cunnane, T.C., and Teramoto, N. (2008). Molecular and biophysical properties of voltage-gated  $\text{Na}^+$  channels in murine vas deferens. *Biophysical Journal*, 94(8), pp.3340-3351.



## **Appendix**

### **A.1 Materials and methods**

#### **A.1.1 Intracellular recording**

Intracellular recording involves inserting a very fine pipette (tip size typically around 0.1-0.01  $\mu\text{m}$ ) into a single cell to measure its electrical activity. While fast electrical events can be recorded with extracellular recordings, subthreshold events in single neurons can only be recorded with intracellular electrodes. Thus, intracellular recording is often chosen to study the membrane signals *in situ*, that is, in tissue, which allows for the measurement of receptor or synaptic potentials.

In this preliminary study, intracellular recording was used to study the resting membrane potential of corpus cavernosum smooth muscle cells. These experiments were performed in collaboration with Professor Sean Ward and Dr SungJin Hwang during a secondment at the University of Nevada, Reno.

#### **A.1.2 Tissue $\text{Ca}^{2+}$ imaging**

Manually sliced CCSM tissue (~1 mm thick) were cut and pinned out on Sylgard-coated (Dow Corning, Weisbaden, Germany) petri dish. Then, the dish was loaded with 10  $\mu\text{M}$  Fluo-4-AM and 0.05% pluronic acid in Krebs solution (solution 1) at room temperature for an hour and a half prior to experiments. During experiments, the dish containing the tissue was continuously perfused with Hanks' solution (solution 3) at  $36 \pm 1^\circ\text{C}$ . Additionally, the tissue under study was continuously superfused by means of a custom-built closed delivery system.

Epifluorescence microscopes are effective at visualising thin samples. However, thicker samples will produce out of focus light. This leads to increased noise and decreased signal, resulting in 'hazy' images. Thus, confocal microscopy was developed to address this issue.

In this study, imaging of intracellular  $\text{Ca}^{2+}$  events in CCSM tissue slice were performed using confocal microscopy. Confocal microscopy excludes out of focus lights using

pinholes, spatially resolving light from a particular depth or plane in an object. Single point illumination, through a Nipkow spinning disc, was focused onto the sample via an objective lens. Returning lights from above or below the focal plane failed to pass through the pinhole. The pinhole, situated at the exact point where the returning light rays focus, filters out any signal that is not the focused light. Focused light that passed through the detector pinhole aperture are collected by a photomultiplier that converts the light signal to an electrical signal that can be subsequently recorded. A simplified illustration demonstrating this principle is shown in Figure App.3.

A krypton-argon laser (Melles Griot, UK) was used to excite the Fluo-4-AM dye at 488 nm, resulting in fluorescent emissions with  $>510$  nm wavelengths. The fluorescent light emitted from the specimen returned through the objective lens and Nipkow disc and was reflected with a dichroic mirror to the focal point. An electron multiplying charge coupled device (EMCCD) camera, Andor iXon 887, (Andor Technology Belfast, UK, 512 x 512 pixels, pixel size 16 x 16  $\mu\text{m}$ ) was coupled to dual Nipkow spinning disc (CSU22, Yokogawa, Electric Corporation, Tokyo, Japan) to image CCSMs.

Experiments were conducted using a Zeiss Axioskop 2 upright microscope, a x20 water-dipping lens (Carl Zeiss MicroImaging GmbH, Jena, Germany), and a frame rate of 15 frames per second (FPS) was employed to capture images with pixel size 0.512 x 0.512  $\mu\text{m}$ . A representative image of the Nipkow spinning disk and micro lens array is shown in Figure App.4.

No image analysis was performed since the experiments were preliminary. However, using ImageJ, background fluorescence from the camera, obtained using a null frame, was subtracted from each frame. A colour-coded system was then imported to display low intensity fluorescence as cold colours (blue/green) and high intensity fluorescence as warm colours (red/yellow).